From stable carbenes to stable Blatter-type radicals

DAVID EDWARD TUCKER

From stable carbenes to stable Blatter–type radicals

David E. Tucker

A thesis submitted in partial fulfilment of the requirements for the degree of Doctor of Philosophy

Department of Chemistry

Durham University

2018

Declaration

The work described in this thesis was carried out at the Department of Chemistry at Durham University between October 2014 and April 2017 under the supervision of Dr. AnnMarie O'Donoghue. The material within has not been previously submitted for a degree at this or any other university. All work has been carried out by the author unless otherwise indicated.

D. E. Tucker

Copyright

Abstract.

The overall theme of this project was investigation of the proton-transfer of stable carbene species. Stable carbenes, such as N-heterocyclic carbenes (NHCs) have recently been the focus of a great deal of research, due to their useful nature as organocatalysts for a wide range of synthetic transformations. As NHCs are typically generated *in situ* by deprotonation of their conjugate acids, the kinetics of proton-transfer of NHCs and related species are highly important areas of research.

Using a kinetic method, the C(3)H acidity of a series of NHC conjugate acids, (imidazolium and triazolium based) was investigated at I = 1.0, 25 °C. The acidity was probed by H/D exchange experiments monitored by ^{1}H NMR spectroscopy in D_2O solutions at varied p*D*, from which the pseudo first-order rate constants of exchange k_{ex} (s^{-1}) could be determined. Comparing the k_{ex} values at various p*Ds* allows determination of the second-order rate constant of exchange k_{DO} (M^{-1} s^{-1}), for each azolium ion, and using a secondary solvent isotope effect (k_{DO}/k_{HO} = 2.4), estimates of pK_a could be made by kinetic acidity, as the reprotonation of carbenes in water is known to be limited by solvent reorganisation ($k_{HOH} = k_{reorg} = 10^{11}$ s^{-1}).

p*D* rate profiles of *ortho*-halogen substituted triazolium salts studied by this method showed an altered dependence on p*D* at low p*D*, an effect which has previously been observed in an N-C_6F_5 triazolium salt. This effect is believed to originate from N1 protonation of the triazolium ring system under acidic conditions, to generate a dicationic triazolium species. *Ortho*-halogen substitution is believed to promote this effect by raising the pK_a of the N1 position.

Two imidazolium salts with fused furan rings and exocyclic nitrogen atoms were also studied by this method and did not show altered dependence on p*D*. The carbon acidity C(3)H positions of these salts was significantly higher than is generally predicted for N-aryl imidazolium salts. The origin of this increased acidity is assigned to increased σ-electron withdrawal and π-donation by the O atom of the fused furan ring.

Bis(amino)cyclopropenylidenes (BACs) are a relatively new field of stable carbenes, and the only family with no α-heteroatoms to the carbene centre. Several BAC conjugate acids were prepared using existing literature procedures, however, attempts to prepare of N-aryl BACs by the use of N-methylaniline produced only trisubstituted cyclopropenium species. Hydrolysis of this to cyclopropenone, followed by

chlorination and reaction with triphenylphosphine produced a phosphonium salt, instead of the desired BAC conjugate acid. Using diethylamine produced a mixture of disubstituted and trisubstituted cyclopropenium salts. The disubstituted product could not be purified after the use of triphenylphosphine. Replacement with triethyl phosphite afforded a stable phosphonato cyclopropenium salt. Base hydrolysis of the phosphonate yielded N-ethyl BAC conjugate acid, with competing elimination of ethanol.

The carbon acidity of the C(3)H position of two bis(amino)cyclopropenium salts was studied by the same kinetic acidity method used to investigate NHC conjugate acids. Control experiments determined a lack of buffer catalysis and confirmed H/D exchange had occurred. The lack of buffer catalysis suggests that as with NHCs, reprotonation of BACs is limited by solvent reorganisation ($k_{HOH} = k_{reorg} = 10^{11}$ s^{-1}). The determined values of k_{DO} could be converted to k_{HO} ($k_{DO}/k_{HO} = 2.4$), which in turn was used to estimate pK_a (~22). This value is between the approximate acidity of N-aryl and N-alkyl imidazolium salts. Despite the lack of α-heteroatoms, the BAC is believed to be stabilised by a highly acute bond angle at the carbene centre and by σ-withdrawal and π-donation from the exocyclic nitrogen substituents.

The unusual hydrolytic behaviour of the phosphonato-cyclopropenium species was investigated. Further phosphonato-cyclopropenium salts were prepared by reaction of alkyl phosphites with chloro-cyclopropenium salts. Hydrolysis of these phosphonates largely favoured elimination of a BAC compared to ethoxide, contrary to what would be expected from the respective pK_a values of the leaving groups. The kinetics of hydrolysis was investigated using ^{31}P NMR spectroscopy at 25°C, I = 1.0 M in various K_2CO_3 buffers in H_2O and D_2O. A first-order dependence on hydroxide/deuteroxide was observed with no significant solvent kinetic isotope effect. Variable temperature experiments suggested an associative mechanism, and at varied temperature, ionic strength and basicity, identical ratios of products were produced. From this information, it is proposed that hydrolysis proceeds *via* either an A_N+D_N or S_N2@P mechanism. The unusual ratio of products could be potentially be explained by rate-limiting pseudorotation during an A_N+D_N mechanism.

Investigation of the organocatalytic chemistry of BACs involved following the BAC-catalysed intramolecular Stetter reaction by ^{1}H NMR spectroscopy at 25 °C. The degree of steric hindrance around the BAC was of vital importance, as the reaction did not

proceed using bulky catalysts. A similar 2-substituent effect of aryl aldehydes in reaction with NHCs was observed with BACs. Several hydroxy-aryl adducts of BACs were prepared and isolated, and the formation of a d_1-acyl anion equivalent was investigated by H/D exchange experiments. Exchange was observed under organocatalytic conditions, and experiments monitored by ^{1}H NMR in highly basic aqueous (D_2O, I = 1.0, 25 °C) conditions found exchange to occur. The second-order rate constants of exchange k_{DO} showed a moderate aryl substituent effect between adducts.

Finally, the serendipitous discovery of a "Blatter"-type radical formed from carbenoid species Nitron found by previous MChem student Jacob A. Grant was investigated. A further radical derivative compound was discovered and both were fully characterised. Further synthetic and spectroscopic experiments suggested a possible mechanism for the formation of these radicals. Both radicals' properties were found to be largely similar to previous examples of "Blatter"-type radicals through cyclic voltammetry and EPR experiments.

TABLE OF CONTENTS

Abbreviations

A	Absorbance
Ac	Acetyl
Ad	Adamantyl
Aq.	Aqueous
BAC	Bis(amino)cyclopropenylidene
Bn	Benzyl
br.	Broad
BPh_4	Tetraphenylborate
Bu	Butyl
BuLi	Butyllithium
°C	degrees Celsius
cat.	Catalytic
C_6F_5	Pentafluorophenyl
$CDCl_3$	d1-chloroform
CHN	Carbon/Hydrogen/Nitrogen elemental analysis
cm^{-1}	Wavenumbers
COSY	Correlation spectroscopy
Cp	Cyclopropenyl
CV	Cyclic voltammetry
Cy	Cyclohexyl
DBU	1,8-Diazabicyclo(5.4.0)undec-7-ene
DCM	Dichloromethane
dec.	Decomposition
DFT	Density Functional Theory
DMF	Dimethylformamide
DMSO	Dimethylsulfoxide
D_2O	Deuterium oxide
e.e.	Enantiomeric excess
Et	Ethyl
EPR	Electron paramagnetic resonance
eq.	Equivalents
ES+	Electrospray Ionisation +
EWG	Electron-withdrawing Group
EXSY	Exchange Spectroscopy NMR
$E_{1/2}$	Half-wave potential
E_{cell}	Cell potential
f.b. (%)	Freebase (percentage)
g	Gram(s)
G	Gauss
γ	Activity coefficient
h	Hours
HPLC	High-performance liquid chromatography
HRMS	High-resolution mass spectrometry
Hz	Hertz (s^{-1})
H_2O	Water
I	Ionic strength
i-	Iso-
IR	Infrared
J	Coupling constant
k	Rate constant
K	Equilibrium constant
K_a	Acid dissociation constant
K_w	Autoprotolysis constant
KHMDS	Potassium bis(trimethylsilyl)amide
L	Litre(s)
L	Lyo- (either H or D)
LCMS	Liquid chromatography-mass spectrometry
ln	Natural logarithm
log	Logarithm (base 10)
M	Molarity **(**$moldm^{-3}$)
mM	Millimolar
µA	Amps
Me	Methyl
MeCN	Acetonitrile
Mes	Mesityl
mg	Milligram
mL	Millilitre
Mol.	Mole
m.p.	Melting point
M.S.	Molecular sieves
mmol	Millimoles
MRI	Magnetic Resonance Imaging
µW	Microwave
m/z	Mass-to-charge ratio
NaOH	Sodium hydroxide
NHC	N-Heterocyclic carbene
ν_{MAX}	Wavenumber (cm^{-1})
NMR	Nuclear Magnetic Resonance
Ox.	Oxidation
Ph	Phenyl
Pr	Propyl
ppm	Parts per million
R	Alkyl substituent
ρ	Hammett reaction constant
RT	Room temperature
s	Second(s)
SOMO	Singularly Occupied Molecular Orbital
SQUID	Superconduting Quantum Interference Device
σ	Hammett substituent constant
TBDPSO	tbutyldiphenylsilyl
T_c	Curie Temperature
TEMPO	2,2,6,6-tetramethylpiperidin-1-yl)oxidanyl
THF	Tetrahydrofuran
THT	Tetrahydrothiophene
Tf	Triflyl
TMEDA	Tetramethylethylenediamine
TMS	Tetramethylsilane
TMS.DAM	Trimethylsilyl diazomethane
Ts	Tosyl
UV	Ultraviolet
V	Volts

Chapter 1 Introduction

1.0 Foreword

The aims of this thesis are focused on three major topics, and the results are divided between four chapters. Chapter 2 is a continuation of previous research into the proton-transfer chemistry of NHCs. Chapters 3 and 4 detail our exploratory research into the chemistry of a relatively young family of stable carbenes, bis(amino)cyclopropenylidenes (BACs). Chapter 3 focusses on the preparation and proton-transfer chemistry of BACs. In the course of these studies novel BAC-phosphonate adducts were isolated; the kinetics and mechanism of hydrolysis of these adducts are also presented in chapter 3. Chapter 4 focusses on a mechanistic evaluation of BACS in benzoin and Stetter organocatalytic transformations. Chapter 5 concerns the preparation of a series of novel stable benzotriazinyl radicals from carbenoid precursors and a detailed evaluation of properties.

This chapter provides an over-arching introduction to the major areas of chemistry within this thesis.

1.1 Carbenes

A carbene is a divalent, uncharged carbon species, with six valence electrons. Four electrons are used in bonding with the two substituents, and two remain localised on the carbon atom. The chemistry of carbenes is broadly categorised by the configuration of these electrons, either in a singlet or triplet state.

Figure 1.1 Orbital structure of carbenes

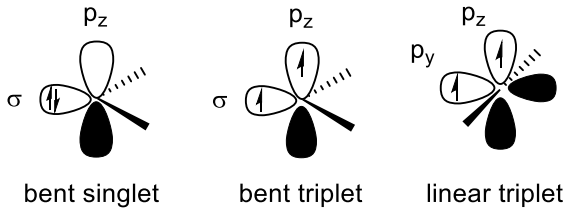

The geometry of the carbene centre can be described as bent or linear, with corresponding stabilization of either the triplet or singlet state through geometry. In a linear carbene, the carbon p-orbitals are degenerate, and therefore the lowest energy state is a triplet configuration. The majority of carbenes are non-linear, however, and the bent geometry stabilises the σ-symmetry orbital, which depending on the angle and substituents, can result in either a singlet (both electrons paired in σ-orbital) or triplet (electrons in separate orbitals) ground state.[1]

Figure 1.2 Representation of relative orbital energies in carbene configurations

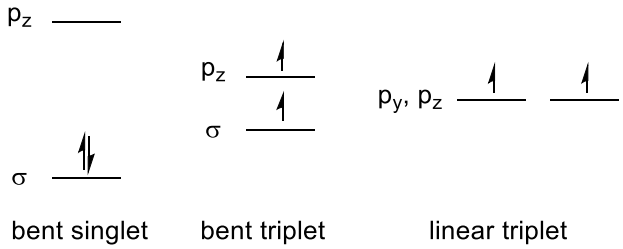

The larger the gap between the σ and π orbital energy, the more likely a given carbene will have a singlet ground state. Singlet carbenes are therefore favoured by σ-withdrawing and π-donating substituents, which both stabilise the occupied σ-orbital, and disfavour occupation of the π-orbital. Triplet carbenes are favoured by the reverse; σ donating and π withdrawing substituents, as these lower the gap between orbitals. If the energy gap between the σ and π orbitals is larger than the energy associated with the spin-pairing of electrons, then the carbene will have a singlet ground state.

The reactivity of a carbene is greatly influenced by electronic configuration. Triplet state carbenes tend to behave similarly to diradical species, whereas singlet carbenes can react as electrophiles or nucleophiles, depending on the substituents. The majority of carbenes, regardless of singlet or triplet configuration, are highly reactive and are therefore typically classed as reactive intermediates prepared *in situ* from a more stable starting material for applications in chemistry.

Scheme 1.1 Carbene mediated alkylation of propan-2-ol

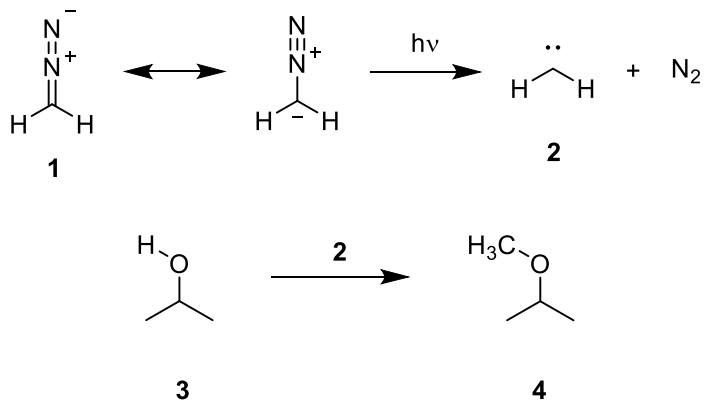

As an example, methylation of isopropanol **3** by diazomethane **1** starts with the photochemical generation of a triplet carbene **2**, which inserts across the O-H bond. Production of nitrogen gas provides a thermodynamic driving force for the reaction.

Figure 1.3 Generation of dichlorocarbene

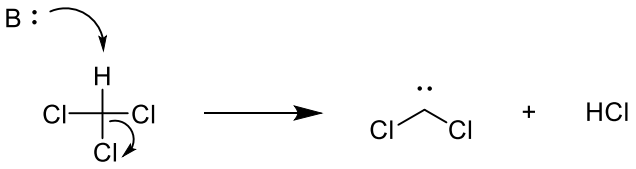

5 **6**

Most traditional carbene chemistry involves this type of *in situ* generation, such as the formation of dichlorocarbene **6** from the α–elimination of HCl from chloroform **5** in the presence of a strong base.

Scheme 1.2 Dichlorocarbene cyclopropanation

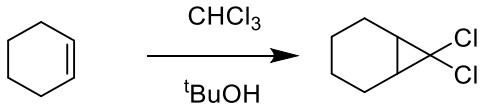

7 **8**

Dihalocarbenes such as dichlorocarbene **6** are commonly used to generate geminal dihalocyclopropanes from alkenes[2]. However, most carbenes are too unstable for direct use, and carbenoid species are used instead, such as in the Simmons-Smith reaction.[3]

1.1.1 Stable Carbenes

Although most carbenes are highly unstable species, existing only as reactive intermediates, there are increasing examples of more stable variants over the last few decades.

Figure 1.4 Stabilisation of diaminocarbenes (Pauling electronegativity indices in italics)

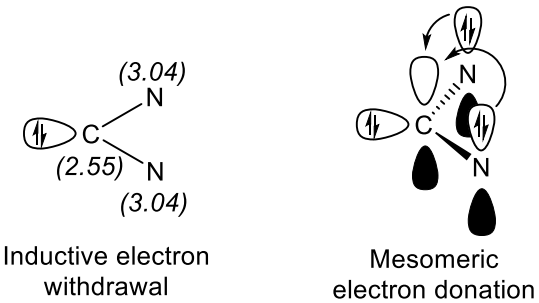

Singlet carbenes are typically stabilised by adjacent heteroatoms (NR_2, OR, SR, F etc.), due to their electronegative nature (σ-withdrawing) and donation of their lone-pair electron density (π-donation). The use of σ-donor and π-acceptor substituents (such as in diborylcarbenes) is

predicted to have singlet rather than triplet multiplicity with linear geometry[4,5], although these species have not been successfully isolated. The singlet configuration is due to the interaction of a vacant π-orbital of the acceptor with one p orbital, but non-interaction with the other, resulting in non-degenerate p orbitals and a singlet ground state[6].

Scheme 1.3 Pyrolysis to generate an NHC

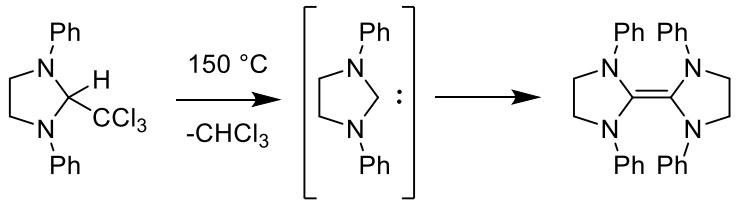

9 **10** **11**

Early attempts at the isolation of a carbene were performed by Wanzlick et. al. in 1960[7]. Using two amino substituents in an attempt to increase the stability of the carbene, 1,3-diphenylimidazolin-2-ylidene **10** was generated by vacuum pyrolysis to eliminate chloroform from **9**. Although reactivity studies with strong electrophiles[8] confirmed the carbene was generated, it could not be isolated due to formation of the dimer **11**. N,N-Diphenyl carbene **10** is a member of the large N-heterocyclic carbene (NHC) family, which contains commonly used families of stable carbenes, such as imidazol-2-ylidenes, triazol-3-ylidenes and thiazolylidenes.

Figure 1.5 Bertrand's phosphinosilyl carbene

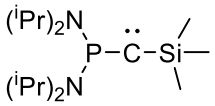

12

The first isolation of a stable carbene was in 1988, when Bertrand et. al.[9] isolated a phosphinosilyl carbene **12**, an example of a push-pull carbene, although it was generally considered that this species had more phosphoacetylene than carbene character. A “push-pull” carbene is named after the differing electronegativities of the phosphoryl and silyl substituents. The partial multiple P-C bond order contributes to the system’s stability.

Scheme 1.4 First isolated stable NHC

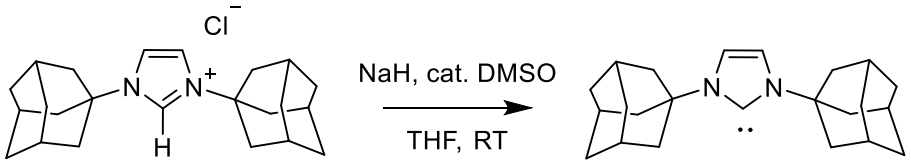

13 **14**

The largest and most studied family of stable carbenes are NHCs. N,N-di-adamantyl imidazolylidene **14** was the first example of an isolated NHC achieved by Arduengo et. al.[10] by deprotonation of its conjugate acid **13** under anhydrous conditions.

Scheme 1.5 Alternative methods to generate NHCs.

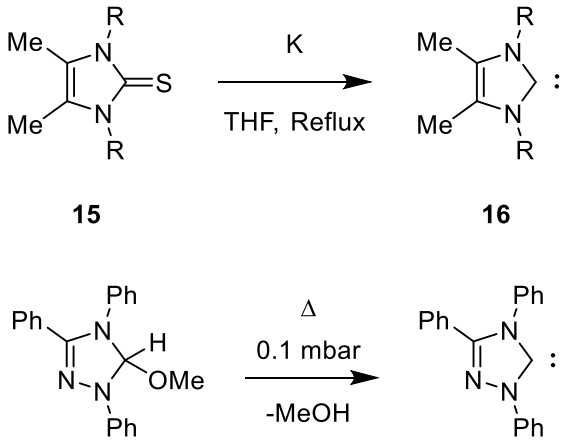

15 **16**

17 **18**

Most NHCs are generated by the deprotonation of their conjugate acids, however, they may also be generated by other methods, such as reduction of the parent imidazole-2-thione **15** using potassium metal to generate carbene **16**[11]. Other methods include the thermal elimination of methanol from **17** at low pressure to generate triazol-3-ylidene **18**[12].

Figure 1.6 Di(amido)carbene

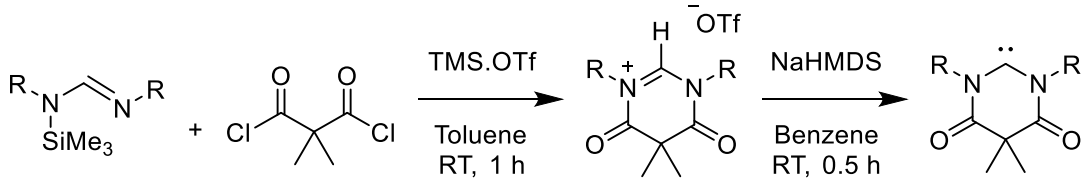

19 **20** **21** **22**

Aside from NHCs, several related families of stable carbenes have been isolated. *N*-*N*-diamidocarbenes (diamidocarbenes or DACs) **22** are distinct from NHCs by the use of amide nitrogen instead of amino groups to stabilise the carbene state. Synthesis of these carbenes involves the condensation of a protected formamidine **19** and a diacid chloride **20** to create the conjugate acid of the carbene **21**[13,14]. As the amido group is a weaker donor than an amine, the singlet-triplet gap is lower in DACs than for NHCs. This suggests that DACs may be more reactive in catalysis than NHCs.[15]

Figure 1.7 Bis(amino)cyclopropenylidenes

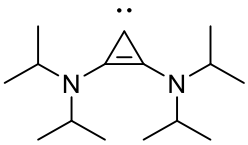

23

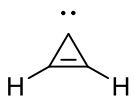

24

A group of stable carbenes of particular interest to this work is cyclopropenylidenes. The first isolated example is bis(amino)cyclopropenylidene **23**, by Lavallo et. al.[16], Cyclopropenylidenes are unique among stable isolated carbenes in that they have no heteroatom substituents directly adjacent to the carbenic centre. Additionally, due to the constraints of the three-membered ring system, cyclopropenylidenes are sterically unhindered. The bis(amino)cyclopropenylidenes (BACs), which are stabilised by the exocyclic nitrogen substituents, are a particularly stable subset of cyclopropenylidene. BACs evaded isolation for some time due to their propensity to form lithium[17] or sodium adducts[16,18], and requirement for specific counterions in their conjugate acids. Additionally, the parent cyclopropenylidene **24** has been observed spectroscopically in the interstellar medium[19]. It has also been prepared by pyrolysis and captured in an argon matrix at 10 K[20].

Figure 1.8 Dianthracyl persistent triplet carbene

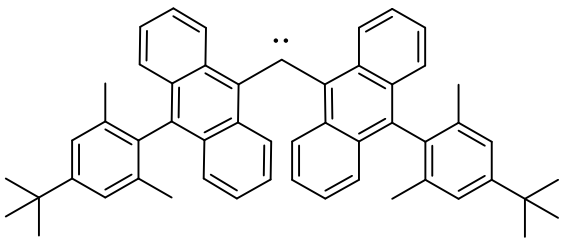

25

Unlike singlet carbenes, there are no examples of isolated triplet carbenes with indefinite stability. Several mildly persistent triplet carbenes have been isolated with lifetimes from

milliseconds to several days at room temperature[21], such as the anthracyl system **25**, with a lifetime of up to 14 days[22]. Most examples of persistent triplet carbenes are stabilized by large conjugated aryl systems, and by steric hindrance providing kinetic stability.

1.2 Organocatalysis

An important role for stable carbenes, in particular N-heterocyclic carbenes, lies in organocatalysis. Since Breslow's seminal mechanistic study on the action of thiamine[23], NHCs have been at the forefront of organocatalytic experimentation.

Figure 1.9 Action of thiamine pyrophosphate in the pyruvate dehydrogenase process.

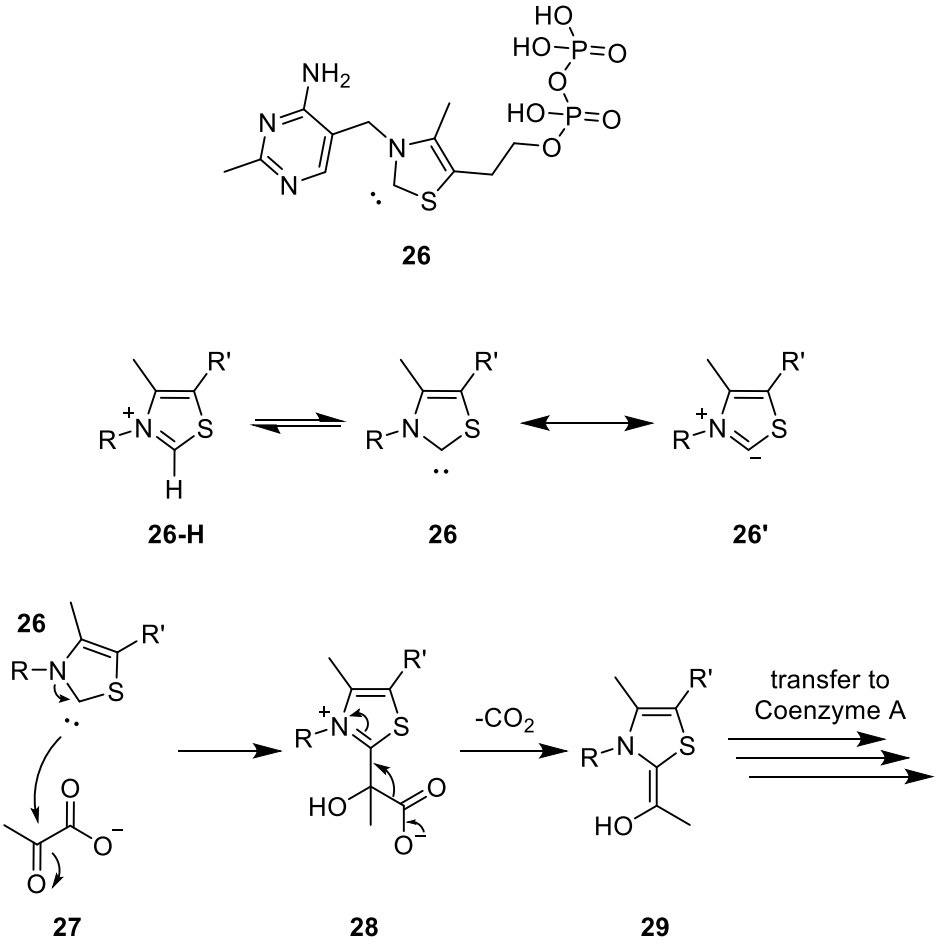

Thiamine (vitamin B1) is a ubiquitous biological example of a NHC precursor used as a coenzyme in a wide variety of enzymatic reactions. Thiamine pyrophosphate (**26-H**) has an NHC conjugate base **26** which is the active nucleophilic catalyst in many enzymatic transformations. In earlier studies, the active form of **26-H** was more commonly drawn as ylide **26'** rather than as thiazolylidene **26**. As one example, the first step in the transformation of pyruvate **27** to acetyl coenzyme A is catalysed by pyruvate decarboxylase, which is dependent

on **26-H**. Acetyl co-enzyme A is subsequently used in the citric acid cycle to produce cellular energy through respiration[24].

The action of the thiamine-derived carbene in this reaction is as an "umpolung" (meaning reversed polarity) reagent, activating the ketone position of pyruvate to allow it to act as an anionic leaving group, which is highly disfavoured in the absence of an umpolung reagent. Umpolung reagents are the primary method of accessing these acyl anion equivalent synthons. Common umpolung reagents include cyanide, dithianes[25] or, increasingly, N-heterocyclic carbenes.

Figure 1.10 Retrosynthetic representation of benzoin and Stetter reactions

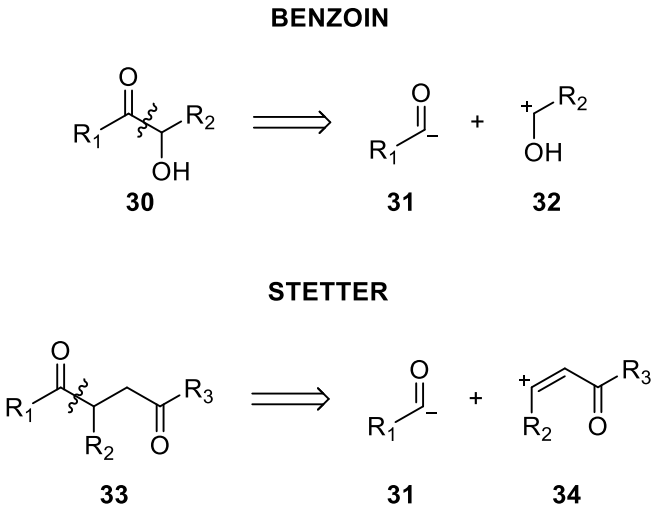

Early NHC organocatalysis was largely focussed on two reactions involving acyl anion equivalents: the benzoin condensation and Stetter reaction. Since then, a much wider variety of NHC catalysed processes has been discovered.

1.2.1 Benzoin condensation

Figure 1.11 Catalytic cycle of the thiamine catalysed benzoin condensation

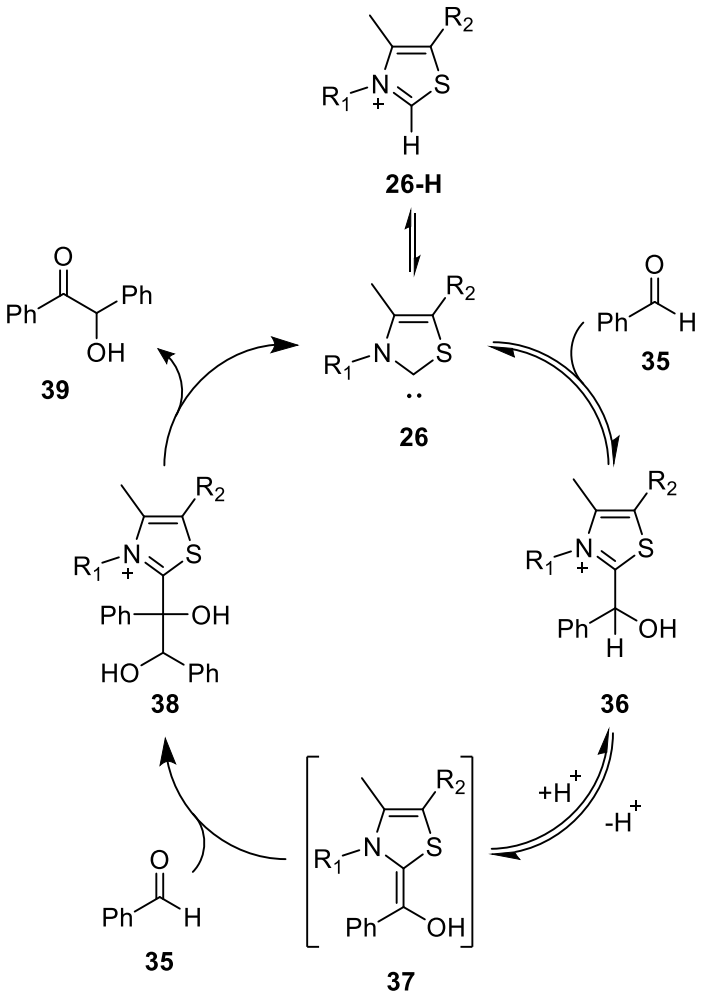

The earliest reports of NHC organocatalysis were in 1943 when Ugai[26] discovered that the benzoin condensation could be performed using thiamine in the presence of base. Breslow[23] proposed the mechanism of this reaction, involving reaction of the conjugate base of **26-H** with aryl aldehydes such as benzaldehyde **35** to give a proposed hydroxy-aryl adduct **36**. Subsequent deprotonation generates an enaminol or "Breslow intermediate" **37**. Finally, reaction with another equivalent of aldehyde, followed by dissociation of the NHC to repeat the catalytic cycle, gives benzoin **39** as product.

Since this early study, a large amount of research has been undertaken to increase the scope of the benzoin condensation, and it is normally the test reaction to evaluate new carbene scaffolds in organocatalysis. Most modern benzoin condensation reactions use triazol-3-ylidene based catalysts in place of thiazol-2-ylidene systems.[27] Asymmetric benzoin condensations can be performed using chiral triazolium salts to produce NHCs.

Figure 1.12 Early Enantioselective NHC catalyst

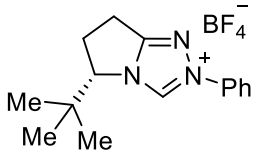

40

Scheme 1.6 Enantioselective benzoin condensation

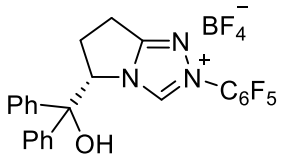

41

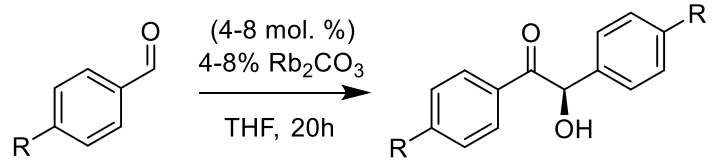

35 R = H
42 R = Cl
43 R = OMe

39 R = H
44 R = Cl
45 R = OMe

Table 1.1 Selected yields and e.e. of Enders' enantioselective benzoin condensation

Product	Yield (%)	e.e. (%)
39	90	>99
44	91	92
45	26	97

Enders et. al. reported an early asymmetric benzoin reaction which found yields of up to 72% and enantiomeric excesses (e.e.s) of up to 86% using catalyst **40**. An improved catalyst **41** was found by this group to give higher yields and e.e.s of up to 99%[28].

The cross-benzoin reaction between different aldehydes still poses significant chemoselectivity challenges, due to poor differentiation between the reactivity of the aldehydes.

Scheme 1.7 Selectivity in the cross-benzoin condensation using two different NHC catalysts

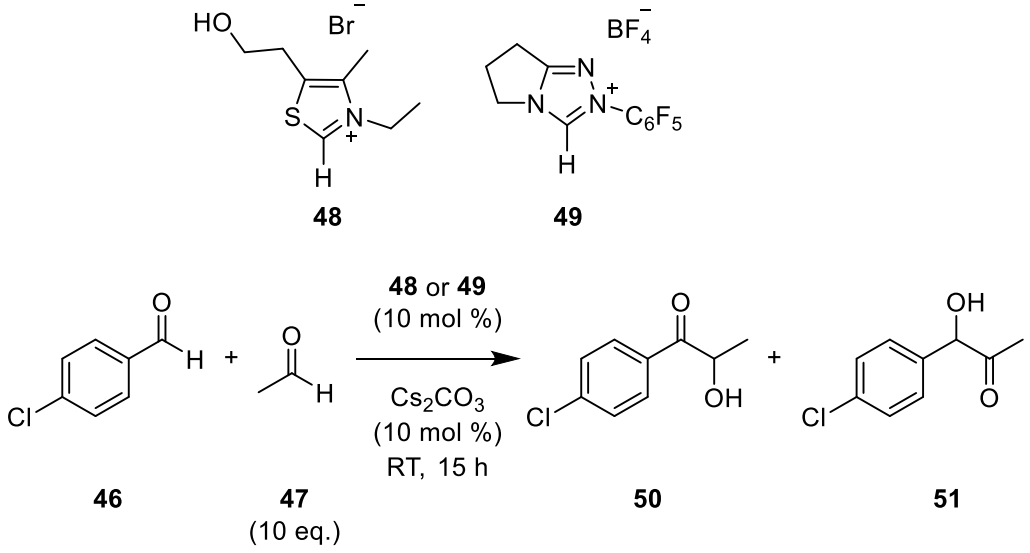

Table 1.2 Product ratios in cross-benzoin condensation

Catalyst	Product Ratio (**50:51**)
48	95:5
49	14:86

One approach to this selectivity problem by Yang et. al.[29] used the different reactivity of thiazolium and triazolium based NHC catalysts. It was found that using thiazolium catalyst **48**, the addition into the aryl aldehyde **46** was preferred, followed by attack on alkyl aldehyde **47**. Triazolium based catalyst **49** showed the opposite selectivity, preferential addition into the alkyl aldehyde, followed by attack on aryl species **46**.

Scheme 1.7 Thiazolium-catalysed cross-benzoin condensation

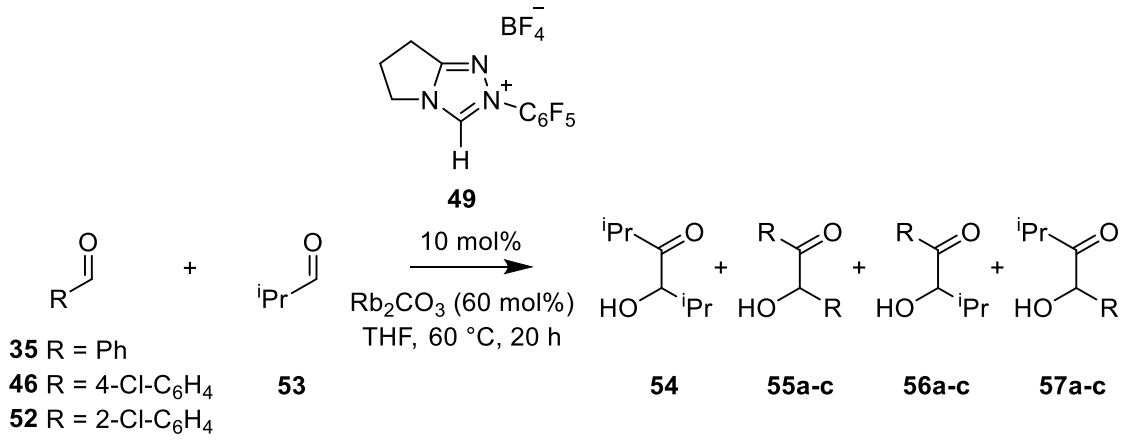

Table 1.3 Yields of cross-benzoin reaction

Aryl Aldehyde	Yield **54** (%)	Yield **55a-c** (%)	Yield **56a-c** (%)	Yield **57a-c** (%)
35	<2	13	<2	61
46	0	7	12	63
52	<2	<2	<2	68

Further experimentation by Zeitler et. al.[30] found using catalyst **49**, high selectivity could be obtained using *ortho* substituted aldehydes such as **52** in the cross-benzoin reaction. It is suggested that the lack of reactivity of 2-substituted aryl aldehyde-NHC adducts is due to steric hindrance. This effect has been used by Glorius et. al.[31] to selectively couple aromatic aldehydes with 2-substituted benzaldehyde derivatives.

The origins of this effect have been investigated by Collett. et. al.[32] It was found that addition to 2-substituted aldehydes by NHCs was significantly favoured, suggesting that this step does not underpin the observed chemoselectivity differences. Instead it was proposed that onward reaction of the Breslow intermediate controls the observed product outcome. One aim of this work is to probe whether this effect is present in BAC organocatalysis (Section 4).

1.2.2 Stetter reaction.

The Stetter reaction involves attack of an acyl anion equivalent on a 1,4-conjugate acceptor such as *trans*-chalcone **46** and was initially identified by Stetter in 1976[33]. This reaction can be somewhat difficult due to the formation of unwanted benzoin side-products, in that further equivalents of aldehyde can be equally reactive towards the acyl anion intermediate as the intended 'Michael-type' acceptor

Scheme 1.8 Enantioselective Stetter reaction

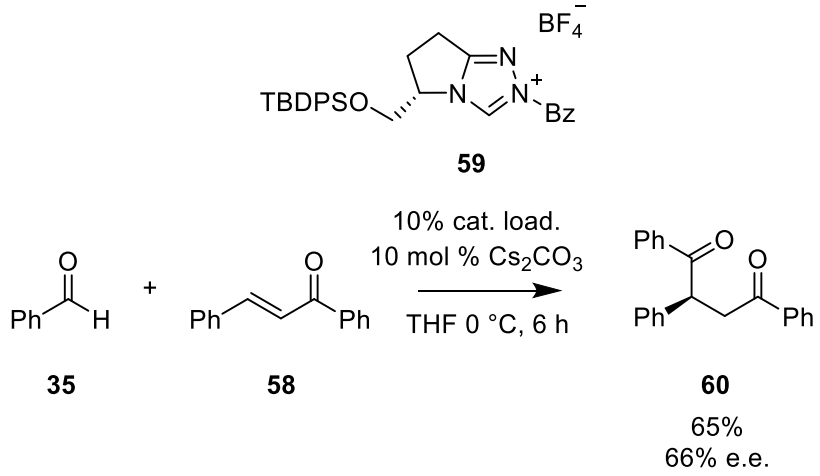

Enders et. al[34] reported the first successful enantioselective intermolecular Stetter reaction using a chiral triazolium catalyst **59** (TBDPSO = ^{t}butyldiphenylsilyl) with reasonable e.e.

Figure 1.13 Proposed silyl Stetter mechanism involving 1,2-brook rearrangement.

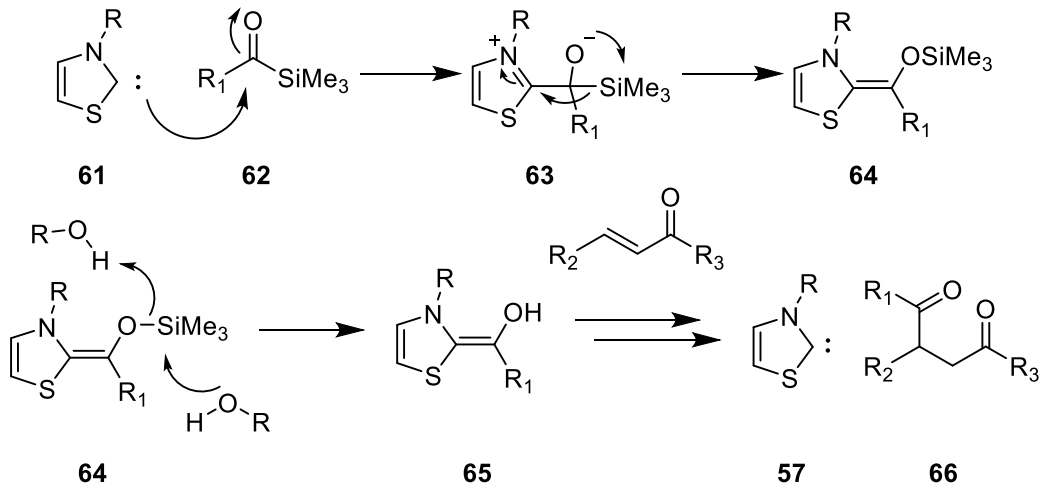

Some groups have approached the problem of unwanted benzoin side-products using acyl silanes **62** in place of aryl aldehydes[35,36]. The sterically congested nature of the trialkylsilyl groups used in these reactions is proposed to prevent the undesired benzoin reactions, in addition to the lower electrophilicity of acyl silanes compared to aldehydes[37]. The acyl anion intermediate **64** is accessed by a 1,2-Brook rearrangement. The silyl group is transferred to the additive alcohol to activate this compound **65**, which completes the Stetter reaction to give **66**.

Another method reported by Gravel et. al.[38] to avoid production of unwanted benzoin products used bis(amino)cyclopropenylidenes in place of conventional NHC. This reaction, and other BAC-catalysed processes are discussed in detail in Section 4.1.

Scheme 1.9 Asymmetric intramolecular Stetter reaction

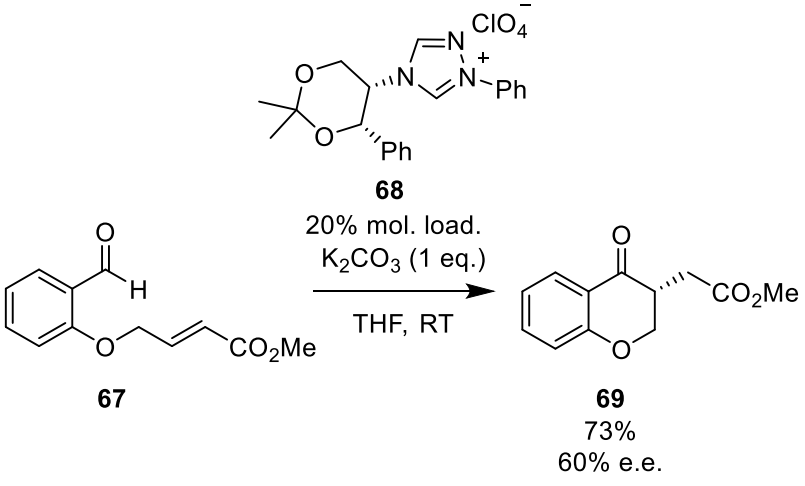

The intramolecular Stetter reaction avoids the chemoselectivity problems associated with the intermolecular Stetter reactions. The first example of an intramolecular Stetter reaction was reported by Ciganek et. al.[39], and the first asymmetric intramolecular Stetter reaction was reported by Enders[34] (Scheme 1.9), using a chiral triazolium catalyst **68**.

Scheme 1.10 Extended Stetter reaction

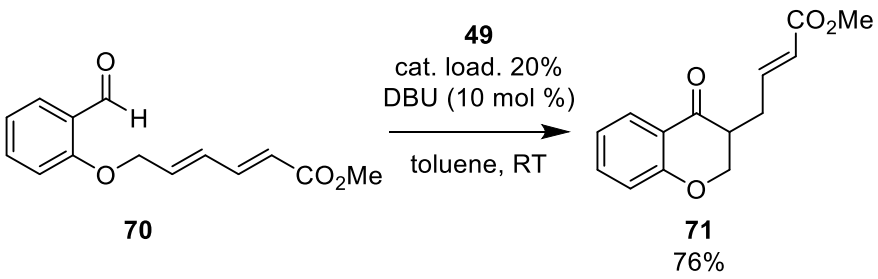

70 **71** 76%

The substrates for the intra- and intermolecular Stetter reaction have been quite varied and versatile, producing an array of products. These include the McErlean et. al. extended Stetter reaction[40], using an α,β,γ,δ-unsaturated ester **70** with a triazolium catalyst **41**.

A wide variety of other organocatalytic processes have utilised NHCs, which are beyond the scope of this thesis. Examples of alternative forms of catalysis by NHCs include enolate and homoenolate processes, transesterification reactions and Lewis base catalysis[27].

An important factor in each of the NHC-catalysed processes is selection of the catalyst. Most procedures favour a triazol-3-ylidene catalyst, and often with a highly electron-withdrawing N-C_6F_5 substituent, whereas occasionally, e.g. in processes involving enals, the *N*-mesityl triazolium salts are preferred. Mechanistic research into benzoin and Stetter reactions using triazolium based catalysts found that *ortho*-substituted (e.g. C_6F_5, 2,4,6-$Cl_3C_6H_2$), N-aryl substituents significantly favoured addition of the carbene to the aldehyde[41]. Research into the potential origins of *ortho*-substituent effects in triazolium salts, and its effects on proton-transfer chemistry are detailed in Section 2.1.

1.3 Radical Chemistry

A free radical is defined as a compound with unpaired valence electrons. Many common inorganic compounds such as molecular oxygen (O_2) and nitrogen monoxide (NO) are stable with unpaired electrons. In contrast, the vast majority of organic radicals are highly unstable, and exist only as intermediates during reaction.

Scheme 1.11 Radical chain bromination of toluene

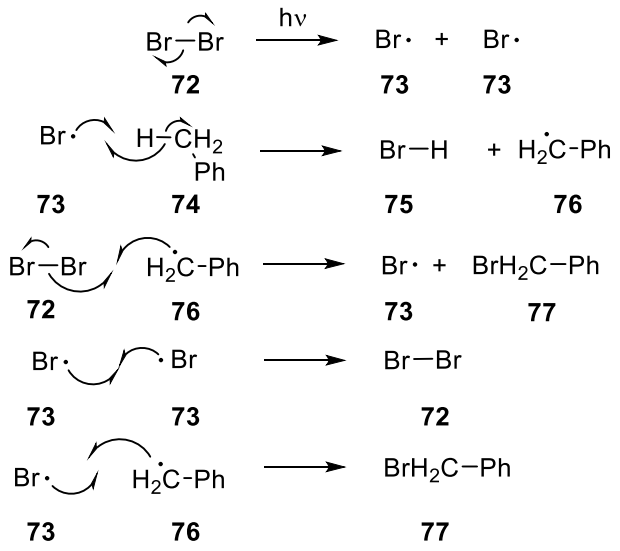

Radical chemistry is a vast and complex area of chemistry, with very wide-ranging applications. Radicals are often generated by the homolysis of a weak bond by heat or light. Common and well-known reactions using radicals include the halogenation of organic compounds, such as toluene **74** (Scheme 1.11), which proceeds *via* a radical chain reaction[24], as well as versatile and often highly selective radical cyclizations.

Although most organic radicals are highly unstable and exist only as reaction intermediates, there are many examples of stable organic radicals. The stabilisation of radicals is broadly centred around two major factors: steric hindrance and electronic stabilization. Steric crowding around the spin-dense areas of the radical can prolong the lifetime of the radicals significantly. Electronic stabilization is often achieved by delocalization of the spin density. Most stable radicals are π-radicals and can be delocalised across the spin system. Electron withdrawing elements also typically stabilize radicals, especially within the π-system, in a similar manner to the stabilization of carbanions. Radicals with the highest stability are typically heteroatom based, in particular when spin-density can be localized on nitrogen, oxygen or sulfur. These electronegative heteroatoms reduce reactivity with molecular oxygen and other oxidizers. Further, the hypothetical σ-dimer of many of these radicals would involve significant unfavourable lone pair interactions, a similar factor to the low bond strength in peroxides and hydrazines.[42]

K. U. Ingold[43] in 1976 defined two broad categories for stable radicals, referring to them as either “stable” or “persistent”. Persistent radicals are radicals which are considered to be

"significantly more stable than a methyl radical" but yet are not stable enough to be isolated under ambient conditions. Stable radicals are defined as radicals, which are stable to moisture, air and dimerization, permitting handling under normal laboratory conditions without particular precautions.

Figure 1.14 Triphenylmethyl radical dimerization

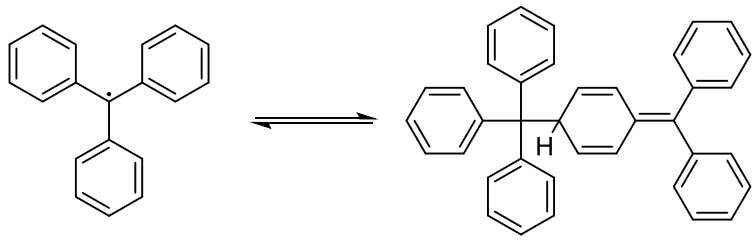

78 **79**

One of the most famous persistent carbon-based radicals is the triphenylmethyl radical 78. This radical exists in equilibrium with its dimer in solution[44], and is stable for several days in the absence of oxygen. The stability of this radical is unusual, compared to other similarly conjugated aromatic radicals, which are transient. This unusual stability is assigned to steric hindrance around the radical centre. This can be demonstrated by the requirement of attack of the radical on the aryl ring of another equivalent to cause dimerization, rather than direct interaction of the radical centres.

Figure 1.15 tris(tri-2,4,6-trichlorophenyl)methyl radical

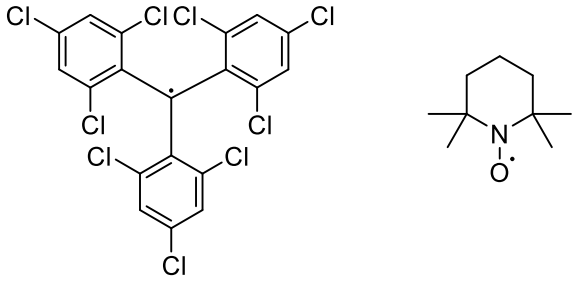

80 **81**

The triphenylmethyl radical can be stabilised further by the addition of chloro substituents to the phenyl ring. The *ortho*-substituents are necessary to stabilise this radical **80**, by crowding at the radical centre[45].

A common family of stable radicals are nitroxide radicals. An example is TEMPO **81**, which can be purchased in its free radical form from suppliers[46], among many other nitroxide radical

species. TEMPO is often used as a catalytic or stoichiometric oxidant in organic chemistry, after first being converted to its N-oxoammonium salt by a harsher oxidant.

Scheme 1.12 Dimerisation and decomposition of diphenylnitroxide

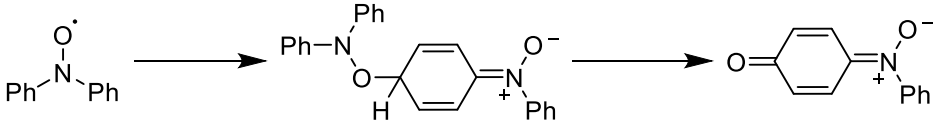

82 **83** **84**

Perhaps counterintuitively, simple aryl substituents, such as diphenylnitroxide **82** on nitroxide radicals cause significant destabilization, by allowing spin-density to delocalize out of the nitroxide system and causing dimerization through the carbon of one with the nitroxide of another.

Figure 1.16 N,N'-diphenyl-N'-picrylhydrazyl

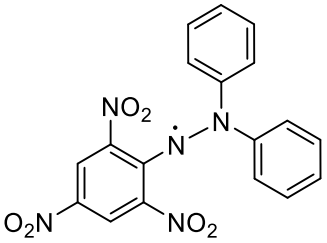

85

Nitrogen-based radicals such as hydrazyl radicals are also common. N,N'-diphenyl-N'-picrylhydrazyl **85** is a well-known stable radical and EPR reference[47]. However, most hydrazyl radicals have significantly less stability than **85**. The conjugated aromatic system and electron withdrawing nitro groups contribute to the high stability of this radical.

Figure 1.17 Verdazyl radical

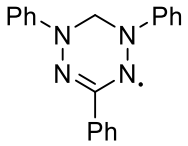

86

Another family of particularly stable radicals are verdazyl systems, of which many unhindered derivatives can be isolated and are stable under atmospheric conditions[48]. Interestingly, spin-

delocalization onto the aromatic ring substituent is prevented by nodal planes in the SOMO (singly occupied molecular orbital)

Figure 1.18 Blatter's Radical

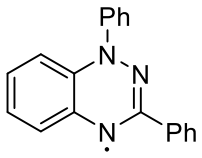

87

The stable radical family of interest to this work is the 1,2,4-benzotriazinyl or Blatter-type radical family[49]. The spin density in this system is largely localized onto the three nitrogen atoms, but is also partially delocalized into the fused aromatic system. Benzotriazinyl radicals are remarkably stable under ambient conditions and are attracting increasing interest in the field of stable radical chemistry.

Benzotriazinyl radicals came to be of relevance to our research group after the serendipitous production of a benzotriazinyl radical from the carbenoid species Nitron by previous student Jacob A. Grant. The chemistry of benzotriazinyl radicals is discussed in detail in Section 5.1

1.3.1 Applications of Stable Radicals.

Stable radicals, although significantly less reactive than other radical species have a wide range of applications, including nitroxide radicals as mediators in radical polymerisation processes[50,51] and the previously mentioned TEMPO oxidation. Other uses of stable radicals include use as radical traps, to terminate ongoing radical chain reactions. Radicals used as radical traps include the previously mentioned picrylhydrazyl **85** or TEMPO **81**. This can be useful as a diagnostic agent – to capture radical intermediates in reactions with unknown mechanisms[52], however, must be used with caution, due to the potential for reactivity of the agent itself modifying the reaction[53]. **85** has also been used as a method to measure the radical-scavenging ability of foodstuffs using spectrophotometric HPLC techniques[54].

Another potential application for stable radicals is as magnetic materials. In a concentrated phase of a paramagnetic substance, the centres of spin are non-dilute, and therefore the unpaired spins on different atoms may couple with each other, in a process termed “magnetic exchange”. Depending on the system in question, this coupling may result in antiferromagnetism or ferromagnetism.

Figure 1.19 Ferromagnetism (left) and Antiferromagnetism (right)

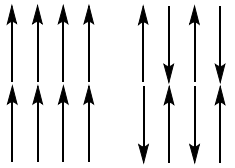

The spins aligning predominantly along one direction in ferromagnetism gives rise to a significant magnetic moment and therefore cause great attraction to magnetic fields. Conversely, in antiferromagnetism the spins align opposite one another and give a very low magnetic moment, resulting in very weak attraction to magnetic fields (lower than simple paramagnetic materials).

Ordered spin systems like antiferromagnetism and ferromagnetism compete with the tendency for random alignment of spins in purely paramagnetic materials. The temperature at which the transition between ordered and disordered systems occurs, is termed the Curie Temperature (T_c) in ferromagnetic and Neel Temperature (T_n) in antiferromagnetic systems. Current attempts at the creation of organic magnetic materials have very low Curie temperatures (< 50 K)[55] in contrast to iron, with a T_c of 1043 K[56].

Another potential application of stable organic radicals is in biological imaging. Using Electron Paramagnetic Resonance (EPR) spectroscopy, the location and concentration of spin-active species can be imaged using 2-dimensional and 3-dimensional techniques. Few applications of this method currently exist, partially due to difficulty in designing the appropriate spin-probes[57]. EPR has the advantage of being more sensitive to low concentrations of probe than NMR based techniques, as well as being useful for three-dimensional mapping of oxygen concentrations *in vivo*, by monitoring the signal broadening of the probe in the presence of high oxygen concentrations[58].

A related application of stable organic radicals is their use as MRI (Magnetic Resonance Imaging) contrast agents. These species have the advantage of avoiding the problems associated with more common gadolinium based systems, namely accumulation in bone, brain and kidney tissue, with associated toxicity[59]. Rajca et. al[60] have reported a successful use of a polymeric nitroxide radical in mice as an MRI contrast agent. Problems with organic radicals in this system include rapid reduction to spin-paired hydroxylamines[61–63] under biological conditions, so this field remains very much in its infancy.

Figure 1.20 Tirapazamine

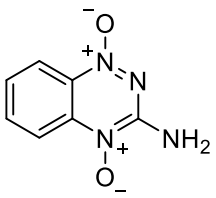

89

A recently developed anticancer agent, Tirapazamine **89**, is administered in an inactive form as a dinitroxide, but is believed to be metabolized *in vivo* to a cytotoxic benzotriazinyl form[64,65]. In particular, it is proposed to become active under hypoxic conditions[66] which is useful for reaction within the hypoxic interior of tumours.

1.4 Summary.

This thesis is split broadly between four major areas of investigations, with the overall common theme of mechanistic investigations in carbene chemistry.

Following from the identification and quantification of unusual *ortho*-substituent effects in N-pentafluorophenyl triazolium based catalysts, further investigations of alternative N-aryl *ortho*-substituents should be explored to shed light on the origins of these effects. Additionally, the presence or absence of similar effects in other NHCs is worthy of investigation.

As the use of BACs is in its infancy, very little mechanistic investigation into either the proton-transfer chemistry or organocatalytic properties have been conducted. Although some limited investigations into proton-transfer[67] have been undertaken, no detailed studies have been presented. Selection of BAC catalyst for example, is largely by trial and error[38,68]. Furthermore, there have been no detailed mechanistic studies of recently identified BAC-organocatalytic transformations.

The novel benzotriazinyl radical prepared by Grant is unique among the benzotriazinyl family in its 3-heteroatom substitution pattern. Additionally, the method of preparation of this type of radical had not yet been optimized, and the mechanism of such an unusual transformation is unknown.

Therefore, the major questions that we wish to address in this thesis are as follows,

1. Does the observed *ortho*-substituent effect in the proton-transfer of triazolium salts continue with the use of other heteroatoms than the C_6F_5 group? Additionally, can this type of substituent effect be found in other groups of N-heterocyclic carbenes?
2. Does the proton-transfer from cyclopropenium salts to form BACs follow an analogous mechanism to those of NHCs, and if so, how do kinetic acidities and pK_as compare to related NHCs?
3. During reactions catalysed by BACs, which intermediates form, can they be isolated and what properties do these isolated intermediates have?
4. What is the mechanism of formation of the benzotriazinyl radical isolated by Grant; what properties do these novel radicals have, and how do they compare to existing examples of benzotriazinyl radicals?

1.5 Bibliography

1 M. Fèvre, J. Pinaud, Y. Gnanou, J. Vignolle and D. Taton, *Chem. Soc. Rev.*, 2013, **42**, 2142–2172.
2 M. Fedoryński, *Chem. Rev.*, 2003, **103**, 1099–1132.
3 A. B. Charette and A. Beauchemin, in *Organic Reactions*, John Wiley & Sons, Inc., 2004.
4 W. W. Schoeller, *J. Chem. Soc., Chem. Commun.*, 1980, 124–125.
5 R. A. Moss, T. Zdrojewski and G.-J. Ho, *J. Chem. Soc., Chem. Commun.*, 1991, 946–947.
6 D. Bourissou, O. Guerret, F. P. Gabbaï and G. Bertrand, *Chem. Rev.*, 2000, **100**, 39–92.
7 H.-W. Wanzlick and E. Schikora, *Angewandte Chemie*, 1960, **72**, 494–494.
8 Wanzlick H. W., *Angew. Chem. Int. Ed.*, 2003, **1**, 75–80.
9 A. Igau, H. Grutzmacher, A. Baceiredo and G. Bertrand, *J. Am. Chem. Soc.*, 1988, **110**, 6463–6466.
10 A. J. Arduengo, R. L. Harlow and M. Kline, *J. Am. Chem. Soc.*, 1991, **113**, 361–363.
11 N. Kuhn and T. Kratz, *Synthesis*, 2002, **1993**, 561–562.
12 D. Enders, K. Breuer, G. Raabe, J. Runsink, J. H. Teles, J.-P. Melder, K. Ebel and S. Brode, *Angew. Chem. Int. Ed. Engl.*, 1995, **34**, 1021–1023.
13 D. Gerbig and P. Schreiner, *Contemporary Carbene Chemistry*, 2013.
14 T. W. Hudnall and C. W. Bielawski, *J. Am. Chem. Soc.*, 2009, **131**, 16039–16041.
15 T. W. Hudnall, E. J. Moorhead, D. G. Gusev and C. W. Bielawski, *J. Org. Chem.*, 2010, **75**, 2763–2766.
16 V. Lavallo, Y. Canac, B. Donnadieu, W. W. Schoeller and G. Bertrand, *Science*, 2006, **312**, 722–724.
17 V. Lavallo, Y. Ishida, B. Donnadieu and G. Bertrand, *Angew Chem Int Ed*, 2006, **45**, 6652–6655.
18 Z. Yoshida and Y. Tawara, *J. Am. Chem. Soc.*, 1971, **93**, 2573–2574.
19 D. Fossé, J. Cernicharo, M. Gerin and P. Cox, *ApJ*, 2001, **552**, 168.
20 H. P. Reisenauer, G. Maier, A. Riemann and R. W. Hoffmann, *Angew. Chem. Int. Ed.*, 1984, **23**, 641–641.
21 K. Hirai, T. Itoh and H. Tomioka, *Chem. Rev.*, 2009, **109**, 3275–3332.
22 E. Iwamoto, K. Hirai and H. Tomioka, *J. Am. Chem. Soc.*, 2003, **125**, 14664–14665.
23 R. Breslow, *J. Am. Chem. Soc.*, 1958, **80**, 3719–3726.
24 J. Clayden, N. Greeves and S. Warren, *Organic Chemistry*, Oxford University Press, Oxford, New York, Second Edition., 2012.
25 D. Seebach and E. J. Corey, *J. Org. Chem.*, 1975, **40**, 231–237.
26 Fudo Ukai, Ryuzo Tanaka and Shun Doukawa, *YAKUGAKU ZASSHI*, 1943, **63**, 296–300.
27 D. M. Flanigan, F. Romanov-Michailidis, N. A. White and T. Rovis, *Chem. Rev.*, 2015, **115**, 9307–9387.
28 L. Baragwanath, C. A. Rose, K. Zeitler and S. J. Connon, *J. Org. Chem.*, 2009, **74**, 9214–9217.
29 M. Y. Jin, S. M. Kim, H. Han, D. H. Ryu and J. W. Yang, *Org. Lett.*, 2011, **13**, 880–883.
30 S. E. O'Toole, C. A. Rose, S. Gundala, K. Zeitler and S. J. Connon, *J. Org. Chem.*, 2011, **76**, 347–357.

31 I. Piel, M. D. Pawelczyk, K. Hirano, R. Fröhlich and F. Glorius, *Eur. J. Org. Chem.*, 2011, **2011**, 5475–5484.
32 C. J. Collett, R. S. Massey, J. E. Taylor, O. R. Maguire, A. C. O'Donoghue and A. D. Smith, *Angew. Chem.*, 2015, **127**, 6991–6996.
33 H. Stetter, *Angew. Chem. Int. Ed.*, 1976, **15**, 639–647.
34 D. Enders, K. Breuer, J. Runsink and J. H. Teles, *HCA*, 1996, **79**, 1899–1902.
35 A. E. Mattson, A. R. Bharadwaj and K. A. Scheidt, *J. Am. Chem. Soc.*, 2004, **126**, 2314–2315.
36 A. R. Bharadwaj and K. A. Scheidt, *Org. Lett.*, 2004, **6**, 2465–2468.
37 E. M. Phillips, A. Chan and K. A. Scheidt, *Aldrichimica Acta*, 2009, **42**, 55–66.
38 M. M. D. Wilde and M. Gravel, *Angew. Chem. Int. Ed.*, 2013, **52**, 12651–12654.
39 E. Ciganek, *Synthesis*, 2000, **1995**, 1311–1314.
40 K. R. Law and C. S. P. McErlean, *Chem. Eur. J.*, 2013, **19**, 15852–15855.
41 C. J. Collett, R. S. Massey, O. R. Maguire, A. S. Batsanov, A. C. O'Donoghue and A. D. Smith, *Chem. Sci.*, 2013, **4**, 1514–1522.
42 R. G. Hicks, *Org. Biomol. Chem.*, 2006, **5**, 1321–1338.
43 D. Griller and K. U. Ingold, *Acc. Chem. Res.*, 1976, **9**, 13–19.
44 H. Lankamp, W. T. Nauta and C. MacLean, *Tetrahedron Letters*, 1968, **9**, 249–254.
45 O. Armet, J. Veciana, C. Rovira, J. Riera, J. Castaner, E. Molins, J. Rius, C. Miravitlles, S. Olivella and J. Brichfeus, *J. Phys. Chem.*, 1987, **91**, 5608–5616.
46 TEMPO 214000, https://www.sigmaaldrich.com/catalog/product/aldrich/214000, (accessed 15 March 2018).
47 N. D. Yordanov and A. Christova, *Appl. Magn. Reson.*, 1994, **6**, 341–345.
48 R. Kuhn and H. Trischmann, *Angew. Chem. Int. Ed. Engl.*, 1963, **2**, 155–155.
49 H. M. Blatter and H. Lukaszewski, *Tetrahedron Lett.*, 1968, **9**, 2701–2705.
50 T. Fukuda, T. Terauchi, A. Goto, K. Ohno, Y. Tsujii, T. Miyamoto, S. Kobatake and B. Yamada, *Macromolecules*, 1996, **29**, 6393–6398.
51 G. Moad and E. Rizzardo, in *Nitroxide Mediated Polymerization*, 2015, pp. 1–44.
52 R. Ciriminna and M. Pagliaro, *Org. Process Res. Dev.*, 2010, **14**, 245–251.
53 A. C. Albéniz, P. Espinet, R. López-Fernández and A. Sen, *J. Am. Chem. Soc.*, 2002, **124**, 11278–11279.
54 T. Yamaguchi, H. Takamura, T. Matoba and J. Terao, *Bioscience, Biotechnology, and Biochemistry*, 1998, **62**, 1201–1204.
55 J. S. Miller, *Materials Today*, 2014, **17**, 224–235.
56 H. Hall, H.E J. R., *Solid State Physics*, Wiley & Sons Ltd., Chichester, 2nd edn., 1991.
57 T. Masumizu, K. Fujii, M. Kohno, S. Nagai, Y. Odagaki, M. Imanari, A. Mori and L. Packer, *IUBMB Life*, 1998, **46**, 707–717.
58 R. Halevy, L. Shtirberg, M. Shklyar and A. Blank, *J Vis Exp*, DOI:10.3791/2122.
59 M. Rogosnitzky and S. Branch, *Biometals*, 2016, **29**, 365–376.
60 A. Rajca, Y. Wang, M. Boska, J. T. Paletta, A. Olankitwanit, M. A. Swanson, D. G. Mitchell, S. S. Eaton, G. R. Eaton and S. Rajca, *J. Am. Chem. Soc.*, 2012, **134**, 15724–15727.
61 J. F. Keana and F. L. Van Nice, *Physiol Chem Phys Med NMR*, 1984, **16**, 477–480.

62 N. Kocherginsky and H. M. Swartz, *Nitroxide Spin Labels: Reactions in Biology and Chemistry*, CRC Press, Boca Raton, Fla, 1 edition., 1995.
63 A. A. Bobko, I. A. Kirilyuk, I. A. Grigor'ev, J. L. Zweier and V. V. Khramtsov, *Free Radic Biol Med*, 2007, **42**, 404–412.
64 S. B. Reddy and S. K. Williamson, *Expert Opinion on Investigational Drugs*, 2009, **18**, 77–87.
65 J. W. Evans, K. Yudoh, Y. M. Delahoussaye and J. M. Brown, *Cancer Res*, 1998, **58**, 2098–2101.
66 B. Muz, P. D. L. Puente, M. J. Luderer, F. Ordikhani and A. K. Azab, *Blood*, 2015, **126**, 4436–4436.
67 R. Weiss and C. Priesner, *Angew. Chem. Int. Ed. Engl.*, 1978, **17**, 445–446.
68 X. Lu and U. Schneider, *Chem. Commun.*, 2016, **52**, 12980–12983.

Chapter 2 – Substituent Effects in the Proton-Transfer Chemistry of N-Heterocyclic Carbenes.

2.0 Foreword

This chapter consists of our research on substituent effects on the proton-transfer chemistry of NHCs. Section 2.1 is a short review of current and relevant literature. The results of our work are presented in Section 2.2.1 for two N-aryl *ortho*-halogen substituted triazolium salts and Section 2.2.2 for two imidazolium derived salts with exocyclic nitrogen substituents. The results and their implications are discussed in Section 2.3 and Section 2.4 is a summary of this chapter.

2.1 Introduction

N-Heterocyclic Carbenes (NHCs) are the widest and most applied group of stable carbenes. NHCs have a very wide range of applications, from their use as ligands in organometallic chemistry to direct use as organocatalysts. As previously discussed in Chapter 1, NHCs are typically generated *in situ* from the deprotonation of their respective conjugate acids. The proton-transfer chemistry of the conjugate acids of NHCs is therefore of great interest in the field of physical organic chemistry and directly influences the activities of these compounds in organocatalysis.

The relative carbon acidities of the conjugate acids of NHCs can be compared by analysis of their pK_a values in water. The concentration of the carbene conjugate base in aqueous solution, however, is always far too low to allow the pK_a to be directly measured from equilibrium concentrations, and, may alternatively be measured by a kinetic acidity method.

2.1.1 Proton-transfer chemistry of NHCs

The proton-transfer chemistry of NHCs can be probed by H/D exchange experiments in deuterium oxide. After deprotonation of the hydrogen containing starting material, the free carbene will be rapidly deuterated by a molecule of D_2O. Owing to the large excess of D_2O relative to HOD and H_2O in solution, the process is considered irreversible. Therefore, the rate of disappearance of the peak in the ^{1}H NMR spectrum corresponding to the removed proton allows the determination of the pseudo first-order rate constant of exchange, k_{ex} (s^{-1}). A second-order rate constant of deuteroxide catalysed H/D exchange, k_{DO} (M^{-1} s^{-1}), can then be determined from a plot of k_{ex} against [DO^-] assuming a simple first order dependence on the concentration of deuteroxide ion. The value of k_{DO} provides an estimate of the kinetic acidity. Using Equation 2.1, where k_{HO} is the second-order rate constant of hydroxide catalysed deprotonation (k_{DO}/k_{HO} = 2.4), k_{HOH} is the rate constant of reprotonation of carbene by solvent

water (~10^{11} s^{-1})[1], the experimental values of k_{DO} can be converted into an estimate of pK_a for the NHC in question. This is further discussed in section 2.3

Scheme 2.1 Acid dissociation of a generic NHC

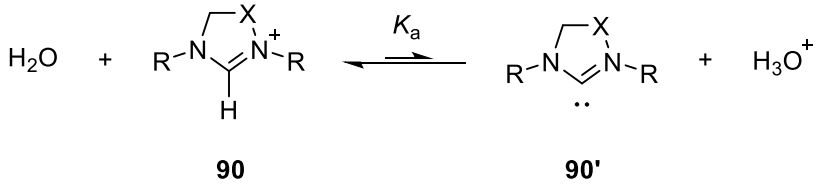

90 **90'**

Equation 2.1* pK_a *from kinetic acidity

$$\mathrm{p}K_a = \mathrm{p}K_w + \log\left(\frac{k_{\mathrm{HOH}}}{k_{\mathrm{HO}}}\right)$$

Scheme 2.2 H/D exchange of thiamine

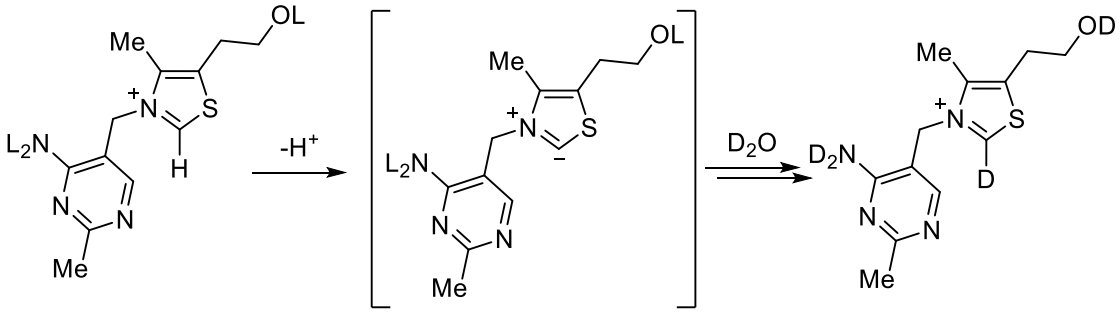

91 **91'** **92**

L = H or D

The earliest report of H/D exchange via an NHC intermediate was in 1957 by Breslow[2] on thiamine **91** (vitamin B1), the chemistry of which was previously discussed (Chapter 1). Breslow discovered that in solutions of neutral D_2O, thiamine underwent a rapid H/D exchange. The original mechanism of exchange assigned by Breslow involved the formation of ylidic intermediate **91'** to give exchange product **92**.

Scheme 2.3 Resonance forms of 2'

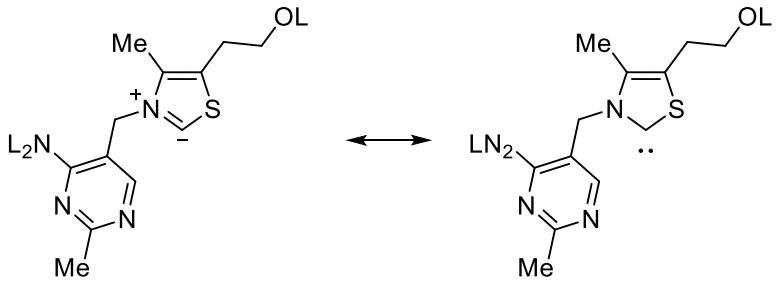

91' **91"**

Ylide **91'** is a resonance form of thiazolylidene **91''**, and shows similar reactivity to other NHCs, for example in organocatalysis.

The first quantitative study of H/D exchange *via* a NHC was in 1964[3], on imidazolium salt **4**. It was found that H/D exchange took place with a first order rate constant of $k_{ex} = 2.6 \times 10^{-3}$ s^{-1}at p*D* 8.92 (borate buffer) at 31 °C. A further study[4] quantitatively determined that the rate constant of exchange for thiazolium salts was 3000-fold faster than the imidazolium analogues

Figure 2.1 Imidazolium salts studied by Amyes et. al.

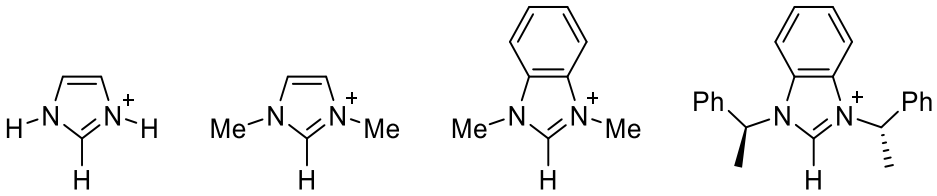

93 **94** **95** **96**

Table 2.1 Results of Amyes et. al. H/D exchange experiments.

Imidazolium Salt	k_{DO} (M^{-1} s^{-1})	k_{HO} (M^{-1} s^{-1})	pK_a
93	36.9	15.4	23.8
94	247	103	23.0
95	5.74×10^3	2.39×10^3	21.6
96	1.48×10^4	6.17×10^3	21.2

In 2004, Amyes et. al.[5] reported a more detailed study into the proton-transfer chemistry of a series of simple N,N-dialkylimidazolium cations. The imidazolium salts were dissolved in D_2O buffers at p*D* 4.33-8.88 and the proton-transfer was studied by ^1H NMR spectroscopy, monitoring the decrease of the signal of the C(2) proton to determine the pseudo first-order rate

constant (k_{ex}). Using this data, estimates of the pK_a of the C2 position were obtained (Equation 2.1).

The variation of pK_as (2.6) was relatively small across the range of imidazolium salts **93-96**. Substituent effects were also studied by Amyes on a further series of NHC structures with different ring systems.

Figure 2.2 Imidazolium, thiazolium and oxazolium salts studied by Amyes et. al.

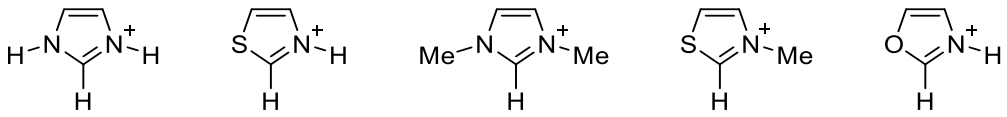

93 **97** **94** **98** **99**

Table 2.2 Results of Amyes et. al. H/D exchange experiments on salts 8-12.

NHC Conjugate Acid	k_{HO} (M^{-1} s^{-1})	pK_a
93	15.4	23.8
97	1.3×10^5	19.9
94	103	23.0
98	3.4×10^5	19.5
99	3.0×10^7	16.9

The difference in pK_a is significantly higher between NHC classes than within the imidazolium family. The thiazolium salts **97** and **98** were found to have significantly lower pK_a (3.5-3.9 pK_a units) than their imidazolium equivalents **93** and **94**. Oxazolium salt **99** had an even larger gap of 6.1 in its pK_a relative to **94**. It is important to note that in these cases, and in others, that the lower pK_a of the thiazolium salt does not indicate that the thiazolylidene carbenes are more stable than the imidazolylidene carbenes. Calculations by Amyes[5] have indicated that imidazolylidenes are actually slightly more stable than thiazolylidenes, but the conjugate acid imidazolium is significantly more stable than the thiazolium salt. In other words, the pK_a is a measure of the relative stability of the conjugate acid and carbene in water, and not an overall measure of absolute carbene stability, although often a lower pK_a does correspond to a more stable carbene state.

Further research into the proton-transfer chemistry was performed by Higgins et al[6]. on a large series of imidazolium, 4,5-dihydroimidazolium and tetrahydropyrimidinium salts.

Figure 2.3 Imidazolium, 4,5-imidazolinium and tetrahydropyrimidinium salts studied by Higgins et. al.

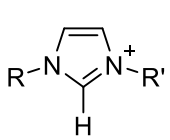

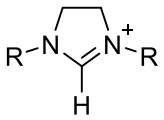

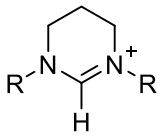

100a R = R' = 4-Chlorophenyl
100b R = R' = 4-Methoxyphenyl
100c R = R' = 2,4,6-Trimethylphenyl
100d R = Et, R' = Me
100e R = Bu, R' = Me

101a R = 4-Methoxyphenyl
101b R = 2,4,6-Trimethylphenyl

102a R = Et
102b R = ^{i}Pr

Table 2.3 Effect of ring size and saturation on NHC proton-transfer.

NHC Conjugate Acid	k_{HO} (M^{-1} s^{-1})	pK_a
100a	3.92×10^{5}	19.8
100b	4.80×10^{4}	20.7
100c	4.08×10^{4}	20.8
100d	2.29×10^{2}	23.0
100e	1.07×10^{2}	23.3
101a	4.26×10^{4}	20.7
101b	1.19×10^{4}	21.3
102a	3.48×10^{-3}	27.8
102b	1.48×10^{-3}	28.2

Varying the N-aryl substituents of **100a-c** had a small effect on the pK_a (< 1 units). Changing from N-aryl to N-alkyl, in **100d-e** resulted in a larger increase of up to 3 pK_a units. Imidazolinium salts **101a-b**, the 4,5-dihydro analogues of **100b-c**, have closely similar pK_a values, showing the double bond has a small effect on the pK_a of this system. **102a-b** show a dramatic increase in pK_a by up to 5.2 units above that of the N,N-dialkyl imidazolium salts. It was suggested that the 6-membered ring disfavours formation of a carbene owing to a requirement for a higher N-C-N bond angle at the carbene centre. More acute N-C-N bond angles at the NHC centre preferentially stabilise the singlet configuration, and as such stabilise the carbene state relative to the conjugate acid, lowering pK_a.

Scheme 2.4 Acyclic nitrogen carbene.

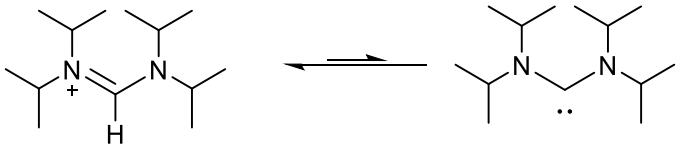

103 **103'**

Deprotonation to acyclic nitrogen carbenes from non-cyclic azolium salt precursors was found to be significantly less favoured than observed for the NHC analogues. In the example studied by Higgins, (6) it was found that H/D exchange for **103** was very slow and outcompeted by hydrolysis, thus only a lower limit estimate, pK_a > 29, could be established.

The pK_a range of a series of imidazolium salts have also been determined by a titration method in DMSO. Chu et al.[7] titrated 12 imidazolium salts in a solution of DMSO using a bracketing indicator method by UV-Visible spectrophotometry. The pK_a range was determined to be 19.5-23.4. To compare with results by kinetic acidity in D_2O, compound **94** studied by Amyes[5] and Chu[7] was found to have a pK_a of 23.0 in H_2O and 22 in DMSO. The lower pK_a in DMSO was assigned to the loss of stabilising effects on the cationic conjugate acid from water.

Using the same bracketing indicator method, Harper et. al.[8] used titration to determine the pK_a of 25 imidazolium salts. The range of pK_a was found to be 18-23.8. The measured pK_a values in DMSO of the studied imidazolium ions had a good correlation with the Hammett σ values of the N-aryl substituents, with a slope of −1.25, indicating that the substituent effect on the pK_a of imidazolium salts in DMSO is greater than in the acid dissociation of substituted benzoic acids. It was also noted that variation of the counter anion did not change the pK_a of the cations.

2.1.2 Triazol-3-ylidenes and *ortho* substituent effects

The triazolium ion conjugate acids of triazol-3-ylidenes were found to be among the most acidic families of the NHCs[9], even more acidic than the thiazolylidenes, due to the presence of three nitrogen atoms in the ring. It was also observed that the N-substituents have a comparatively small effect on the carbon acidity of the triazolium salts in agreement with previous studies of imidazolium and thiazolium salts. Triazolium salts are of particular interest due to their comparatively high catalytic ability, and the high enantioselectivity associated with certain asymmetric triazolium catalysts[10].

Figure 2.4 and Table 2.4 show data acquired by R. Massey[9] et al. in their study on the proton-transfer chemistry of 1,2,4-triazolium salts.

***Figure 2.4 Plot of* $\log_{10} k_{ex}$ *against* p*D for triazolium salts, 49* (◆), *104*(●), *105*(■), *106* (▲), *107* (▼), *108* (■)**

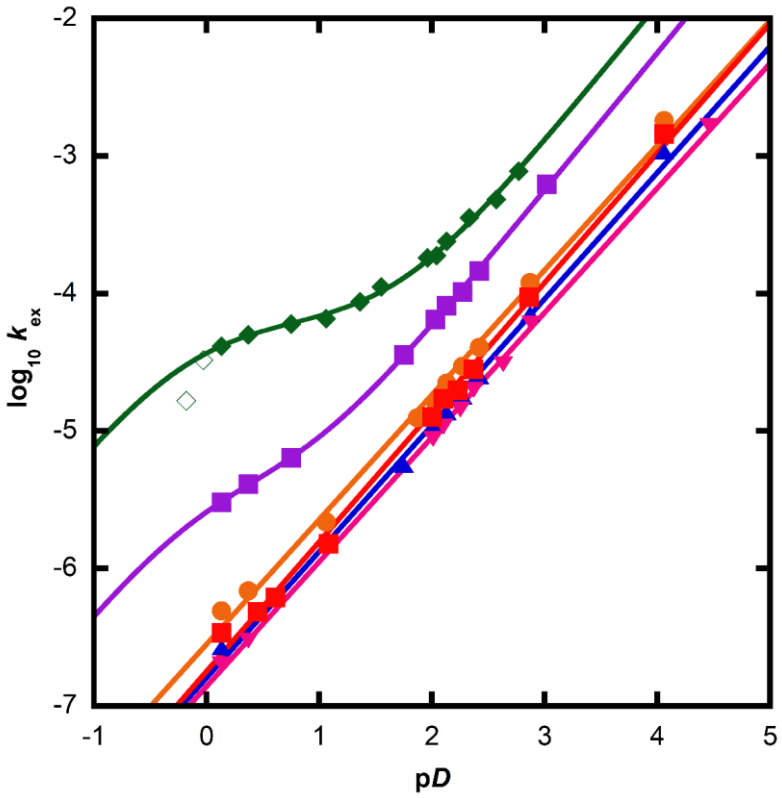

49, 104-108

Table 2.4 Triazolium* k_{DO} *and* pK_a *values.

Triazolium	R =	k_{DO} (M^{-1} s^{-1})	pK_a
49[a]	C_6F_5	6.82×10^{8}	16.5
104	4-FC_6H_4	8.66×10^{7}	17.4
105	Ph	6.82×10^{7}	17.5
106	Mesityl	5.29×10^{7}	17.7
107	4-$MeOC_6H_4$	4.20×10^{7}	17.8
108	4-CNC_6H_4	3.18×10^{8}	16.9

[a]The points at pD < 0 have I > 1.0 M are marked with unfilled markers, and are not accounted for in the fit.

Four of the triazolium salts studied show the usual NHC behaviour of a linear log k_{ex} dependence on pD for the entire range of tested pDs with a slope of unity consistent with a

simple first order dependence on the concentration of deuteroxide ion. Two (**49** and **108**) deviated upwards from the unity slope at low p*D*s, which suggests a change in the predominant mechanism of H/D exchange. The rate constant again appeared to decrease at the very lowest p*D*s studied. This unexpected increase in rate constant at low p*D* is suggested to be as a result of one of two kinetically indistinguishable mechanisms (Figure 2.5). This behaviour was particularly pronounced in the case of pentafluorophenyl triazolium salt **49.**

Figure 2.5 Suggested mechanistic pathways of H/D exchange

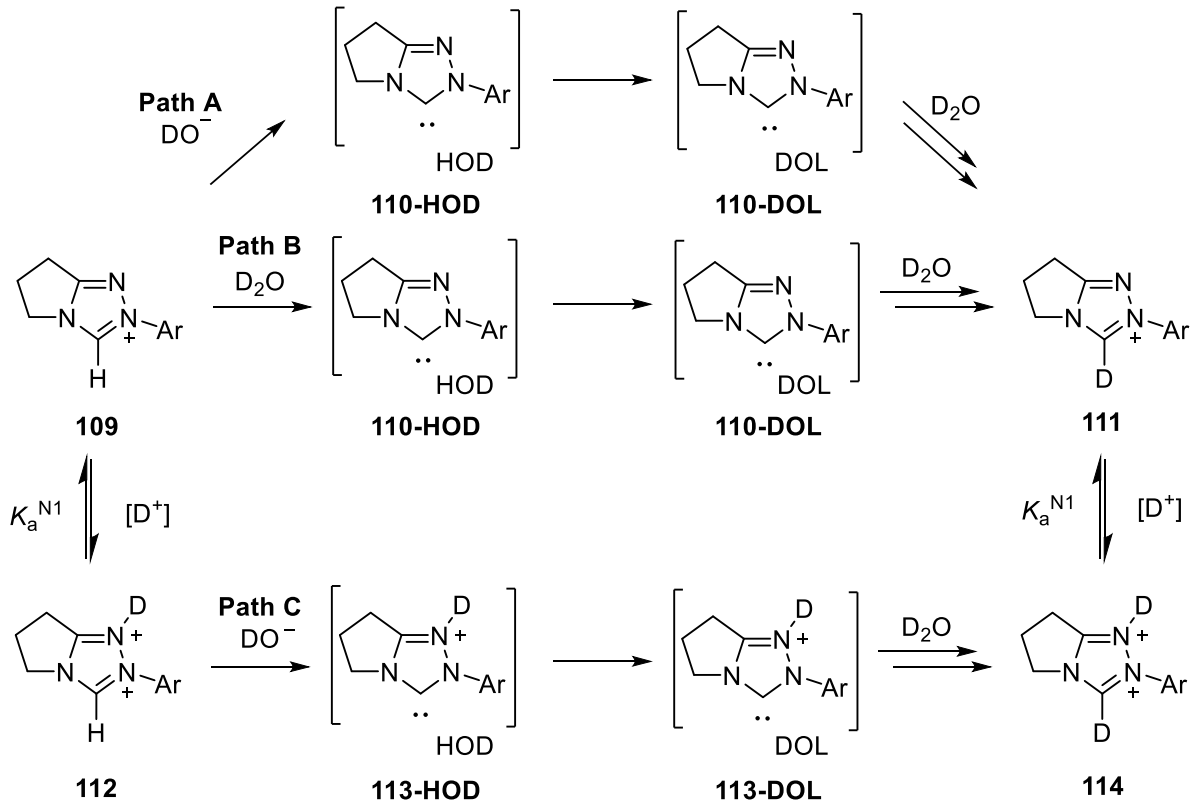

Path A is the normal pathway for H/D exchange. Path B involves initial deprotonation of the substrate by neutral D_2O rather than deuteroxide, which after solvent reorganisation and redeuteration yields the deuterated product **111**. Path C involves the initial protonation/deuteration at the N1 position to form a dicationic intermediate **112** which is subsequently deprotonated on the C3 position by deuteroxide to form a monocationic carbene **113** which is deuterated by D_2O after solvent reorganisation to give **114**. Both pathways could account kinetically for an upward deviation in the slope of the p*D*-log k_{ex} plot as p*D* is decreased and the subsequent downward trend at lower p*D*s, as shown particularly by pentafluoro salt **49**.

To explain the origin of this change in mechanism, it was suggested that the presence of the *ortho*-heteroatom on the aryl ring, e.g. fluorine, could potentially favour protonation (deuteration) at N1 by a through-space interaction, which would result in particular prevalence of this altered behaviour for **49** in the accessible p*D* range, by raising of the pK_a of the N1 position. This increase in N1 pK_a could be as a result of suppression of an unfavourable nitrogen-fluorine electrostatic interaction, or as a result of a stabilizing effect of N^+-H…F interactions in the protonated state.

Scheme 2.5 Condensed triazolium-catalysed mechanism of benzoin condensation

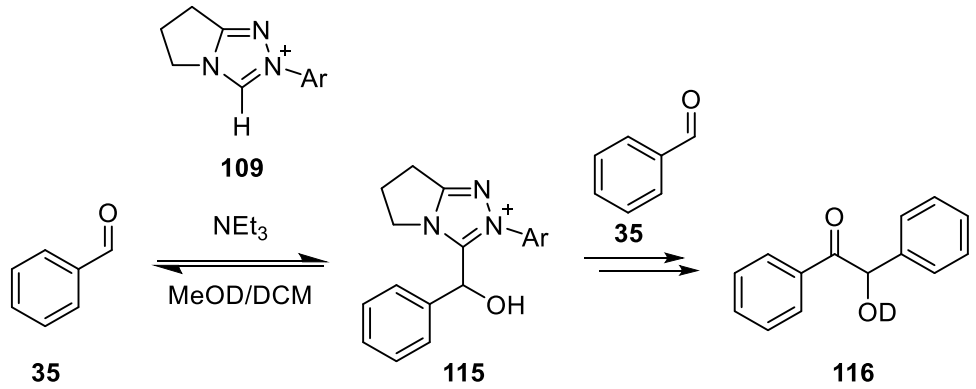

This effect is of general interest as many previous synthetic studies have noted that a variation of the triazolium N-aryl substituent can have dramatic effects on the yields and selectivities of triazolylidene catalysed reaction, unlike the relatively small observed effects on pK_a. Triazolylidene catalysed benzoin and Stetter reactions have been previously found to have unexpected *ortho*-heteroatom substituent effects related to the common first step of both reactions, involving a hydroxy-aryl-triazolium intermediate species (Scheme 2.5). N-Aryl *ortho*-heteroatoms on triazolium rings have been observed to significantly increase the rate and equilibrium constants for the formation of the adducts[11], compared to their *para*-substituted or *ortho*-alkyl equivalents. A possible explanation for this effect is the presence of an O-D…X interaction in the intermediate stage, similar to the proposed N^+-H…F effect proposed for **49**.

2.1.3 Recent developments

As stated in the Foreword (Section 1), part of Chapter 2 has been published previously in the Journal of Physical Organic Chemistry[12]. Part of this work, contributed by P. Quinn and R. Massey, included a study on the proton-transfer chemistry of two other triazolium salts with pyridyl **117** and pyrimidyl **118** substituents. My contribution was the study of the proton-

transfer chemistry of two triazolium salts, **120** and **121**, which had been previously prepared by C. Bramley, of our research group.

Figure 2.6 Pyridyl and pyrimidyl substituted triazolium salts

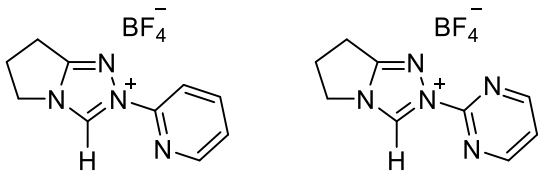

117 **118**

The objective of this study was to determine whether pyridyl and pyrimidyl *ortho*-nitrogen substituents would have similar effects to *ortho*-fluorines in the H/D exchange of the C3 proton of other triazolium salts. The results of these experiments are summarised in Figure 2.7.

Figure 2.7 Comparison of* $\log_{10} k_{ex}$ *against* p*D for triazolium salts 49* (◆)*, 118* (▼)*, 117* (▲)*, and 108* (●)*at 25 C and I = 1.0 M.

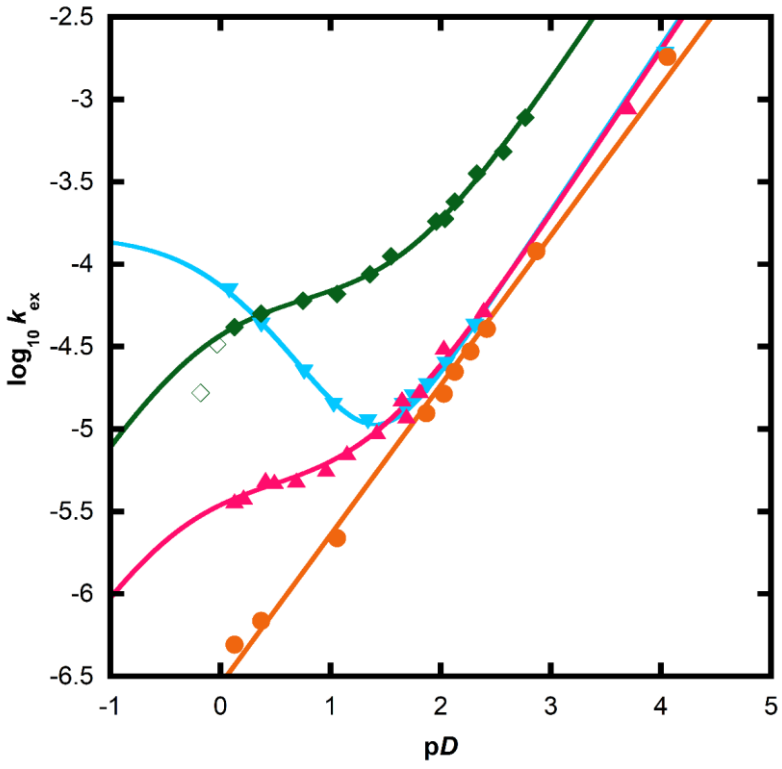

Pyrimidyl substituted triazolium salt **118** showed similar behaviour to pentafluorophenyl analogue **49**[9], in an upwards deviation from unity slope at low p*D*, suggesting a similar mechanism for H/D exchange. The pyridyl substituted triazolium salt **117** however showed very different behaviour, deviating significantly *upwards* with a slope of –1 consistent with

formal acid-catalysis of H/D exchange. This acid-catalysed process has not been observed for any other known NHC.

Scheme 2.6 Proposed mechanism of acid-catalysed H/D exchange of 117

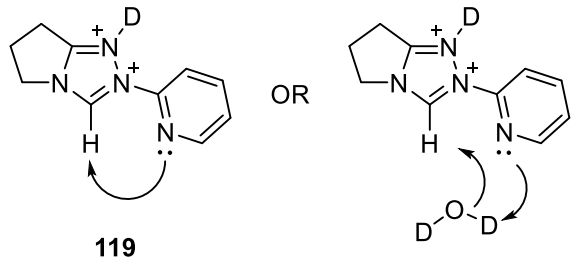

119

Several mechanisms were proposed for the acid-catalysed H/D exchange of **117**, however the most likely is shown in Scheme 2.6. The mechanism involves a protonation of the N1 position on the triazolium ring to give protonated triazolium **119**, followed by either intramolecular proton transfer to the pyridyl nitrogen, or a proton-transfer via a molecule of D_2O. This mechanism would explain the lack of acid-catalysis in the other studied NHCs. Pyrimidine substituted triazolium **118** is less likely to undergo this mechanism because of the significantly reduced basicity of free pyrimidine ($pK_a = 1.3$), compared to pyridine ($pK_a = 5.2$)[4], suggesting the group will be less basic.

2.2 Results

Figure 2.8 Ortho substituted N-aryl triazolium salts.

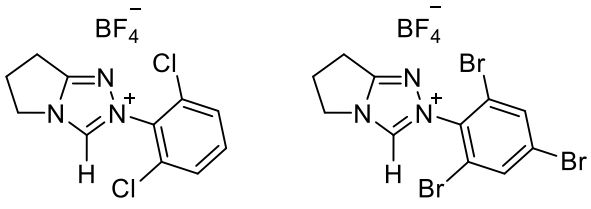

120 **121**

In order to further probe the origin of the *ortho* substituent effects discussed in section 2.1.2, it was decided to study the proton-transfer chemistry of two further triazolium salts **120** and **121.** These triazolium salts were prepared by a previous fourth year undergraduate MChem student Christopher Bramley. The proton-transfer chemistry of **120** and **121** is further explored in section 2.2.1.

Figure 2.9 Two studied furoimidazolium salts.

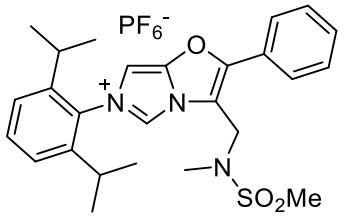

122

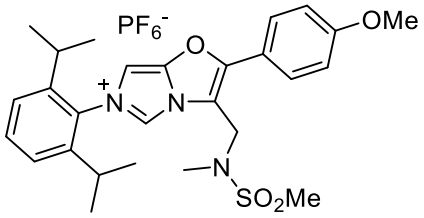

123

Two imidazolium salts with sterically rigid backbones were prepared by Dr. Paul Davies of the University of Birmingham.

These salts were partly of interest because of the fused bicyclic imidazolium motif, which had not been studied previously by the group. In addition, the pendant sulfonamide group has the potential to act as an intramolecular general base akin to proton-transfer behaviour for N-pyridyl triazolium salt **117**.

The proton-transfer chemistry of **120**-**123** is explored in sections 2.2.1 and 2.2.2.

2.2.1 Proton-transfer chemistry of triazolium salts 120 and 121

Scheme 2.7 H/D exchange of triazolium salt

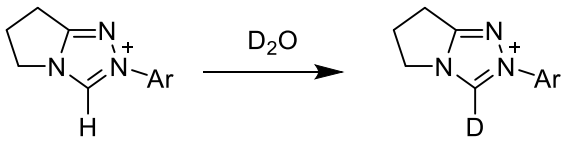

109 **111**

Deuterium exchange experiments were carried out in D_2O solutions of either dilute DCl or acetate buffer in the range of 0-3.65 p*D* at 25 °C and I = 1.0 M (KCl), with an internal standard of tetramethylammonium deuteriosulfate (~1 mM).

The progress of the deuterium exchange was followed by the decrease of the area of the singlet signal at ~10 ppm, corresponding to the C(3) proton of the triazolium salts. All peaks were integrated relative to the internal standard peak at ~3 ppm, corresponding to the twelve methyl protons of NMe_4 DSO_4, which are known to be non-exchanging under these conditions.

Equation 2.2

$$f(s) = \frac{\left(A_{\mathrm{C(3)H}}/A_{\mathrm{std}}\right)_{\mathrm{t}}}{\left(A_{\mathrm{C(3)H}}/A_{\mathrm{std}}\right)_{\mathrm{t0}}}$$

The fraction of protonated substrate remaining was determined using Equation 2.2. Pseudo-first order rate constants for exchange, k_{ex} (s^{-1}), were determined from plots of f(s) against time, using non-linear least square fitting of f(s) against time to a first-order exponential decay.

Equation 2.3

$$f(\mathrm{s}) = \mathrm{e}^{-k\mathrm{t}}$$

From the data obtained in these experiments second-order rate constants for deuteroxide catalysed exchange, k_{DO} (M^{-1} s^{-1}), could be determined. From analysis of the rate constants, an estimate of pK_a could be determined.

Representative spectra taken at three time points during the reaction of dichlorophenyl salt **120** at pD 0.53 (0.5 M DCl) are shown in Figure 2.10. Disappearance of the singlet at 9.6 ppm over time is assigned to hydrogen-deuterium exchange of the C(3)-H atom. Other signals corresponding to cyclic methylene protons are present at 4.1, 2.9 and 2.5 ppm, and aryl protons at 7.3 ppm. No change was observed in the integrated areas of these other peaks, relative to the internal standard, which indicates that neither H/D exchange nor other chemical reactions occurred in any significant amount under these conditions.

Figure 2.10 Representative ^{1}H NMR spectra at 400 MHz of triazolium salt 120 (5 mM,* p*D 0.53), obtained during exchange of the C3-H (s, 9.7ppm) for deuterium in D_2O at 25 °C and I = 1.0 (KCl). [Internal standard, tetramethylammonium deuteriosulfate (s, 3.17 ppm)]

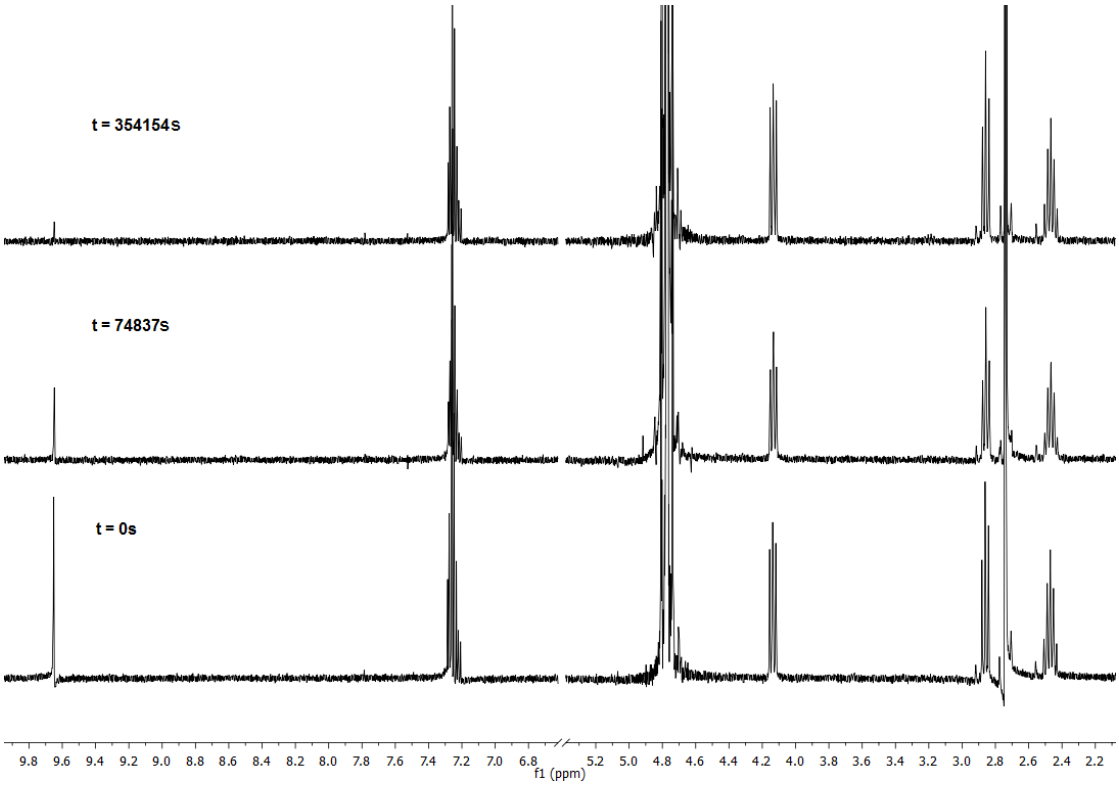

In a similar manner, hydrogen-deuterium exchange was followed for 2,4,6-tribromophenyl triazolium salt **121.** Representative spectra taken at three times at p*D* 0.97 (0.1 M DCl) are shown in Figure 2.11. As with **120**, there was no change in the integration of other peaks relative to the internal standard of NMe_4 DSO_4.

Figure 2.11 Representative ^{1}H NMR spectra at 400 MHz of triazolium salt 121 (5 mM,* p*D 0.97), obtained during exchange of the C3-H (s, 10.10 ppm) for deuterium in D_2O at 25 °C and I = 1.0 (KCl). [Internal standard, tetramethylammonium deuteriosulfate (s, 3.17 ppm)]

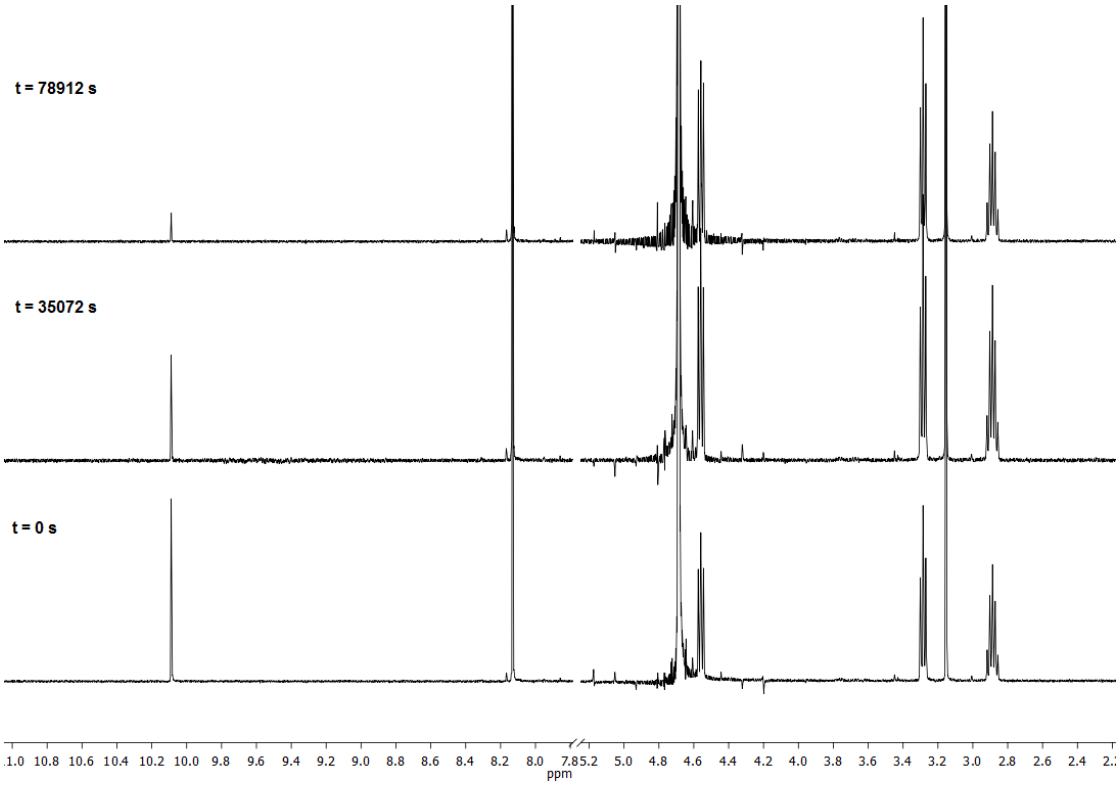

Experimentally observed pseudo first-order rate constants for exchange, k_{ex} (s^{-1}), were determined using non-linear least square fitting of *f*(s) against time to a first-order exponential decay. Example plots of *f*(s) against time with non-linear least square fitting are below (Figure 2.12).

Figure 2.12 (a-b) Representative plot of fraction of substrate remaining against time for triazolium salt a) 120 at 25 ºC, I = 1.0 at* p*D 0.53, b) 121 at 25 ºC, I = 1.0 at* p*D 0.97

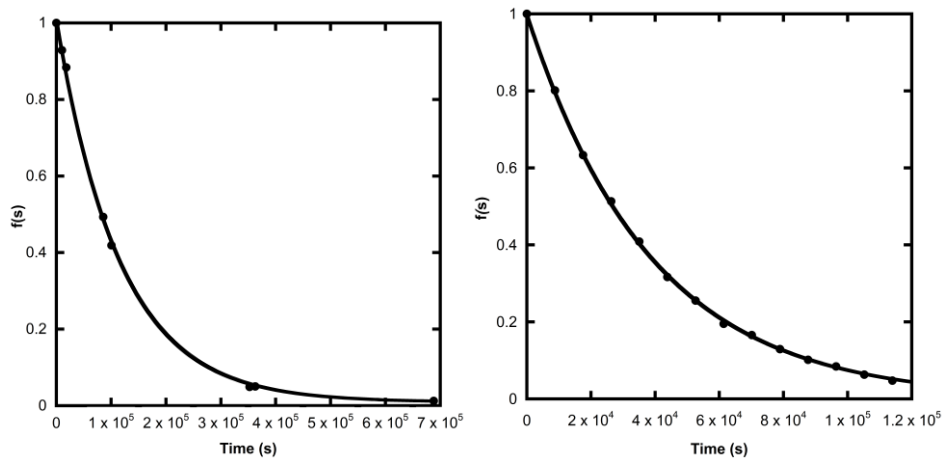

Table Table 2.5 details the reaction data and k_{ex} values. The concentration of deuteroxide is given by Equation 2.4 where K_w is the ionic product of D_2O under standard conditions ($10^{-14.87}$ M^2). The apparent activity coefficient of deuteroxide γ_{DO} = 0.73 has been previously determined at I = 1.0 M (KCl), under identical conditions.

Equation 2.4

$$[DO^-] = \frac{10^{(pD - pK_W)}}{\gamma_{DO}}$$

Table 2.5 Reaction data and first-order rate constants for exchange of the C3 proton of triazolium salts 35 and 36 at 25 ºC, I = 1.0

Triazolium Salt	[DCl] M	p*D*	[DO^-] M	k_{ex} (s^{-1})
120	2[a]	−0.10	1.07×10^{-15}	2.29×10^{-6}
	1	0.37	3.17×10^{-15}	6.71×10^{-6}
	0.75	0.61	5.51×10^{-15}	8.13×10^{-6}
	0.5	0.53	4.58×10^{-15}	8.61×10^{-6}
	0.25	0.71	6.93×10^{-15}	9.52×10^{-6}
	0.175	1.17	2.00×10^{-14}	1.28×10^{-5}
	0.1	1.09	1.66×10^{-14}	1.40×10^{-5}
	0.05	1.41	3.47×10^{-14}	2.08×10^{-5}
	0.025	1.80	8.53×10^{-14}	4.30×10^{-5}
	0.01	2.99	1.32×10^{-12}	5.73×10^{-4}
	Acetate Buffer	2.2	2.14×10^{-13}	8.21×10^{-5}
	Acetate Buffer	3.4	3.40×10^{-12}	1.01×10^{-3}
	Acetate Buffer	3.65	6.04×10^{-12}	2.42×10^{-3}
121	2[a]	−0.13	1.03×10^{-15}	4.59×10^{-6}
	1	0.22	2.24×10^{-15}	1.37×10^{-5}
	0.5	0.43	3.64×10^{-15}	1.70×10^{-5}
	0.25	0.70	6.78×10^{-15}	1.91×10^{-5}
	0.1	0.97	1.26×10^{-14}	2.58×10^{-5}
	0.05	1.25	2.40×10^{-14}	3.37×10^{-5}
	0.025	1.60	5.38×10^{-14}	4.98×10^{-5}
	0.005	2.25	2.40×10^{-13}	1.50×10^{-4}

0.0015	2.45	3.81×10^{-13}	2.48×10^{-4}
0.001	2.55	4.80×10^{-13}	3.14×10^{-4}

[a]I > 1 M points not included in fitting.

2.2.1.1. Determination of second-order rate constants and pK_a of 122 and 123

Typically, the observed pseudo first-order rate constant for exchange, k_{ex} (s^{-1}) includes kinetic terms for dependence on deuteroxide ion concentration, $k_{DO}[DO^-]$, and potentially additional terms for deprotonation by solvent, k_{D2O}, or buffer base $k_B[B]$.

Equation 2.5

$$k_{ex} = k_{DO}[DO^-] + k_{D2O} + k_B[B]$$

In most of our experiments no buffer was used, so there is no contribution from $k_B[B]$. Previous assessment by Massey and Collett showed general base catalysis to be insignificant for the deuterium exchange reaction of a broad range of triazolium salts, thus it is also assumed that the $k_B[B]$ term does not have a significant contribution.

An overall simple first-order dependence on the contribution from deuteroxide is expected from this mechanism, which would result in a straight line with a slope of unity in a plot of $\log_{10} k_{ex}$ against p*D*.

The data acquired from these experiments shows a significant deviation from this trend, and the deviation is assigned to the mechanism shown previously in Figure 2.5 (Section 2.1) for pentafluoro triazolium **49**, involving either reaction of the triazolium ions **120** and **121** with solvent D_2O directly (Path B), or pre-equilibrium protonation of the N1 position followed by deprotonation by deuteroxide (Path C). Equations 2.6 and 2.7 allow for the influence of path B and C respectively.

Equation 2.6 Fitting equation accounting for pathway B.

$$\log_{10} k_{ex} = \log_{10}\left[\frac{K_a^{N1}\left(\left(\frac{k_{DO}K_w}{\gamma_w}\right)10^{pD}\right)+\left(K_a^{N1}k_{D2O}\right)}{K_a^{N1}+10^{-pD}}\right]$$

Equation 2.7 Fitting equation accounting for pathway C.

$$\log_{10} k_{ex} = \log_{10} \left[\frac{K_a^{N1} \left(\left(\frac{k_{DO} K_w}{\gamma_w} \right) 10^{pD} \right) + \left(\frac{k'_{DO} K_w}{\gamma_w} \right)}{K_a^{N1} + 10^{-pD}} \right]$$

Figure 2.13 Plot of* $\log_{10} k_{ex}$ *against* p*D for 120* (■) *and 121* (▲) *at 25°C, I = 1.0, fitted to equations 2.6 and 2.7.

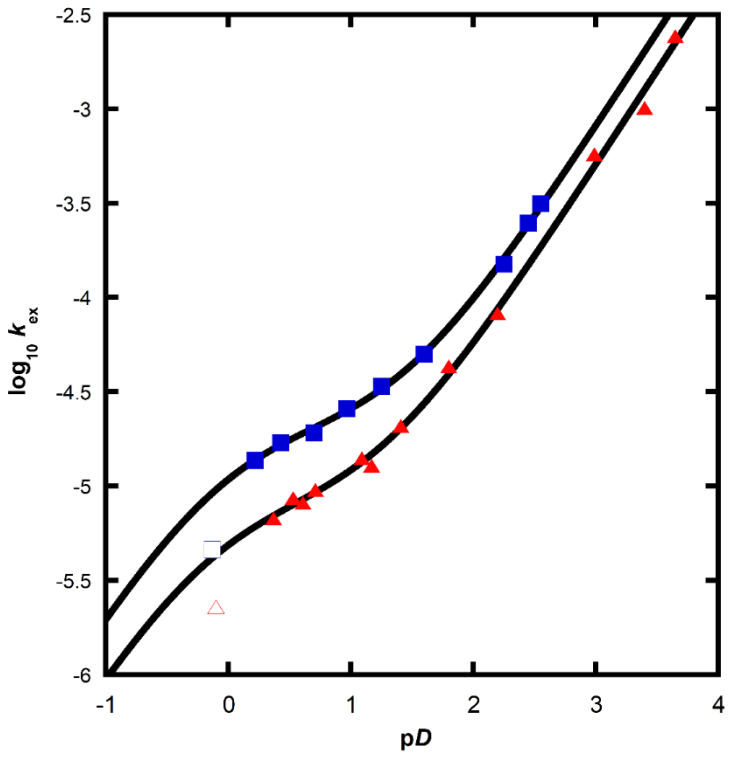

The points below p*D* = 0 are marked with hollow data points and are not included in the fit due to their variation in ionic strength. As deduced for **49**, the data for **120** and **121** also fit equations 2.6 and 2.7 well, which suggests that the mechanism responsible for exchange in these triazolium salts is the mechanism of Figure 2.13. Other fitting options were considered, such as linear dependence on p*D* and a plot allowing for the influence of protonation of N1 but disallowing path B or C (see appendix B), all of which fit poorly to the acquired data.

Due to equations 2.6 and 2.7 being kinetically indistinguishable by analysis of fitting alone, it is not possible to determine which mechanism of pathways B and C is present. The results of fitting to these equations are presented in Table 2.6

Table 2.6 Kinetic Parameters from Equations 2.6 and 2.7.

Triazolium	k_{DO} (M^{-1} s^{-1})	k_{D2O} (s^{-1})	k'_{DO} (M^{-1} s^{-1})	K_a^{N1}	pK_a^{N1}
120	2.71×10^8	8.0×10^{-6}	5.7×10^9	1.3	−0.11
121	4.29×10^8	2.0×10^{-5}	1.2×10^{10}	1.1	−0.04

2.2.1.2 Estimation of k_{HOH}, k_{HO} and pK_a

The second-order rate constants for deuteroxide catalysed exchange k_{DO} (M^{-1} s^{-1}) previously determined for **120** and **121** can be used to make an estimate of their pK_a. Using the kinetic acidity method, a modified version of the Henderson-Hasselbalch equation derives an estimate of pK_a from exchange data. K_w is the dissociation constant of water, k_{HO} (M^{-1} s^{-1}) is the second-order rate constant of exchange by hydroxide and k_{HOH} (s^{-1}) is the solvent reorganisation rate constant of water. This is discussed further in section 2.3.

Equation 2.8

$$pK_a = pK_W + \log_{10}\left(\frac{k_{HOH}}{k_{HO}}\right)$$

As previously discussed, the mechanism of H/D exchange for triazolium salts **120-121** has a rate-determining step of solvent reorganisation, due to the previously found lack of buffer catalysis. This means that the proton-transfer step must exist as a pre-equilibrium for this reaction.

The value of k_{HO} can be determined from k_{DO} using the secondary solvent isotope effect relationship, $k_{DO}/k_{HO} = 2.4$, where proton-transfer occurs as a pre-equilibrium. The secondary solvent kinetic isotope effect is as a result of the higher basicity of DO^- relative to that of HO^-.

Due to solvent reorganisation being the rate-determining step in this reaction, the principle of microscopic reversibility dictates that solvent reorganisation will also be rate-determining for the protonation of the carbene, from which it follows that the rate constant of solvent reorganisation may be assigned to the rate constant of protonation of the carbene by water (Equation 2.9)

Equation 2.9

$$k_{HOH} = k_{reorg} \approx 10^{11} s^{-1}$$

With the estimate of k_{HOH} and the value of k_{HO}, an estimate of the carbon acid pK_a can be made from equation 2.10, where pK_w = 14 (ionic product of water $K_w = 10^{-14}$).

Table 2.7 Second-order rate constants of exchange and estimates of pK_a of triazolium salts 120 and 121.

Triazolium	k_{DO} ($M^{-1}\,s^{-1}$)	k_{HO} ($M^{-1}\,s^{-1}$)	pK_a^{C3}
120	2.71×10^8	1.13×10^8	16.9
121	4.29×10^8	1.79×10^8	16.7

The estimation of pK_a and the origin of equations 2.9-2.11 are discussed further in section 2.3.

2.2.2 Proton-transfer chemistry of imidazolium salts 122 and 123

Figure 2.14 Two imidazolium based salts with exocyclic nitrogen substituents.

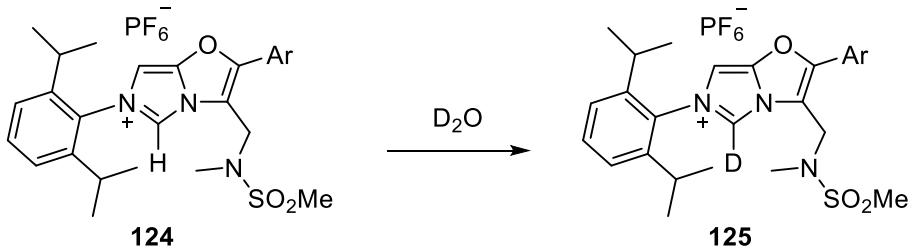

Deuterium exchange experiments were carried out in D_2O solutions with a 40 % acetonitrile cosolvent. The p*D* was maintained with formate and acetate buffers in the range of p*D* 2-5. The experiments were maintained at a constant ionic strength (I = 0.4) and temperature (25 °C).

The progress of deuterium exchange was followed by the decrease of the area of the singlet signal at ~9.5 ppm, corresponding to the C(3) proton of the imidazolium salts. All peaks were integrated relative to the internal standard peak at ~3 ppm, corresponding to the twelve methyl protons of NMe4 DSO_4, which are known to be non-exchanging under these conditions[13].

Equation 2.10

$$f(\mathrm{s}) = \frac{\left(A_{\mathrm{C(3)H}}/A_{\mathrm{std}}\right)_{\mathrm{t}}}{\left(A_{\mathrm{C(3)H}}/A_{\mathrm{std}}\right)_{\mathrm{t0}}}$$

The fraction of protonated substrate remaining was determined using Equation 2.10. Pseudo-first order rate constants for exchange, k_{ex} (s^{-1}), were determined from plots of *f*(s) against time, using non-linear least square fitting of *f*(s) against time to a first-order exponential decay.

Equation 2.11

$$f(\mathrm{s}) = \mathrm{e}^{-k\mathrm{t}}$$

From the data obtained in these experiments second-order rate constants for deuteroxide catalysed exchange, k_{DO} (M^{-1} s^{-1}), could be determined. From analysis of the rate constants, an estimate of pK_a could be determined

Representative spectra taken at three time points during the reaction of imidazolium salt **122** in conditions of pD_{obs} 4.50 (0.2 M formate buffer) are shown in Figure 2.15. Disappearance of the singlet at 9.6 ppm over time is assigned to hydrogen-deuterium exchange of the C(3)-H atom. Other signals corresponding to non-exchanging groups are present: aryl protons from 8.4 to 7.8 ppm, alkyl singlets at 3.8 and 3.6 along with isopropyl group protons at 2.8 and 1.6 ppm. No change was observed in the integrated areas of the other peaks, relative to the internal standard, which indicates that neither H/D exchange nor other chemical reactions at these positions occurred in any significant amount under these conditions.

Figure 2.15 Representative ^{1}H NMR spectra at 400 MHz of imidazolium salt 122 (5 mM, pD_{obs} 4.50), obtained during exchange of the C3-H (s, 9.6 ppm) for deuterium in D_2O at 25 °C and I = 0.40 M (KCl). [Internal standard, tetramethylammonium deuteriosulfate (s, 3.17 ppm)]

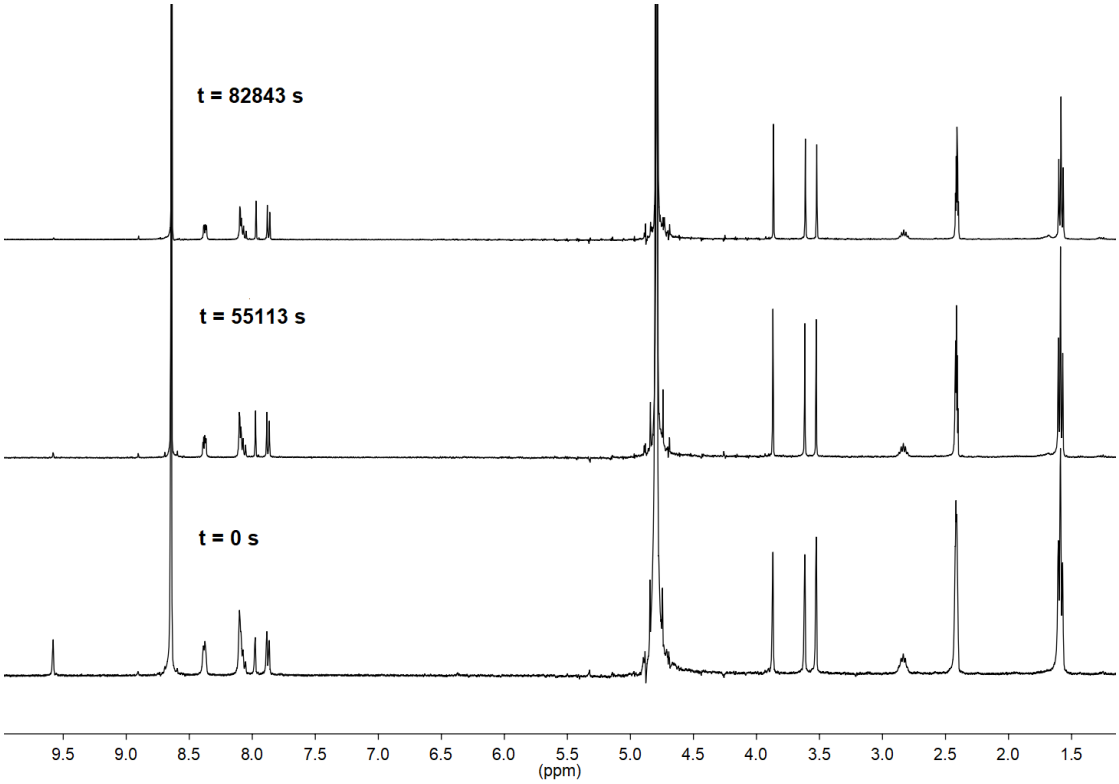

In a similar manner, hydrogen-deuterium exchange was followed for **123**. Representative spectra taken at three time points at pD_{obs} 3.36 (formate 0.2 M) are shown in Figure 2.16. As with **122**, there was no change in the integration of the other peaks relative to the internal standard of NMe_4 DSO_4

Figure 2.16 Representative ^1H NMR spectra at 400 MHz of imidazolium salt 123 (5 mM, pD_{obs} 3.36), obtained during exchange of the C3-H (s, 9.36 ppm) for deuterium in D_2O at 25 °C and I = 0.40 M (KCl). [Internal standard, tetramethylammonium deuteriosulfate (s, 3.17 ppm)]

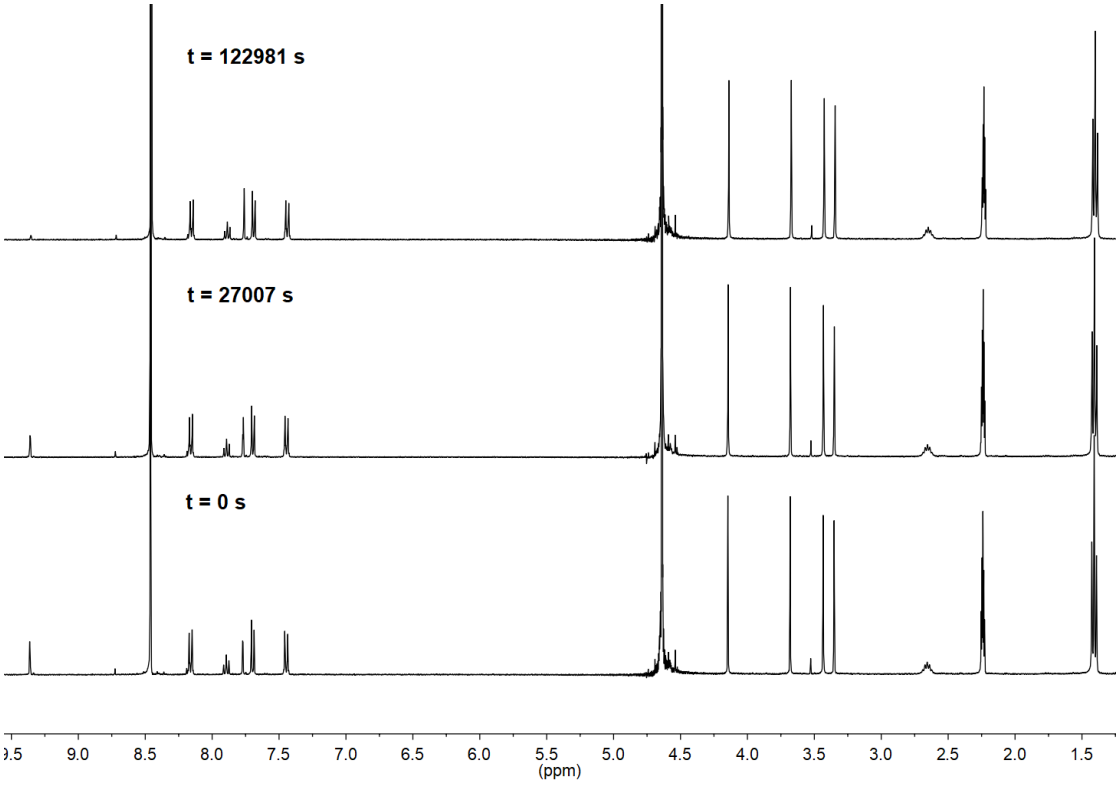

Experimentally observed pseudo first-order rate constants for exchange, k_{ex} (s^{-1}) were determined using non-linear least square fitting of *f*(s) against time to a first-order exponential decay. Example plots of *f*(s) against time with non-linear least square fitting is below.

Figure 2.17 (a-b) Representative plots of fraction of substrate remaining against time for (a) 122 at 25 ºC, I = 0.40 at* pD_{obs} *4.50 (b) 123 at 25 ºC, I = 0.40 at* pD_{obs} *3.36

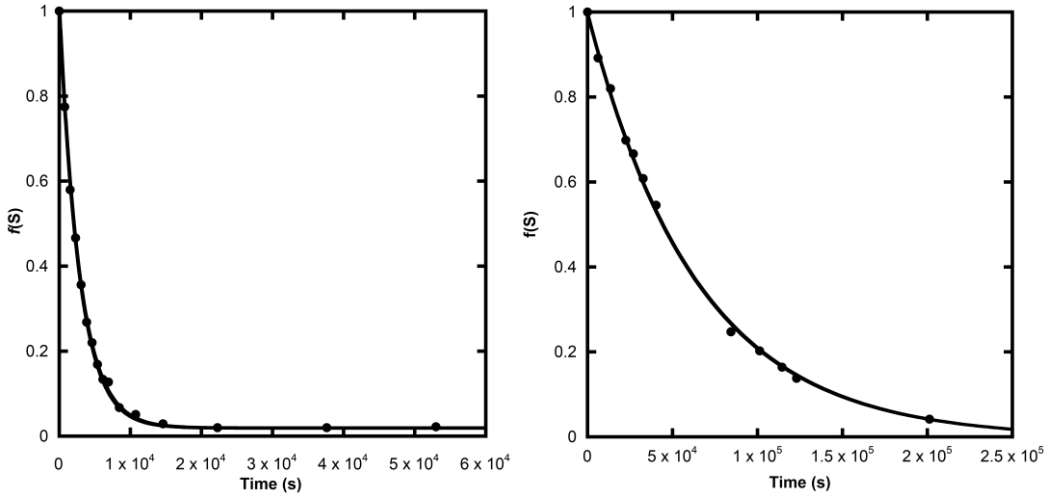

Table 2.8 details the reaction data and k_{ex} values. The effects of the addition of the acetonitrile cosolvent are compensated for by the subtraction of δ from the pD_{obs} valueto give p$D_{corr.}$ δ is an empirically determined correction factor for variation in pH in mixtures of water and other organic solvents[14].

Equation 2.12

$$[\mathrm{DO^-}] = (10^{\mathrm{p}D_{corr} - \mathrm{p}K_{AP})})/\gamma_{\mathrm{DO}}$$

[DO^-] was calculated from equation 2.12 where pK_{AP} = 15.92 for a mixture of D_2O:Acetonitrile (2:3) (v/v). This value is derived from the autoionization constant of H_2O:Acetonitrile (X_i = 0.19) at 25 °C ($K_{AP} = 10^{-15.05}$)[15] under the assumption that the ratio of K_{AP} (H_2O)/ K_{AP}(D_2O) = 7.4[16] is consistent with H_2O:Acetonitrile mixtures.

The activity coefficient γ_{DO} is presumed to be similar to the experimentally determined activity coefficient of activity of hydroxide γ_{HO} of 0.80 at I = 0.4 (Section 6).

Table 2.8 Reaction data and first-order rate constants for exchange of the C3 proton of imidazolium salts 122 and 123 at 25 ºC, I = 0.4, formate buffer 0.2 M.

Imidazolium Salt	Buffer	% (f.b.)	pD_{obs}	pD_{corr}	[DO^-] (M)	k_{ex} (s^{-1})
122	Formate	10%	3.00	3.20	2.38×10^{-13}	1.20×10^{-5}
		17.5%	3.32	3.52	4.98×10^{-13}	2.09×10^{-5}

		25%	3.48	3.68	7.19×10^{-13}	3.37×10^{-5}
		50%	4.00	4.20	2.55×10^{-12}	1.04×10^{-4}
		75%	4.50	4.70	9.93×10^{-12}	3.55×10^{-4}
	Formate	10%	3.16	3.36	3.44×10^{-13}	7.52×10^{-6}
		17.5%	3.36	3.56	5.46×10^{-13}	1.55×10^{-5}
123		25 %	3.48	3.68	7.19×10^{-13}	2.72×10^{-5}
		50 %	4.03	4.23	2.55×10^{-12}	7.44×10^{-5}
	Acetate	25 %	4.62	4.82	9.93×10^{-12}	4.63×10^{-4}

Figure 2.18 Second-order rate plot of C(3) exchange of imidazolium salt 122 at 25°C, I = 0.4 M in 0.2 M formate buffer.

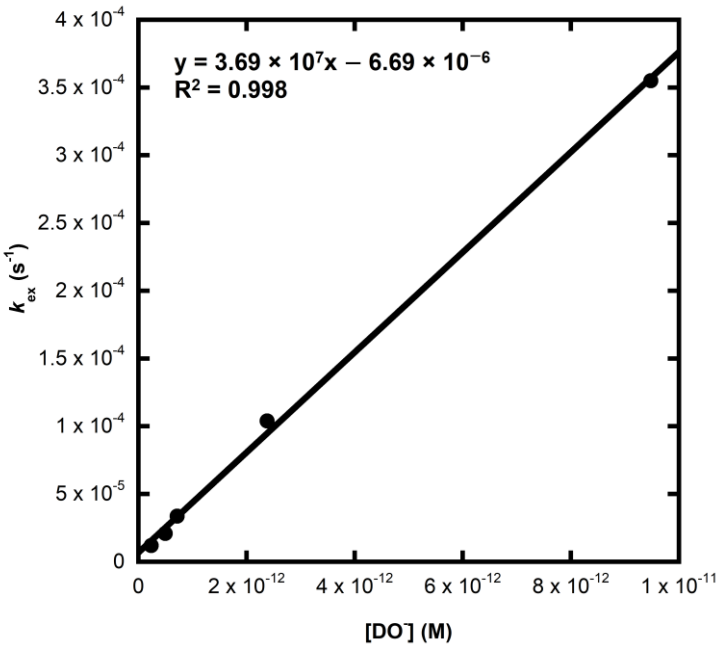

Figure 2.19 Second-order rate plot of C(3) exchange of imidazolium salt 123 at 25°C, I = 0.4 M in 0.2 M formate buffer.

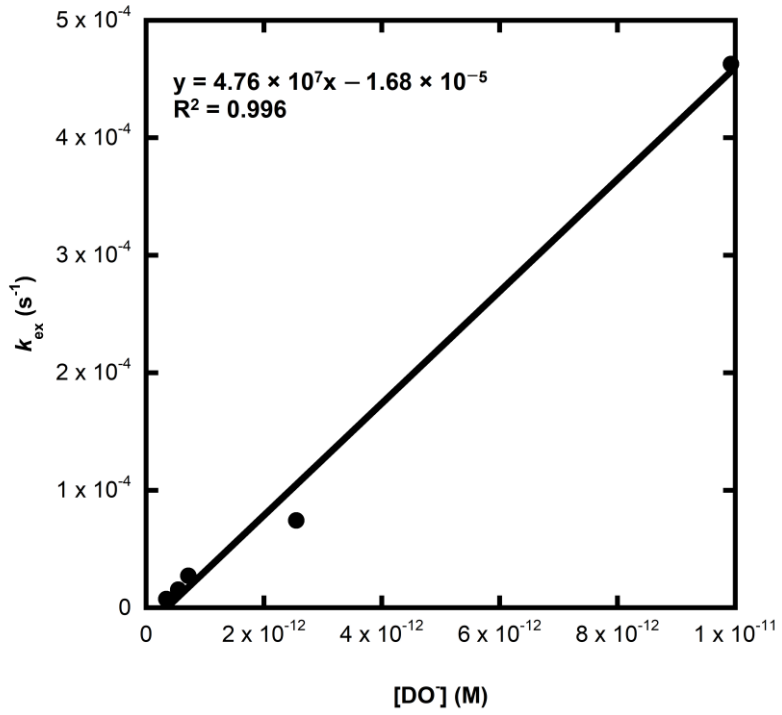

2.2.2.3 Determination of second-order rate constants and pK_a of 122 and 123

In Section 2.2.1.3, it was discussed that the pseudo first-order rate constant for exchange k_{ex} includes terms for H/D exchange catalysed by deuteroxide k_{DO}, as well as potential terms for reaction with solvent k_{D2O} and buffer base k_B (Equation 2.13).

Equation 2.13

$$k_{ex} = k_{DO}[DO^-] + k_{D2O} + k_B[B]$$

Previous research on the H/D exchange experiments of imidazolylidenes by Amyes[5] and Higgins[6] has determined that the mechanism is exclusively specific-base catalysed for each experiment, with no significant contribution from buffer catalysis. In addition, the lack of a significant contribution from k_{D2O} is expected due to its greatly lower basicity compared to deuteroxide.

There was no deviation from unity dependence on p*D* in either salt at low p*D*s, which indicates a lack of change in mechanism from deuteroxide-catalysed H/D exchange.

Additional experiments were performed on imidazolium salt **122**, in dilute DCl solutions of 0.1 M and 0.01 M, neither of which showed observable H/D exchange over several days, consistent with expected behaviour extrapolated from the second-order rate plots.

The mechanism of this reaction is assumed to be the same as the previously determined mechanism of H/D exchange of imidazolium salts, a mechanism analogous to the previously discussed path A in the H/D exchange of triazolium salts.

2.2.1.3.1 Estimation of k_{HOH}, k_{HO} and pK_a

As in section 2.2.1 the previously determined second-order rate constants of deuteroxide catalysed exchange k_{DO} (M^{-1} s^{-1}) can be used to make an estimate of pK_a and carbon acidity by use of equation 18.

Equation 2.14

$$pK_a = pK_W + \log_{10}\left(\frac{k_{HOH}}{k_{HO}}\right)$$

The H/D exchange of imidazolium salts **122** and **123** can be assumed to follow the same mechanism of previous examples of imidazolium salts studied by Amyes et. al. in the mechanism of exchange via an NHC with a rate-determining step of solvent reorganisation. The secondary solvent isotope effect (k_{DO}/k_{HO} = 2.4) is also the same as previously discussed. This allows for an estimate of pK_a, assuming $k_{reorg} = 10^{11}$ s^{-1} and where pK_w = 14 using Equation 2.8, the results of which are presented in Table 2.9.

Table 2.9 Second-order rate constants and estimated pK_a of 122 and 123

Imidazolium	k_{DO} (M^{-1} s^{-1})	k_{HO} (M^{-1} s^{-1})	pK_a^{C3}
122	3.70×10^7	1.54×10^7	17.8
123	4.76×10^7	1.98×10^7	17.7

2.3 Discussion

The kinetic acidities of triazolium salts **120-121** and imidazolium salts **122-123** were investigated by H/D exchange reactions followed by ^{1}H NMR (400/500 MHz) spectroscopy in D_2O solutions at 25 °C. The H/D exchange of the C(3) position is suggested to proceed *via* the general mechanism in Scheme 2.8

Scheme 2.8 General mechanism of NHC H/D exchange.

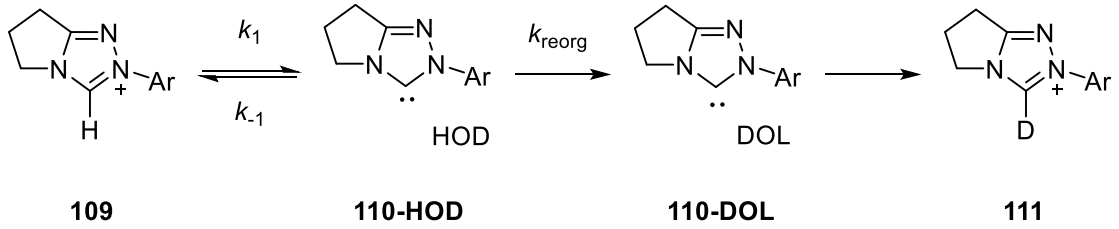

Reversible deprotonation (k_1/k_{-1}) of the cationic species **109** generates an intimately bound complex of NHC **110** and a molecule of HOD. Solvent reorganisation results in complex DOL, where the DOL molecule is positioned to deuterate the carbene **110**, yielding the product, **111**. The H/D exchange reaction is considered to be essentially irreversible due to the large excess of solvent D_2O to the sources of protons from the substrate.

The rate of reprotonation of **110** is considered to be limited by solvent reorganisation, with an approximate rate constant of $k_{reorg} = 10^{11}$ s^{-1} [17]. The rate of proton-transfer from alcoholic solvents to singlet diphenylcarbene has been directly shown by femtosecond spectroscopy to be limited by solvent reorganisation[1].

As previously mentioned, the absence of significant buffer catalysis in the H/D exchange of imidazolium[5,6] and triazolium[6,9] salts suggests specific base-catalysis thus requiring solvent reorganisation to be rate-limiting.

These effects allow the assumption that $k_{reorg} = k_{HOH} \approx 10^{11}$ s^{-1}, and therefore k_{DO}, to be converted to an estimate of pK_a by equation 2.15 using a secondary solvent kinetic isotope effect of $k_{DO}/k_{HO} = 2.4$ [18]for proton-transfer limited by solvent reorganisation.

Equation 2.15

$$pK_a = pK_w + \log\left(\frac{k_{HOH}}{k_{HO}}\right)$$

The objective of this research was to investigate further NHC proton-transfer behaviour, and in particular to probe the unusual *ortho* substituent effects reported by Massey et. al.[9]

2.3.1 Proton-transfer chemistry of 1,2,4-triazolium ions

Values of k_{DO} and pK_a, **120** and **121** are similar in acidity to those reported by Massey et. al.[9] for a broader range of triazolium salts. Relatively little variation is reported across the series of

triazolium ions studied, with only a 16-fold difference in k_{DO} between the most acidic N-C_6F_5 substituted triazolium **49** to the least acidic N-C_6H_4OMe substituted **107**.

Figure 2.20 Exchange data and* pK_a *for selected triazolium salts.

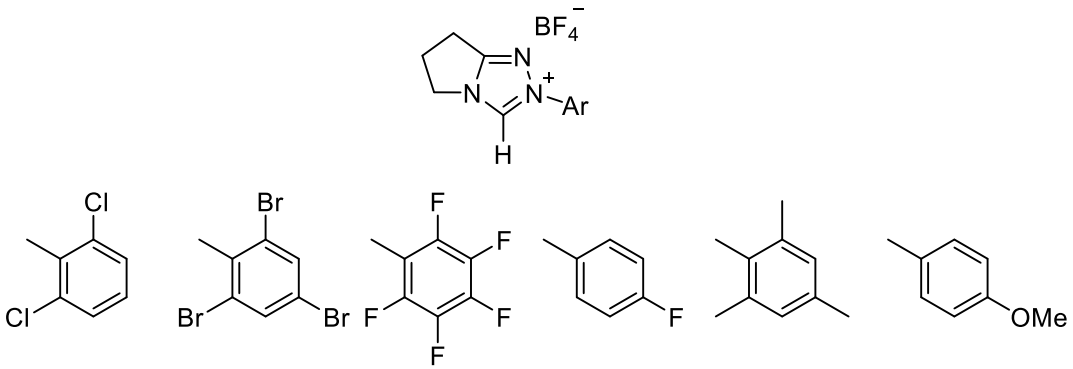

Table 2.10 Second-order rate constants and estimates of* pK_a *for selected triazolium salts.

Triazolium	k_{DO} (M^{-1} s^{-1})	pK_a^{C3}
120[a]	2.71×10^8	16.9
121[a]	4.29×10^8	16.7
49[b]	6.82×10^8	16.5
104[b]	8.66×10^7	17.4
106[b]	5.29×10^7	17.7
107[b]	4.20×10^7	17.8

a. From this work. b. Taken from Massey et. al.[9]

From the fitting of the regions of unity linear dependence on p*D*, triazolium ions **120** and **121** are amongst the most acidic of those studied, however, less acidic than the N-C_6F_5 salt **49**. The k_{DO} values **120**, **121**, and **49** increases in order **121**<**120**<**49**, which is in order of increasing halogen substitution, however there is only a 2.5-fold difference in k_{DO}, similar to the remainder of the series of triazolium salts. This behaviour is expected given the relatively electron-withdrawing halogenated N-aryl substituents of **120** and **121**.

As with previous examples of NHCs, the electron-withdrawing substituents destabilise the cationic conjugate acids **120** and **121** relative to their electronically neutral NHC state, which results in a higher value of k_{DO} and lower pK_a.

The relatively low difference in k_{DO} values between triazolium salts has been assigned to a non-planar orientation of the N-aryl ring with the 1,2,4-triazolium system[9,19], resulting in a lack of conjugation between rings, and limiting the effect of aryl substituents on the electronic

properties of the 1,2,4-triazolium system. It should be noted that this effect is common to the other families of NHCs, such as imidazolium[5] based systems, which show similarly small N-substituent effects.

Figure 2.21 Comparison of **$\log_{10} k_{ex}$** ***against*** **p*D*** ***for triazolium salts 49*** **(◆)**, ***120*** **(■)**, ***121*** **(▲)**, ***104*** **(●)**, ***107*** **(▼)**

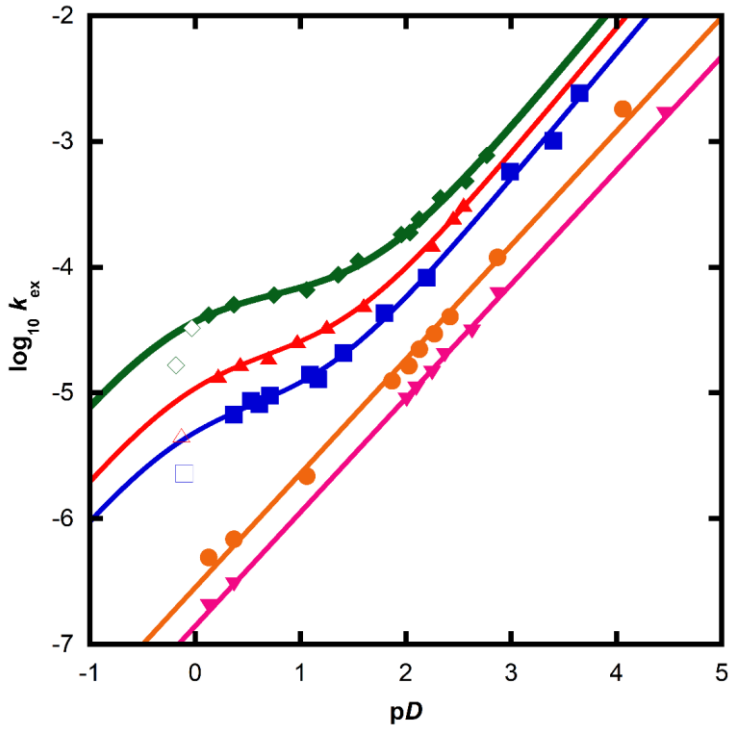

120, **121** and **49** all showed good fit to equations 2.6 and 2.7, which is consistent with the proposed mechanisms from Figure 2.5. The fitting parameters are presented in Table 2.7

Triazolium salts **120** and **121** were chosen for examination mainly owing to their *ortho*-halogenated aryl substituents. We were interested in probing whether the unexpected change in the log k_{ex} – p*D* dependence observed for **49** would also extend to other *ortho*-halo substituted salts. Clearly **120** and **121** also show altered dependence on p*D* under highly acidic conditions, which further supports the hypothesis of an *ortho*-substituent effect favouring reaction pathway C by raising the pK_a of the N1 position.

The acidity constants at N1 also have relatively little variation, with pK_a^{N1} values of −0.04 to −0.18 across the series, with **121**>**120**>**49** however the fitting errors for K_a^{N1} are relatively large. This is due to the partial protonation of this position at accessible p*D*s, considering constraints of ionic strength and diminished usefulness of p*D* below 0.

It is also notable that although the values of k_{DO} for di-chloro **120** and 4-cyano **108** triazolium salts are very similar (**108** $k_{DO} = 3.18\times 10^8$), **108** shows much less significant deviation from unity linear dependence on p*D* under highly acidic conditions. This is consistent with the proposed *ortho* substituent effect.

The k'_{DO} values for the dicationic forms of **120**, **121** and **49** are on the order of 10^{10} M^{-1} s^{-1}, which is near the diffusional limit. Considering that the monocationic triazolium ions have k_{DO} values as high as 6.82×10^8 M^{-1} s^{-1}, the higher values for the far more reactive dicationic triazolium system are expected. The values of k'_{DO} would place the dicationic triazolium ions as the most acidic of the known NHC precursors with estimated pK_a values of approximately 14.6-15.6.

2.3.2 Proton-transfer chemistry of two imidazolium ions

The objective of this research was to investigate the proton-transfer chemistry of **122** and **123**, and to determine if there were any unusual substituent effects such as the *ortho* effect of triazolium salts **120**, **121** and **49**, or the alternative effect imparted by pyridyl substituted triazolium salt **117**.

Figure 2.22 Studied imidazolium salts 122 and 123

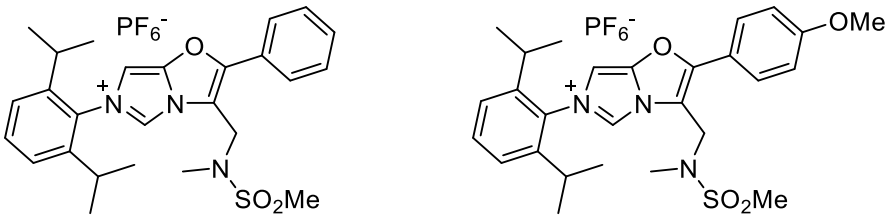

Due to the large hydrophobic substituents of **122** and **123**, they were insufficiently soluble in D_2O to allow monitoring by ^{1}H NMR spectroscopy. The addition of acetonitrile cosolvent has previously been used in studies of NHC proton-transfer chemistry, with relatively little effect on the kinetics of H/D exchange. It was found **122** and **123** were only sufficiently soluble with cosolvent addition of 40% (v/v) acetonitrile. At this concentration of acetonitrile, higher ionic strengths (I > 0.5 M) were found to form biphasic mixtures, requiring the use of lower ionic strength values than in previous studies. Despite these changes, it is expected that the results of H/D exchange experiments under these conditions are comparable to the results of previous studies; Massey et. al.[9] report a 1.2 fold increase in reported k_{DO} value in 33% (v/v) acetonitrile

solutions. This increase is assigned to either increased basicity of deuteroxide in the mixed solvent system or destabilization of the cationic conjugate acid.

***Figure 2.23 Plot of* $\log_{10} k_{ex}$ *against* p*D for imidazolium salts 122* (▲) *and 123* (●)**

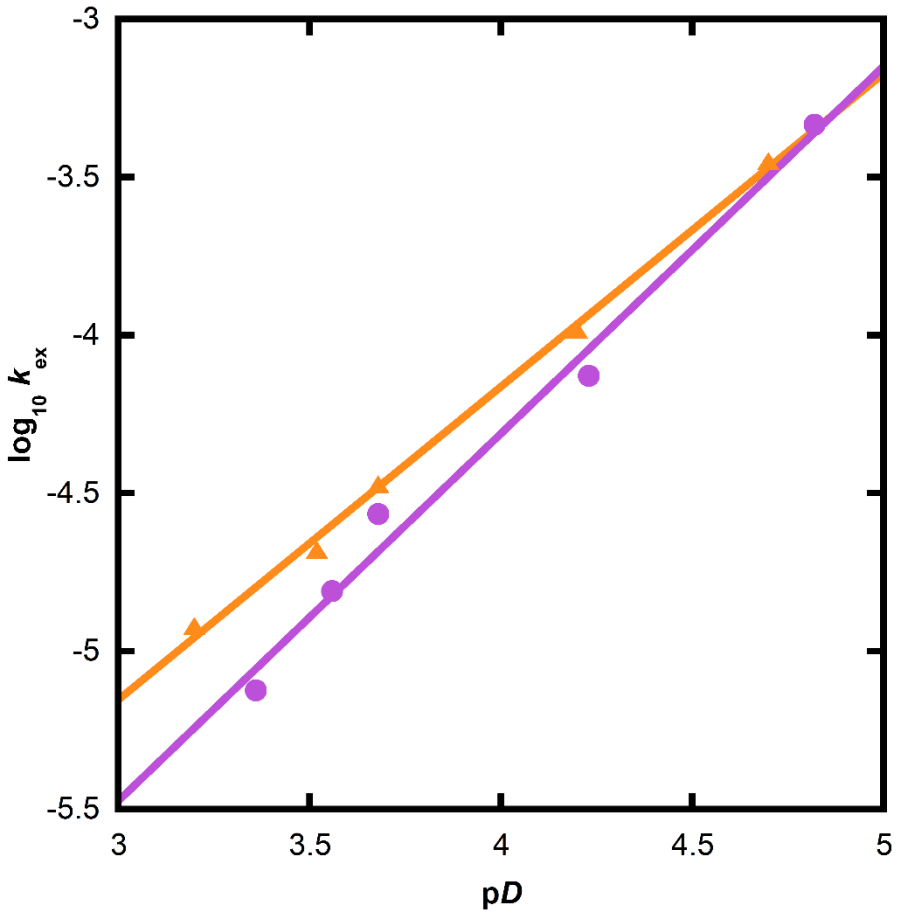

The p*D* rate profiles of **122** and **123** do not show any deviation from a slope of unity linear dependence on p*D*. The structures of **122** and **123** differ from the triazolium salts where altered dependence on p*D* was observed, in that they lack the N1 position that is protonated in these mechanisms. The only possible site of protonation is the furyl oxygen atom, however, the low basicity of furan ($pK_a = -10$)[20] combined with the positively charged ring system suggests that it is highly unlikely this site is protonated under the studied conditions.

The sulfonamide substituent of **122** and **123** has very poor basicity, and is also unlikely to be involved in the mechanism of proton-transfer of these imidazolium salts.

The determined values of k_{DO} from fitting of k_{ex} against [DO^-] for **122** and **123**, along with estimates of k_{HO} and pK_a^{C3} are shown in Table 2.12

***Table 2.12 Imidazolium second-order rate constants of exchange and* pK_a**

Imidazolium	k_{DO} ($M^{-1}\,s^{-1}$)	k_{HO} ($M^{-1}\,s^{-1}$)	pK_a^{C3}
122	3.70×10^7	1.54×10^7	17.8
123	4.76×10^7	1.98×10^7	17.7

The k_{DO} values are significantly higher than those reported for imidazolium salts, and even the N-alkyl thiazolium salts by Amyes. et. al.[5] and Higgins et. al.[6] The reported values are also similar to the less acidic triazolium ions reported by Massey[8]. Several relevant structural details have the potential to explain the large increase in carbon acidity. The addition of the oxygen heteroatom, although γ to the NHC centre, could have a large contribution to lowering the pK_a by increasing the stability of the NHC *via* the push-pull effect. The system also contains a larger conjugated aromatic system, with two aryl substituents to the main aromatic ring that could have a contribution to the lower pK_a.

Figure 2.24 Two NHC conjugate acids studied by Higgins et. al.

Table 2.13 Compared proton-transfer chemistry of 100b and 101a

Conjugate Acid	k_{DO} ($M^{-1}\,s^{-1}$)	pK_a
100b	2.00×10^4	20.7
101a	1.44×10^4	20.7

Previous literature data suggests that increases in the size of the conjugated aromatic system for previous imidazolium salts has a relatively small effect on their carbon acidity. Higgins et. al.[6] found that the change from imidazolium to imidazolinium did not lead to a significant change in k_{DO} for **100b** and **101a**.

Figure 2.25 Imidazolium and benzoimidazolium

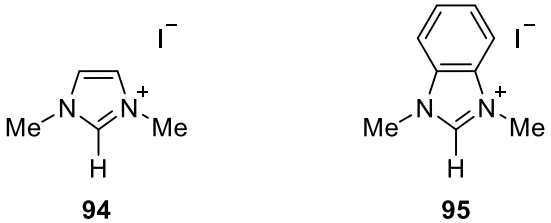

Table 2.14 Compared proton-transfer chemistry of 94 and 95

Conjugate Acid	k_{DO} (M^{-1} s^{-1})	pK_a
94	247	23.0
95	5.74×10^3	21.7

In contrast, studies on **94** and **95** by Amyes et. al.[5] found a ~25-fold increase in k_{DO} by the change from imidazolium to benzimidazolium ring. This change is smaller than the change from *N*-alkyl to *N*-aryl substituents (~2-3 pK_a units)

Figure 2.26 Imidazolium, thiazolium and oxazolium

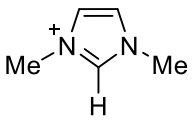

94

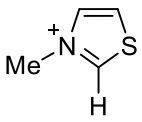

97

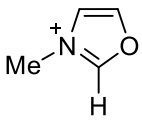

99

Table 2.15 Compared proton-transfer chemistry of 94, 97 and 99

Conjugate Acid	k_{DO} (M^{-1} s^{-1})	pK_a
94	247	23.0
97	3.4×10^5	19.5
99	3×10^7	16.9

Heteroatomic substitution on the NHC ring system was found to have a large effect on pK_a. Both the number and type of heteroatomic substitutions was found to be of high importance. Changing from an imidazolium to a substituted thiazolium or oxazolium system gives a decrease from a pK_a of 23.0 for the di-*N*-methyl substituted imidazolium **94** to 19.5 for the thiazolium **97** and 16.9 for oxazolium **99**[5]. The addition of a third nitrogen atom in the change from imidazolium to triazolium also gives a large decrease in pK_a e.g. comparing 4-methoxyphenyl substituted salts **100b** and **107** corresponds to a 3 unit difference in pK_a.

Figure 2.27 Triazolium salts 126 and 105

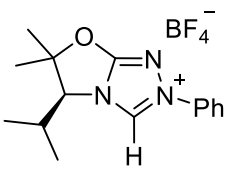

126

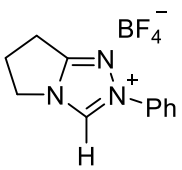

105

A further triazolium structure, **126** studied by Massey et. al.[9] has an oxygen heteroatom γ to the carbene centre similar to **122** and **123**. However, unlike the studied imidazolium salts, **126** has only a 1.3-fold increase in k_{DO} compared to analogous triazolium **105** in 33% acetonitrile solution. A possible explanation is that the oxygen of **126** is not within a conjugated ring system, unlike **122** and **123**. This could reduce the effect of the somewhat distant heteroatom on the pK_a of this triazolium ion.

Figure 2.28 Nitron and triphenyl-1,2-4-triazolium tetrafluoroborate.

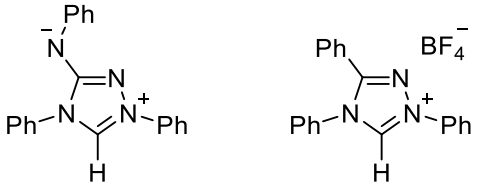

127 **128**

Additionally, we have recently demonstrated that Nitron[21] **127** has a pK_a significantly below that of the analogous triphenyl 1,2,4-triazolium salt **128** (pK_a = 16.8)[9], although H/D exchange occurred too rapidly even under highly acidic conditions to allow a reasonably accurate estimate of pK_a. An upper bound on the pK_a of Nitron was tentatively assigned as pK_a < 15 (see Section 5).

The higher values of k_{DO} and therefore lower pK_a of **122** and **123** are considered most likely to be a result of the additional fused furyl ring, and particularly its oxygen atom 3 bonds from the C3 position. The π-donation and σ-withdrawing nature of the oxygen atom is considered to be likely highly effective at influencing the behaviour at the C3 position, resulting in the observed higher rate of H/D exchange. Due to the increased distance from the NHC centre this effect is less pronounced than for oxazolium **99** but is consistent with the differences in other NHC groups, such as the example of Nitron.

Less significantly, there was a small difference between the second-order rate constants of deprotonation by deuteroxide of **122** and **123**. In contrast to previous examples of 4-methoxyphenyl substituents of triazolium salts resulting in a small decrease in k_{DO} relative to the phenyl salt **122**, the 4-methoxy substituted **123** is slightly (1.3-fold) faster in H/D exchange. The values are likely within fitting error of one another, and further experiments would likely show the values are similar, due to the distant position of the substituent from the reaction centre of deprotonation.

2.4 Conclusions

As NHCs are typically generated by the deprotonation of their conjugate acids, studies of the proton-transfer chemistry of these compounds is of high importance in the field of carbene chemistry. The previous discoveries by Massey et. al.[9] of an unusual mechanism of proton-transfer of pentafluorophenyl triazolium ion **49** and by Quinn et. al.[12] of an unusual proton-transfer mechanism of pyridyl triazolium ion **117** lead to our studies of four species: triazolium salts **120** and **121** and imidazolium salts **122** and **123**.

Figure 2.29 Four NHC conjugate acids studied in this section.

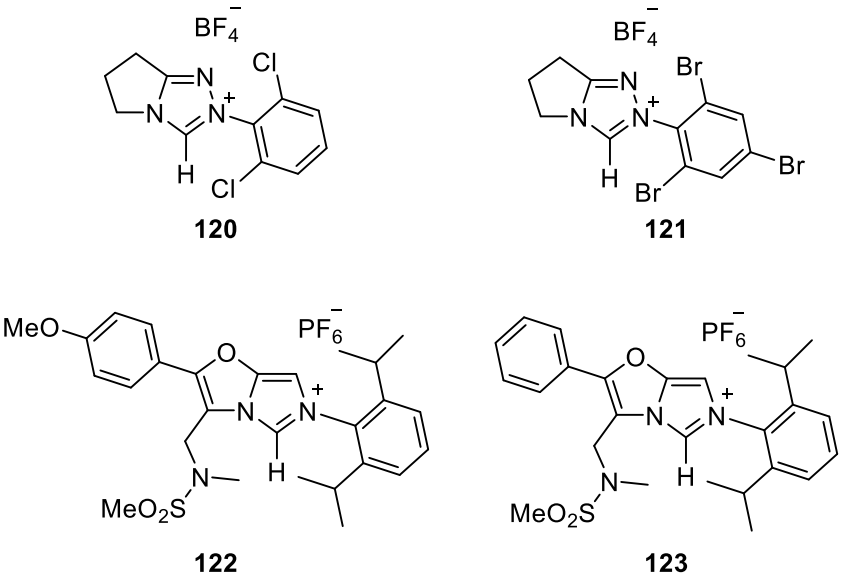

The proton-transfer chemistry of these species was investigated by a series of H/D exchange experiments monitored by ^{1}H NMR spectroscopy in D_2O solutions at 25 °C. The data from these experiments was used to discern information about the mechanism for H/D exchange by fitting to the respective functions, as well as determining the second-order rate constant of deprotonation by deuteroxide k_{DO} (M^{-1} s^{-1}) and from this making an estimate of the pK_a of each NHC conjugate acid.

Triazolium salts **120** and **121** were found to be similarly acidic at C3 to previous examples of triazolium salts, with estimated pK_a of 16.9 and 16.7 respectively. **120** and **121** also showed similar deviation from unity linear dependence of $\log_{10} k_{ex}$ on p*D* under acidic conditions to pentafluoro substituted triazolium **49**. Fitting the data to equation 2.7 takes into account the presence of the second proposed mechanism of H/D exchange involving protonation of N1 to give a more reactive dicationic species. The *ortho* halogen substituents of triazolium salts **120** and **121** give further credence to the proposed mechanism of pathway C of Figure 2.5, as

through-space interactions could affect protonation at N1. The estimated pK_a of N1 of these species (−0.2 to 0) is consistent with structurally similar dicationic nitrogen acids, which further supports the proposed mechanism.

Imidazolium salts **122** and **123** did not display the same change in mechanism of H/D exchange at low p*D* as the studied triazolium salts. The lack of this mechanism is assigned to a combined lack of suitable protonation sites to allow an analogous mechanism to pyridyl triazolium salt **117** and to the insufficient basicity of the aliphatic sulfonamide group to significantly affect the mechanism of the reaction. Values of k_{DO} were obtained by fitting the slope of the second-order plot of k_{ex} against concentration of deuteroxide ion. The k_{DO} of these imidazolium salts was found to be about 100 to 1000-fold higher than those obtained for previous N-aryl imidazolium salts, corresponding to a decrease of 2-3 pK_a units. This increased acidity was assigned to the addition of the fused furyl ring to the imidazolium system and in particular the effects of the additional oxygen heteroatom.

2.5 References

1 J. Peon, D. Polshakov and B. Kohler, *J. Am. Chem. Soc.*, 2002, **124**, 6428–6438.
2 R. Breslow, *J. Am. Chem. Soc.*, 1957, **79**, 1762–1763.
3 R. A. Olofson, W. R. Thompson and J. S. Michelman, *J. Am. Chem. Soc.*, 1964, **86**, 1865–1866.
4 P. Haake, L. P. Bausher and W. B. Miller, *J. Am. Chem. Soc.*, 1969, **91**, 1113–1119.
5 T. L. Amyes, S. T. Diver, J. P. Richard, F. M. Rivas and K. Toth, *J. Am. Chem. Soc.*, 2004, **126**, 4366–4374.
6 E. M. Higgins, J. A. Sherwood, A. G. Lindsay, J. Armstrong, R. S. Massey, R. W. Alder and A. C. O'Donoghue, *Chem. Commun.*, 2011, **47**, 1559–1561.
7 Y. Chu, H. Deng and J.-P. Cheng, *J. Org. Chem.*, 2007, **72**, 7790–7793.
8 M. H. Dunn, N. Konstandaras, M. L. Cole and J. B. Harper, *J. Org. Chem.*, 2017, **82**, 7324–7331.
9 R. S. Massey, C. J. Collett, A. G. Lindsay, A. D. Smith and A. C. O'Donoghue, *J. Am. Chem. Soc.*, 2012, **134**, 20421–20432.
10 L. Baragwanath, C. A. Rose, K. Zeitler and S. J. Connon, *J. Org. Chem.*, 2009, **74**, 9214–9217.
11 C. J. Collett, R. S. Massey, O. R. Maguire, A. S. Batsanov, A. C. O'Donoghue and A. D. Smith, *Chem. Sci.*, 2013, **4**, 1514–1522.
12 D. E. Tucker, P. Quinn, R. S. Massey, C. J. Collett, D. J. Jasiewicz, C. R. Bramley, A. D. Smith and A. C. O'Donoghue, *J. Phys. Org. Chem.*, 2015, **28**, 108–115.
13 A. Rios, A. C. O'Donoghue, T. L. Amyes and J. P. Richard, *Can. J. Chem.*, 2005, **83**, 1536–1542.
14 G. Douhéret, *Bull. Société Chim. Fr.*, 1968, 3122–3131.
15 J. Barbosa and V. Sanz-Nebot, *Anal. Chim. Acta*, 1991, **244**, 183–191.

16 A. K. Covington, R. A. Robinson and R. G. Bates, *J. Phys. Chem.*, 1966, **70**, 3820–3824.
17 U. Kaatze, R. Pottel and A. Schumacher, *J. Phys. Chem.*, 1992, **96**, 6017–6020.
18 R. More O'Ferall, A. J. Kresge and M. F. Powell, *Isotopes in Organic Chemistry*, Elsevier, New York, 1987, vol. 7.
19 D. A. DiRocco, K. M. Oberg and T. Rovis, *J. Am. Chem. Soc.*, 2012, **134**, 6143–6145.
20 M. P. Carmody, M. J. Cook and R. D. Tack, *Tetrahedron*, 1976, **32**, 1767–1771.
21 J. A. Grant, Z. Lu, D. E. Tucker, B. M. Hockin, D. S. Yufit, M. A. Fox, R. Kataky, V. Chechik and A. C. O'Donoghue, *Nat. Commun.*, 2017, **8**, 15088.

Chapter 3 Proton-Transfer Chemistry of Bis(amino)cyclopropenylidenes.

3.0 Foreword

This chapter consists of our investigations into the preparation of BACs, their proton-transfer chemistry and research into novel aminocyclopropenium phosphonates, and their unusual hydrolytic mechanism. Section 3.1 is a short review of relevant literature. Section 3.2.1 details the results of our investigations into the preparation of BACs, Section 3.2.2 presents our research on the proton-transfer of BACs and Section 3.2.3 shows novel cyclopropenium phosphonates and probes the mechanism of their hydrolysis. Discussion on these results and their implications is in Section 3.3 and Section 3.4 summarises the chapter.

3.1 Introduction

Bis(amino)cyclopropenylidenes (BACs) are a relatively modern class of stable carbene, first isolated and characterised in 2006 by Bertrand et. al.[1] Bertrand prepared bis(diisopropylamino)cylopropenylidene **23** from its conjugate acid tetraphenylborate salt **129** by deprotonation with KHMDS in dry diethyl ether at −78 °C.

Scheme 3.1 First preparation and isolation of BAC 23.

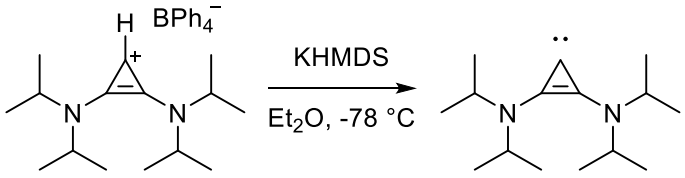

129 **23**

BAC **23** was characterised by crystallography and ^{13}C NMR spectroscopy and is the first reported example of an isolated carbene with no α-heteroatoms to the carbene centre. The carbene was reported to be highly sensitive to air and moisture, however, thermally stable and largely intact after heating to 80 °C in dry toluene for 2 hours.

Overall, there have been relatively few reports on the properties and applications of BACs due to their relatively recent discovery but the field is rapidly expanding.

3.1.1 Cyclopropenium Chemistry

Scheme 3.2 Preparation of triphenylcyclopropenium tetrafluoroborate 132

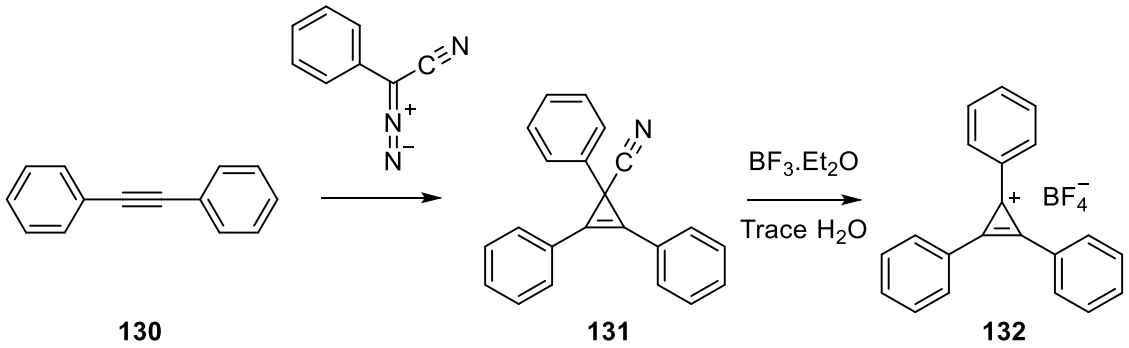

As with the majority of N-heterocyclic carbenes, BACs are typically generated through deprotonation of their conjugate acids, aminocyclopropenium ions. Although BACs were only isolated as recently as 2006, cyclopropenium chemistry dates back to 1958 with Breslow's[2] preparation of the first example, triphenylcyclopropenium tetrafluoroborate **132**. Reaction of phenyldiazoacetonitrile with diphenylacetylene **130** yielded cyano-cyclopropene **131**. Boron trifluoride etherate was used to remove the cyanide group and generate cyclopropenium salt **132**, which was found to be relatively stable to air and water. The stability was attributed to the 2π electron aromaticity of the ring, as well as charge distribution over the three phenyl rings.

The range of known cyclopropenium chemistry is wide. Relevant aspects are discussed in this section with a particular emphasis on synthetic developments.

Scheme 3.3 Lewis acid promoted reaction of tetrachlorocyclopropene 133.

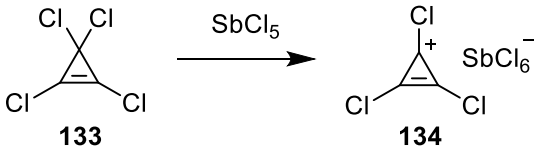

Trichlorocyclopropenium salts were prepared by addition of strong Lewis acids such as $SbCl_5$ or $AlCl_3$ to tetrachlorocyclopropene.[3] Quenching these salts with water was found to regenerate the starting tetrachlorocyclopropene.

Scheme 3.4 Preparation of trialkylthiocyclopropenium salts.

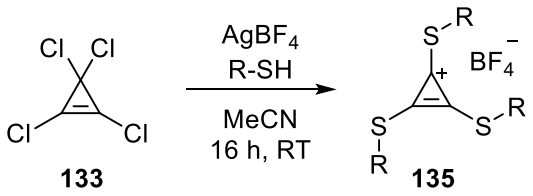

Trialkylthiocyclopropenium salts **135** have also been prepared, by addition of silver tetrafluoroborate to **133** in acetonitrile solution, followed by addition of a thiol.[4] These salts were found to have similar stability to the triphenylcyclopropenium salts. Use of alcohols as nucleophiles in place of thiols was not successful, instead forming ring-opened species[5]

Scheme 3.5 Friedel-Crafts reactions to prepare cyclopropenium compounds.

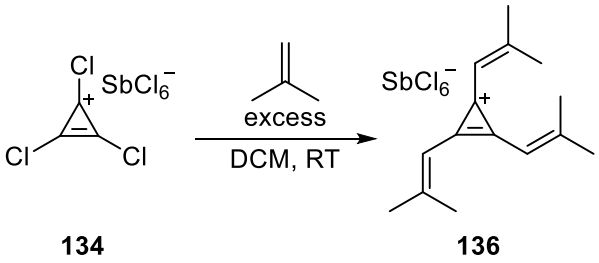

As aromatic ring systems, Friedel-Crafts reactions have been used to prepare cyclopropenium derivatives from trihalocyclopropenium ions, with careful counterion control.[6] A trivinyl derivative **136** was prepared by addition of isobutylene to a stirring solution of the hexachloroantimonate salt **134** at 0 °C in DCM, which was left to stand for several days at −30 °C in diethyl ether, forming crystals of the product **136**.

A wide variety of other, more exotic derivatives have been prepared in the literature, including ferrocenyl cyclopropenium salts[7], however the species of particular interest to this work are amino cyclopropenium ions.

3.1.1.1 Aminocyclopropenium Chemistry.

Scheme 3.6 Yoshida's Preparation of aminocyclopropenium salts 137 and 138

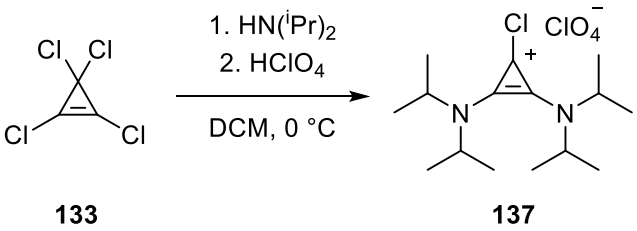

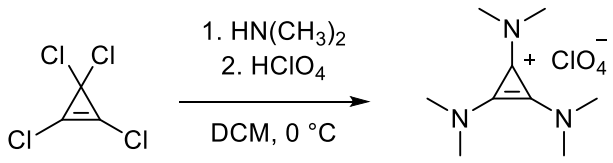

133 **138**

BACs are prepared from the bis(amino)cyclopropenium family of cyclopropenyl cations. Amino cyclopropenium chemistry was first developed in 1971 by the preparation of several tri- and disubstituted cyclopropenium ring systems by Yoshida et al.[8] Starting from commercially available tetrachlorocyclopropene, reaction with bulky secondary amines such as diisopropylamine produced disubstituted products such as **137**. Less bulky amines, such as dimethylamine, diethylamine, N-methylaniline, piperidine or morpholine were reported to produce exclusively the trisubstituted product such as **138**. These alkylaminocyclopropenium salts proved highly stable to water, even at high temperatures, by contrast to those of triphenylcyclopropenium cations.

Possibly owing to the ease of preparation of tris(amino)cyclopropenium salts over their disubstituted equivalents, there has been a comparative lack of novel BACs in the literature.

Scheme 3.7 Preparation of di(amino)substituted cyclopropenium salt 140

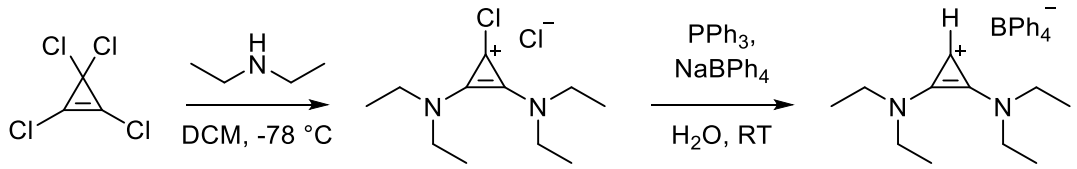

133 **139** **140**

Yoshida[8] found the reaction of diethylamine with tetrachlorocyclopropene produced trisubstituted cyclopropenium rings. More recently, Gravel et. al.[9] reported that slow addition of two equivalents of diethylamine to **133** at −78 °C produced the disubstituted chloro cyclopropenium **139**, which was dechlorinated using PPh_3 to give **140**. Higher temperatures gave largely the trisubstituted product. Di(amino)cyclopropenium salt **139** was found to have more effective organocatalytic behaviour (see section 4.1) due to its lower steric bulk compared to diisopropyl salt **129**.

Scheme 3.8 Preparation of 142

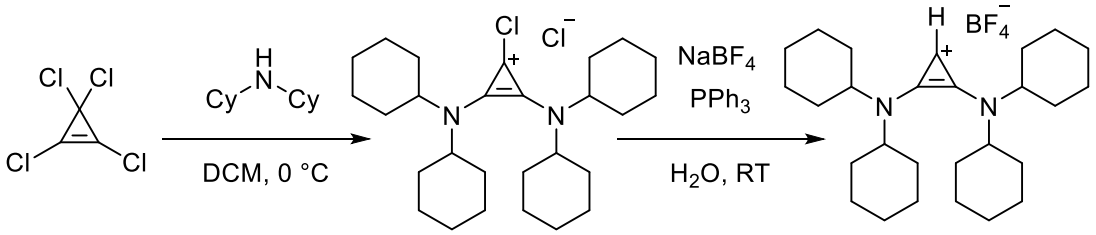

133 **141** **142**

Use of bulky dicyclohexylamine by Bertrand et. al enabled the successful preparation of a dicyclohexylamino BAC precursor.[10] Reaction conditions were essentially identical to those employed for their previous preparation of the diisopropyl salt **129**, with a modified method of purification.

Figure 3.1 Chiral BAC precursors

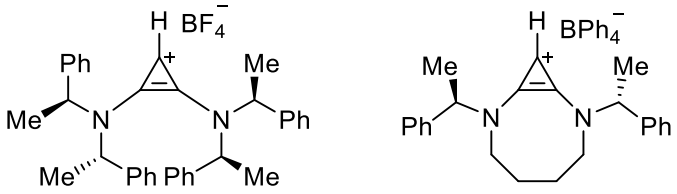

143 **144**

Chiral BACs and their precursors are also reported in the literature. Bis(*R*-1-phenylethyl)amine was used to prepare cyclopropenium salt **143** from tetrachlorocyclopropene[11]. Although **143** is chiral, very poor e.e. values resulted from its use in organocatalysis attributed to the free rotation of the amino substituents (see section 4 for more detail). This free rotation was avoided in a later work by Gravel[9], using N,N'-bis[(S)-α-phenylethyl]butane-1,4-diamine to produce BAC precursor **144**, which resulted in significantly improved e.e.

Scheme 3.9 Counterion-dependent preparation of substituted aminocyclopropenium salts

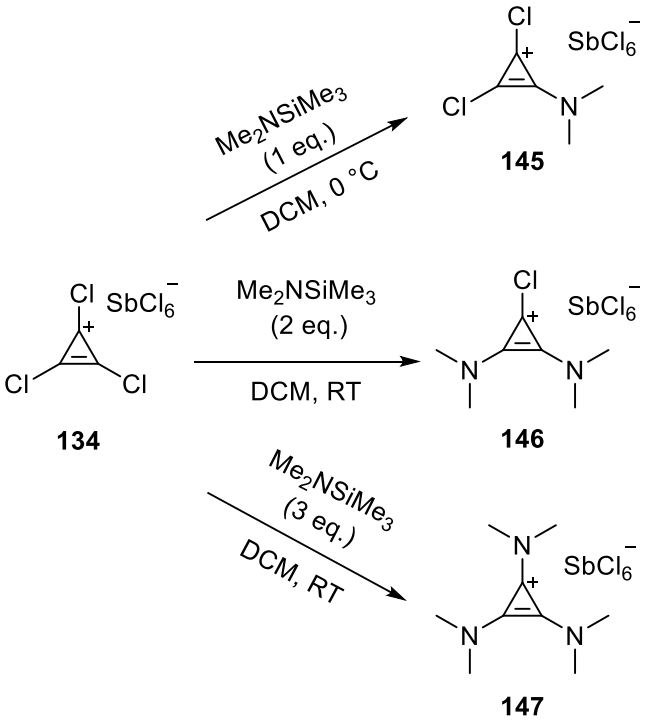

Weiss found that the use of the hexachloroantimonate salt of a trichlorocyclopropenium ion allowed for selective mono, di or trisubstitution with silyl dimethylamine[12]. Furthermore, it was found that the mono substituted product **18** spontaneously disproportionated in organic solvents to give the disubstituted product **19** and starting material **7**. This selective substitution was found to be impossible with any other counterion (Cl^-, BF_4^-, TfO^-) that was tested. This methodology has not been applied to the formation of BACs, likely due to the difficulty of using hexachloroantimonate salts.

3.1.1.1.1 Properties and Applications of Aminocyclopropenium Ions.

As an unusually stable carbocationic moiety, aminocyclopropenium ions are suited to a wide range of applications. Due to their high-lying LUMO, they are highly resistant to nucleophilic attack, which results in high stability against hydrolysis The pK_{R+} values of trisubstituted cyclopropenium ions in water have been calculated to be >13, extrapolated from experiments with trialkylcyclopropenium and trihalocyclopropenium ions[3] and from vibrational data.[13]

Figure 3.2 Stable phenol-chloride adduct of aminocyclopropenium ion

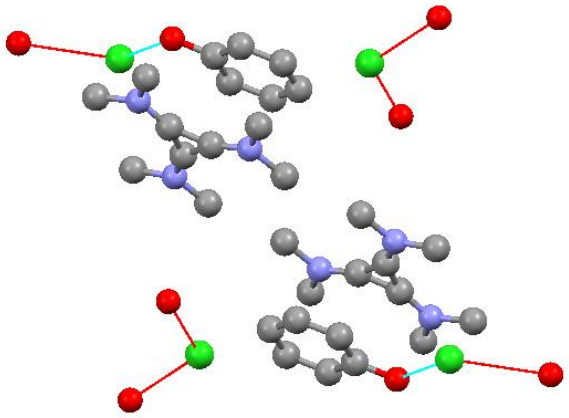

Aminocyclopropenium ions are suggested to experience an "ion pair strain" interaction, due to the electron-rich nature of the carbocation substituents if paired with an electron rich counterion. Weiss et. al.[14] prepared several charge transfer salts due to this interaction, resulting in strong hydrogen bonding interactions between carboxylic acids and the "naked" chloride ion produced by the strained ion pair.

Scheme 3.10 Yoshida's preparation of bis(N-methylanilino)-cyclopropenone.

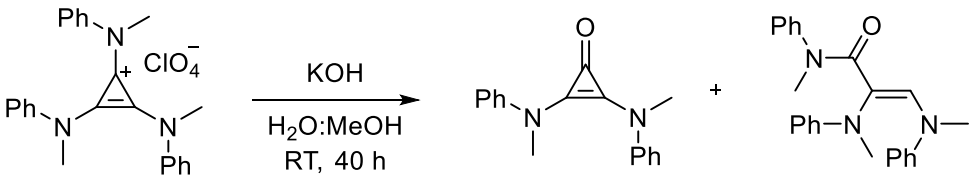

The basic hydrolysis of tris(amino)cylopropenium ion **148** provides diaminocyclopropenone **149**, in competition with a ring-opening reaction to produce α-β unsaturated amide **150**[15–17].

Scheme 3.11 Pyrolysis and cycloreversion from a cyclopropenone

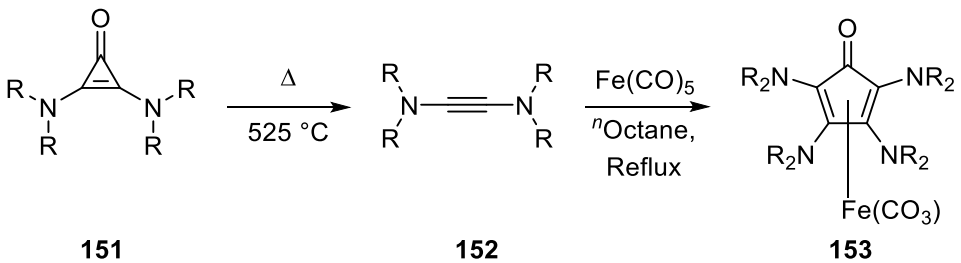

Diaminocyclopropenones can undergo pyrolysis to access synthetically useful ynediamines, through loss of a carbon monoxide molecule *via* a [2+1] cycloreversion.[18] This synthetic methodology was applied successfully by Breslow et. al. to produce an iron complex **153** by addition of iron pentacarbonyl under reflux to the ynediamine produced by pyrolysis at 525 °C[19].

3.1.2 Applications of BACs

Although BACs are a relatively recent discovery, a range of applications are now reported. Organocatalysis using BACs is a field which is rapidly increasing in scope due to the versatility and unique catalytic properties of these carbenes, and is discussed in detail in section 4.1.

Scheme 3.12 Preparation of BAC-Pd Complex

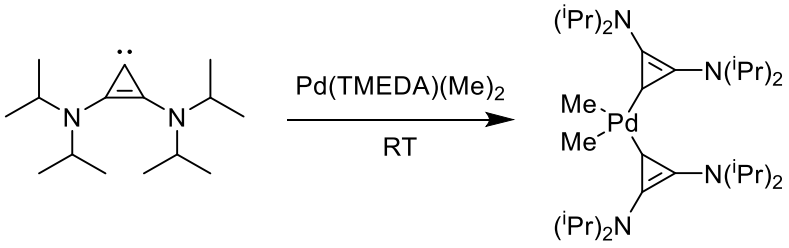

23 **154**

Similarly, to NHCs, several examples of organometallic complexes of BACs are present in the literature. The first examples of organometallic BAC complexes were prepared by Bertrand et. al.[20] by ligand exchange of Pd, Ni and Rh complexes.

Scheme 3.13 Preparation of BAC-Cu complex

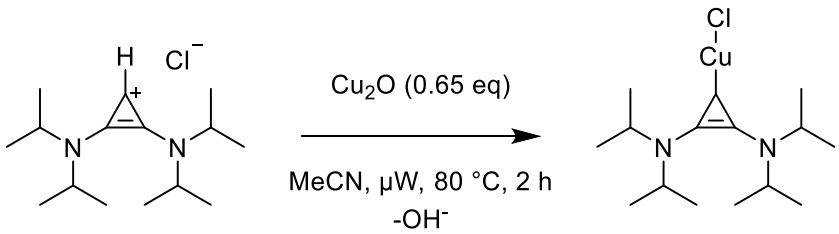

155 **156**

A BAC-Cu complex **156** was prepared through addition of the chloride salt **155** to Cu_2O and heating to give a pale yellow solid[21]. This copper complex was then used as the starting point for transmetallation reactions to form complexes of Pd, Au, Ir, and Rh. The Cu complex **156** was found to be an effective catalyst for "click" chemistry with a variety of azide substrates to form 1,2,3-triazoles.

Scheme 3.14 Preparation of BAC-Au complex

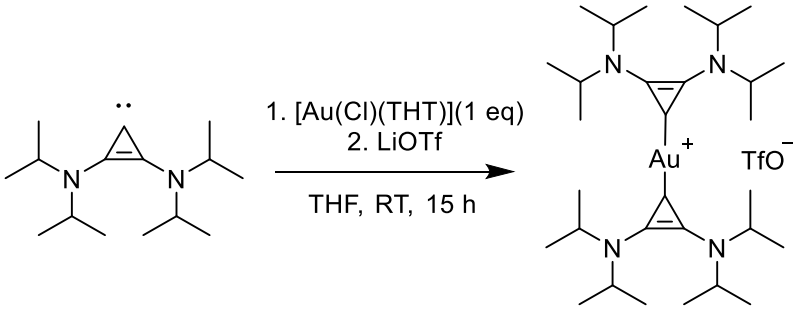

23 **157**

A doubly BAC substituted Au complex **157** was prepared through addition of the active carbene **2** to solution of [Au(Cl)THT] in THF (THT = Tetrahydrothiophene).

Scheme 3.15 Preparation of dicyclohexylhydroborate-BAC complex

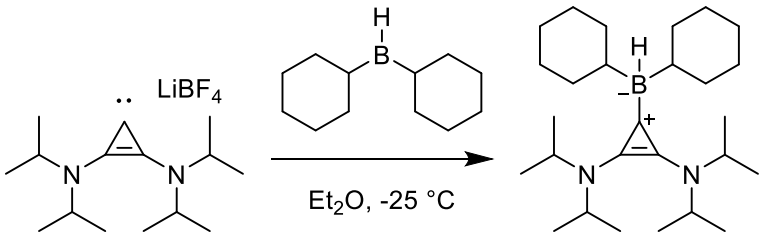

158 **159**

BAC-borane adducts such as **159** have been prepared by combination of a BAC lithium BF_4 adduct with borane dimethylsulfate, boron trifluoride etherate or dicyclohexylcarborane[22].

Scheme 3.16 Borenium ion catalysed ketimine reduction

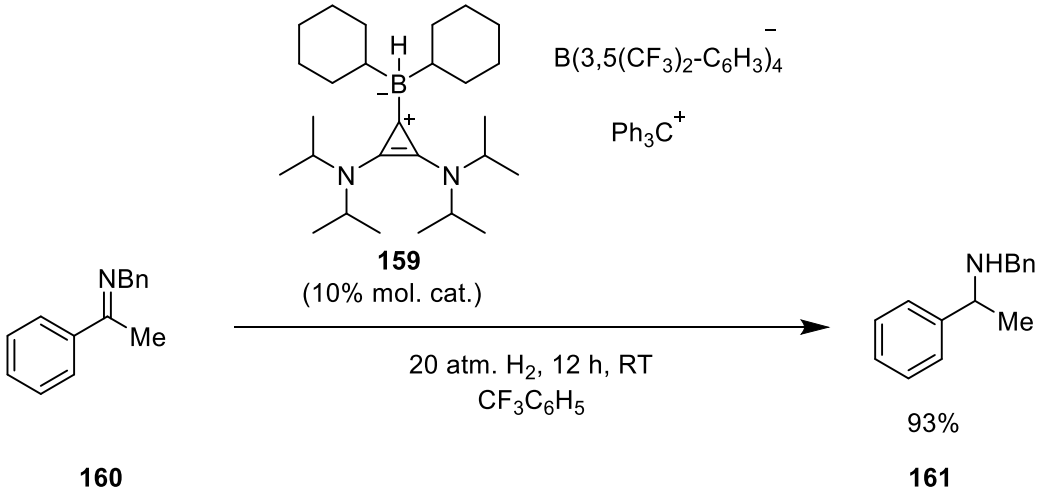

160 **161**

An *in situ* preparation of a borenium ion from dicyclohexylborane adduct **159** by hydride abstraction using trityl BArFate was found to be a useful catalyst for the reduction of unhindered benzyl ketimines, using hydrogen as the terminal reducing agent.

3.2 Results

3.2.1 Preparation of Bis(amino)cyclopropenium Salts

In order to prepare BAC precursors to investigate their proton-transfer chemistry, several methods from the literature were investigated and modified to enable access to the desired cyclopropenium salts.

3.2.1.1 Adapting Literature Procedures for Preparation of Bis(amino)cyclopropenium Salts

Scheme 3.17 Preparation of 129

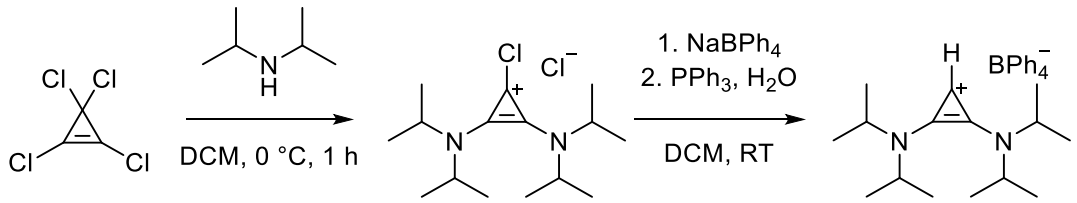

133 **162** **129**

The first method investigated was that employed by Bertrand[1], the synthetic methodology of which was adapted from the earlier Weiss[23] and Yoshida[8] work on cyclopropenium salts. Using the common starting material tetrachlorocyclopropene **133**, an excess of diisopropylamine was added at 0 °C. The reaction was exothermic and liberated HCl gas. To this solution, sodium tetraphenylborate was added, followed by addition of triphenylphosphine and water. Purification and isolation yielded **129** as an off-white solid. The proton-transfer chemistry of BAC **129** could not be explored due to solubility and stability difficulties associated with the tetraphenylborate counterion in water (Section 3.2.2).

Figure 3.3 Tetrafluoroborate salts 163 and 142

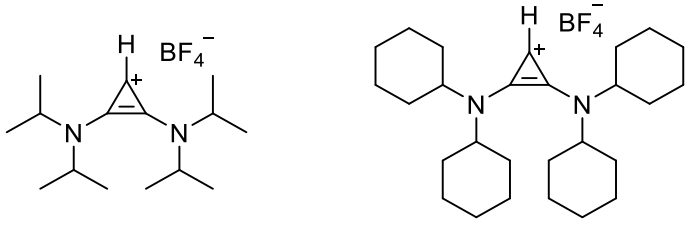

163 **142**

The procedure was modified by replacing sodium tetraphenylborate with $NaBF_4$ and with purification by recrystallization from cold DCM:Et_2O. This resulted in product **163**, which was found to be more suitable for further studies.

A second cyclopropenium salt **142** was prepared using dicyclohexylamine in place of diisopropylamine, following a literature procedure[10]. The large hydrophobic cyclohexyl groups of **142** necessitated purification by recrystallization from hot THF, due to increased solubility in diethyl ether.

3.2.1.2 Method Development for Preparation of Bis(1,2-diethylamino)cyclopropenium Tetrafluoroborate

Preparation of a BAC precursor using diethylamine proved more difficult. As found by Yoshida[8], diethylamine has insufficient steric bulk to prevent trisubstitution of the cyclopropenium ring. Wilde[9] reported that cooling to −78 °C with slow addition of diethylamine to the tetrachlorocyclopropene solution produced disubstituted chlorocyclopropenium **39**, the tetraphenylborate salt of which was purified by successive recrystallizations from hot methanol/H_2O and cold DCM/Et_2O.

Scheme 3.18 Preparation of 140

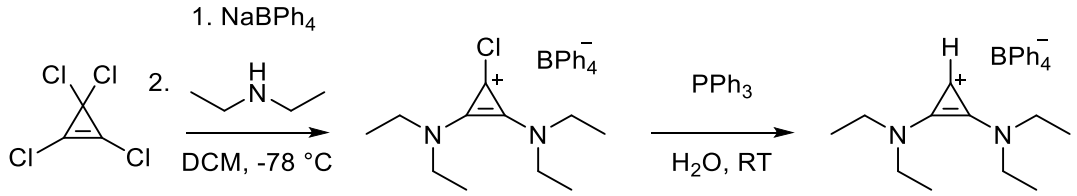

Early attempts following the procedure developed by Wilde were at first unsuccessful. The production of the disubstituted product **140** was contaminated by large amounts of competing trisubstituted product, which made the purification more difficult. It was found that pre-addition of sodium tetraphenylborate to a stirring solution of **133** before the addition of diethylamine provided purely disubstituted chlorocyclopropenium ion **164** (as determined by LCMS), with no trisubstitution. The use of triphenylphosphine successfully dechlorinated **164**. Purification of **140** was achieved by washing with cold water, sonication under diethyl ether and recrystallization from hot methanol and water. Allowing the methanol-water mixture to remain hot (~90 °C) for extended periods of time appeared to cause degradation of **140**.

Scheme 3.19 Preparation of 165 with contaminant 166

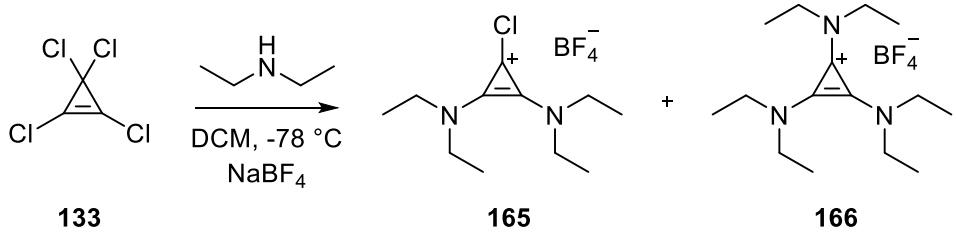

133 **165** **166**

Preparation of a BF_4^- analogue of **140** using the same method was not successful. Addition of $NaBF_4$ before diethylamine did not have the same effect of preventing the competing production of **40**. It was found that the amount of **40** produced could be limited by careful maintenance of the temperature at −78 °C, while adding diethylamine slowly with the use of a syringe pump. Two equivalents of diethylamine diluted in DCM were added over the course of 1 hour.

Scheme 3.20 Dechlorination of 166

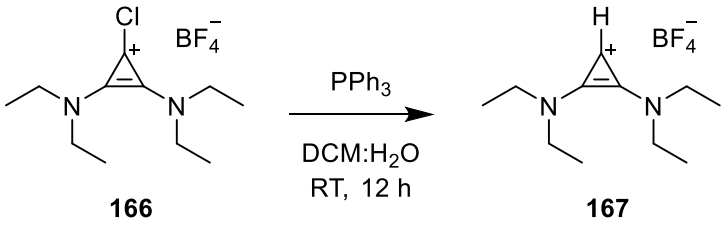

166 **167**

Unlike the preparations of **163** and **142**, cyclopropenium salt **167** could not be purified by any of the previously discussed methods. The crude mixture from this experiment contained large amounts of contaminating **166**, as well as by-products of triphenylphosphine use. A wide variety of conditions were employed in attempts to purify **167**, including trituration and recrystallization from a range of solvents. Although repeated trituration with diethyl ether removed the majority of triphenylphosphine oxide, various unidentified phosphorus containing species were detected (by ^{31}P and ^{1}H NMR spectroscopy) in the impure mixture, along with **166**.

Column chromatography under a range of conditions proved unsuccessful, only managing to separate triphenylphosphine oxide from the mixture. The other components co-eluted, and only under highly eluting conditions of acetonitrile or acetone.

Scheme 3.21 Representation of ion-exchange purification

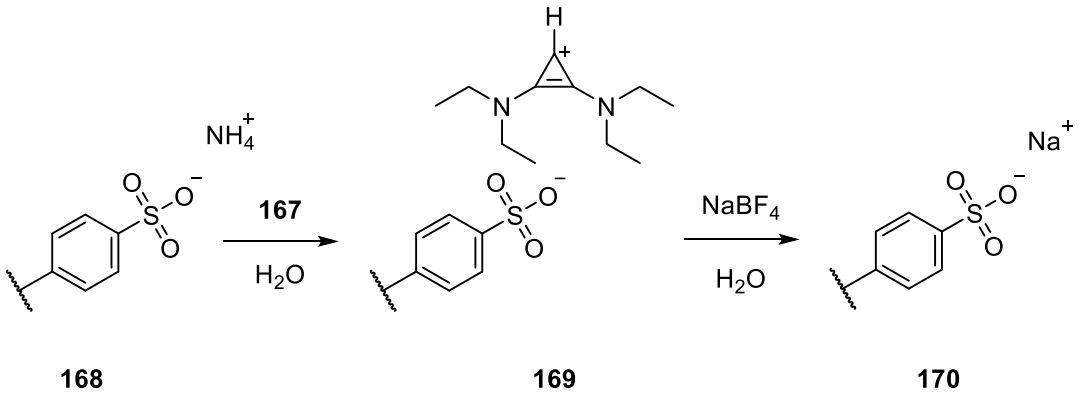

168 **169** **170**

The use of ion-exchange resin DOWEX 50X8[24] was investigated, in order to separate ionic **169** from non-ionic phosphine oxides and related by-products. The primed resin **168** was stirred over an aqueous solution of the impure **167** and was subsequently filtered off. The resin was then washed with aqueous tetrafluoroborate solution to elute **167**, however, with large amounts of phosphorus containing impurities. The use of reverse-phase HPLC purification also failed due to poor resolution of the product and contaminants.

Due to difficulties primarily assigned to the use of triphenylphosphine and its decomposition products, alternative methods for dechlorination of **165** were investigated. Alternative commercially available phosphines were considered to be either too pyrophoric (such as trimethylphosphine[25]) or to have by-products that would likely insufficiently differ in solubility and polarity to the already attempted triphenylphosphine (such as tributylphosphine). The other group of phosphorus(III) species that were investigated were phosphites, principally triethyl phosphite. Triethyl phosphite was chosen due to its inexpensive commercial availability and because triethyl phosphite **171** and decomposition product triethyl phosphate are highly soluble in hexane (unlike triphenylphosphine oxide), which was anticipated to ease purification.

Scheme 3.22 Triethyl phosphite method

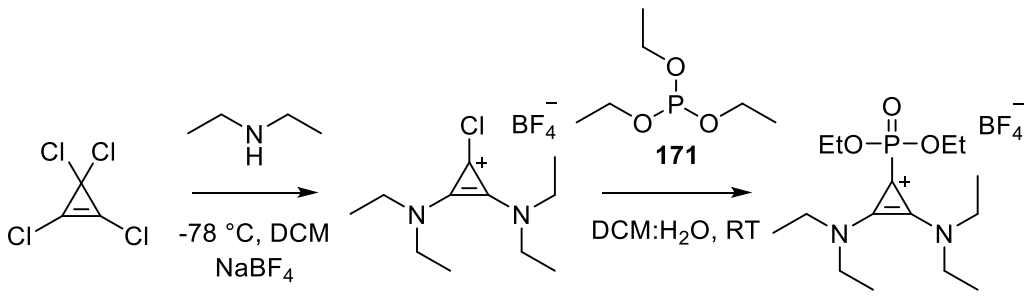

133 **165** **172**

Modification of the procedure to replace triphenylphosphine with triethyl phosphite did not result in the desired product **167**, but instead yielded the novel cyclopropenium phosphonate **172**, in an impure mixture with trisubstituted **166**.

Scheme 3.23 Hydrolysis of 172

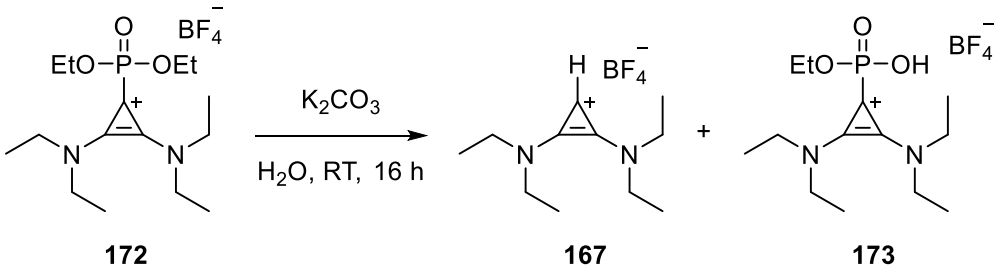

172 **167** **173**

Phosphonate **172** was stable and characterised by ^{31}P NMR and LCMS in the mixture Although stable to neutral water and acidic conditions, phosphonate **172** could be hydrolysed by two simultaneous routes by mild bases such as K_2CO_3, to give the desired cyclopropenium salt **167** and phosphonate **173**, presumably by removal of a BAC or ethanol respectively. Phosphonate **173** is likely zwitterionic in basic aqueous solutions (Me_2HPO_4 pK_a = 1.39)[26] and did not decompose further. It could be isolated from the reaction mixture by washing with DCM and collecting the aqueous layer, followed by evaporation and extraction using DCM of the residue. Subsequent filtration and concentration under reduced pressure yielded a brown ionic liquid **173**, which was characterised by HRMS, ^{1}H, ^{13}C and ^{31}P NMR spectroscopy as well as 2-dimensional NMR techniques.

The separated organic phase was found to contain a mixture of disubstituted product **167** with trisubstituted product **166**, and a smaller concentration of phosphorus containing by-products. Purification of this mixture was performed by HPLC, using a reverse phase Sunfire C18 19x100mm 5 µm column with an isocratic water:methanol (80:20) system at 10 mL/min with UV-Visible detector, to yield the pure product **167**, as a brown ionic liquid in overall poor yield (0.4%).

3.2.1.3 Further Preparation of Bis(amino)cyclopropenium Salts

The preparation of further BAC precursors was then explored. The synthetic methodology employed has been outlined previously for the preparation of diamino cyclopropenium salts[27–29] using secondary amines with low steric bulk. Starting from the easily accessible tris(amino)cyclopropenium salts, basic hydrolysis is used to obtain the corresponding cyclopropenone, which is then converted to the bis(amino)-chlorocyclopropenium salt by

reaction with oxalyl chloride. The chloro salt can theoretically be converted to the corresponding BAC precursor **178** by use of triphenylphosphine.

Scheme 3.24 Preparation of bis(dimethylamino)cyclopropenium tetrafluoroborate

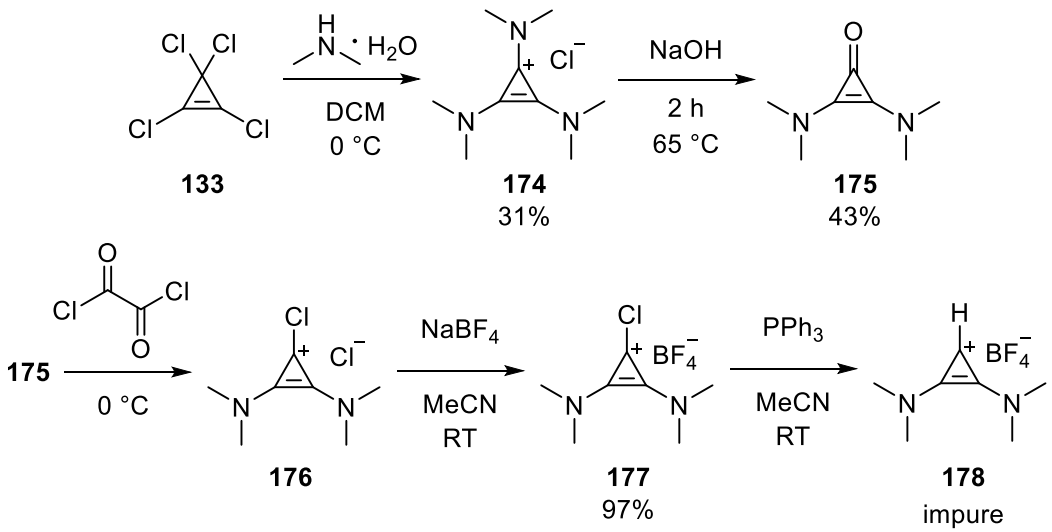

A preparation of the dimethylamino cyclopropenium ion **178** reported by Landau et. al[27] was repeated. As dimethylamine is gaseous at room temperature, commercially available solutions of dimethylamine in water and THF were used in these experiments, rather than neat amine. Due to the significantly greater nucleophilicity of dimethylamine compared to water, there was little competing hydrolysis of tetrachlorocyclopropene over the timescale studied, leading to high conversions to **174** in each case. Landau reported that purification of product **178** was not achieved (a later product in the process was successfully purified), a finding mirrored in our preparation of **178**. Although the presence of product **178** could be detected by ^{1}H and ^{13}C NMR spectroscopy and by mass spectrometry, purification proved impossible.

An area of particular interest to our studies was replacing the secondary alkyl amines with secondary anilines. Previous research on the proton-transfer of NHCs has shown reasonably large differences in the C2-H pK_as of N-alkyl imidazolium salts compared to their N-aryl equivalents[30]. Furthermore, there have been no reported literature examples of N-aryl BACs.

Figure 3.4* pK_a *of secondary amines

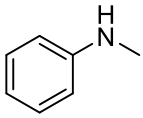

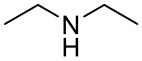

pK_a	4.85	10.84
	179	**180**

N-methylaniline **179** was chosen as the first aryl amine as a simple secondary aniline. Compared to diethylamine **180** for example, N-methylaniline has a significantly lower pK_a, potentially corresponding to a lower nucleophilicity (Figure 3.4)[31]. It was hoped that this lower nucleophilicity would lead to a more manageable reactivity with tetrachlorocyclopropene.

Scheme 3.25 Preparation of tris(N-methylanilino)cyclopropenium tetrafluoroborate 181.

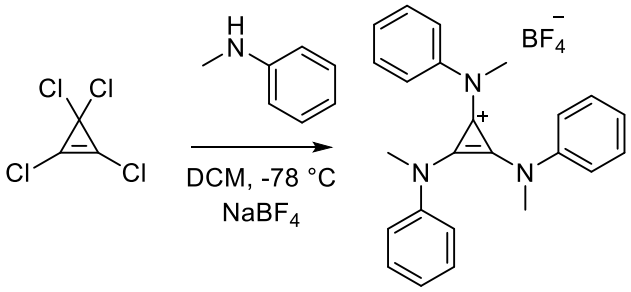

133 **181** 71%

Adding N-methylaniline to a stirring solution of tetrachlorocyclopropene in DCM at 0 °C yielded only trisubstituted product **181**, even when added slowly. Changing conditions to −78 °C and adding slowly with a syringe pump also yielded only **181**, with no detectable amount of the desired disubstituted cyclopropenium species by LCMS or NMR spectroscopy. The addition of sodium tetraphenylborate before addition of N-methylaniline also yielded only **181**, in contrast to experiments with diethylamine.

Scheme 3.26 Formation of 184 by hydrolysis of 181 to cyclopropenone 149 and chlorination by oxalyl chloride.

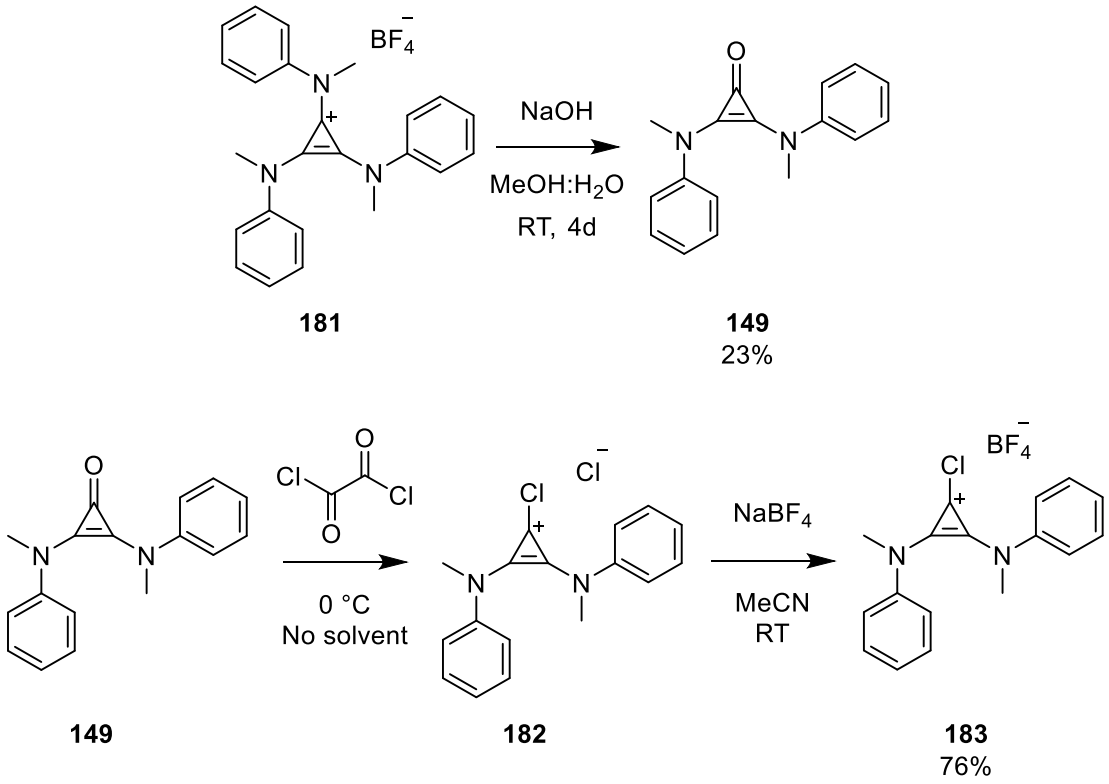

Hydrolysis of trisubstituted product **181** to the cyclopropenone **149** followed by chlorination with oxalyl chloride following a literature procedure formed chloride salt **182**. Ion exchange of chloride ion for tetrafluoroborate gave **183**, which was used directly in reaction with triphenylphosphine.

Scheme 3.27 Phosphorylation of 183

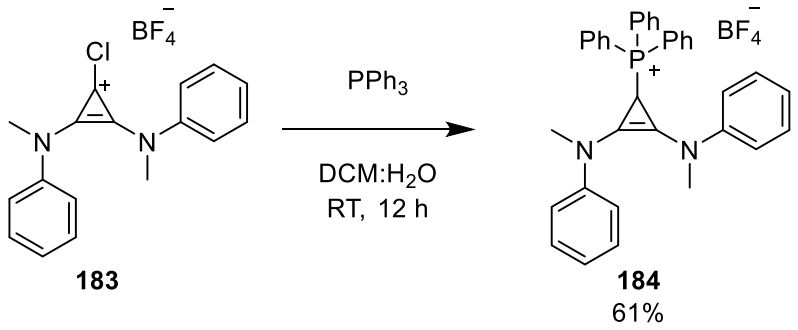

The desired product was however not obtained, instead forming a phosphonium species **184**. Stirring **184** in water at room temperature and at reflux did not yield the desired BAC precursor.

Scheme 3.28 Attempted BAC precursor preparation using 2-nitroaniline 185.

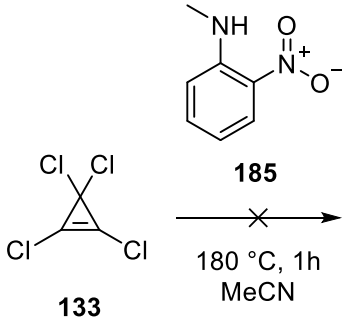

N-Methyl-2-nitroaniline failed to react with tetrachlorocyclopropene at room temperature overnight, and after heating to 180 °C by microwave for 1 hour also did not yield any identifiable reaction products. The parent 2-nitroaniline has a pK_a of −0.26[31], therefore it is likely that the secondary amine equivalent **185** has similarly low basicity and poor nucleophilicity in addition to being sterically bulky.

Scheme 3.29 Attempted preparation of BAC precursors with highly bulky amines

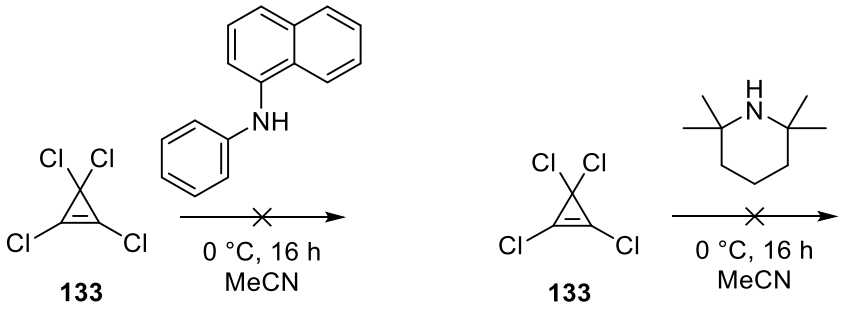

The use of very bulky amines such as 2,2,6,6-tetramethylpiperidine and N-(2-napthyl) phenylamine did not show any reaction with **133** overnight, in contrast to other amines. This effect is assigned to excessive steric hindrance preventing formation of either disubstituted or trisubstituted products.

3.2.2 Proton-Transfer Chemistry of Bis(amino)cyclopropenium Salts

The proton-transfer chemistry of BACs has not been previously studied in detail. Limited H/D exchange experiments were conducted by Weiss[23,32], which determined that H/D exchange under highly acidic conditions occurred with an electrophilic aromatic substitution mechanism through a dicationic intermediate.

Scheme 3.30 Acid-catalysed H/D exchange in cyclopropenium salts

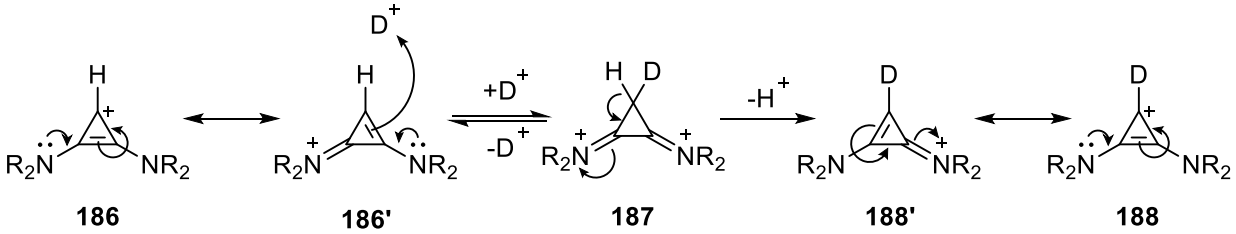

Weiss[23] did not find that BAC precursors underwent H/D exchange at neutral p*H*, suggesting that the pK_a is relatively high, provided that the mechanism follows the typical mechanism of H/D exchange *via* a carbene.

Scheme 3.31 Early H/D exchange experiments

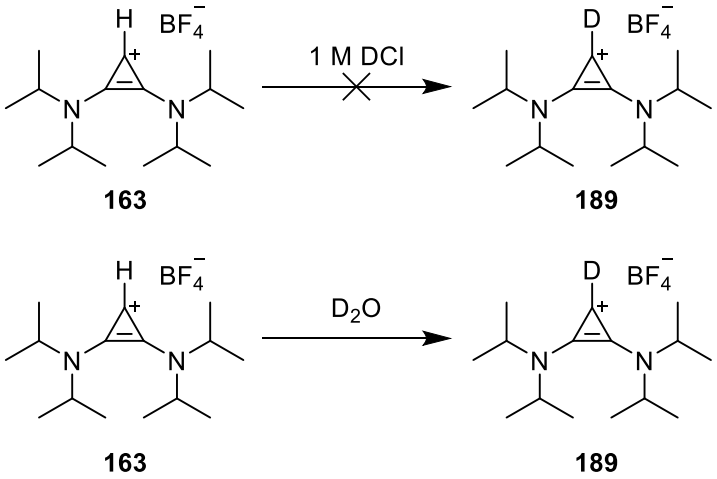

These early H/D exchange experiments reported that bis(diisopropylamino)cyclopropenium tetraphenylborate **140** was poorly soluble in water. The tetraphenylborate counterion was also found to be vulnerable to protonolysis over time (to triphenylborane and benzene)[33,34], under acidic conditions. Replacement of the tetraphenylborate salt **140** with the tetrafluoroborate salt **163** resulted in far greater stability and solubility. Small samples of tetrafluoroborate salt **163** were dissolved in 1 M DCl solution, neutral D_2O and 1 M NaOD solution. No H/D exchange was observed under acidic conditions, whereas very slow H/D exchange was observed in neutral D_2O and complete H/D exchange in under 5 minutes was observed under the strongly basic conditions.

Figure 3.5 Simple alkyl aminocyclopropenium salts

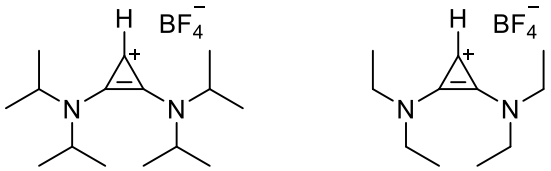

163 **167**

Deuterium exchange reactions on **163** and **167** were carried out in buffered D_2O solutions of acetate or phosphate, in the p*D* range of ~3-8 and I = 1.0 (KCl) with an internal standard of tetramethylammonium deuteriosulfate (~1 mM).

Exchange of the C(3)-H proton for deuterium was followed by ^{1}H NMR spectroscopy (400 and 500 MHz). Representative spectra of the H/D exchange of **163** are shown in Figure 3.6. Disappearance of the singlet at 7.4 ppm over time is assigned to hydrogen-deuterium exchange of the C(3)-H atom. Other signals corresponding to the isopropyl amino group protons are present as septets and doublets at 3.9 and 1.3 ppm. No change was observed in the integrated areas of the other peaks, relative to the internal standard, which indicates that neither H/D exchange nor other chemical reactions occurred in any significant amount under these conditions.

Figure 3.6 Representative ^{1}H NMR (500 MHz) spectra of 163 at* p*D 7.70 obtained during exchange of the C3-H (s, 7.4 ppm) for deuterium in D_2O at 25 °C and I = 1.0 (KCl).

[Internal standard, tetramethylammonium deuteriosulfate (s, 3.17 ppm)] over time at 25 °C, I = 1.0

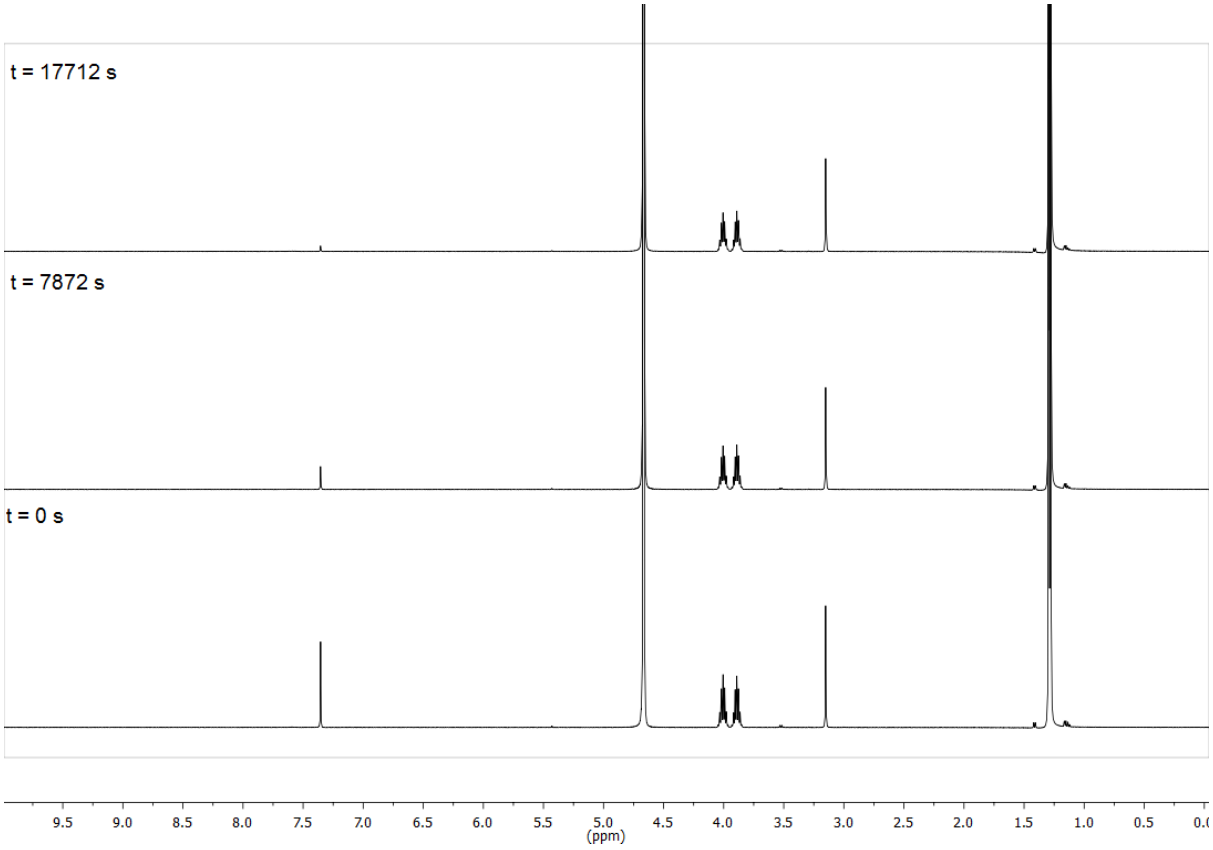

In a similar manner, hydrogen-deuterium exchange was followed for N-ethyl cyclopropenium salt **167**. Representative spectra taken over time at p*D* 7.56 are shown in Figure 3.7. As with **163**, there was no change in the integration of other peaks relative to the internal standard of NMe_4 DSO_4.

Figure 3.7 Representative ^{1}H NMR (500 MHz) spectra of 167 at* pD *7.56 over time at 25 °C, I = 1.0

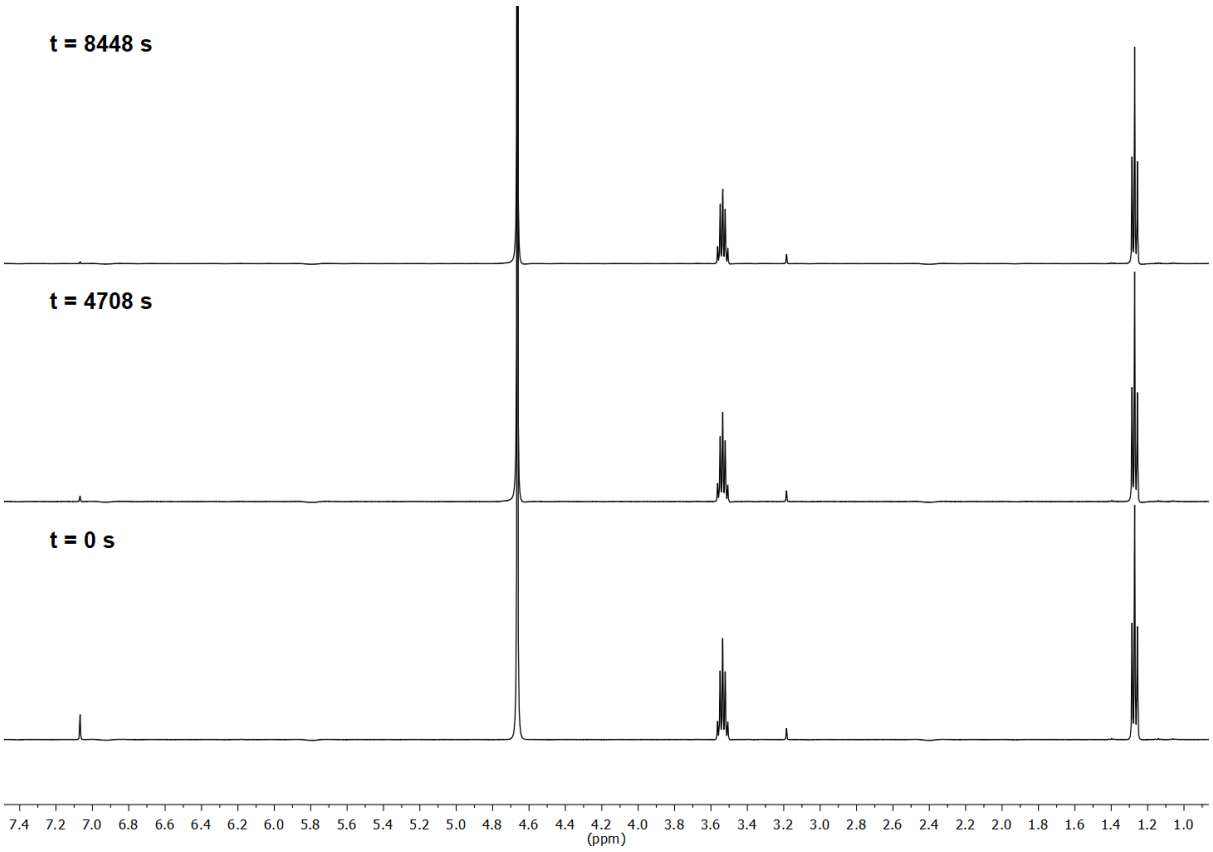

The progress of the deuterium exchange reaction was followed by the decrease of the area of the singlet signal at ~7.4 ppm, corresponding to the C(3) proton of the cyclopropenium ions, against the internal standard peak at ~3 ppm, corresponding to the twelve methyl protons of NMe_4 DSO_4, which are known to be non-exchanging under these conditions.

Equation 3.1

$$f(s) = \frac{\left(A_{C(3)H}/A_{std}\right)_t}{\left(A_{C(3)H}/A_{std}\right)_{t0}}$$

The fraction of protonated substrate remaining was determined using Equation 3.1. Representative plots of *f*(s) against time with non-linear least square fitting are shown in Figure 3.8 for **163** and **167**. Experimentally observed pseudo first-order rate constants for exchange, k_{ex} (s^{-1}), were determined using non-linear least square fitting of *f*(s) against time to a first-order exponential decay (Equation 3.2)

Equation 3.2

$$f(s) = e^{-kt}$$

Figure 3.8 (a-b) Example plots of first-order decay of C(3)H signal over time of a) 163 at 25 °C I = 1.0* p*D 7.70 b) 167 at 25 °C I = 1.0* p*D 7.56

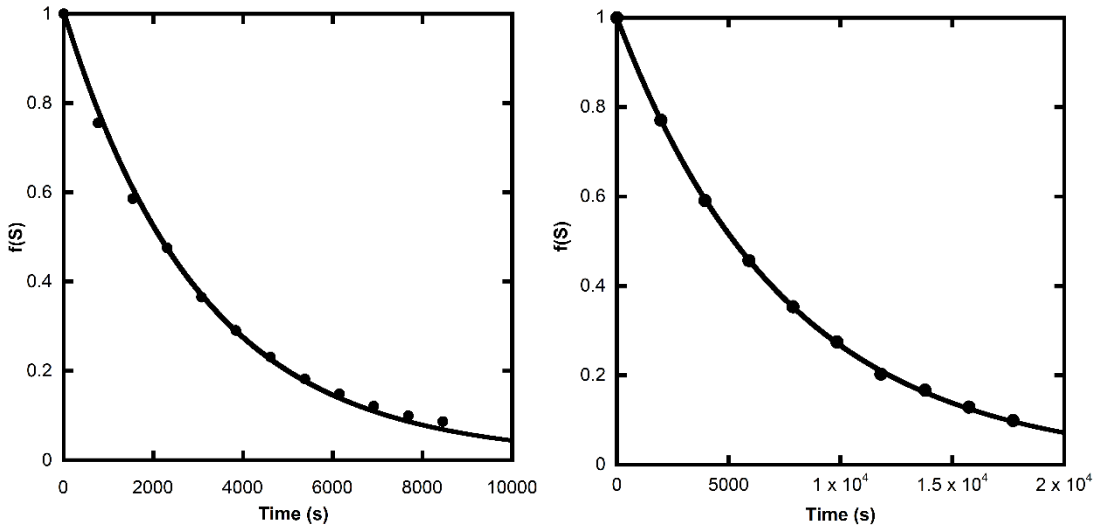

Table 3.1 details the reaction data and k_{ex} values. The concentration of deuteroxide is given by Equation 3.3 where K_w is the ionic product of D_2O under standard conditions ($10^{-14.87}$ M^2). The apparent activity coefficient of deuteroxide γ_{DO} = 0.73 has been previously determined at I = 1.0 (KCl)[35].

Equation 1.3

$$[DO^-] = \frac{10^{(pD - pK_W)}}{\gamma_{DO}}$$

Table 3.1 Reaction data and first-order rate constants for exchange of the C3 proton of cyclopropenium salts at 25 ºC, I = 1.0

Cyclopropenium	Buffer	p*D*	[DO^-] (M)	k_{ex} (s^{-1})
163	10% DPO_4^{2-}	5.51	5.98×10^{-10}	1.04×10^{-6}
	25% DPO_4^{2-}	6.13	2.49×10^{-9}	3.30×10^{-6}
	50% DPO_4^{2-}	6.73	9.92×10^{-9}	1.95×10^{-5}
	75% DPO_4^{2-}	7.13	2.49×10^{-8}	2.98×10^{-5}

	90% DPO_4^{2-}	7.70	9.26×10^{-8}	1.33×10^{-4}
	75% fb AcO^-	5.52	6.13×10^{-10}	2.58×10^{-6}
	10% DPO_4^{2-}	5.88	1.40×10^{-9}	6.58×10^{-6}
167	50% DPO_4^{2-}	6.90	1.47×10^{-8}	8.11×10^{-5}
	75% DPO_4^{2-}	7.48	5.58×10^{-8}	2.52×10^{-4}
	90% DPO_4^{2-}	7.56	6.72×10^{-8}	3.29×10^{-4}

From this data, second-order rate constants for deuteroxide catalysed exchange k_{DO} (M^{-1} s^{-1}) were obtained as the slopes of plots of k_{ex} (s^{-1}) against the concentration of DO^-. Assuming the mechanism is the same as for NHCs, an estimate of pK_a can be determined from analysis of these rate constants.

Figure 3.9 Plot of k_{ex} against* [DO]$^-$ *for cyclopropenium salt 163 at 25 °C, I = 1.0

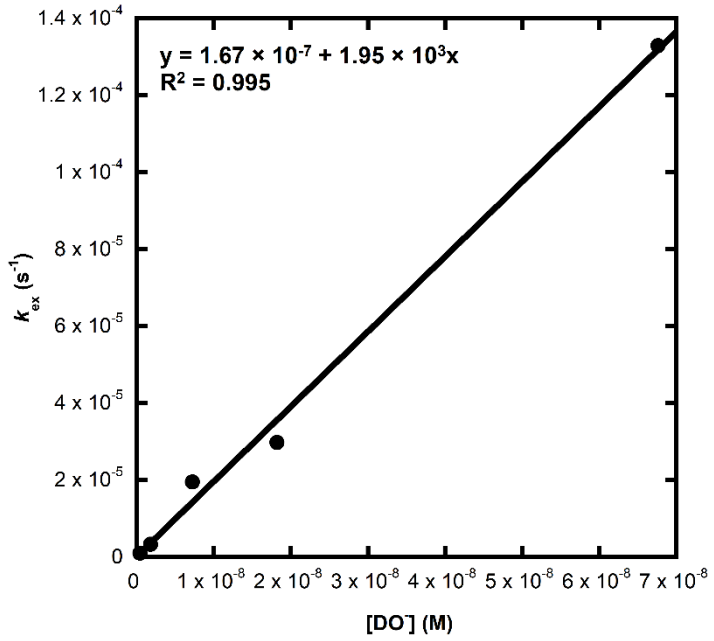

Figure 3.10 Plot of k_{ex} against $[DO]^-$ for cyclopropenium salt 167 at 25 °C, I = 1.0.

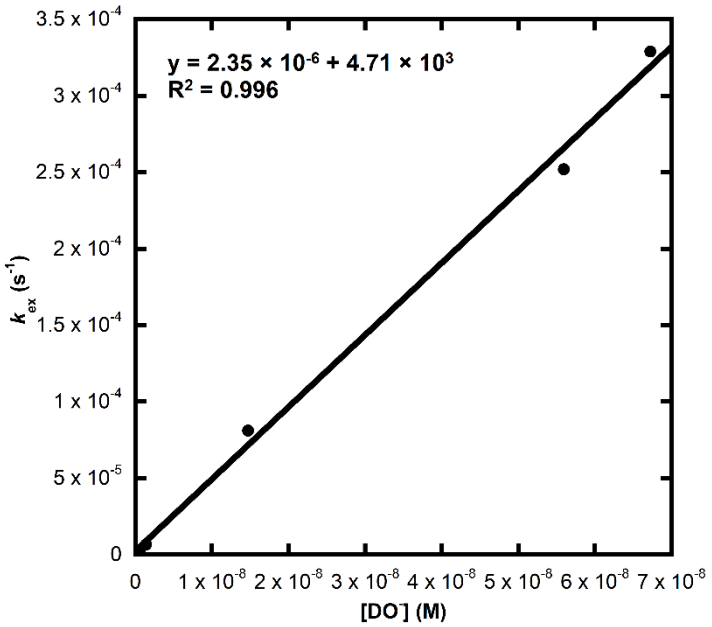

3.2.2.1 Further Evidence for C(3)-H/D exchange

In order to investigate the mechanism of proton-transfer chemistry of **163** and **167**, further experiments were performed. The disappearance of the C(3)H peak was confirmed to be a result of H/D exchange as opposed to decomposition by the use of ^{2}H NMR spectroscopy. ^{13}C NMR spectroscopy experiments were predicted to show a triplet signal at C3, however due to the relatively low solubility of **189** in D_2O and, loss of Nuclear Overhauser Effect enhancement, a signal could not be identified.

Figure 3.111 ^{2}H NMR (107 MHz) spectrum of 189 in D_2O solution.

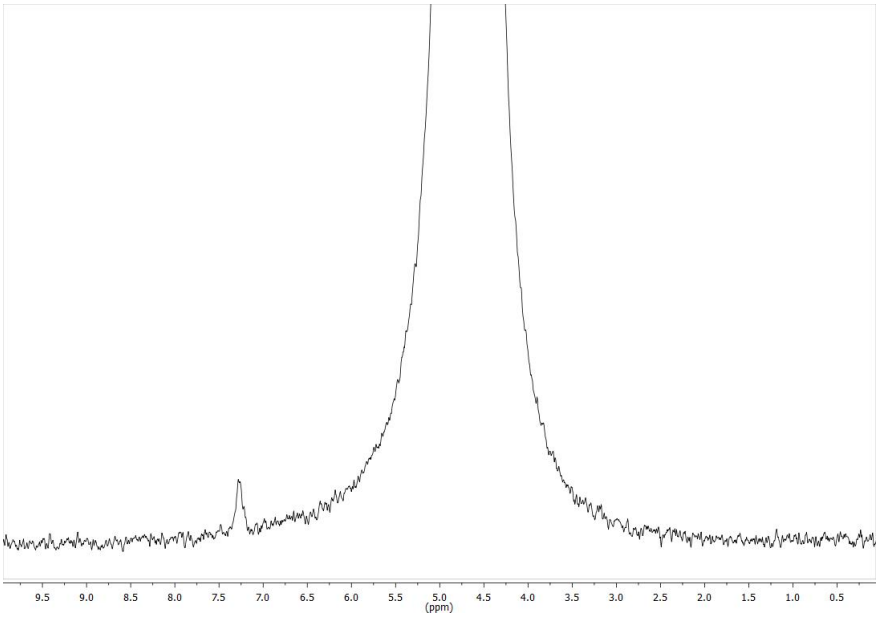

The ^{2}H NMR spectroscopy experiment showed two signals: a very large signal corresponding to D_2O and a small singlet signal at 7.27 ppm. This signal is within error of the previous C(3)H proton at 7.35 ppm, and was assigned to the product of H/D exchange **189**.

The effect of varying buffer concentration was also studied. Previous examples of NHC H/D exchange do not show any significant buffer catalysis.

Table 3.2 Reaction data and first-order rate constants for exchange of the C3 proton of cyclopropenium salt 163 at 25 ºC, I = 1.0 at varied phosphate buffer concentration.

[B$^-$] M	p*D*	[B$^-$]/[DO$^-$]	k_{ex} (s^{-1})	k_{rel}
0.025	6.13	1.37×10^{7}	3.30×10^{-6}	0.93
0.0125	6.20	5.85×10^{6}	4.00×10^{-6}	0.95
0.00625	6.17	3.13×10^{6}	3.66×10^{-6}	0.94

Exchange experiments with varied concentration of phosphate buffers were performed at fixed p*D*, constant ionic strength and temperature. Figure 3.12 shows a plot of k_{rel} (Equation 3.4) against [B$^-$]/[DO$^-$], accounting for the slight variation in p*D* from dilution of buffer at constant ionic strength. The slope of this graph is the ratio of rate constants of buffer catalysis over deuteroxide catalysed exchange.

Equation 3.4

$$k_{\mathrm{rel}} = \frac{k_{\mathrm{ex}}}{k_{\mathrm{DO}}[\mathrm{DO}^-]} = \frac{(k_{\mathrm{DO}}[\mathrm{DO}^-] + k_{\mathrm{B}}[\mathrm{B}^-])}{k_{\mathrm{DO}}[\mathrm{DO}^-]} = 1 + \frac{k_{\mathrm{B}}[\mathrm{B}^-]}{k_{\mathrm{DO}}[\mathrm{DO}^-]}$$

Figure 3.12 Plot of k_{rel} against [B⁻]/[DO⁻] for cyclopropenium salt 163 at 25 °C, I = 1.0.

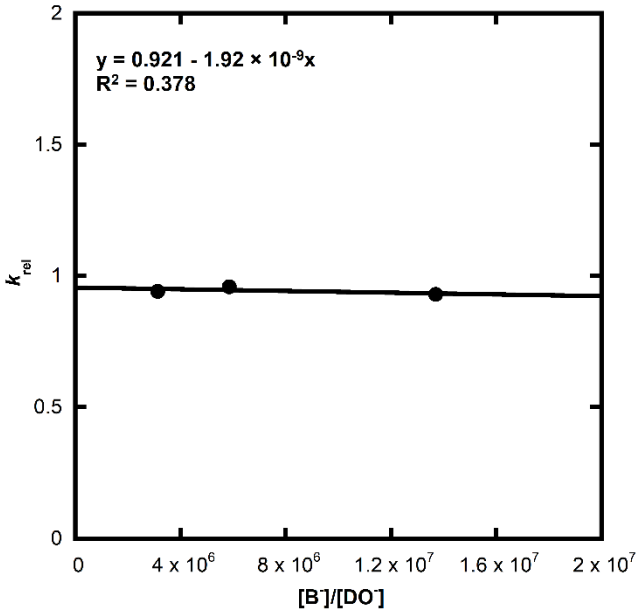

The slope of this graph is within error of zero, indicating that buffer catalysis is insignificant for this reaction. The R^2 value of 0.378 indicates poor quality of fit, due to the very small magnitude of the slope and fitting to three similar points of data.

3.2.2.2 Determination of k_{HO} and pK_a of BACs

As discussed in Chapter 2, the pseudo first-order rate constant for H/D exchange, k_{ex}, Equation 3.5 potentially includes terms for catalysis by deuteroxide (k_{DO}, M^{-1} s^{-1}), buffer base (k_B (M^{-1} s^{-1}), as well as for reaction with solvent (k_{D2O}, s^{-1}).

Equation 3.5

$$k_{ex} = k_{DO}[DO^-] + k_{D2O} + k_B[B]$$

Our experiments in 1 M DCl did not reveal any H/D exchange over 3 days, suggesting that rate constants continue to decrease with p*D* rather than levelling to a p*D*-independent reaction. Additionally, the data analysis in Figure 3.12 indicates a lack of significant buffer catalysis. From this, we can reasonably assume the mechanism of H/D exchange is *via* a BAC, with deuteroxide-catalysis analogous to that observed for the NHCs. Additionally, there was no deviation from a linear dependence on deuteroxide, indicating a single mechanism of exchange.

The previously determined second-order rate constants of deuteroxide exchange can be used to make an estimate of pK_a and carbon acidity by Equation 3.6

Equation 3.6

$$\mathrm{p}K_a = \mathrm{p}K_W + \log_{10}\left(\frac{k_{\mathrm{HOH}}}{k_{\mathrm{HO}}}\right)$$

As exchange is believed to proceed *via* a BAC, with rate-determining solvent reorganisation, the secondary solvent kinetic isotope effect ($\underline{k}_{\mathrm{DO}}/k_{\mathrm{HO}}$ = 2.4) is the same as in NHC experiments. Furthermore, as previously discussed, the rate of reprotonation is also assumed to be the same as that of NHCs, $k_{\mathrm{HOH}} = k_{\mathrm{reorg}} = 10^{11}$ s^{-1}. The results are presented in Table 3.3Table , using Equation 3.6 where pK_{w} = 14.

Table 3.3 Second-order rate constant and estimate of* pK_{a} *of BACs

Cyclopropenium	k_{DO} (M^{-1} s^{-1})	k_{HO} (M^{-1} s^{-1})	pK_{a}
163	1.95×10^3	8.12×10^2	22.1
167	4.71×10^3	1.96×10^3	21.7

3.2.3 Novel Cyclopropenium Phosphonates and Mechanistic Studies of Hydrolysis.

Scheme 3.32 Products of hydrolysis of phosphonate 172

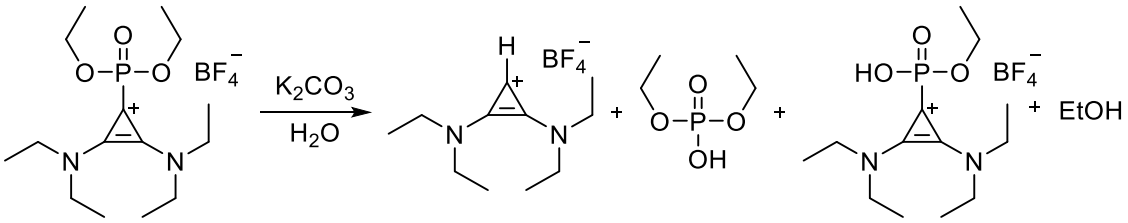

172 **167** **173**

In the synthetic preparation of the diethylamine-derived cyclopropenium **167** (Section 3.2.1.2), it was serendipitously discovered that novel cyclopropenium phosphonate **172** could be produced from the reaction of the chlorocyclopropenium **165** with triethyl phosphite. Furthermore, the hydrolysis of **172** led to an unusual partitioning of products, presumably from the competitive elimination of ethoxide ion compared to cyclopropenylidene to give **167**. This was of particular interest, as there is the potential for a comparison of leaving group ability of the bis(amino)cyclopropenylidenes against a nucleofuge, ethoxide ion, of well-established basicity. This could provide further insight into the relative nucleophilicity, stability and proton-transfer chemistry of bis(amino)cyclopropenylidenes.

3.2.3.1 Preparation of Phosphonato Cyclopropenium Salts

Purification of the original **172** was not accomplished, due to the seemingly unavoidable simultaneous production of trisubstituted **166**, therefore further synthetic procedures were developed.

Scheme 3.33 Preparation of 191

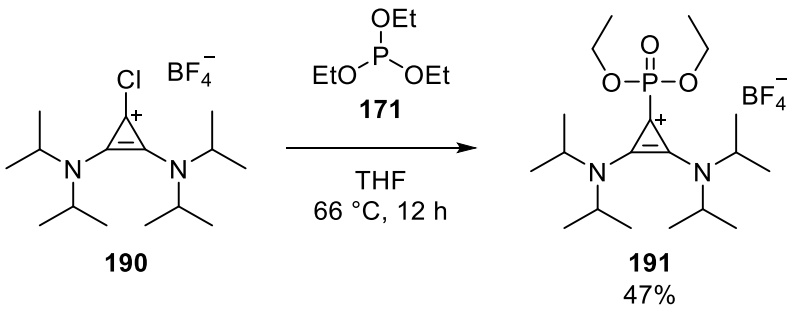

Easily accessible **190** was obtained by reaction of diisopropylamine and tetrachlorocyclopropene, stirring over sodium tetrafluoroborate, followed by recrystallization from DCM:Et_2O. When **190** was stirred overnight in a solution of triethyl phosphite in DCM, no reaction was observed by LCMS, ^{1}H and ^{31}P NMR spectroscopy. Repeating this experiment overnight in refluxing THF proved successful, producing **191** in reasonable yield after purification by trituration with diethyl ether to remove excess phosphite and by-products, followed by recrystallization from DCM/Et_2O. Characterisation was performed by ^{1}H, ^{13}C and ^{31}P NMR spectroscopy, along with mass spectrometry, IR and single crystal X-ray diffraction, which confirmed the suggested structure.

Figure 3.13 Crystal structure of 191

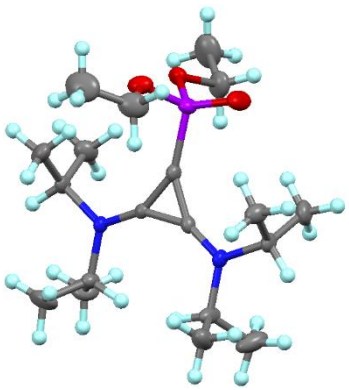

Scheme 3.34 Preparation of cyclopropenium phosphonates by microwave heating

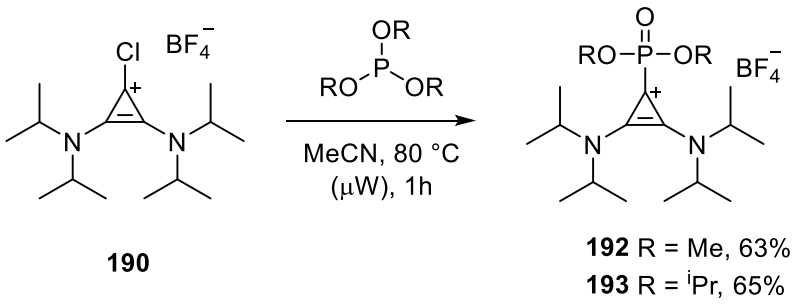

190

192 R = Me, 63%
193 R = ^{i}Pr, 65%

Further modification of the procedure by changing from an overnight reflux in THF to shorter microwave heating (1 h, 80 °C) in acetonitrile was successful in obtaining two further phosphonates: **66** and **67**, in higher yield than the diethyl equivalent. A structure of **67** obtained by single-crystal X-ray diffraction confirms is analogous those obtained for **47** and **65**.

Figure 3.14 Crystal structure of cation of 193

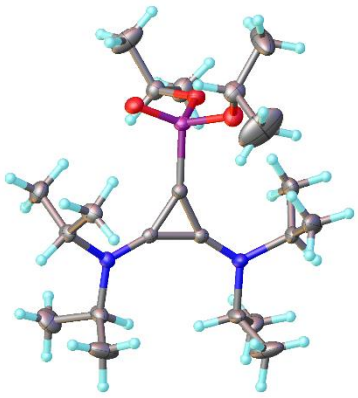

The use of electron-poor phosphites to form cyclopropenium phosphonates was investigated, due to their potentially different chemistry from better leaving group ability of their corresponding alcohols.

Triphenyl phosphite and tris(2,2,2-trifluoroethyl) phosphite were chosen for their commercial availability and lower pK_a of their corresponding alcohol leaving groups, phenol (pK_a = 10.0) and 2,2,2-trifluoroethanol (pK_a = 12.4) respectively, compared to ethanol (pK_a = 16.0)[36,37]. Reactions at room temperature did not yield any of the desired products with either phosphite by LCMS or ^{31}P NMR. Reactions at 55 °C overnight in $CDCl_3$ also did not produce the desired products, with partial decomposition of the phosphites to their respective phosphates observed.

Scheme 3.35 Attempted preparation of O-phenyl cyclopropenium phosphonate 194

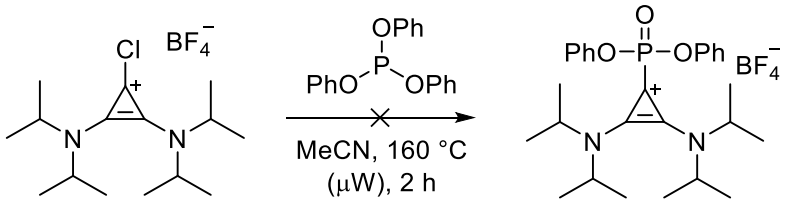

190 **194**

Higher temperatures and longer reaction times were applied. Heating at 100 and 140 °C gave minimal reaction but the reaction of triphenyl phosphite with **190** at 160 °C for 2 hours gave a small peak in crude LCMS of the correct molecular formula, which was confirmed by high resolution mass spectrometry. Attempts at purification, however, yielded only cyclopropenium **163** and what is believed to be triphenyl phosphate. ^{31}P and ^{1}H NMR peaks assignable to the desired **194** were either not present or masked entirely by large amounts of impurities, suggesting that the overall yield of **194** is very small, and unsuitable for purification.

Scheme 3.36 Attempted preparation of cyclopropenium phosphonate 195

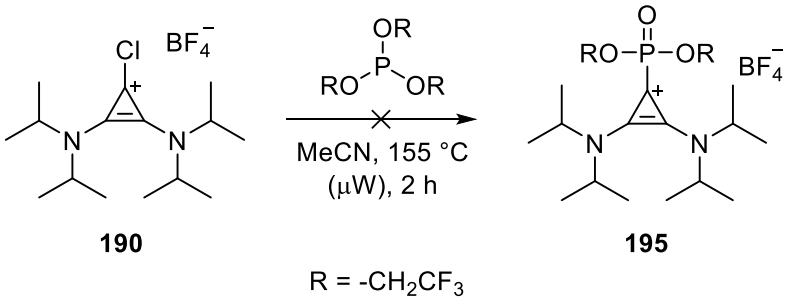

190 **195**

Reactions with tris(2,2,2-trifluoroethyl) phosphite at 155 °C for 2 hours or 140 °C for 30 minutes did not yield any detectable quantity of the desired product **195**.

Scheme 3.37 Cyclopropenium Finkelstein-like reaction

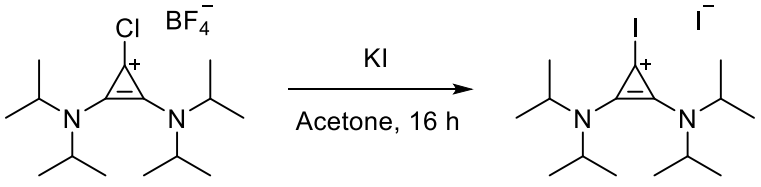

190 **196**
74%

It was postulated that the lack of reaction in previous examples was due to a combination of the poor nucleophilicity of the phosphites in conjunction with the poor leaving group ability

and nucleophilicity of the chloride leaving group. The chlorine atom of **190** was replaced by iodine using the Finkelstein reaction based on a literature procedure[38] stirring overnight in acetone with a large excess of sodium iodide, which produced bis-1,2-(diisopropylamino)-3-iodocyclopropenium iodide **196**.

Figure 3.15 Unusual crystal structure of 196.

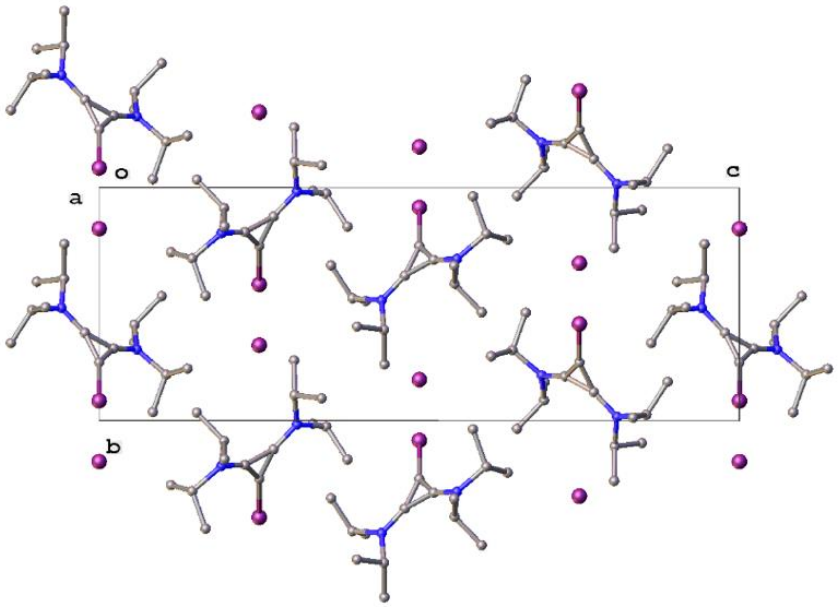

Interestingly, **196** has a highly unusual crystal structure. Both cation and anion are located in special positions on a 2-fold axis, meaning that the centre of cation and anion are within symmetry elements of the crystal structure. The unusual positioning of these groups is possibly due to poor coordination from the cyclopropenium ion and the iodide, resulting in preferential interactions between the "naked" iodide and the electron-poor cyclopropenium iodine[14,39].

Scheme 3.38 Ion-exchange of 197.

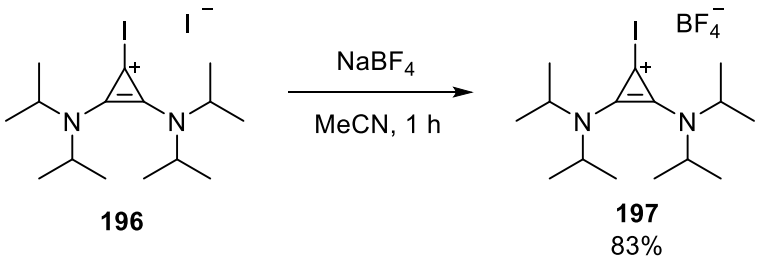

It was considered that the presence of the somewhat nucleophilic iodide counterion could interfere with further reactions, so tetrafluoroborate salt **197** was prepared by stirring **196** in a suspension of sodium tetrafluoroborate.

The use of 1,2-bis(diisopropylamino)-3-iodocyclopropenium tetrafluoroborate **197** in the reaction with electron-deficient phosphites did not produce any of the desired phosphonate products, instead producing a higher yield of **163** than from the reaction with chloride equivalent **190**.

3.2.3.2 Hydrolysis of Phosphonato Cyclopropenium Salts

As previously discussed, phosphonate **172** showed unusual products of hydrolysis under basic conditions. Contrary to what would be suggested by the previously determined pK_a of BACs and ethanol, significant proportions of BAC were eliminated from the complex. As the pK_a of cyclopropenium **163** is significantly greater than of ethanol, the predominant expulsion of ethoxide ion could be predicted based on the lower basicity.

A series of ^{31}P NMR spectroscopic experiments were performed in order to probe the kinetics of the hydrolysis of phosphonate **191**. Initial experiments on the hydrolysis of **191** determined that hydrolysis did not occur at p$D \approx 1$ or in neutral D_2O over a week. Hydrolysis occurred on an accessible timescale in approximately the pD 9-11 range, and increasing in rate at higher pD.

Figure 3.39 Hydrolysis products of 191.

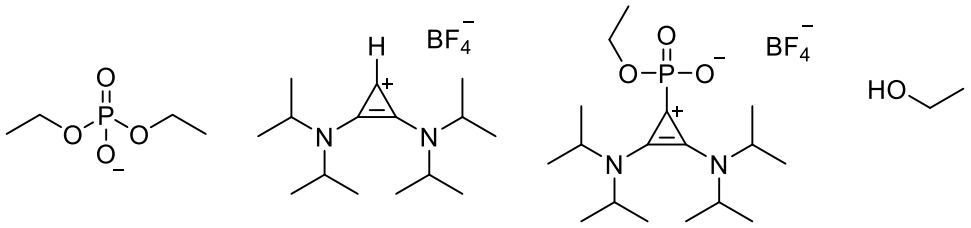

163 **198**

The products of hydrolysis (Figure 3.16) were characterised *in situ* by ^{1}H and ^{31}P NMR spectroscopy and mass spectrometry. Diethyl phosphoric acid has a pK_a of 1.39[26], and the zwitterionic phosphonate **198** is likely to have a significantly lower pK_a than ethyl phosphonic acid (pK_a = 2.39)[40], due to the effect of the positively charged cyclopropenium substituent. It is therefore assumed that both products will be fully deprotonated in the studied pH range. Therefore, each mole of hydrolysis product will donate one mole of protons to solution.

Due to the product acidity, relatively concentrated buffers were required in order to keep reasonably consistent pH through the course of the reaction. This also reduced the amount of phosphonate that could be used (~4 mg, at least 1:9 **191**:CO_3^{2-}) which limits the precision of the measurements.

3.2.3.2.1 Kinetic Analysis of Cyclopropenium Phosphonate Hydrolysis

Hydrolysis experiments were performed in aqueous solutions of **191** buffered with K_2CO_3 (0.5 M) in the range of 9-10 p*H* at 25 °C and I = 1.0 (KCl). An internal standard of K_3PO_4 (sat.) in a D_2O lock tube was used in each experiment. The experiments were initiated by addition of buffered aqueous solution to a sealed vial of **191**, which was quickly agitated to ensure full solution. The reactions were monitored by 162 MHz ^{31}P NMR spectroscopy and incubated in a water bath thermostated at 25 °C. Faster reactions ($t_{1/2}$ < 4 h) required monitoring by a thermostated 202 MHz ^{31}P NMR spectrometer at 25 °C directly.

The progress of the reaction was followed by the decrease of the quintet signal corresponding to the phosphorus atom of **191** at −2.25 ppm, compared to that of the internal standard K_3PO_4 at approximately 0 ppm.

Equation 3.7

$$f(s) = \frac{(A_P/A_{std})_t}{(A_P/A_{std})_{t0}}$$

The fraction of remaining phosphonate f(s) **191** was determined using Equation 3.7 from which observed pseudo first-order rate constants of decomposition k_{obs} (s^{-1}) can be determined by least-squares fitting the decrease of the signal corresponding to the P atom of **191** over time to a pseudo first-order exponential decrease.

Representative spectra of three-time points during the hydrolysis of **191** at conditions of p*H* 9.73 (0.5 M K_2CO_3) are shown below (Figure 3.17). Disappearance of the quintet at −2.25 ppm is simultaneous to the increase of a quintet at +0.5 ppm corresponding to diethyl phosphate and triplet at −7.5 ppm corresponding to phosphonate **198**. This latter peak was assigned to **198** by comparison with the NMR spectroscopy data of **173**, correct ^{31}P multiplicity and the confirmation by HRMS of the presence of **198**. Diethyl phosphate was also identified by HRMS. The internal standard phosphate is present at +4.5 ppm. Also visible is a singlet peak corresponding to contaminant pyrophosphate (−6.4 ppm) in the internal standard, formed during flame annealing.

Figure 3.17 Representative ^{31}P NMR (162 MHz) spectra of the hydrolysis of 191 in H_2O solution at 25 C, I = 1.0,* p*H = 9.73

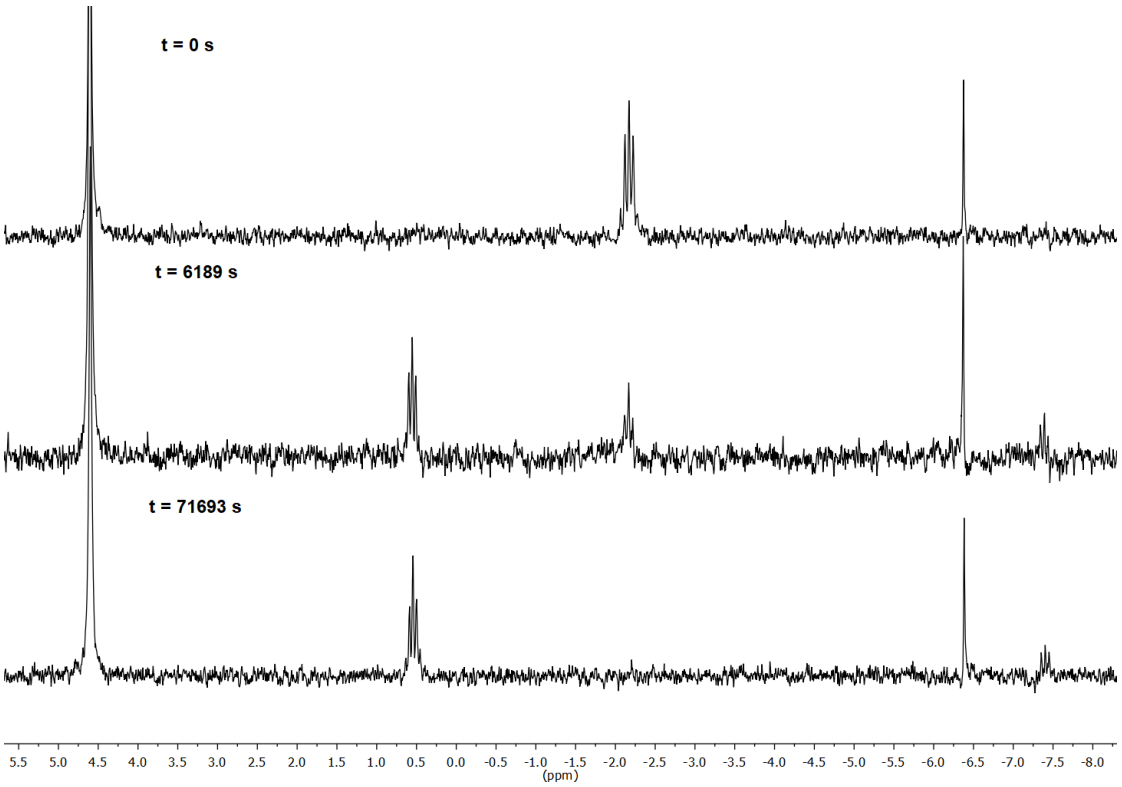

Table 3.4 shows the reaction data and fitted k_{obs} values. The values of p*H* were obtained at the start of the reaction, after addition of phosphonate **191**. Due to the formation of acidic by-products, the p*H* decreased over the course of the reaction but in each case there is less than a 0.05 decrease in p*H* units.

Equation 3.8

$$[\mathrm{HO}^-] = (10^{\mathrm{p}H-\mathrm{p}Ka)})/\gamma_{\mathrm{DO}}$$

The concentration of hydroxide, [HO^-] (M) is determined by Equation 3.8 in which pK_w is the dissociation constant of water (14.0) and γ_{HO} is the activity coefficient of water under these conditions, which has been previously determined as 0.73.

Table 3.4 Kinetic data for the hydrolysis of 191 in H_2O solutions at I = 1.0, 25 °C

f.b % [CO_3^{2-}]	p*H*	[HO^-] M	k_{obs} (s^{-1})
20%	9.32	2.86×10^{-5}	3.71×10^{-5}
30%	9.51	4.43×10^{-5}	7.92×10^{-5}
40%	9.73	7.36×10^{-5}	1.29×10^{-4}

50%	9.91	1.11×10^{-4}	1.94×10^{-4}

Figure 3.18 Second-order rate plot of k_{obs} against [HO⁻] for 191 in H_2O solutions at 25 °C, I = 1.0 (KCl)

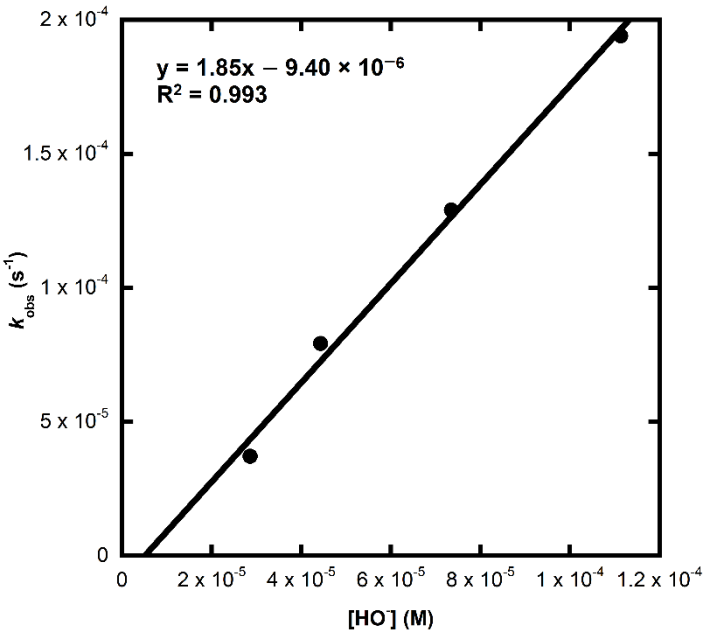

$$y = 1.85\,x - 9.40 \times 10^{-6}$$

$$R^2 = 0.993$$

Figure 3.18 is a second-order rate plot of k_{obs} against [HO⁻]. The slope of this plot is the observed second-order rate constant of hydrolysis with respect to hydroxide, k_{HO} (M^{-1} s^{-1}) at 25 °C, I = 1.0.

Equation 3.9

$$k_{obs} = k_{HO}[HO^-] + k_B[CO_3{}^{2-}] + k_{H2O}$$

The pseudo first-order rate constant of hydrolysis k_{obs} potentially consists of three components as shown in Equation 3.9. $k_{HO,}$ is the second-order rate constant hydroxide-catalysed reaction, k_B is the second-order rate constant of buffer catalysis, and k_{H2O} is the p*H*-independent rate constant of hydrolysis. The lack of reaction under acidic conditions implies that k_{H2O} has a negligible contribution and can be ignored.

In order to analyse the contribution from buffer catalysis, the buffer concentration was varied at a constant freebase ratio. As previously shown, a mitigating factor is unimolecular production of acid from the reaction product, resulting in stoichiometric acidification of the

buffer. This effect is greater at lower concentrations of freebase carbonate. Due to this effect, the p*H* values from the end of the experiments are used.

The hydrolysis of **191** was monitored at a consistent 40 % freebase ratio. Due to the doubly charged carbonate ion, ionic strength could not be regulated at I = 1 for the experiment at $[CO_3^{2-}]$ = 0.4 M.

Table 3.5 Varied buffer concentration in the hydrolysis of 191.

f.b. $[CO_3^{2-}]$ M	pH_{start}	pH_{end}	$[B^-]/[HO^-]$	k_{obs} (s^{-1})	k_{rel} (s^{-1})
0.40	9.76	9.77	4959	1.51×10^{-4}	0.91
0.20	9.73	9.72	2782	1.29×10^{-4}	0.87
0.10	9.76	9.59	1876	9.69×10^{-5}	0.88

Figure 3.19 Buffer-catalysis plot of the hydrolysis of 191 in H_2O solutions at 25 °C.

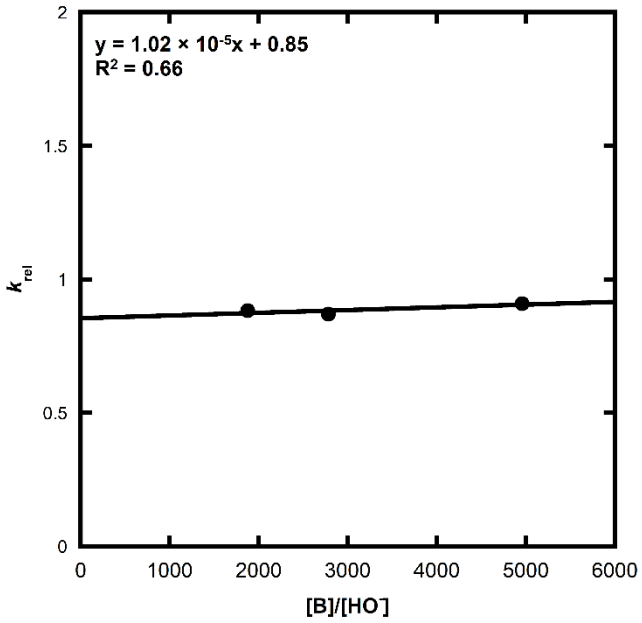

$$y = 1.02 \times 10^{-5}x + 0.85$$

$$R^2 = 0.66$$

The slope of the plot in Figure 3.19 gives a value for k_B/k_{HO} of 1.0×10^{-5}. This ratio gives a small value of for k_{rel} compared to the changes in the concentration of buffer base. The maximal contribution from buffer catalysis to rate from this value is approximately 8%, within the error margin of the values of k_{HO} value found previously

Hydrolysis experiments were repeated in D_2O solutions buffered by K_2CO_3 at I = 1.0 in order to investigate the kinetic isotope effect on phosphonate hydrolysis.

Table 3.6 Kinetic data for the hydrolysis of 191 in D_2O solutions at I = 1.0, 25 °C

f.b % [CO_3^{2-}]	p*D*	[DO^-] M	k_{obs} (s^{-1})
20%	9.24	3.21×10^{-6}	6.06×10^{-6}
30%	10.29	3.60×10^{-5}	6.83×10^{-5}
40%	10.70	9.26×10^{-5}	1.83×10^{-4}
50%	10.29	3.60×10^{-5}	8.20×10^{-5}

Figure 3.20 Second-order rate plot of k_{obs} against* [DO^-] *for 191 in D_2O solutions at 25 °C I = 1.0 (KCl)

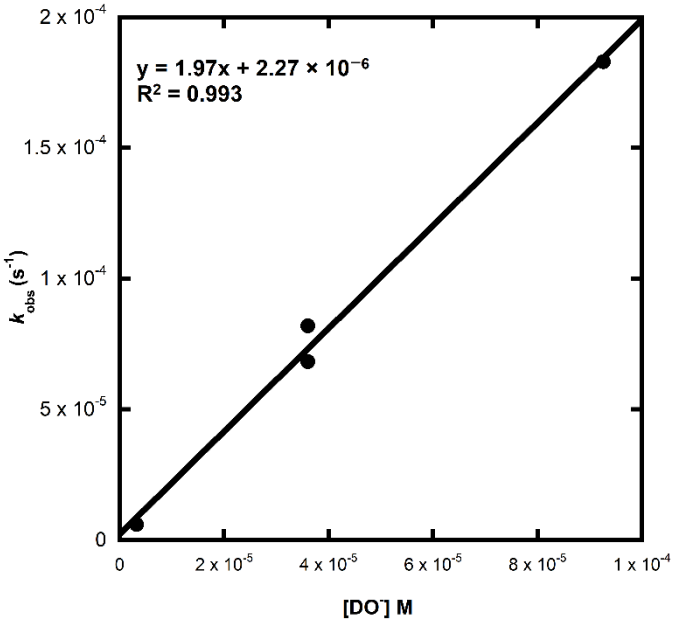

$$y = 1.97x + 2.27 \times 10^{-6}$$

$$R^2 = 0.993$$

The ratio of k_{HO}/k_{DO} is 0.94. We estimate the error in k_{DO} or k_{HO} is ± 10%, thus this value is within error of 1, and therefore indicates a lack of significant kinetic isotope effect (KIE) on this reaction. Clearly a primary KIE is not observed.

3.2.3.2.2 Activation Parameters of Cyclopropenium Phosphonate Hydrolysis

In order to further probe the mechanism of cyclopropenium phosphonate hydrolysis, the activation parameters were probed by varying the temperature of the hydrolysis of **65**. The kinetic data can be used in the Eyring equation (Equation 3.10) to provide further information about the mechanism.

Equation 3.10 Eyring Equation.

$$\ln\left(\frac{k}{\mathrm{T}}\right) = -\frac{\Delta \mathrm{H}^{\ddagger}}{\mathrm{RT}} + \ln\left(\frac{\mathrm{k_B}}{\mathrm{h}}\right) + \frac{\Delta S^{\ddagger}}{R}$$

Where k is the rate constant of reaction, T is temperature, R is the gas constant, k_B is the Boltzmann constant, h is the Planck constant, $\Delta H^{\ddagger}$ is the enthalpy of activation and $\Delta S^{\ddagger}$ is the entropy of activation.

Hydrolysis experiments were carried out in D_2O solutions with the same K_2CO_3 buffer solution, at I = 1.0 (KCl) and pD measured as 10.29 at 25 °C. Experiments from 25-50 °C were monitored by 202 MHz ^{31}P NMR spectroscopy. The experiment at 4 °C was kept at constant temperature by a water vessel inside a refrigerator and monitored by 162 MHz ^{31}P NMR spectroscopy. The refrigerator temperature was checked periodically with a thermometer and found to be consistent ± 1 °C. The experiments were initiated by addition of buffered water solution to a sealed vial of **191**, which was agitated to ensure full solution. The reactions were then quickly brought to the correct temperature before monitoring began.

The differences in the autoionization constant (pK_w) of D_2O with variation in temperature are accounted for by standard data obtained from Covington et. al.[41] Additionally, the changes in pK_a of carbonate at higher temperatures are accounted for by empirical data also obtained by Covington et. al.[42]

Due to the fact that $[K^+]$ and $[CO_3]_{tot}$ are considered to remain the same at varied temperatures, the concentration freebase ratio is approximated not to change. Using literature values of pK_a' at raised temperature, combined with literature values of pK_w increases, this allows us to estimate pD', and therefore $[DO^-]$, to a reasonable accuracy, on the assumption that γ_{DO} is broadly similar at varied temperature using Equations 3.11 and 3.12.

Equation 3.11

$$\mathrm{p}D' = \mathrm{p}K_{\mathrm{a}}' + \log_{10}\left(\frac{[\mathrm{A}^-]}{[\mathrm{HA}]}\right)$$

Equation 3.12

$$[\mathrm{DO}^-] = \frac{10^{(\mathrm{p}D\prime - \mathrm{p}K_W)}}{\gamma_{\mathrm{DO}}}$$

From the obtained [DO⁻] value, k_{DO} can be determined by division of k_{obs} by [DO⁻]

Figure 3.21 Eyring plot of the hydrolysis of 191

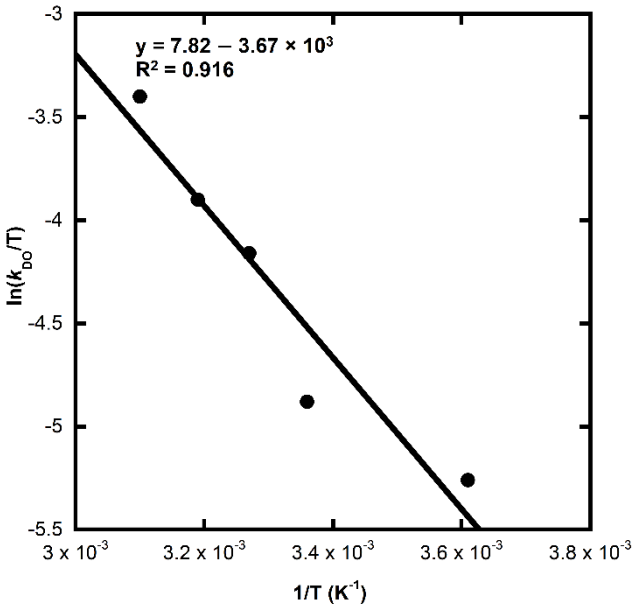

Table 3.7 Variable temperature hydrolysis of 191.

T (K)	k_{obs} (s^{-1})	k_{DO} (M^{-1} s^{-1})	ln(k_{DO}/T)	1/T (K^{-1})
277	1.43×10^{-5}	1.46	−5.24	3.61×10^{-3}
298	8.20×10^{-5}	2.27	−4.88	3.36×10^{-3}
305.5	2.62×10^{-4}	4.71	−4.17	3.27×10^{-3}
313	5.44×10^{-4}	6.65	−3.85	3.19×10^{-3}
323	1.54×10^{-3}	11.40	−3.34	3.10×10^{-3}

From the fit of Figure 3.21, estimates of the entropy and enthalpy of activation can be obtained from the slopes and intercepts of the plots, respectively.

Table 3.8 Enthalpy and entropy of activation

$\Delta H^{\ddagger}$	$\Delta S^{\ddagger}$
30.5 kJ mol^{-1}	−132.5 J K^{-1} mol^{-1}

3.2.3.2.3 Stoichiometry of Hydrolysis Products

Hydrolysis of **191** was determined to have no variation in the ratio of hydrolysis products with changes of temperature or p*H* or changing from H_2O to D_2O. The product analysis was performed by ^{31}P NMR spectroscopy (700 MHz) with a high recycle delay (> 30 s) in order to ensure full relaxation between scans.

Table 3.9 Product analysis of hydrolysis of 191

Solvent	Buffer	I (M)	T (°C)	Diethyl phosphate (%)	**198** (%)
H_2O	1 M K_2CO_3	3.0	25	89.8	10.2
D_2O	0.5 M K_2CO_3 (40% f.b.)	1.0	25	89.8	10.2
D_2O	0.5 M K_2CO_3 (50% f.b.)	1.0	40	89.9	10.1

Each of these results is well within the margin of error associated with ^{31}P NMR spectroscopy and therefore are likely identical.

In order to further probe the mechanism, the product stoichiometry of basic hydrolysis of **192** and **193** was determined by high resolution ^{1}H and ^{31}P NMR.

Samples (~10 mg) of each phosphonate were placed in NMR tubes and dissolved in 2 M K_2CO_3 solution in D_2O. After 10 minutes at room temperature, additional cosolvent d_4-MeOD (10% v/v) was added to ensure full dissolution (**192** was not fully soluble in D_2O) and the contents were characterised by ^{31}P NMR spectroscopy, revealing the reaction had gone to completion. High resolution NMR spectra were then acquired to more accurately determine relative concentrations of products.

Figure 3.22a-b ^{31}P NMR Spectra of Hydrolysis Products of a) 192 (212 MHz) and b) 193 (162 MHz)

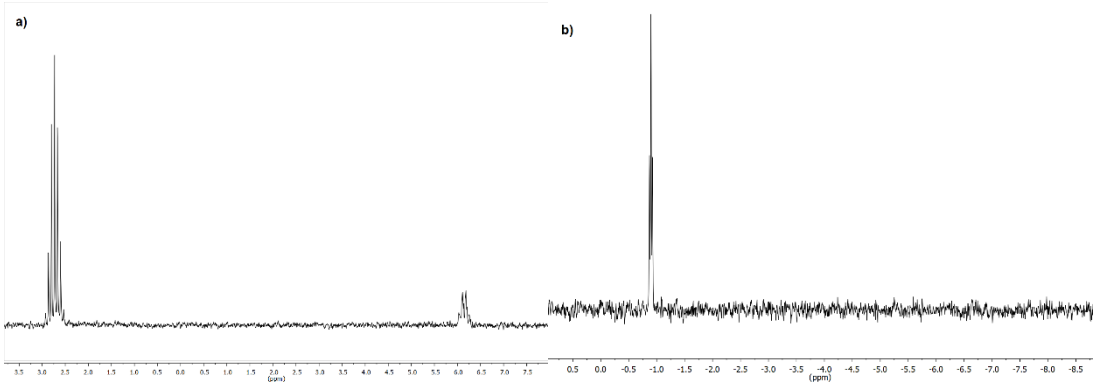

A sufficiently high recycle delay of 30s with a pulse width of 45° was used, due to potentially relatively high T_1 relaxation times (~10s in the case of diethyl phosphate) with an acquisition time of 1s over 64 transients. The identity of the products of hydrolysis were confirmed by analysis of the ^{1}H and ^{31}P spectra combined with high-resolution mass-spectrometry. Table 3.10 details the determined product stoichiometry

Table 3.10 Stoichiometry of phosphonate hydrolysis products

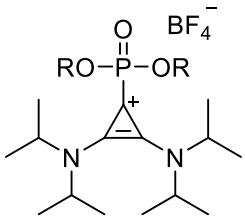

191-193

Phosphonate	R =	C-O/P-O Cleavage	P-C Cleavage
192	Me	19%	81%
191	Et	10%	90%
193	^{i}Pr	0%	100%

In each case, the favoured reaction is the breakage of the P-C bond to form the BAC **23** and respective dialkylphosphate. Greater substitution of the alkyl substituent favours P-C bond breakage further. Discussion of these results takes place in section 3.3.3.

3.3 Discussion

The first section of this work was focussed on the preparation of literature and novel BAC precursor cyclopropenium salts. Literature examples of organocatalytic procedures, as well as other chemical examples, use only a few examples of BAC structures (Section 4.1). This is in contrast to the very wide number of structural variations available for NHCs, of which many different examples are used in organocatalysis.[43] This lack of variety in applied BACs is possibly indicative of the synthetic problems associated with the preparation of BAC precursors with varied substituents.

Preparation of BAC precursors with varied substituents proved difficult. It was found in the use of dialkylamines, any secondary amine with less bulky substituents than diisopropylamine proved difficult to restrict to the desired disubstituted product. Only diethylamine proved capable of producing the disubstituted product, under restrictive conditions. Bulkier amines,

such as 2,2,6,6-tetramethylpiperidine proved totally unreactive under these conditions, suggesting that substituents which are overly bulky are also incompatible with the system.

Using less nucleophilic *N*-methylaniline gave only trisubstituted product **181**. Even the use of low temperatures and bulky counterions did not produce any detectable disubstituted cyclopropenium species, in contrast to diethylamine. The very poorly nucleophilic *N*-methyl-2-nitroaniline **185** did not yield any product.

Using the alternative route, the phosphonium salt **184** could be produced using N-methylaniline but hydrolysis did not give the desired BAC conjugate acid. Potentially, the use of a phosphite in place of triphenylphosphine could generate a phosphonate, the hydrolysis of which could produce an N-aryl cyclopropenium salt.

It has previously been determined that in organic solvents without the presence of strong Lewis acids such as $SbCl_5$, tetrachlorocyclopropene exists as its non-aromatic state[3] **133**, but following addition of these Lewis acids, chloride is extracted to form the aromatic salt **134**. Water causes hydrolysis of the counterion $SbCl_6^-$, returning **134** to its non-aromatic state **133**. In contrast to tetrachlorocyclopropene, salts of aminocyclopropenium ions exist in the aromatic state without any Lewis acid presence.

Figure 3.23 Proposed equilibrium limited* S_NAr *formation of aminocyclopropenium salts

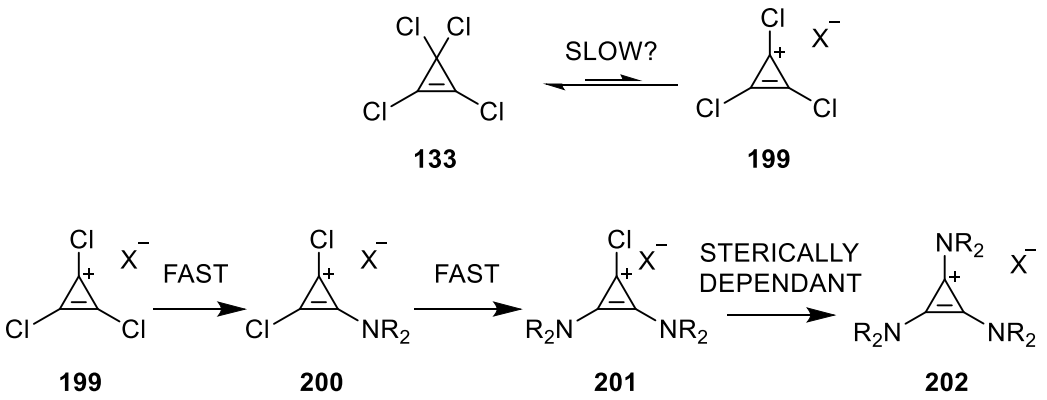

Nucleophilic aromatic substitution therefore provides a plausible explanation to the observed behaviour. Assuming that the non-aromatic state of **133** is unreactive, it exists in a disfavoured equilibrium with its aromatic counterpart **199**. The small amount of **199** reacts very rapidly with amines, to form a monosubstituted product **200**, which remains highly reactive to additional equivalents of amine. This means that the effectively low concentration of the reactive form of **199** limits the number of equivalents available to react with amine. The second

and third additions of amines would be slower due to their being more electron-rich and therefore less reactive, but they could remain overall more reactive than non-aromatic **133**, in particular if the rate of formation of **199** is slow.

The lack of disubstituted or monosubstituted product appearance despite slow addition of low equivalents of unhindered amines at low temperature supports this hypothesis. This hypothesis is further supported by Weiss'[6] observation of successful mono and disubstitution of aminocyclopropenium systems using antimony pentachloride to generate the trichlorocyclopropenium chloride system before addition of amine.

Scheme 3.39 S_NAr Mechanism of Aminochlorocyclopropenium substitution

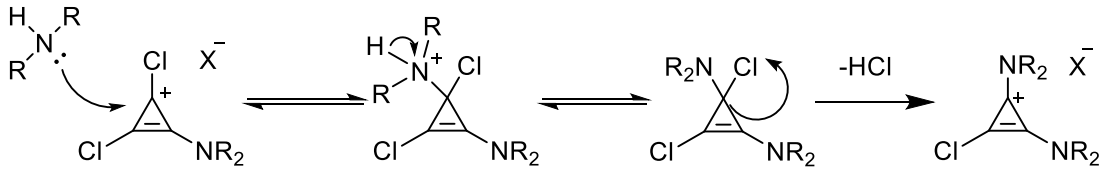

200 **203** **204** **201**

The alternative possible mechanism is an S_N2 attack on a non-aromatic form of **133**. This mechanism is not likely to be predominant due to the somewhat narrow angle to approach the antibonding orbital of the C−Cl bond. Further, the very high rate of reaction does not suggest an S_N2 mechanism, due to the mediocre chloride leaving group. Additionally, further substitution on the ring would disfavour this mechanism, due to an increasingly electron-rich ring favouring the cyclopropenium state over the S_N2 capable non-aromatic state. The increasingly electron-rich cyclopropenium ring of the more substituted species would also disfavour nucleophilic attack. This is in contradiction to the observation of purely trisubstituted cyclopropenium rings being formed in reactions with insufficient equivalents of amines.

Scheme 3.40 Lack of onward reaction to 205.

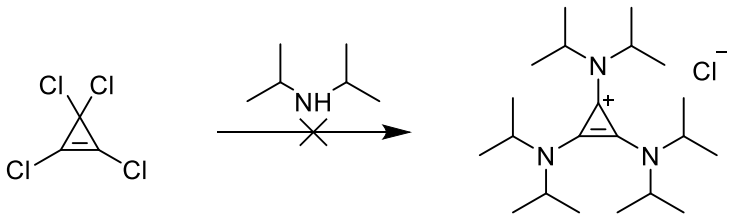

133 **205**

The production of disubstituted **163** and **142** with diisopropyl and dicyclohexyl substituents respectively is considered most likely a result of steric clashing in their trisubstituted equivalents. Addition of excess amine in these two cases does not result in further substitution.

Diethylamino cyclopropenium **166** is an anomaly among these results giving both di- and trisubstitution. At low temperature, the disubstituted **165** was produced preferentially to the trisubstituted **166**, but with significant trisubstituted contaminant. Addition of sodium tetraphenylborate before the addition of diethylamine however prevented significant formation of **166**. This effect is assigned to the formation of a close ion pair in organic solvents between the large bulky tetraphenylborate and cyclopropenium ions. This effect can possibly be observed by the varying chemical shift between the C3 proton of **129** and **163** and between **140** and **167** (Chapter 6).

The formation of the disubstituted **164** or **165** could be explained by the steric bulk of these groups. While insufficient to prevent onward reaction in the presence of excess amine, the ethyl groups of **164** may be required to change conformation to allow addition of the third equivalent of amine. Rotation of the amine groups of diisopropyl **163** are relatively slow at room temperature[1], hence their appearance as two distinct peaks in ^{1}H NMR spectroscopy. It is therefore feasible for this effect to prevent trisubstitution at −78 °C.

To summarise, the proposed mechanism is likely nucleophilic aromatic substitution to form **201** involving a disfavoured pre-equilibrium from tetrachlorocyclopropene. This mechanism could potentially explain the observed data from this work and reported in the literature on the preferential formation of trisubstituted aminocyclopropenium ions. Steric effects leading to unstable products could explain the disubstituted products **141** and **162**. Diethylaminocyclopropenium **165** is a borderline case where a third substitution is possible, but can be kinetically disfavoured by steric hindrance.

3.3.1 Proton-transfer chemistry of BACs

Previous literature has no examples of studies of proton-transfer *via* BAC, however Weiss et. al.[23,32] found that aminocyclopropenium ions underwent electrophilic aromatic substitution in concentrated D_2SO_4. The proton-transfer behaviour was therefore of high interest due the potential similarities and differences between BACs and the more studied NHCs.

Using H/D exchange experiments in D_2O, the proton-transfer chemistry of three BACs was probed. **163** and **166** were studied under standard conditions of I = 1.0 and 25 °C, in order to provide the best comparison to existing NHC data. Early experiments showed very slow

exchange in neutral D_2O, no exchange in 1 M DCl and rapid exchange in 1 M NaOD solutions. Each conjugate acid proved to be stable over several weeks in D_2O solutions at p*D* 1-8, however at the highest basicity (p*D* ~ 14) a slow decomposition of every cyclopropenium system is noted (Chapter 4). Decomposition of conjugate acids is not considered to be competing with H/D exchange, as no experiment noted any detectable decomposition in the range of p*D*s studied (~5-8).

H/D exchange in each case showed an expected pseudo first-order decay of the signal corresponding to the C3(H), and analysis of this data permitted determination of pseudo first-order rate constants of exchange, k_{ex} (s^{-1}). The slopes of the plots of k_{ex} of **163** and **166** against deuteroxide concentration showed a first order dependence on the concentration of deuteroxide, similar to NHCs. There was no detected deviation from linear dependence of k_{ex} on deuteroxide, indicating a single mechanism at each studied p*D*.

Buffer catalysis was shown to be insignificant (Table 3.2), indicating a specific-base catalysed H/D exchange process. This allows linear fitting of the slope of the second-order rate plot to give the second-order rate constant of H/D exchange, k_{DO} ($M^{-1}\,s^{-1}$).

The use of ^2H NMR detected a peak at 7.4 ppm after a H/D exchange experiment of **163**. The chemical shift corresponds well with a predicted shift of this position, compared to the ^1H NMR spectrum (7.4 ppm). Combined with the lack of change in the other ^1H NMR peaks during the exchange experiments, this indicates that the decrease in the signal of the C3 position is due to H/D exchange, and not due to decomposition of **163**.

Figure 3.24 Mechanism of H/D exchange via BAC

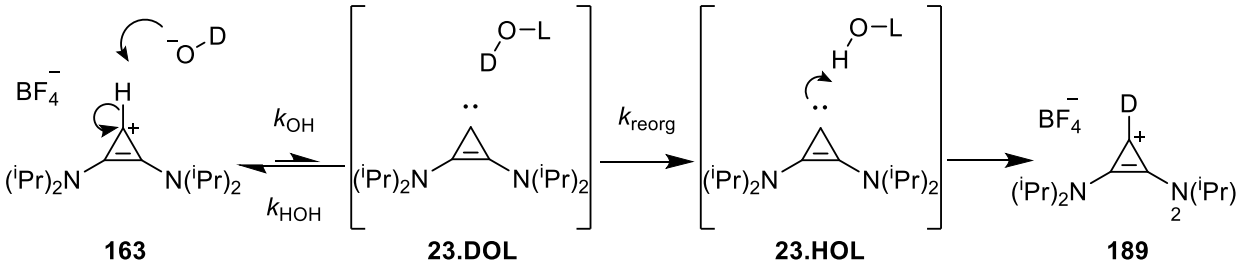

From the evidence obtained from these experiments, the suggested mechanism of the observed H/D exchange is analogous to that of NHCs. Like the NHC mechanism, a pre-equilibrium of addition and removal of the C3 proton is followed by rate-determining solvent reorganisation and deuteration of the C3 position to give the product **189**. Additionally, carbene chemistry has

been observed by deprotonation of BACs in protic solvents (section 4), suggesting that the deprotonated species has BAC character.

Unlike Weiss' observations, no acid-catalysed electrophilic aromatic substitution was observed under the conditions of these experiments. This is to be expected, due to the most acidic experiment (1 M DCl in D_2O) having significantly less acidity than the concentrated D_2SO_4 solutions used by Weiss[32].

Figure 3.25 Selected NHCs and BAC

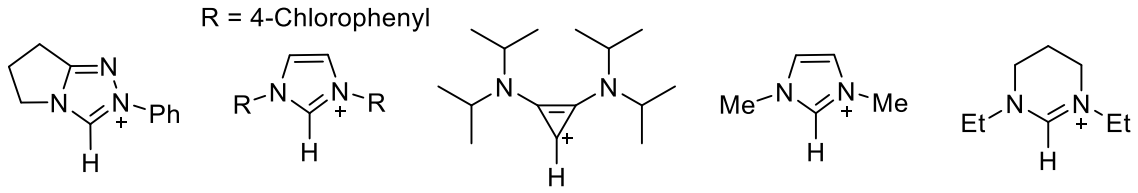

105 **100a** **163** **94** **102a**

Table 3.11 Comparative* pK_a *of NHCs and BACs

Conjugate Acid	pK_a
105[35]	17.5
100a[30]	19.8
163	22.1
94[44]	23.0
102a[30]	27.8

When compared to the data obtained from the various families of N-heterocyclic carbenes, it becomes clear that BACs have a lower carbon acidity than N-aryl imidazolium salts, but are more acidic than N-alkyl imidazolium salts. Considering the absence of the stabilising α-heteroatoms in bis(amino)cyclopropenylidene conjugate acids **163** and **167**, BACs appear to be unusually stable.

A possible explanation for the unexpectedly low pK_a of these BACs could be the three membered cyclopropenium ring. When comparing pyrimidinium salts to imidazolinium salts, the increase from five-membered to six-membered ring size causes a large increase in the pK_a of ~5 units. This effect can be ascribed to the more obtuse N-C-N constrained bond angle of the pyrimidinium ring, which destabilises the carbene state significantly relative to the

conjugate acid. As every known NHC has a singlet ground state, the destabilising effect of this bond angle on the carbene state is significant, thereby favouring the protonated state.

Figure 3.26 Crystal structure of 163

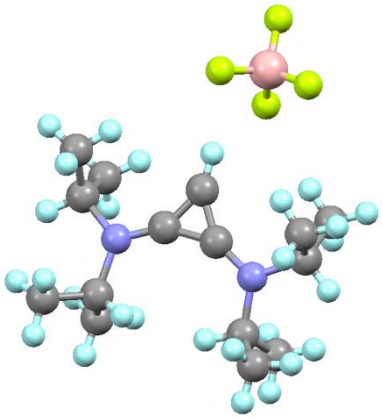

Comparing the crystal structure data of **23** from Lavallo et. al[1] and our structure of **163** (Figure 3.26) it can be seen that the change from the conjugate acid **163** to BAC **23** results in a constraining of the C-C-C bond angle from 62.3 ° to 57.2 °. The highly acute bond angle is far narrower than that for the known NHCs (typically ~ 102-105 °), which could be provide a compensatory stabilising effect that counteracts the lack of the stabilising effect of the α-heteroatoms in the BAC structure.

Figure 3.27 π-donation from nitrogen into empty p orbital of a BAC

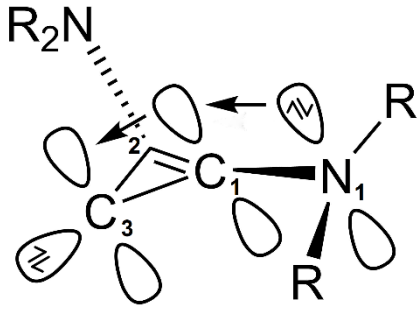

The β-amino substituents are also suggested to be important in the stabilisation of the BAC state. The σ-withdrawing and π-donating nature of these heteroatoms is highly stabilising to the singlet ground state of the carbene, however, the distance from the carbene centre would lessen their effects on stability. The C1-N1 bond lengths obtained by Lavallo et. al. for carbene **23** are significantly shorter than a typical C-N amine single bond (~1.47 Å), and are more similar to that of amides[45]. Additionally, the C-N bond lengths are longer in the carbene **23** (1.332 Å) than in its conjugate acid **163** (1.306 Å). This is due to the higher degree of π-

donation of the nitrogen lone pairs into the positively charged carbocation **163** than the neutral carbene state. The C-N bond lengths indicate the importance of the π-donation on stabilising the BAC.

Previous examples, such as triazolium based systems (Chapter 2), show that heteroatom substitution further than one bond from the carbene centre can have significant effects on carbene stability and pK_a. Combining the effects of the β-heteroatoms on the aromatic system with the highly acute bond angle at the carbene centre therefore can explain the relatively low pK_a of the BAC system.

3.3.2 Novel Phosphonate Chemistry

The preparation of the first of the cyclopropenium phosphonates was a serendipitous result of the difficulties in the preparation of N-ethyl salt **167**. Of further interest was the interesting behaviour during hydrolysis of **172**; two separate pathways of hydrolysis were observed, leading to different products.

The first attempt at an alternative synthesis and purification of N-isopropyl cyclopropenium phosphonate ester involved stirring chloro precursor **190** in solution with triethyl phosphite at room temperature overnight. No reaction was observed under these conditions, unlike the reaction with the N-ethyl **165**. Heating to reflux in THF however, resulted in the reaction going to completion to the desired product **191**.

The preparation of other simple alkyl cyclopropenium phosphonates *via* this method was facile, and was improved by the use of microwave heating for shorter periods of time in acetonitrile, resulting in decent yields and straightforward purification by recrystallization.

Due to the potentially different behaviour in hydrolysis (see section 3.3.3), it was considered important to prepare phosphonates from more electron-poor phosphites. Due to commercial availability, triphenyl phosphite and tris-(2,2,2-trifluoroethyl) phosphite were chosen. Even under very high temperatures (160 °C), preparations of the desired phosphonates were not successful, with only potential traces of product detectable by LCMS, under the detection limit of ^{31}P NMR. The lack of reaction with these phosphonates was assigned to the electron-withdrawing nature of the phosphite substituents, causing poor phosphorus nucleophilicity.

Iodo cyclopropenium salt **197** was prepared, *via* a similar Finkelstein-like reaction to existing literature procedures[38] to improve reactivity with the unreactive phosphites. This was not successful, and there was no observed increased yield of the desired phosphonates. Instead an

increase in the formation of the side product **163** was observed. The increased yield of **163** is possibly a result of preferential attack of the phosphite on the iodine position rather than carbon, resulting in the formation of a carbene which rapidly reprotonates using opportunistic protons to form **163**.

Figure 3.28 Arbuzov-like proposed mechanism

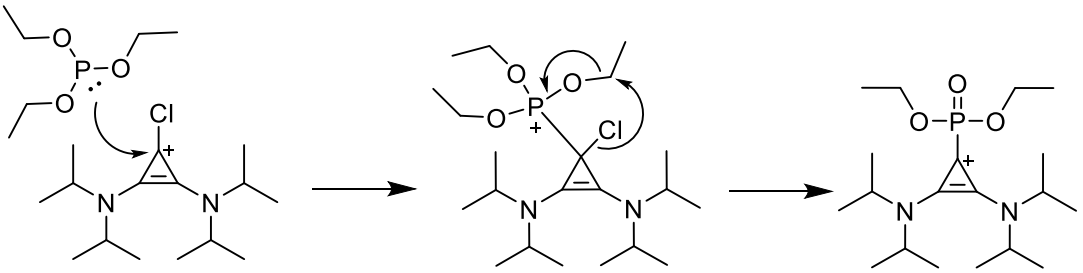

The proposed mechanism for the formation of cyclopropenium phosphonates is analogous to the Arbuzov reaction[46], with initial attack of phosphorus forming an intermediate **206**. From there, the chloride attacks the carbon shown, forming the P=O double bond through a 5-membered ring transition state, eliminating chloroethane. The higher degree of steric hindrance in N-isopropyl salt **190** gives the reaction a higher activation energy compared to N-ethyl **165**, requiring heating to drive the reaction. The poor nucleophilicity of the phosphites with electron-withdrawing substituents makes them a poor route to their respective phosphonates, and other methods of preparing these phosphonates are required.

3.3.3 Hydrolysis of cyclopropenium phosphonate esters.

Hydrolysis of **172** had the unexpected result of removal of the BAC in preference to less basic ethoxide ion. In order to further probe the origins of this outcome, hydrolysis experiments were performed on a range of phosphonate esters.

Figure 3.29* S_N2@C *mechanism

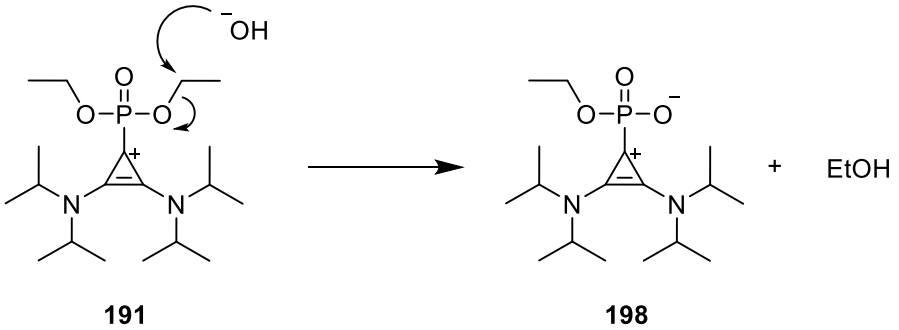

Figure 3.30* S_N2@P *mechanism

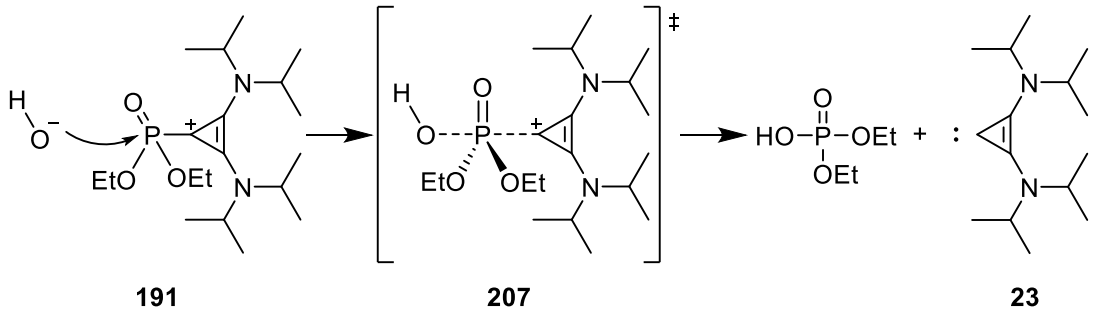

Figure 3.31* $A_N + D_N$ *mechanism

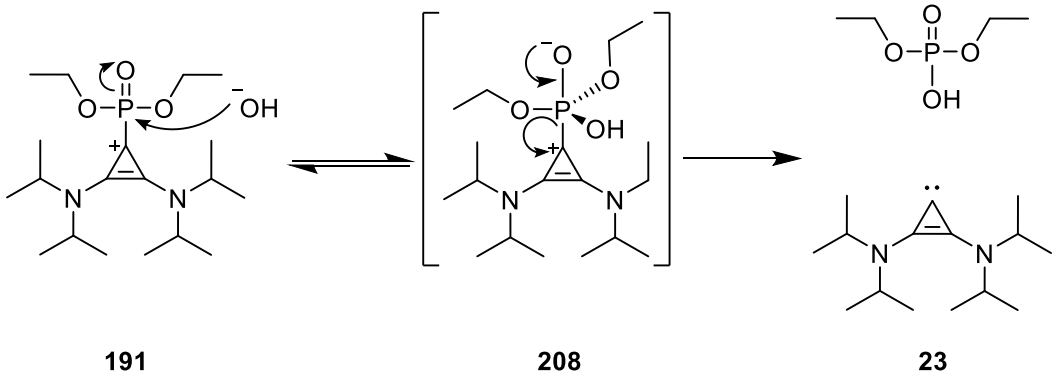

Hydrolysis of phosphonate esters generally proceeds *via* three mechanisms: S_N2@C, S_N2@P or A_N+D_N (Figure 3.29-3.31). The hydrolysis of **191** has the potential to be *via* one or a combination of these mechanisms.

Initial findings determined that the major product of hydrolysis of phosphonate **191** was **163**, and diethyl phosphate, as opposed to **198** and ethanol. This finding is surprising given the relative pK_as of BACs and ethoxide, as the product with the higher pK_a is preferentially eliminated. Hydrolysis proceeded at a measurable rate by ^{31}P NMR spectroscopy at around the p*H* of carbonate buffers, with a second-order rate constant with respect to hydroxide (k_{HO}) of 1.97 M^{-1} s^{-1}. Buffer catalysis could not conclusively be ruled out, but was found to contribute less than 10% of the observed rate constant at maximum. Changing from hydroxide to deuteroxide was not found to have a significant effect on the rate constant. A slight increase in rate constant was observed, but k_H/k_D is within error of unity.

An Eyring plot (Figure 3.21) was obtained by determining rate constants of hydrolysis at various temperatures, and after correcting for the changing concentration of deuteroxide at

varied temperature, it was found that $\Delta H^{\ddagger}$ is small and positive, and $\Delta S^{\ddagger}$ is negative for the hydrolysis of **191**.

The ratio of products was determined by high resolution ^{31}P NMR and was found to be identical at each studied temperature, and between D_2O and H_2O solutions for one phosphonate **191**.

The lack of variation of product ratio with temperature or isotope experiments suggests that hydrolysis is likely to proceed by a single mechanism. Attack of hydroxide at the C3 position of the cyclopropenium ring is also likely to be disfavoured, due to the dearomatisation that would occur. Furthermore, base hydrolysis of cyclopropenium rings has previously generated cyclopropenones, which were not detected as products of this reaction. As the preferentially eliminated product is the BAC, then it is unlikely that S_N2@C is the major pathway.

The Eyring plot shows a negative value for entropy of activation. This could indicate an S_N2 reaction or a rate determining step of addition in an $A_N + D_N$ reaction. Both S_N2@P and $A_N + D_N$ would be facilitated by the electron-withdrawing cyclopropenium substituent.

Table 3.12* pK_a *of BAC compared with simple alcohols

Conjugate Acid	pK_a
163	22.1
Methanol[36]	15.5
Ethanol[36]	16.0
Isopropanol[36]	17.1

The unexpected elimination of BAC preferentially to alcohol could be explained by several means. It is possible that the breakage of a weaker P-C bond compared to a P-O bond[31] could result in faster elimination of the BAC, despite its significantly higher pK_a. In addition to this, the more substituted alcohols are eliminated less readily, which is consistent with the trend in pK_a within leaving groups.

Figure 3.32 Pseudorotation of a 5-coordinate phosphorus intermediate 208

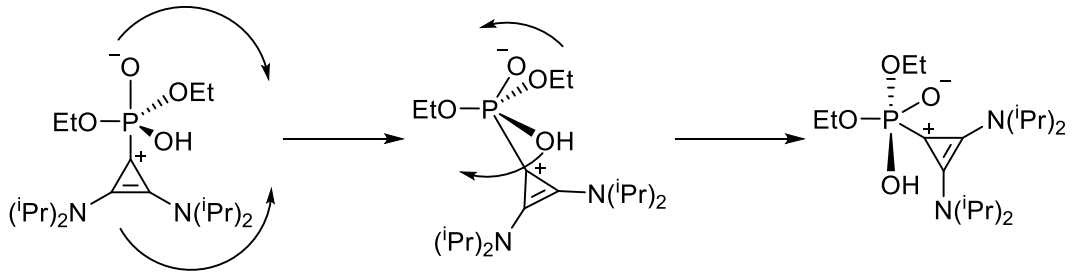

Another possible explanation involves the differing steric bulk of the cyclopropenium and alcohol substituents. If the reaction proceeds *via* a $A_N + D_N$ mechanism, then elimination from the trigonal bipyramidal intermediate should proceed *via* the two axial substituents.

We propose that the bis(amino)cyclopropenylidene moiety is likely to be located in the axial position in the pentacoordinate intermediate. Typically, in pentacoordinate phosphorus species, sterically bulkier species are positioned equatorially. However, it has also been noted that π-acceptors are typically positioned axially, as are strong σ-donors. BACs such as **23** have been characterized as strong σ-donors and also as π-acceptors.[10,20] When π-acceptors are equatorial, their vacant π-orbitals are positioned along the equatorial plane, which could potentially result in unfavourable interactions between the diisopropyl groups and other substituents of the pentacoordinate intermediate[47]. The ethoxy substituents on the other hand are π-donors and may preferentially position themselves equatorially in this case, despite alkoxy substituents usually being positioned axially.

Due to elimination taking place across axial ligands, this could explain the preferential elimination of the BAC over alkoxide leaving groups. Rate-limiting pseudorotation[48] (Figure 3.32) is a possible explanation for the observed trend across the series, that more sterically bulky alcohols are eliminated less often. Bulkier groups could slow pseudorotation, as well as favour their position being equatorial over axial.

Steric effects on the pseudorotation of simple methyl phosphoranes have been documented by Szele et. al.[49], where the pseudorotation of highly hindered methyltetrakis(2,6-dimethylphenoxy)phosphonium triflate could be measured on an NMR timescale at −65 °C, unlike the unhindered pseudorotation of less hindered phosphoranes.

In conclusion, the hydrolysis of phosphonate esters **191-193** likely proceeds *via* a single associative mechanism. The current set of data is unable to distinguish between an S_N2@P or

$A_N + D_N$ process. Reasonable arguments can be made for either mechanism from the existing data, such as the potential for pseudorotational barriers to the elimination of alcohols from the trigonal bipyramidal intermediate, or more simply more rapid S_N2 breaking the P-C bond to form the BAC.

3.4 Summary

This work had the original goal of the preparation of several simple BACs, and the investigation of their proton-transfer chemistry.

The preparation of BAC precursors from literature procedures was repeated successfully, however novel preparations of BACs were less successful. Preparation of an N-aryl BAC was unsuccessful, instead resulting in related phosphonium salt **184**. Other aryl secondary anilines did not form aminocyclopropenium salts, either due to their low nucleophilicity or high steric hindrance around the small cyclopropenium ring. N-ethyl compound **167** was successfully prepared *via* hydrolysis of a novel phosphonate intermediate **172**, however the final stage required HPLC purification.

The successful formation of exclusively disubstituted aminocyclopropenium salts in the case of diethylamine was found to be highly counterion dependant, with bulky tetraphenylborate seeming to prevent formation of the trisubstituted by-product **166**.

The mechanism of aminocyclopropenium formation from tetrachlorocyclopropene **6** is assigned to an S_NAr reaction, with potential slow equilibria between **133** and **134** resulting in exclusive formation of trisubstituted products in reactions with unhindered amines.

The proton-transfer chemistry of two BACs were investigated by determination of their pK_a through H/D exchange experiments. Values of k_{DO} (M^{-1} s^{-1}) were obtained by the slope of a second-order plot of the obtained pseudo first-order rate constants of exchange k_{ex} (s^{-1}) against deuteroxide concentration. As with related NHC compounds, k_{DO} values were converted to k_{HO} (M^{-1} s^{-1}) by a secondary solvent kinetic isotope relation (k_{DO}/k_{HO} = 2.4). Using the additional assumption that BAC reprotonation is similar in rate to other carbene reprotonation (k_{HOH} = k_{reorg} = 10^{11} s^{-1}), pK_a could be estimated through the kinetic acidity method. The obtained pK_a values (~22) were compared to those of NHCs and were found to be similar to the conjugate acids of imidazolylidenes. The process of H/D exchange was confirmed through ^{2}H NMR spectroscopy.

The unusual hydrolysis of cyclopropenium phosphonates seen in the preparation of **167** prompted further investigation. Cyclopropenium phosphonates were prepared in a process using similar conditions to a typical Arbuzov reaction. The hydrolysis of these compounds was investigated and unusually the predominant leaving group was the less stable BAC, compared to alkoxide. Kinetic analysis by ^{31}P NMR spectroscopy showed no variation in product ratio by change of conditions, and variable temperature analysis suggests an associative transition state. From this information, it is suggested that the reaction proceeds through either an $S_N2@P$ or $A_N + D_N$ process with rate-limiting pseudorotation, but this cannot be conclusively proven from current data.

3.5 Bibliography

1 V. Lavallo, Y. Canac, B. Donnadieu, W. W. Schoeller and G. Bertrand, *Science*, 2006, **312**, 722–724.
2 R. Breslow, *J. Am. Chem. Soc.*, 1957, **79**, 5318–5318.
3 R. West, A. Sadô and S. W. Tobey, *J. Am. Chem. Soc.*, 1966, **88**, 2488–2494.
4 Z. Yoshida, S. Miki and S. Yoneda, *Tetrahedron Lett.*, 1973, **14**, 4731–4734.
5 S. W. Tobey and R. West, *Tetrahedron Lett.*, 1963, **4**, 1179–1182.
6 R. Weiss, H. Koelbl and C. Schlierf, *J. Org. Chem.*, 1976, **41**, 2258–2262.
7 E. I. Klimova, T. K. Berestneva, S. H. Ortega, D. M. Iturbide, A. G. Marquez and M. M. García, *J. Organomet. Chem.*, 2005, **690**, 3333–3339.
8 Z. Yoshida and Y. Tawara, *J. Am. Chem. Soc.*, 1971, **93**, 2573–2574.
9 M. M. D. Wilde and M. Gravel, *Angew. Chem. Int. Ed.*, 2013, **52**, 12651–12654.
10 G. Kuchenbeiser, M. Soleilhavoup, B. Donnadieu and G. Bertrand, *Chem. - Asian J.*, 2009, **4**, 1745–1750.
11 D. Holschumacher, C. G. Hrib, P. G. Jones and M. Tamm, *Chem. Commun.*, 2007, **0**, 3661–3663.
12 J. Bandar and T. Lambert, *Synthesis*, 2013, **45**, 2485–2498.
13 Z. Yoshida, H. Ogoshi and S. Hirota, *Tetrahedron Lett.*, 1973, **14**, 869–872.
14 R. Weiss, T. Brenner, F. Hampel and A. Wolski, *Angew. Chem. Int. Ed. Engl.*, 1995, **34**, 439–441.
15 Z. Yoshida, H. Konishi, Y. Tawara, K. Nishikawa and H. Ogoshi, *Tetrahedron Lett.*, 1973, **14**, 2619–2622.
16 Z. Yoshida, H. Konishi, Y. Tawara and H. Ogoshi, *J. Am. Chem. Soc.*, 1973, **95**, 3043–3045.
17 G. Mehler, P. Linowski, J. Carreras, A. Zanardi, J. W. Dube and M. Alcarazo, *Chem. – Eur. J.*, 2016, **22**, 15320–15327.
18 R. Breslow, T. Eicher, A. Krebs, R. A. Peterson and J. Posner, *J. Am. Chem. Soc.*, 1965, **87**, 1320–1325.
19 C. Wilcox and R. Breslow, *Tetrahedron Lett.*, 1980, **21**, 3241–3242.

20 G. Kuchenbeiser, B. Donnadieu and G. Bertrand, *J. Organomet. Chem.*, 2008, **693**, 899–904.
21 Y. D. Bidal, M. Lesieur, M. Melaimi, D. B. Cordes, A. M. Z. Slawin, G. Bertrand and C. S. J. Cazin, *Chem. Commun.*, 2015, **51**, 4778–4781.
22 B. S. N. Huchenski, M. R. Adams, R. McDonald, M. J. Ferguson and A. W. H. Speed, *Organometallics*, 2016, **35**, 3101–3104.
23 R. Weiss and C. Priesner, *Angew. Chem. Int. Ed. Engl.*, 1978, **17**, 445–446.
24 J. Eames, in *Encyclopedia of Reagents for Organic Synthesis*, John Wiley & Sons, Ltd, 2001.
25 Sigma Aldrich.
26 W. D. Kumler and J. J. Eiler, *J. Am. Chem. Soc.*, 1943, **65**, 2355–2361.
27 A. Landau and G. Seitz, *Chem. Ber.*, 1991, **124**, 665–669.
28 K. Komatsu and T. Kitagawa, *Chem. Rev.*, 2003, **103**, 1371–1428.
29 Y. Jiang, J. L. Freyer, P. Cotanda, S. D. Brucks, K. L. Killops, J. S. Bandar, C. Torsitano, N. P. Balsara, T. H. Lambert and L. M. Campos, *Nat. Commun.*, 2015, **6**, 5950.
30 E. M. Higgins, J. A. Sherwood, A. G. Lindsay, J. Armstrong, R. S. Massey, R. W. Alder and A. C. O'Donoghue, *Chem. Commun.*, 2011, **47**, 1559–1561.
31 W. M. Haynes, D. R. Lide, T. J. Bruno and CRC Press, *CRC handbook of chemistry and physics: a ready-reference book of chemical and physical data*, 2013.
32 T. Clark and R. Weiss, *J. Org. Chem.*, 1980, **45**, 1790–1794.
33 G. Wittig, G. Keicher, A. Ruckert and P. Raff, *Ann. Chem.-Justus Liebig*, 1949, **563**, 110–126.
34 D. H. Geske, *J. Phys. Chem.*, 1959, **63**, 1062–1070.
35 R. S. Massey, C. J. Collett, A. G. Lindsay, A. D. Smith and A. C. O'Donoghue, *J. Am. Chem. Soc.*, 2012, **134**, 20421–20432.
36 J. Clayden, N. Greeves and S. Warren, *Organic Chemistry*, Oxford University Press, Oxford, New York, Second Edition., 2012.
37 P. Ballinger and F. A. Long, *J. Am. Chem. Soc.*, 1959, **81**, 1050–1053.
38 J. W. Dube, Y. Zheng, W. Thiel and M. Alcarazo, *J. Am. Chem. Soc.*, 2016, **138**, 6869–6877.
39 R. Weiss, M. Rechinger, F. Hampel and A. Wolski, *Angew. Chem. Int. Ed. Engl.*, 1995, **34**, 441–443.
40 L. D. Freedman and G. O. Doak, *Chem. Rev.*, 1957, **57**, 479–523.
41 A. K. Covington, R. A. Robinson and R. G. Bates, *J. Phys. Chem.*, 1966, **70**, 3820–3824.
42 A. K. Covington, R. G. Bates and R. A. Durst, *Pure Appl. Chem.*, 2009, **57**, 531–542.
43 D. M. Flanigan, F. Romanov-Michailidis, N. A. White and T. Rovis, *Chem. Rev.*, 2015, **115**, 9307–9387.
44 T. L. Amyes, S. T. Diver, J. P. Richard, F. M. Rivas and K. Toth, *J. Am. Chem. Soc.*, 2004, **126**, 4366–4374.
45 W. C. Hamilton, *Acta Crystallogr.*, 1965, **18**, 866–870.
46 A. K. Bhattacharya and G. Thyagarajan, *Chem. Rev.*, 1981, **81**, 415–430.
47 R. Hoffmann, J. M. Howell and E. L. Muetterties, *J. Am. Chem. Soc.*, 1972, **94**, 3047–3058.
48 K. C. Kumara Swamy and N. Satish Kumar, *Acc. Chem. Res.*, 2006, **39**, 324–333.

49 I. Szele, S. J. Kubisen and F. H. Westheimer, *J. Am. Chem. Soc.*, 1976, **98**, 3533–3536.

Chapter 4 Mechanistic Studies on Bis(amino)cyclopropenylidenes in Organocatalysis.

4.0 Foreword

As a direct research on the mechanistic details of organocatalysis by BACs. Section 4.1 provides a concise review of the applications of BAC chemistry to organocatalytic reactions, and their orthogonal reactivity to the related NHC family of carbenes. Section 4.2.1 details the results of kinetic analysis by NMR spectroscopy of the reaction of benzoin and Stetter-type substrates in the presence of BACs. Section 4.2.2 focuses particularly on mechanistic aspects of the formation of acyl anion equivalents using BACs. Section 4.3 discusses the implications of these findings, relative to analogous NHC chemistry and Section 4.4 provides an overall summary and perspective in addition to suggestions for further avenues of research in this area.

4.1 Introduction

BACs are a relatively recently-identified class of stable carbenes and are of increasing interest for a variety of applications including organocatalysis. The earliest example of a BAC- organocatalytic process was reported by Wilde et. al.[1] in 2013 where BACs were shown to efficiently promote the intermolecular Stetter reaction. A proposed mechanism, analogous to the established NHC-catalysed route is shown in Scheme 4.1 although this has not been experimentally proven to date. The proposed mechanism involves initial attack of BAC **211** on an equivalent of aryl aldehyde to generate a hydroxy-aryl adduct **212**. Deprotonation to a "Breslow" intermediate and subsequent reaction with an α,β-unsaturated ketone generates a 1,4-dicarbonyl product **60**. The character of the intermediates in every BAC catalysed reaction is unknown, as to whether there is a strained alkenol "Breslow" intermediate **213**,[2] or an ylidic form **213'**, or whether the reaction proceeds *via* another unknown mechanism. The enaminol "Breslow" intermediate structure has been confirmed by NMR spectroscopy and X-ray crystallography for NHCs by Berkessel et. al[3], however, has not been confirmed for BACs.

Scheme 4.1 Proposed catalytic cycle of the BAC-catalysed intermolecular Stetter reaction

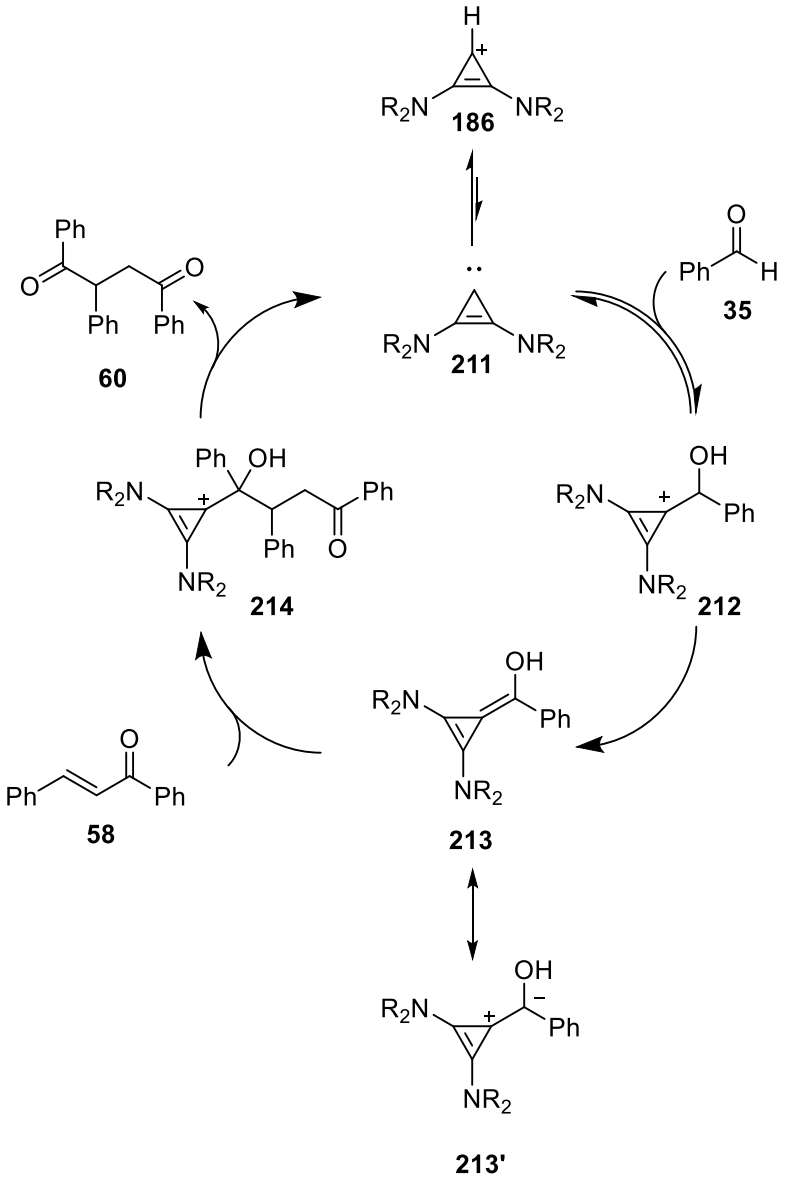

The NHC-catalysed intermolecular Stetter reaction is still considered a relatively challenging synthetic procedure, partially due to strong competition from the competing benzoin condensation. Significantly, Wilde et. al. observed that the BAC catalysed Stetter reactions did not produce any of the competing benzoin product, resulting in substantially higher yields of the desired 1,4-dicarbonyl Stetter product **60** and providing an easier purification.

Scheme 4.2 BAC-catalysis of the Stetter reaction

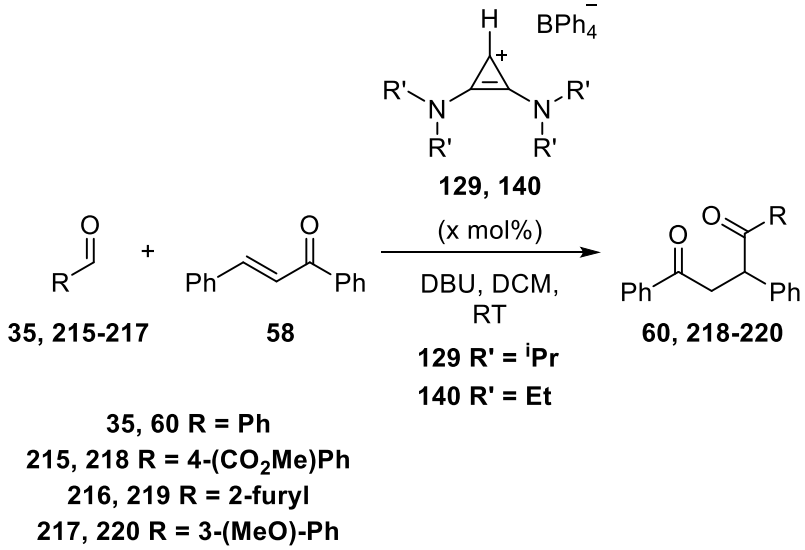

Table 4.1 Comparison of BACs in the Stetter reaction between aryl aldehydes and trans-chalcone.

Aldehyde	BAC	Cat. Load (x) (mol. %)	Product	Yield (%)
215	**129**	10	**218**	<10
215	**129**	30	**218**	24
215	**140**	10	**218**	98
216	**140**	10	**219**	99
217	**140**	10	**220**	72
35	**140**	20	**60**	65

Our initial experiments demonstrated that BACs have lower kinetic acidities and higher pK_as than the more common thiazolium- and triazolium-derived NHCs (see chapter 3). Practically, this necessitates the use of DBU over the less basic triethylamine to provide a convenient timescale for kinetic analysis. As observed by Wilde et. al. changing from a di-isopropylamino **129** to a diethylamino-derived **140** BAC dramatically increased both the yield and rate of reaction. This suggests that the substituents of the catalyst are also very important in determining the reactivity of BACs.

Scheme 4.3 Comparative Stetter reaction between BACs and common NHC catalysts

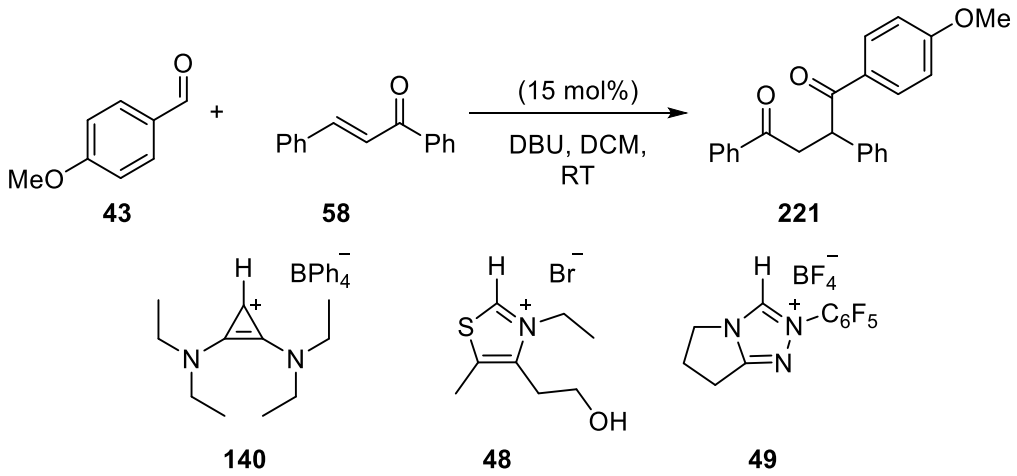

Table 4.2 Comparison of BACs and NHCs in catalysis

Catalyst	**140**	**48**	**49**
Yield (%)	76	14	9

In comparison to the more commonly used thiazolium **48** and triazolium **49** derived NHCs, BACs gave consistently higher yields, even in the use of more "difficult" Stetter reagents, such as electron-rich aldehydes (Scheme 4.3) or β-alkyl substituted-(α,β-unsaturated)-ketone acceptors. Also notable was a lack of competing benzoin side product in each of the BAC-catalysed reactions.

Scheme 4.4 Competition Stetter reaction

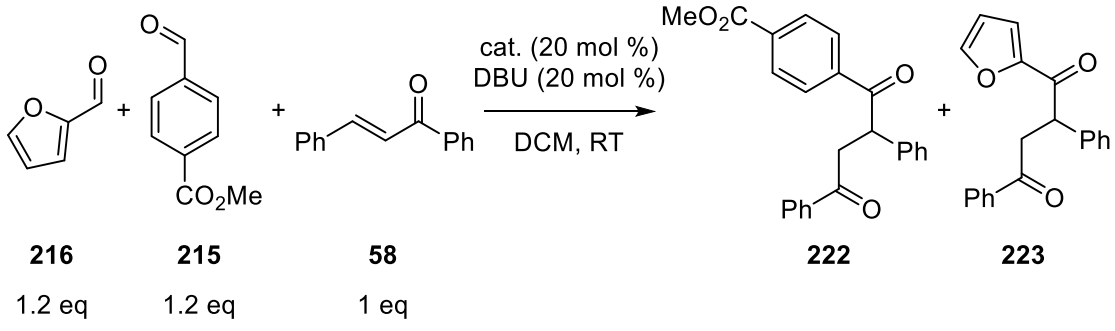

Table 4.3 Competition Stetter Reaction.

Catalyst	Product ratio **222:223**[a]	Combined Yield (%)[b]

140	85:15	99
48	37:63	80
49	12:88	85

[a] Ratio determined by ^{1}H NMR spectroscopy of crude reaction mixture. [b] Isolated mixture of **222** and **223**

Wilde[1] also performed competition experiments with two aldehydes reacting with the acceptor *trans*-chalcone. Less hindered, but more electron-rich furfural **216** and more hindered, electron-poor methyl 4-formylbenzoate **215** were used. BAC **140** was found to preferentially react to form **222** from the more hindered aldehyde **215**, whereas NHCs **48** and **49** were found to favour product **223** from furfural **216**. This is hypothesised to be a result of the lower steric hindrance around the BAC carbene centre, relative to that of the two NHCs, resulting in preferential reactivity with the more electronically favourable aldehyde. Control experiments with monitoring by ^{1}H NMR spectroscopy determined that the product distribution was not as a result of kinetic resolution towards a more thermodynamically stable product.

Scheme 4.5 Chiral Stetter reaction

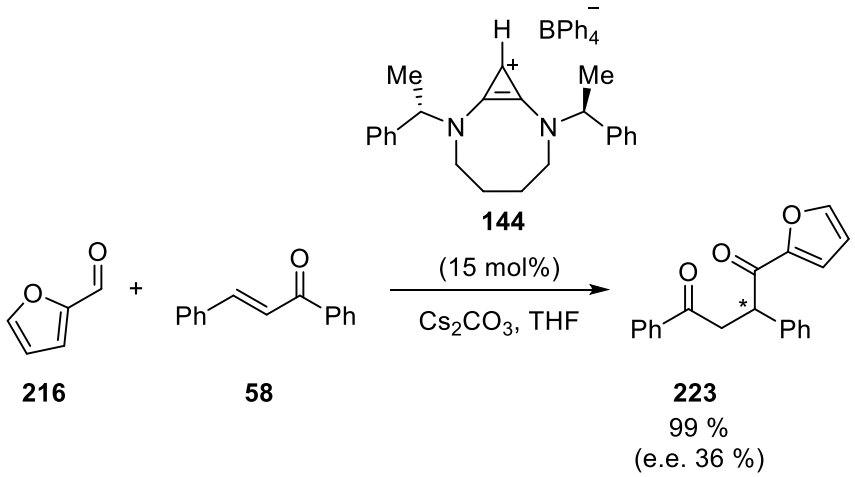

An enantioselective Stetter reaction was performed using chiral BAC **144**, which resulted in a high yield, however, a poor e.e. (36 %). NHC catalysis has achieved greater enantioselectivity in the intermolecular Stetter reaction[4], however, with limited substrate suitability.

Scheme 4.6 BAC-catalysed homoenolate reaction

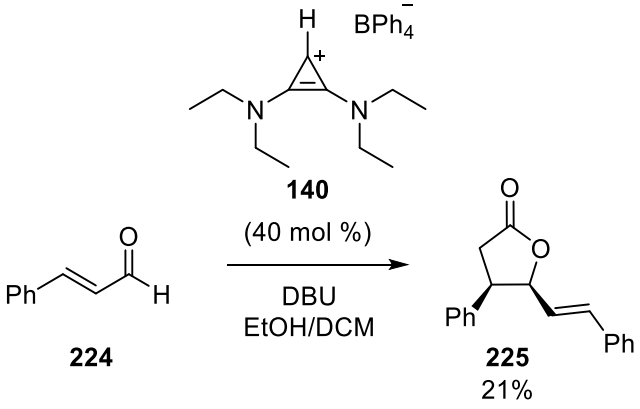

Other than the intermolecular Stetter reaction, several other reactions catalysed by BACs have been performed. Wilde. et. al[1], in the same 2013 publication, reported a BAC-catalysed reaction of cinnamaldehyde to produce lactone **225**, *via* homoenolate formation, with a poor yield.

Scheme 4.7 Aza-benzoin reaction

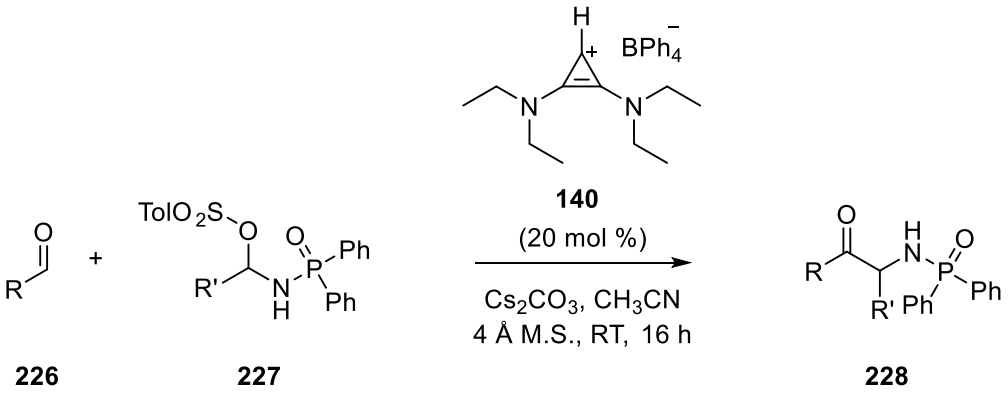

Further research by the same group used BACs as organocatalysts in the aza-benzoin reaction[5] between aldehydes **226** and phosphinoyl imines **227** formed *in situ*. As with the Stetter reaction, a major difficulty with the aza-benzoin reaction is usually the simultaneous formation of the competing homobenzoin product.[5] BAC catalyst **140** once again showed a complete lack of formation of the competing benzoin product, in contrast to NHCs **48** and **49**. This reaction, however, was less versatile in the use of electron-rich aldehydes, showing far slower reactions and lower yields, than the previous Stetter examples[1].

Scheme 4.8 Lack of retrobenzoin activity from BAC catalysis

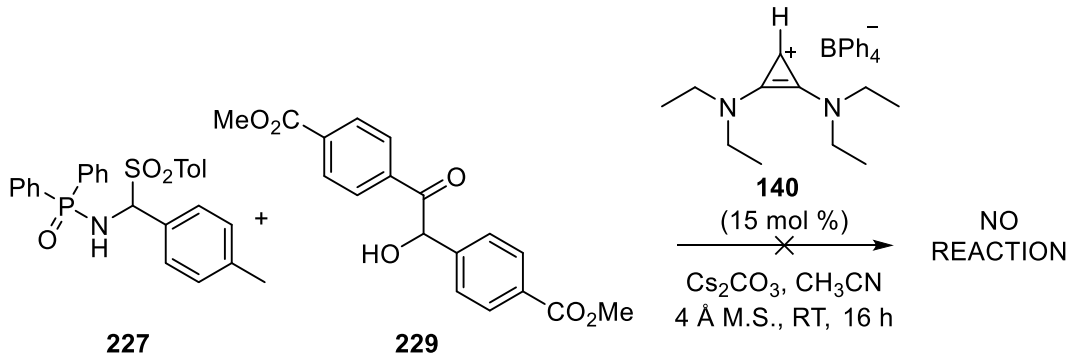

An attempted retrobenzoin-azabenzoin reaction was also reported in the same publication, showing no reaction at all. This indicates that the lack of competing benzoin product formation in the previous reactions is not as a result of a rapid retrobenzoin reaction.

Scheme 4.9 Chiral BAC-catalysed aza-benzoin reaction

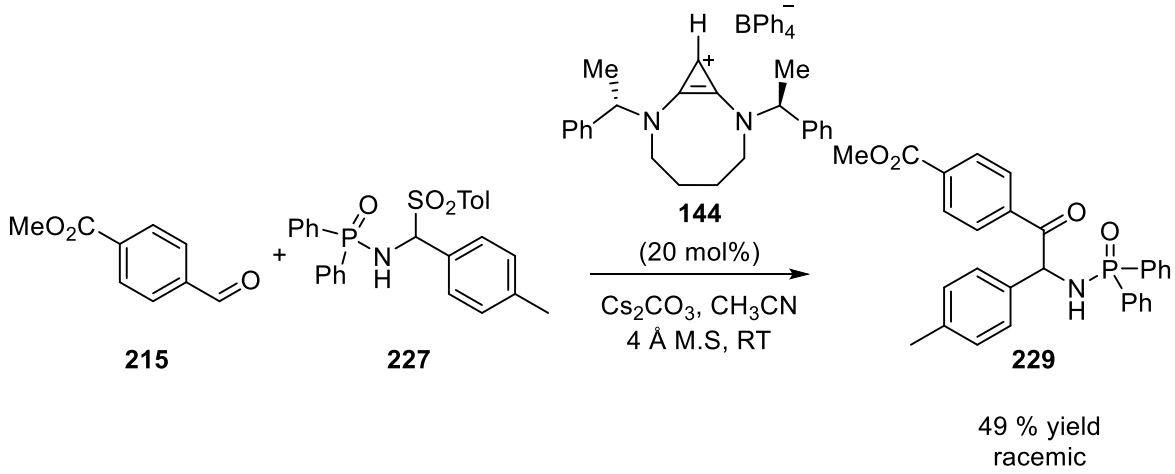

Unlike the enantioselective Stetter reactions performed using BAC organocatalysis, the aza-benzoin reaction performed with chiral catalyst **114** produced only racemic product **229**. The lack of enantioselectivity is assigned to racemisation *via* a rapid retro-aza-benzoin reaction, in contrast to the lack of retrobenzoin activity of BACs.

Scheme 4.10 α,α'-Diarylated ketones from BAC catalysis

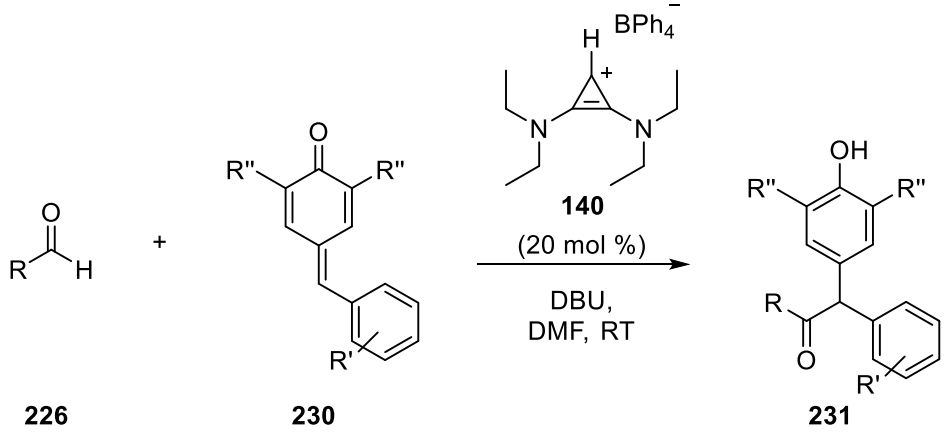

A variety of other examples of BAC organocatalysis are present in the recent literature. BAC-catalysis has been used to generate a range of α,α'-diarylated ketones in yields ranging from moderate to excellent from the reaction of aldehydes with *p*-quinone methides[6].

Scheme 4.11 Aza−Morita–Baylis–Hillman reaction catalysed by BACs

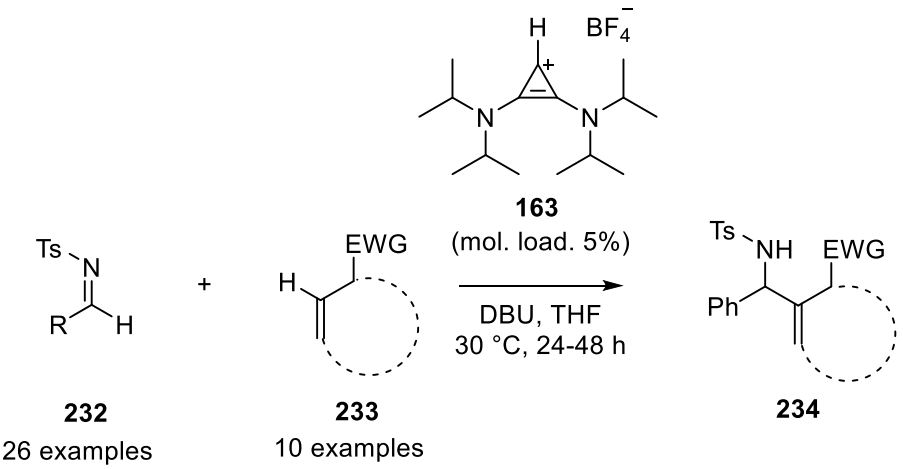

The Aza−Morita–Baylis–Hillman reaction has been catalysed using BACs[7]. Typically, Aza−Morita–Baylis–Hillman reactions are catalysed with an amine or phosphine (e.g. triphenylphosphine) initially reacting with a Michael acceptor by conjugate addition, followed by proton-transfer, addition to an imine and regeneration of the catalyst. BACs were chosen for their high σ-donor ability[8], and low steric hindrance around the carbene centre. In this work, various aromatic, aliphatic or heteroaromatic imines were reacted successfully with a wide range of electron deficient alkenes.

Scheme 4.12 Comparative Aza−Morita–Baylis–Hillman reaction between BAC catalysts

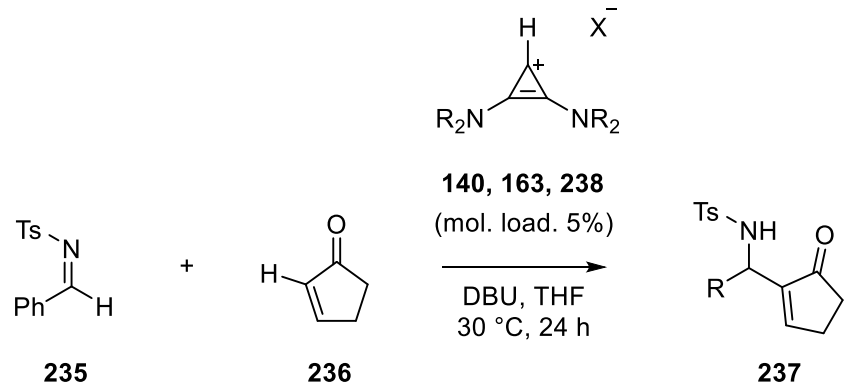

Table 4.4 Comparison of BACs as Aza-Morita-Baylis-Hillman catalysts.

BAC	R	X^-	Yield (%)
163	^{i}Pr	BF_4^-	94
140	Et	BPh_4^-	34
238	Cy	BPh_4^-	26

Unlike the previous examples, this work found significantly higher yield was obtained with the use of N-^{i}Pr catalyst **163** compared to the N-Et catalyst **140**, (and N-Cy catalyst **238**) despite the higher degree of steric hindrance around the reaction centre. Chiral BACs were used in a single example of an asymmetric Aza−Morita–Baylis–Hillman reaction, with relatively poor stereoselectivity (35% e.e.), similar to previous examples.

Additionally, the tetrafluoroborate salt of **140** was used in place of the more common tetraphenylborate counterion in this reaction. Previous research has demonstrated that the free carbene **23** is somewhat difficult to isolate, due to formation of complexes with some group I metals such as lithium and potassium, and possible interactions with the tetrafluoroborate counterion[9,10]. In this case, the *in situ* generation of a carbenoid species was functional regardless of the choice of counterion.

4.1.1 Mechanistic Studies into the NHC Catalysed Stetter Reaction.

The focus of this chapter is a mechanistic investigation of BAC organocatalysis, with particular focus on the Stetter reaction. Previous research into the similar NHC catalysed Stetter reaction, and NHC umpolung reactions in general, have uncovered

significant mechanistic details. This section reviews a few of the areas that are of particular relevance to the topic of BAC catalysed reactions.

Scheme 4.13 NHC-catalysed intramolecular Stetter reaction

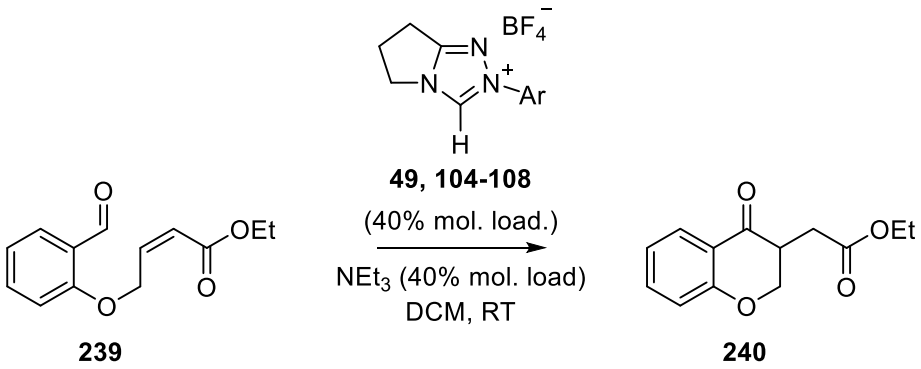

As previously detailed (Chapter 2), Collett, Massey et. al.[11] probed mechanistic aspects of the triazolin-2-ylidene catalysed benzoin and Stetter reactions. The rate of the NHC-catalysed intramolecular Stetter reaction was found to be significantly dependant on the N-aryl substituent, with the N-C_6F_5 catalyst resulting in 1000-fold higher rate constants than the N-2,4,6-trimethylphenyl substituted triazolium equivalent.

Kinetic analysis determined that the reaction involved a reversible first step to form a hydroxy-aryl adduct, followed by slower onwards reaction to form the Stetter product **240**. The equilibrium constant for formation of the adduct from aldehyde and triazolium pre-catalyst was determined by NMR spectroscopic experiments. The value of *K* was found to be highly dependant on the NHC N-aryl substituent. NHCs with electron withdrawing or 2,6-disubstituted N-aryl groups had significantly higher values of *K*. Variation of the 4-substituent, however, had a significantly smaller effect on *K*.

Later research by Collett, Massey et. al. reported an interesting effect of 2-substitution of the benzaldehyde substituent in the formation of the hydroxy-aryl adduct in the benzoin condensation.[12]

Scheme 4.14 Studies on hydroxy-aryl adduct formation in the NHC-catalysed benzoin condensation

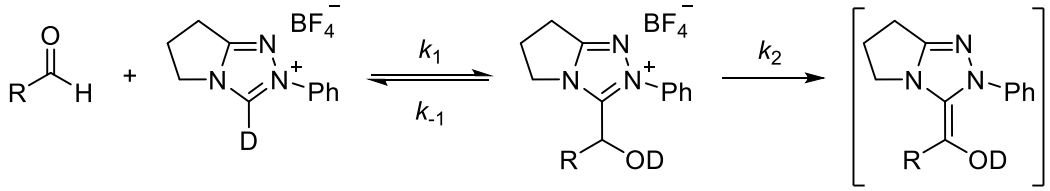

35, 43, 242-246 **241** **247** **248**

Table 4.5 Rate constants in studies of NHC-catalysed benzoin condensation.

Aldehyde	R	k_1 (M^{-1} s^{-1})	k_{-1} (s^{-1})	K_{exp} (M^{-1})	k_2 (s^{-1})
35	Ph	1.33×10^{-2}	1.17×10^{-3}	11.4	9.45×10^{-6}
242	2−$MeOC_6H_4$	3.44×10^{-2}	2.92×10^{-4}	118	5.67×10^{-6}
43	4−$MeOC_6H_4$	2.86×10^{-3}	1.49×10^{-4}	1.92	1.50×10^{-6}
243	2−ROC_6H_4[c]	4.79×10^{-2}	2.98×10^{-4}	16	9.87×10^{-6}
244	4−ROC_6H_4[b,c]	3.58×10^{-3}	1.00×10^{-3}	3.58	–
245	2−$RCH_2C_6H_4$[b,c]	8.87×10^{-3}	1.31×10^{-3}	6.76	–
246	2−MeC_6H_4	1.15×10^{-2}	7.82×10^{-4}	14.7	3.59×10^{-6}
246	4−MeC_6H_4	6.71×10^{-2}	1.11×10^{-3}	6.02	4.57×10^{-6}

[a] Starting concentrations: aldehyde (0.04 M), NHC precatalyst **47** (0.04 M) in CD_3OD and 0.18 M Et_3N:Et_3N·HCl (2:1) buffer at 25 °C. [b] Reaction monitored at 15 °C. [c] R=*E*−CH_2CH=CHCOOEt.

There was a notable increase in *K* in the case of 2-substituted aldehydes. For 2-methoxy substitution, the increase appeared to be as a result of an increased k_1 value in particular, as opposed to a decrease in k_{-1}, although this effect is not the sole factor influencing changes in K_{exp}.

Scheme 4.15 Equilibrium constants in d_2-DCM

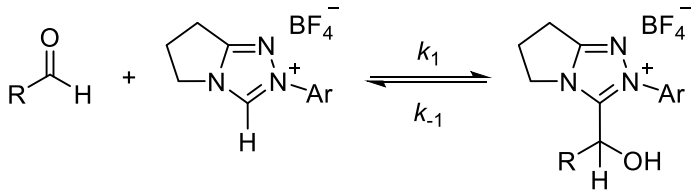

35, 242, 249, 250 **105, 106** **251-254**

Table 4.6 Further rate constants in studies of NHC-catalysed benzoin condensation.

NHC	Ar	Aldehyde	R	Adduct	K^{exp} (M^{-1})
105	Ph	**35**	Ph	**251**	3
105	Ph	**242**	2-MeO-Ph	**252**	56
106	Mes	**35**	Ph	**251**	31
106	Mes	**242**	2-MeO-Ph	**252**	143
106	Mes	**249**	2-Br-Ph	**253**	332
106	Mes	**250**	4-Br-Ph	**254**	15

2-Substituted aldehydes showed a notable increase in the values of *K*, which was particularly pronounced in the use of **106** with a N-mesityl ring. The origin of this effect is possibly as a result of steric hindrance from the *ortho*-substituent forcing the aldehyde out of conformation with the aryl ring. A destabilisation of the ground state of the substituent could be responsible for the increase in k_1 and consequent increase in equilibrium constant.

This type of detailed mechanistic investigation into NHC organocatalysis has not been conducted for analogous BAC reactions. Therefore, this chapter focusses on our investigations into the mechanism of BAC catalysed processes, including the identification and isolation of BAC-hydroxy-aryl adducts, and studies of their properties.

4.2 Results

4.2.1 Organocatalysis by bis(amino)cyclopropenylidenes.

In order to investigate the d_1-acyl anion behaviour of BACs, several reactions with suitable aryl aldehydes were performed and monitored by ^{1}H NMR spectroscopy.

Figure 4.1 Cyclopropenium BAC precatalysts.

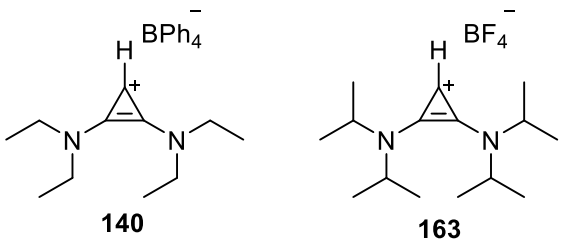

Previously (Chapter 3), four relevant cyclopropenium BAC precursors were prepared, **129**, **140 142** and **163**. Of these, catalysts **140** and **163** were selected as the case studies of this work due to the ease of their preparation in sufficient quantities, and previous use in literature examples of BAC organocatalysis.[1,7]

Scheme 4.16 Reaction of BAC 3 with benzaldehyde using triethylamine

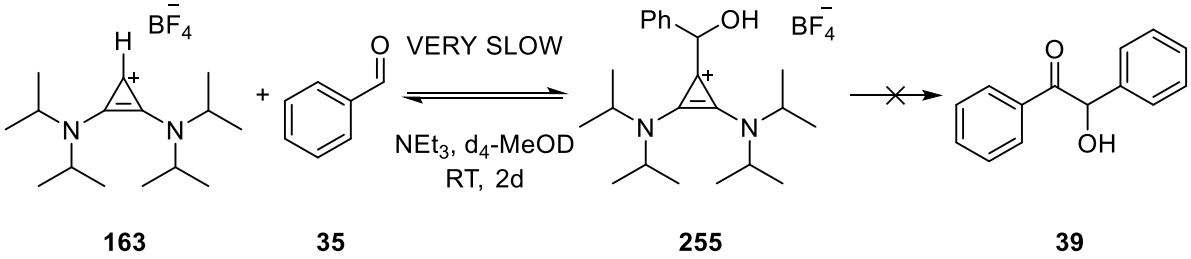

163 **35** **255** **39**

First, using standard conditions utilised by Collett, Massey et. al.[11], a reaction was attempted using a triethylamine buffered solution (2:1 NEt_3/NEt_3HCl) of **163** and benzaldehyde in d_4-MeOD, however, no detectable reaction was observed. As previously highlighted, NEt_3 was predicted to be insufficiently basic to effectively deprotonate **163**. Changing from a triethylamine buffer to pure triethylamine only showed slow formation of a hydroxyaryl adduct over several days and did not show onward reaction.

Switching the base to DBU showed a rapid formation of a hydroxy-aryl adduct **255**, followed by slower onward reactions to low levels of multiple products of unknown identities. Benzoin **39** was not detected by ^1H NMR spectroscopy or by LCMS. Owing to the large number of peaks generated, it was difficult to identify the products of this reaction. The reaction of BAC-precatalyst **163** alone and DBU in d_4-MeOD, without aldehyde, also showed slow decomposition over time, which likely contributes to the mixture of products observed for reaction in the presence of aldehyde.

Figure 4.2 Hemiacetal formation and dedeuteration by DBU

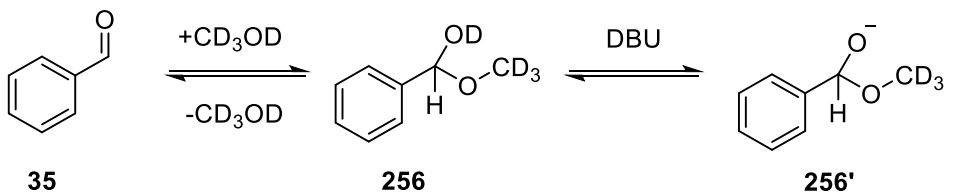

35 **256** **256'**

Owing to the high basicity of DBU, a complicating factor arose in the formation of hemiacetal **256**, through subsequent acid dissociation of the hemiacetal at the hydroxyl

group. This is observed as a broadening of peaks due to aryl and the aldehydic hydrogens in the ^{1}H NMR spectra of these reactions. Due to this process, later reactions were performed in d_2-DCM to simplify analysis.

4.2.1.1 Intramolecular Stetter reaction.

The second area of investigation was the intramolecular Stetter reaction of *ortho*-salicylaldehyde derivative **257**, which had previously been studied extensively in the presence of a range of NHCs.

Scheme 4.17 Preparation of 239

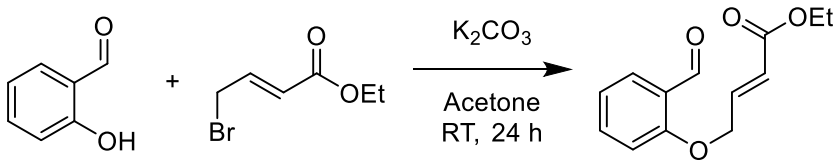

257 **258** **239**

Aldehyde **257** was prepared according to a literature procedure[11] from ethyl 4-bromocrotonate and salicylaldehyde, and purified by column chromatography followed by recrystallization from cold ethyl acetate.

Scheme 4.18 Intramolecular Stetter reaction

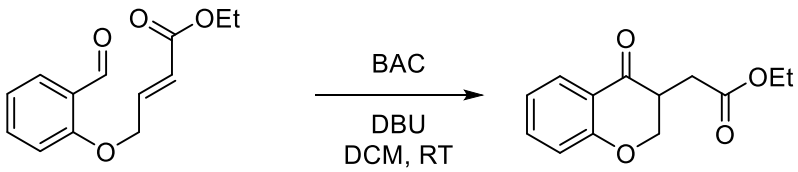

239 **240**

Based on previous analogous NHC-experiments, an intramolecular Stetter reaction was anticipated with ring-closure following d_1-acyl anion generation at the aldehyde position of **239**.

Figure 4.3 Representative ^{1}H NMR spectra (400 MHz) in the reaction of 239 with 163 in d_2-DCM solution with DBU.

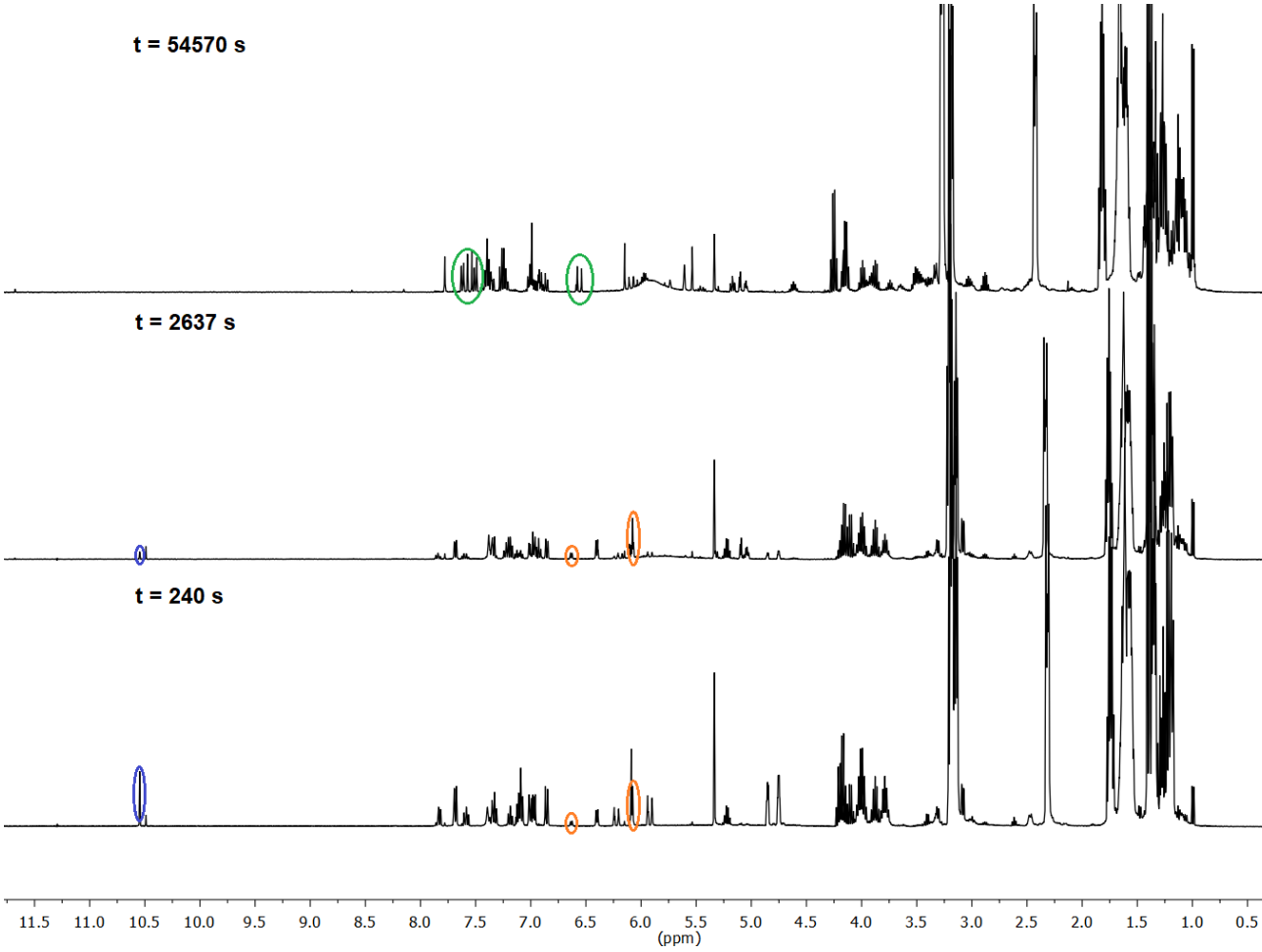

The progress of reaction was followed by ^{1}H NMR spectroscopy in d_2-DCM. **239** can be observed by its aldehydic proton at 10.5 ppm (circled in blue), as well as peaks in the aryl region. DBU is present as a large series of peaks from 4.25-1.2 ppm, including large peaks at 3.2 and 2.3 ppm. The C(3) proton of **163** is obscured by the aryl groups of **239**, but the pair of septets corresponding to the N-C**H** peaks of **163** are visible at ~3.8 ppm. The formation of a hydroxyaryl adduct was suggested by the generation of a new peak at 6.6 ppm (dt, 1H), which is assigned to the EtO_2C-C(H)=C-**H** peak of the presumed adduct **259**. Additionally, a singlet peak at ~6 ppm is assigned to the BAC-C(OH)**H** of this adduct. Both of these adduct peaks are circled in orange in Figure 4.3.

Figure 4.4 Proposed intermediate 259 with bolded hydrogen atoms referring to marked peaks in Figure 4.3.

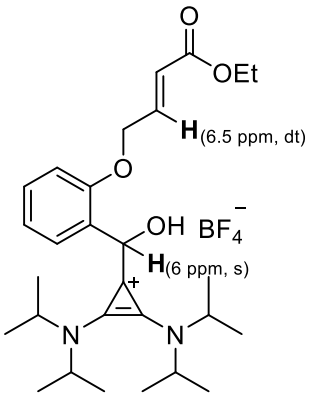

259

Peaks consistent with the formation of the product **240** were unexpectedly not observed in this reaction, instead giving a previously unobserved species.

Figure 4.5 ^{1}H NMR spectra (400 MHz) of the products of reaction of 239 in DBU in the presence (top) and absence (bottom) of 163.

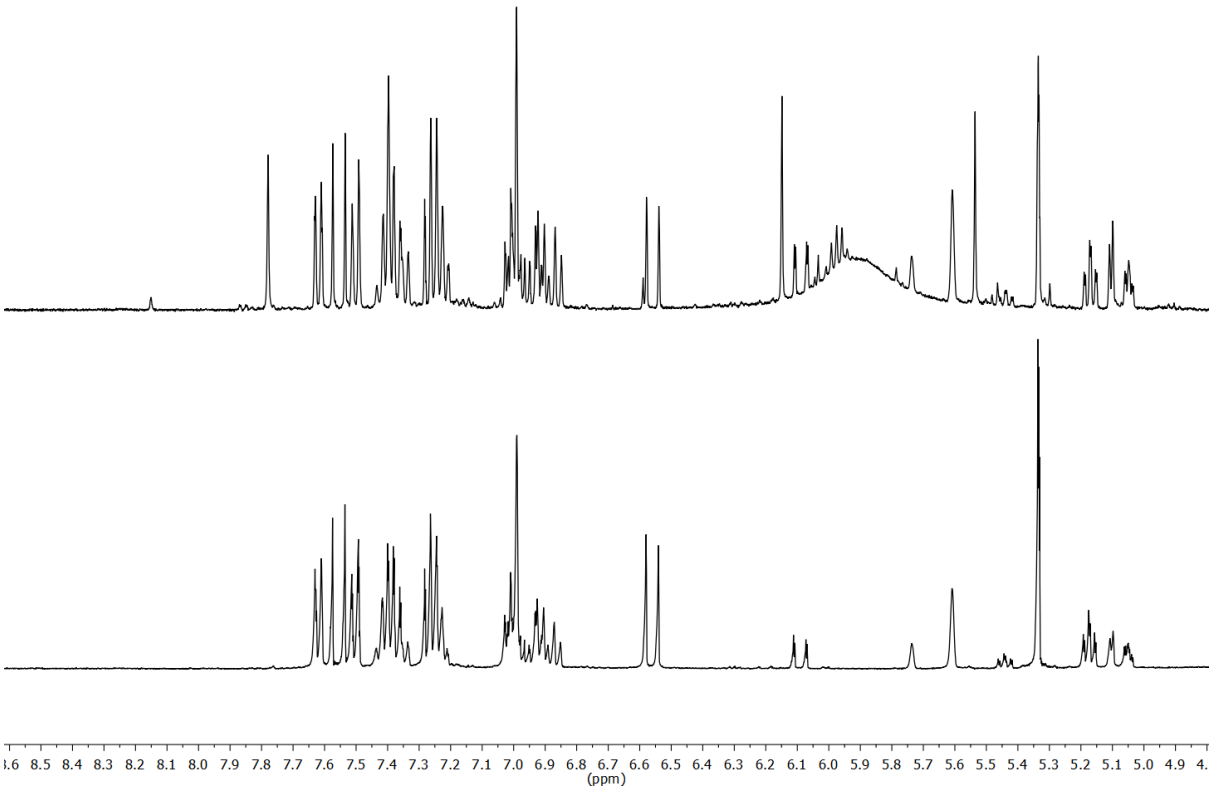

It was found that solutions of **239** and DBU in the absence of a catalyst produced the same unknown product as observed in the presence of BAC **163**. Figure 4.5 compares the ~5-12 ppm region of ^{1}H NMR spectra of reactions with and without a BAC catalyst. In both cases, the aryl region is similar, notably the pattern of the peaks from 7.6-7.45

ppm (doublet, singlet and multiplet). Also notable is the new doublet peak at 6.6 ppm, which is not attributable to **239**, **259** or **240**. While BAC **163** clearly produces additional unknown species, the major product in both cases is the same.

Scheme 4.19 Production of benzofuran 260 from 239

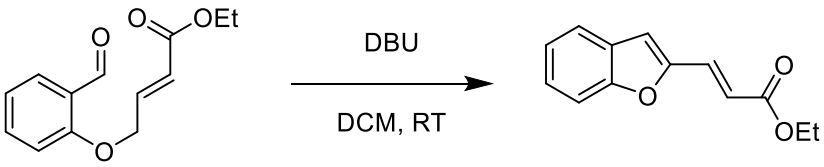

239 **260**

The product of the reactions was identified as **260** from ^{1}H NMR peak assignments and LCMS analysis. The occurrence of this reaction has been previously reported by Reddy et. al[13], using DBU or Cs_2CO_3 as bases in organic solvents. This decomposition reaction was not previously observed in reactions using buffered NEt_3 solutions. The process is likely initiated by removal of a proton α to the ether group of **239**, which is not deprotonated by weaker bases such as triethylamine. Clearly, for bulkier BAC **163**, reaction to the potential intramolecular Stetter product does not compete with benzofuran formation.

Scheme 4.20 Successful Stetter reaction

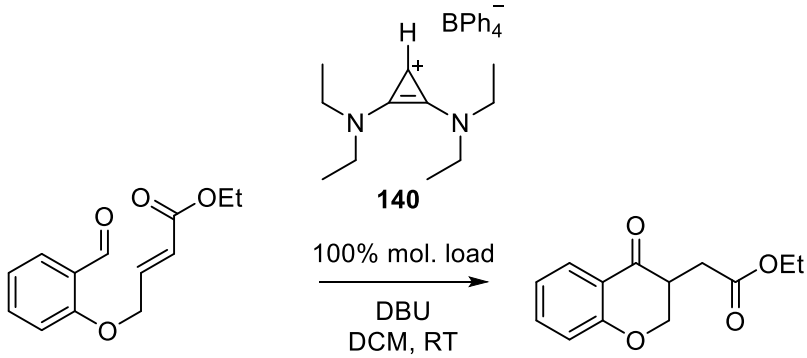

239 **240**

Another series of Stetter reactions of **239** were followed using **140** as a BAC precatalyst. A solution of 0.05 M **239** and **140** in d_2-DCM was prepared, and equimolar DBU was added to initiate the reaction. In contrast to the reactions using isopropyl BAC **163**, reactions using ethyl catalyst **140** successfully produced the intramolecular Stetter product **240** as the major component identified by comparison to literature ^{1}H NMR spectra of **240**.

Figure 4.6 Representative ^{1}H NMR spectra (500 MHz) of the intramolecular Stetter reaction of 239 catalysed by 140

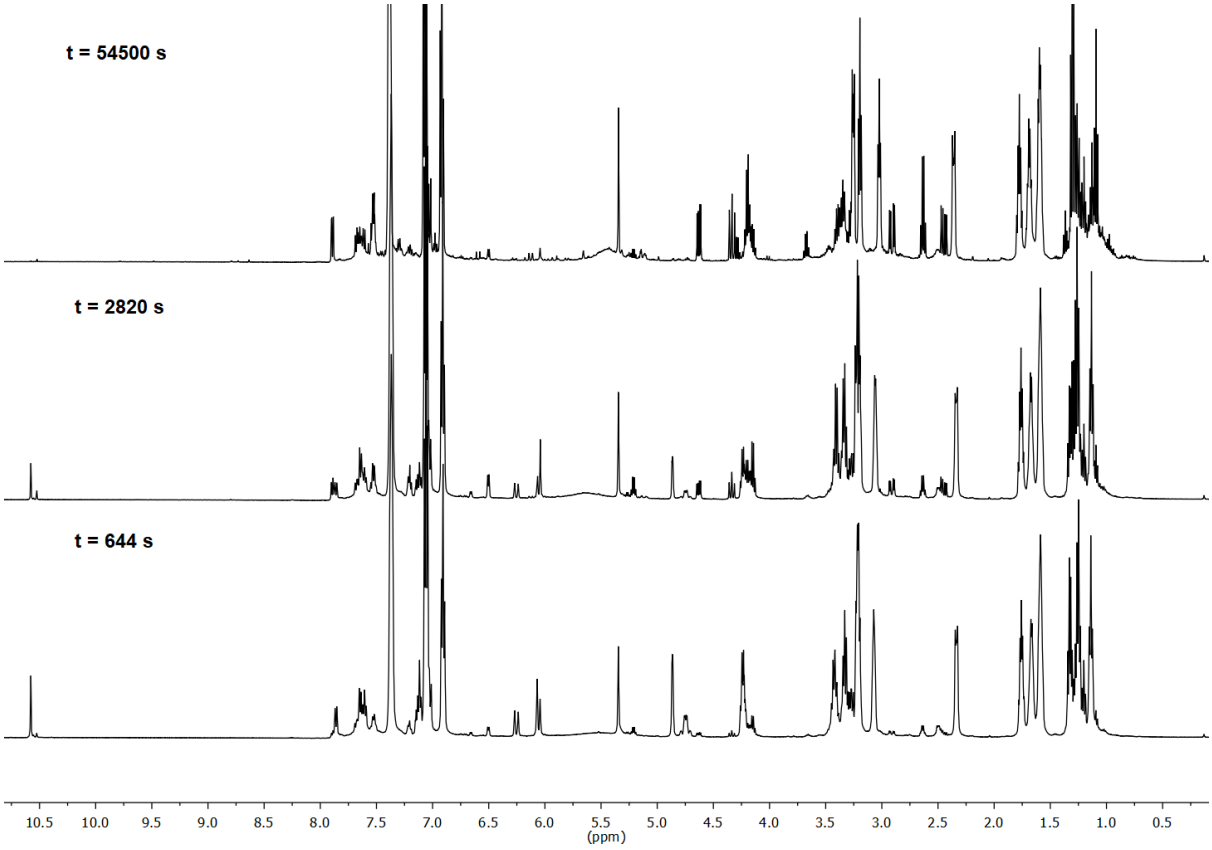

Figure 4.7 Expanded ^{1}H NMR spectra in region 6.8-3.8 ppm of the intramolecular Stetter reaction of 239 catalysed by 140

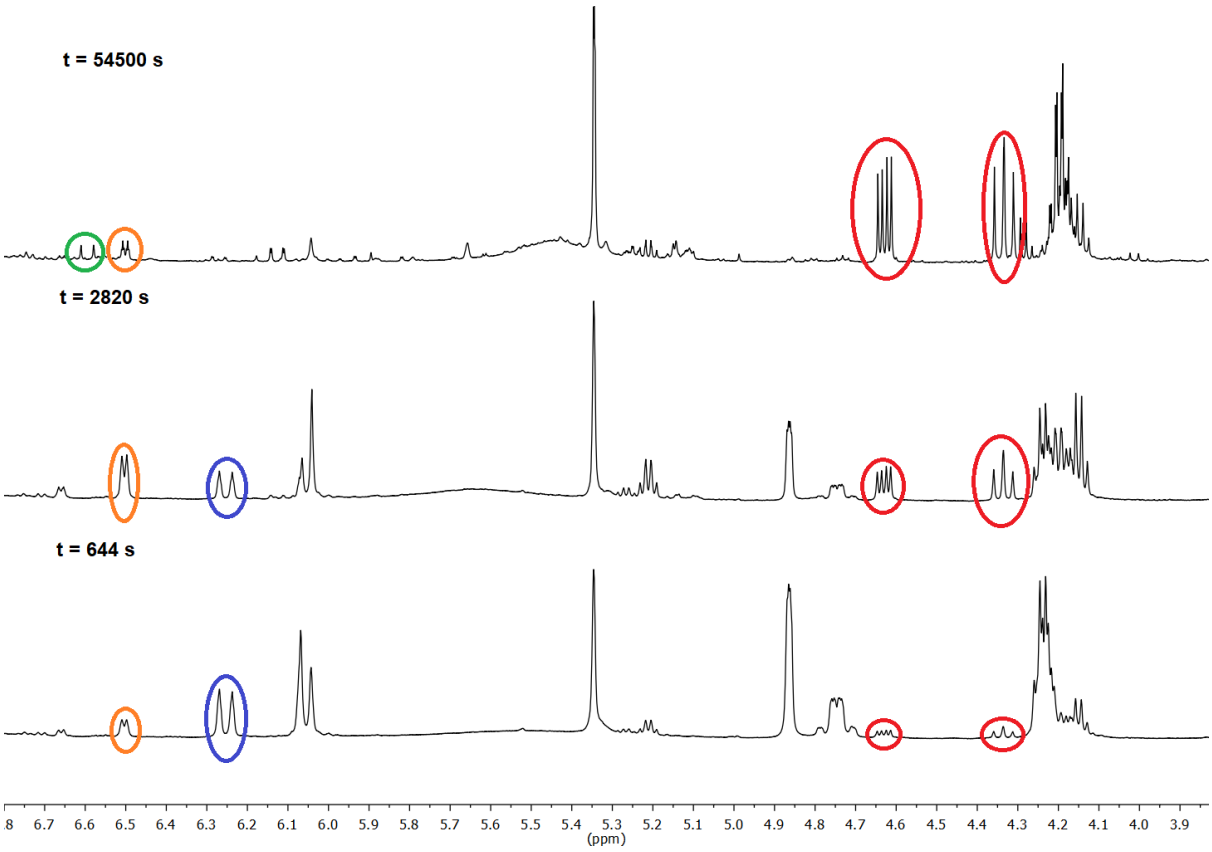

In this experiment, a decrease in the aldehydic proton of **239** as a singlet at 10.5 ppm is observed over the course of the reaction and a concurrent decrease in the doublet at 6.25 ppm owing to decomposition of **239** (circled in blue). Other peaks attributable to **239** are also observed to decrease concurrently, including a doublet of doublets at 6.2 ppm due to the EtO_2C-C(**H**)=C-H group of **239**. Rapid initial formation of a hydroxy-aryl adduct can be observed from the appearance of a peak at ~6.5 ppm (dt, 1H) of the EtO_2C-C(H)=C-**H** group (circled in blue), as well as a partially obscured peak at ~6.05 ppm (1H, s), believed to be BAC-C(OH)**H** proton, and these peaks subsequently decrease over time. The concentration of product **240** steadily increases over time, which is observed as the increase of the triplet at 4.35 ppm and a doublet of doublets at 4.65 ppm (circled in red). These peaks are confirmed to correspond to the ^{1}H NMR spectrum of an independently-prepared and purified sample of **240** using triazolium catalyst **49**. Other peaks arise during this reaction, and while **240** is the major product, many other species were generated, including very small amounts of **260** (circled in green) among other uncharacterised species.

4.2.2 Preparation of Hydroxy-aryl Adducts

4.2.2.1 Preparation of Hydroxy-aryl adducts

As previously discussed, reactions of aryl aldehydes with BACs progress as far as the first step in the catalytic mechanism of the analogous NHC-catalysed reaction, creating the "hydroxy-aryl adduct" but appear to not proceed further. In order to further probe this first step, several hydroxy-aryl adducts were prepared.

Scheme 4.21 Preparation of 255

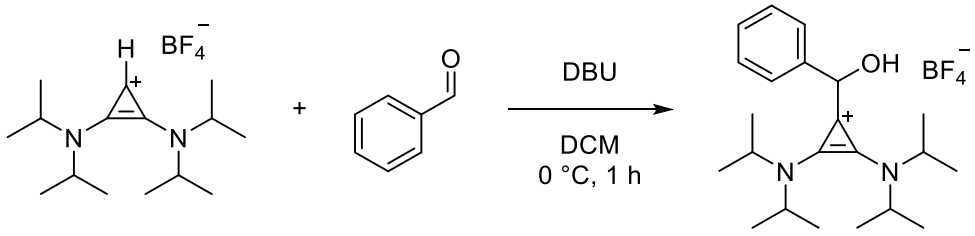

163 **35** **255** 54%

Starting from previously prepared **163** (Chapter 3.2), dissolved in dry DCM, benzaldehyde was added, followed by DBU, and stirred for 1 hour. Purification by careful recrystallization from DCM:Et_2O separated **255** from catalyst **163**. The adduct **255** was found to be stable to air and water.

Figure 4.8 X-ray crystal structures of adduct 255 and ketone oxidation product 261

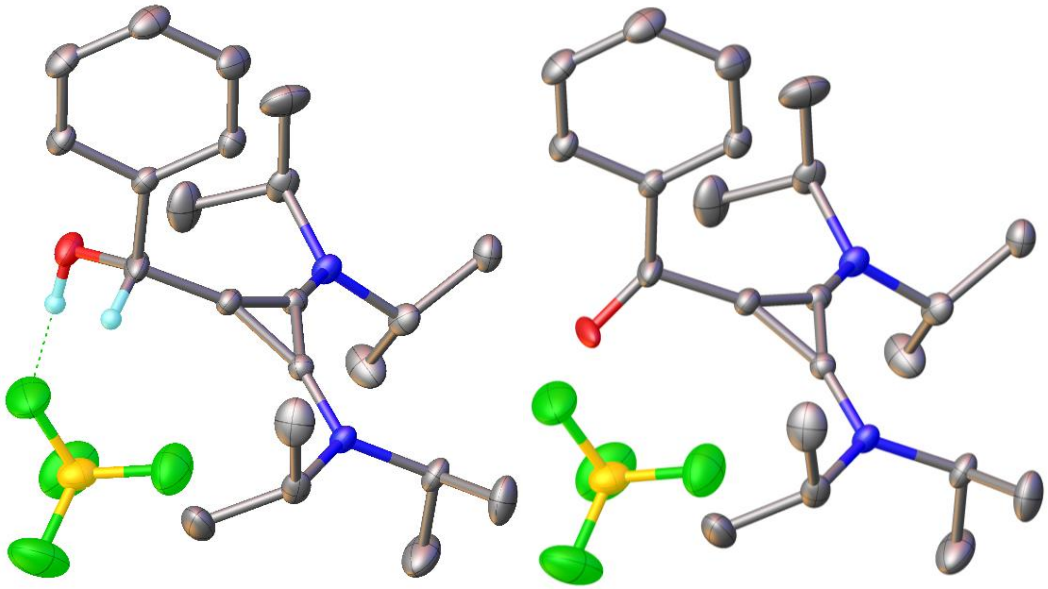

The structure of **255** was confirmed by ^{1}H and ^{13}C NMR spectroscopy, mass spectrometry, IR spectroscopy and by single-crystal X-ray analysis of a crystal formed by slow evaporation of a concentrated solution in acetone.

Figure 4.9 Ketone oxidation product

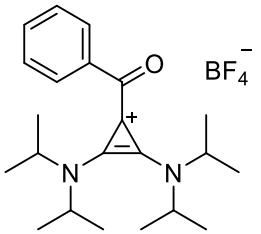

261

The resulting crystal structure is a solid-solution of the hydroxy-aryl adduct **255** and its ketone oxidation product **261** (85:15), presumably formed by atmospheric oxidation during the slow evaporation of acetone while exposed to air and light. Ketone **261** was not observed by ^{1}H, ^{13}C NMR spectroscopy or LCMS of previous samples.

Scheme 4.22 Preparation of 4-fluorophenyl BAC adduct 263

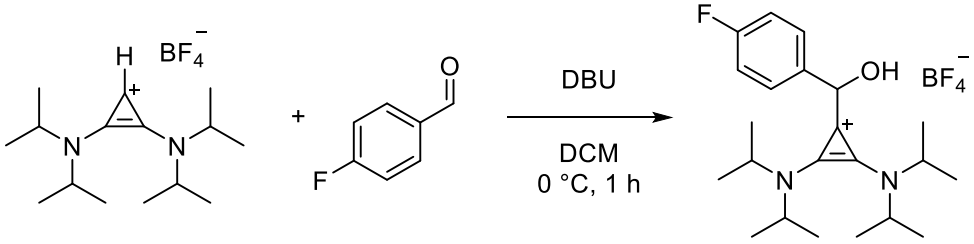

163 **262** **263**
41%

Three other hydroxy-aryl adducts were prepared. Using 4-fluorobenzaldehyde **262** with few alterations to the procedure, the adduct **263** was successfully obtained. The use of electron-rich aldehyde, 4-anisaldehyde **43**, required a modified procedure compared to electron-poor aldehydes as adduct formation was less favoured in the former case.

Scheme 4.23 Preparation of 264 and 265

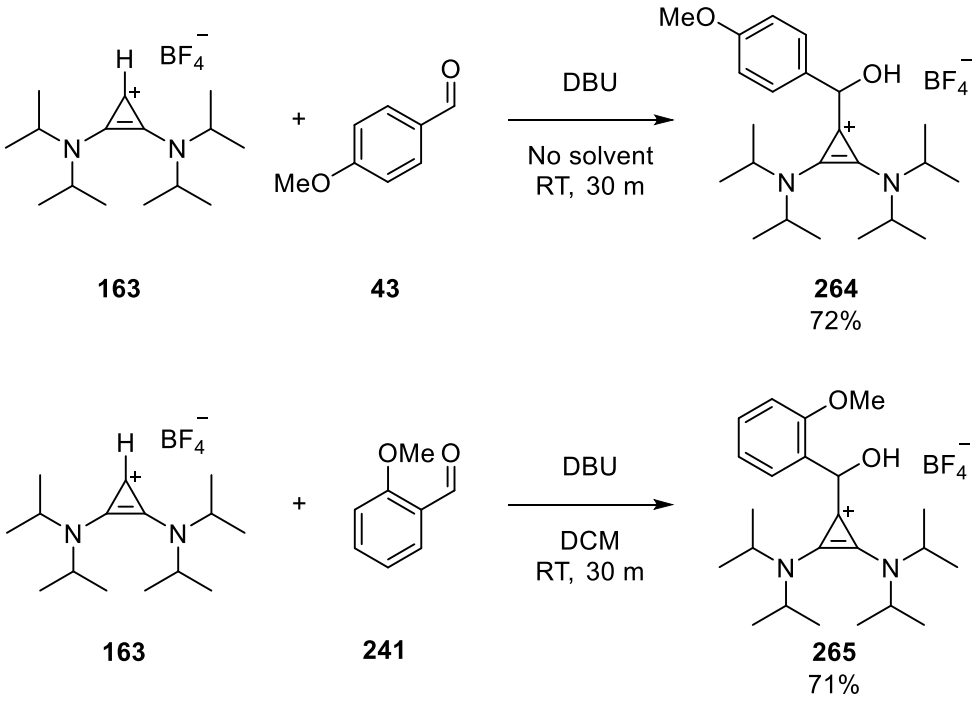

Based on our studies of the reactions of NHCs and aldehydes, the hydroxyaryl adduct exists in equilibrium with starting materials with lower equilibrium constants for more electron rich aldehydes (although this trend is broken for 2-substituents). In order to force the equilibrium towards the product, the concentration of aldehyde was increased, to the extreme of performing the reaction in neat 4-anisaldehyde (m.p. −1 °C), which was highly effective in producing the desired adduct **264**. 2-Anisaldehyde (m.p. 34-40 °C) **241** was added in minimal DCM, which also successfully produced the pure adduct **265**.

Figure 4.10 ^{1}H NMR spectra (600 MHz [a]/700 MHz [b-d]) of isolated adducts (a) 255, (b) 263, (c) 264 and (d) 265 in $CDCl_3$.

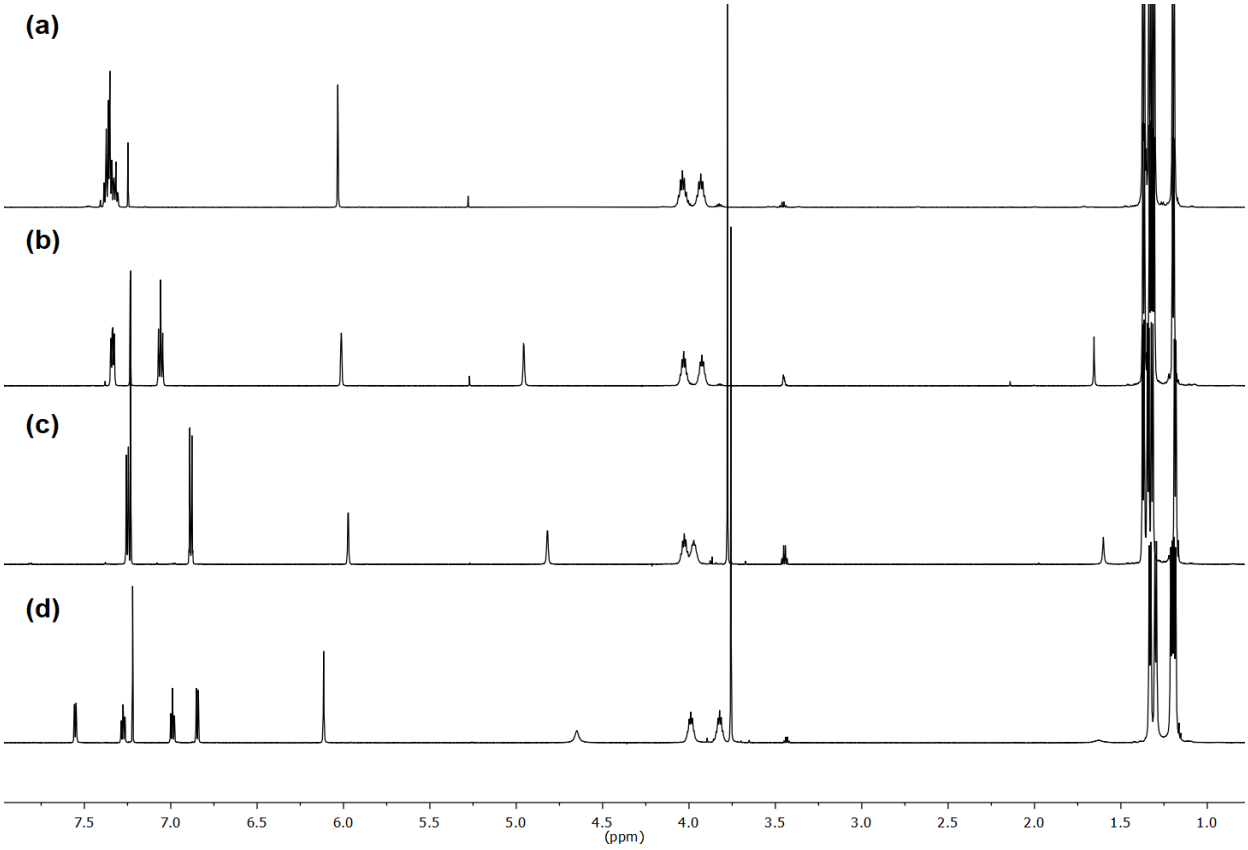

The ^{1}H NMR spectra of adducts **255** and **263-265** are shown in Figure 4.10. Each spectrum shows a peak at ~ 6 ppm corresponding to the benzylic C-*H*. This peak has been noted in our previous ^{1}H NMR spectroscopy monitoring of reactions of **140** and **163** with aryl aldehydes, and isolation has allowed a conclusive analysis of the identity of this species. Additionally, depending on solvent conditions, a broad peak at ~ 5-4.5 ppm is observable corresponding to the O-H proton. Additional peaks are present at ~4 ppm (two septets) and at ~1.3 ppm (sets of doublets), corresponding to the diisopropylamino groups in each example. Methoxy group signals are present as a sharp singlet at ~3.7 ppm in the spectra of **264** and **265**. The aryl peaks are from 7.6-6.8 ppm, varying in each case: **255** aryl peaks are present as a single multiplet, 4-fluoro substituted **263** shows coupling to fluorine, 4-methoxy substituted **264** has two sets of doublets and 2-methoxy substituted **77** has 4 separate peaks. The identities of these compounds were confirmed by HRMS, elemental analysis and IR spectroscopy. The yields presented in the schemes are the best obtained, but are by no means optimized, and it is likely that improvements could be made. Minor solvent impurities are present

in some of these spectra, such as DCM (5.3 ppm, s), diethyl ether (3.5 ppm, q), and HOD (1.5 ppm, s), which could be removed by extensive drying.

Scheme 4.24 Preparation of 267.

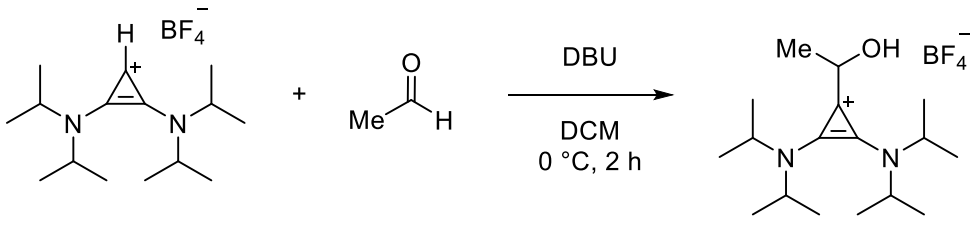

163 **266** **267** 53%

A further hydroxy-alkyl adduct **267** was prepared by use of acetaldehyde **266** in large excess (>80 eq.). This large excess was used due to the low cost and high volatility (b.p. 21 °C) of acetaldehyde, facilitating the purification and increasing the yield of the obtained adduct. The obtained adduct was purified by recrystallization and characterised by NMR, MS and IR spectroscopy.

4.2.2.3 Alkylation of Hydroxyaryl adducts.

Previous studies of hydroxy-aryl adducts of triazolium based NHCs have resulted in difficulties measuring the rate of deprotonation at the C(4) position due to reversion to NHC and aldehyde in basic solutions (See Section 4.2.3 for studies on this subject with BACs). The solution to this problem previously used by our group was to approximate the behaviour of the hydroxy-aryl adduct to its ether derivative, with the latter accessed by alkylation of the alcohol group of the adducts.

Scheme 4.25 Attempted alkylation of 255

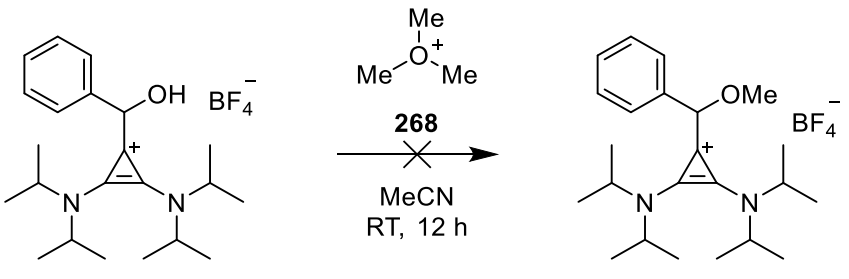

255 **269**

Firstly, to explore the O-alkylation reaction on an NMR scale, adduct **255** was dissolved in d_3-MeCN and trimethyloxonium tetrafluoroborate **268** was added. No reaction was

observed by ^{1}H NMR spectroscopy except the slow decomposition of trimethyloxonium tetrafluoroborate, presumably by reaction with trace water to generate methanol and dimethyl ether, and no trace of the desired product could be detected by LCMS. Using mild base (NEt_3) also failed to give any of the desired product, and only increased the rate of decomposition of **255**. As discussed later (Section 4.2.3), triethylamine did not cause decomposition of adduct **255** to carbene and aldehyde, presumably due to not being sufficiently basic to quantitatively deprotonate the alcohol group.

Scheme 4.26 Attempted alkylation using iodomethane

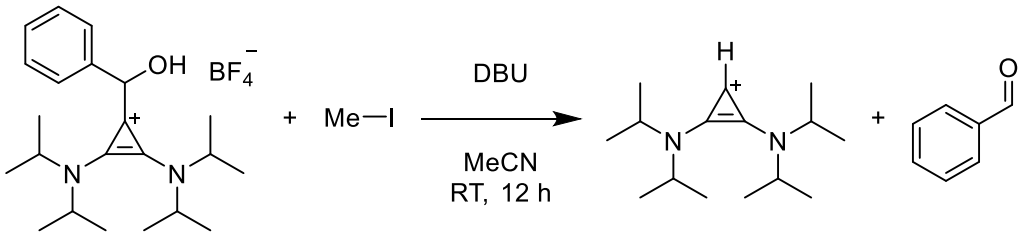

255 **270** **163** **35**

The use of iodomethane **270** as an alkylating agent was similarly unsuccessful in the alkylation of **255**. In the presence of DBU, reversal to BAC conjugate acid **163** and benzaldehyde **35** was observed, however, no O-alkylated product was obtained. From these results, adduct **255** is seemingly incompatible with sufficiently basic conditions, instead equilibrating relatively rapidly to precursor cyclopropenium and aldehyde before alkylation occurs.

An acidic alkylation method employing TMS.diazomethane **271** was then investigated, which had been previously successful in the O-alkylation of NHC-hydroxy-aryl adducts albeit resulting in very low yields.

Scheme 4.27 Partial preparation of 269 using acidified 271.

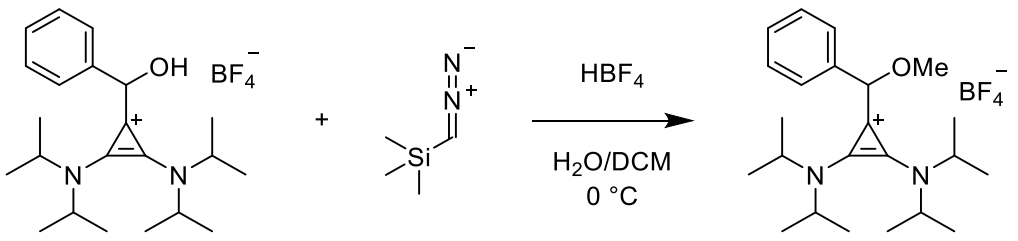

255 **271** **269**

Partial Conversion

The proposed mechanism for this alkylation involves the *in-situ* preparation of diazomethane **1** slowly from the acidic tetrafluoroboric acid mixture. After a large excess (> 10 eq.) of TMS.DAM **271** was added dropwise to the acidic solution of **255**, partial alkylation was observed. Further equivalents of **271** saw diminishing returns of alkylation. Purification of **269** was attempted by fractional recrystallization, which failed to separate **261** from **255**. TLC experiments under various highly eluting conditions (e.g. DCM:MeOH 90:10) failed to show significant separation of the two salts. The direct use of diazomethane was precluded by its high toxicity and its nature as a highly sensitive explosive, requiring specialist glassware and equipment.

Figure 4.11 Alkylation of 255 by acidic etheration

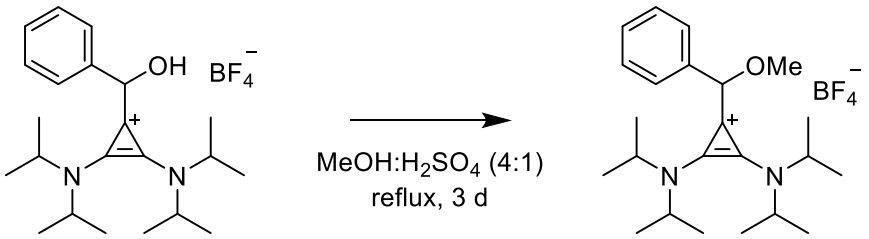

255 **269** 64%

A new methodology was instead developed resulting in the successful alkylation of the hydroxy-aryl adduct **255**. A solution of **255** in a mixture of (4:1) MeOH:H_2SO_4 was heated under reflux (~90 °C) over 3 days. The reaction was monitored by ^{1}H NMR spectroscopy of small quenched aliquots of the reaction mixture, comparing to the results of the previous partial alkylation by **271** above. The reaction mixture was carefully quenched with aqueous $KHCO_3$, to give presumably the sulfate salt of **269**, which was stirred over $NaBF_4$ to give the tetrafluoroborate salt **269**. The pure product **269** was characterised by ^{1}H and ^{13}C NMR spectroscopy, as well as high resolution mass spectrometry.

Figure 4.12 Further adducts

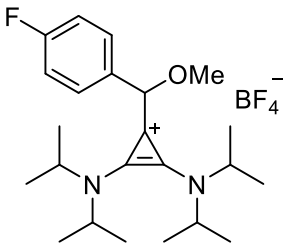

272
63%

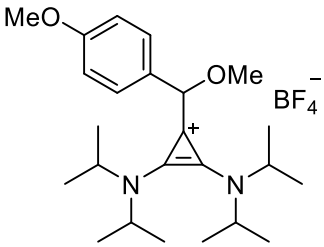

273
85%

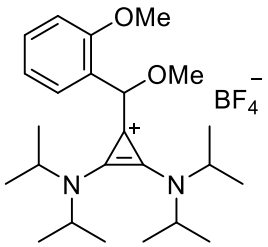

274
95%

The same method was applied to the methylation of the three other adducts, **272-274**. Notably, the reaction of more electron-deficient **272** reached completion significantly more slowly than the electron-rich substrates **273** and **274**, presumably due to the higher nucleophilicity of the latter alcohols. This method is therefore reasonably versatile towards a variety of hydroxy-aryl adducts, however, would possibly not be tolerant of several chemical groups which are acid sensitive, such as esters, amides and nitriles.

4.2.3 Properties of hydroxyaryl adducts

4.2.3.1 Early experiments on hydroxyaryl adducts.

Adducts **255** and **263-265** were found to be stable at room temperature to air and moisture, which aided further mechanistic experimentation.

Figure 4.13 Representative ^{1}H NMR spectra of 255 in d_4-MeOD solution with NEt_3 buffer (2:1 fb, 0.16 M) over time at 25 °C

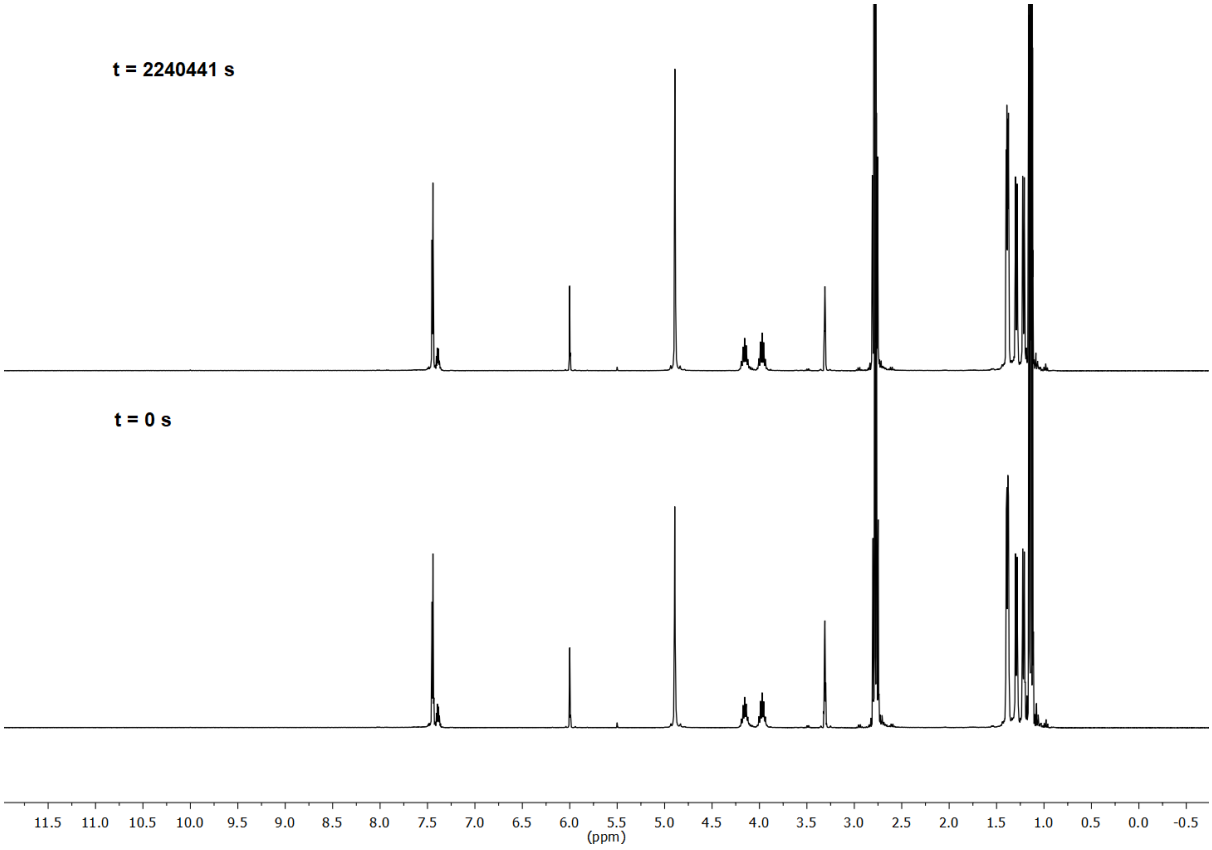

Firstly, the reaction of adduct **255** (5 mM) was explored in various conditions similar to those used in typical organocatalysis experiments. In buffered NEt_3 (2:1 fb ratio, 0.16 M) in d_4-MeOD, <1% reversion to aldehyde was observed, and minimal H/D exchange of the C(4)-H position was observed over the course of 1 month (Figure 4.13)

Figure 4.14 Representative ^{1}H NMR spectra (400 MHz) of the decomposition of 255 in d_4-MeOD solution over time with DBU.

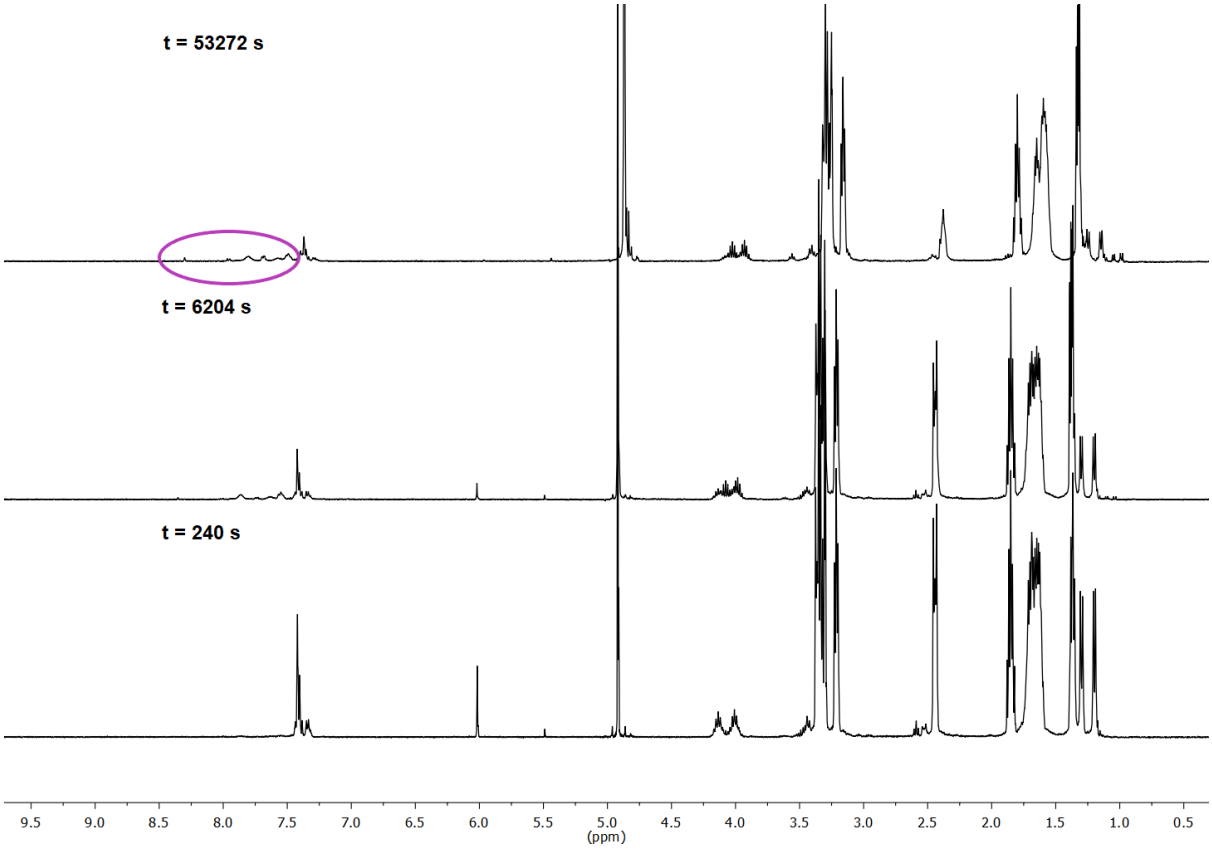

Replacing NEt_3 with unbuffered DBU resulted in the reaction of **255** overnight with significant formation of hemiacetal **256'** as shown by the decrease of the aryl multiplet at 7.4 ppm and increase in broad peaks in the region of ~8-7.4 ppm. It is unclear whether the decay of the peak at 6.0 ppm is due to H/D exchange at the C(4) position of **255** or equilibration to precursor aldehyde and cyclopropenium ion.

Figure 4.15 ^{1}H NMR (400 MHz) spectrum of 263 in $CDCl_3$ solution immediately before (bottom) and after (top) (~4min) addition of DBU

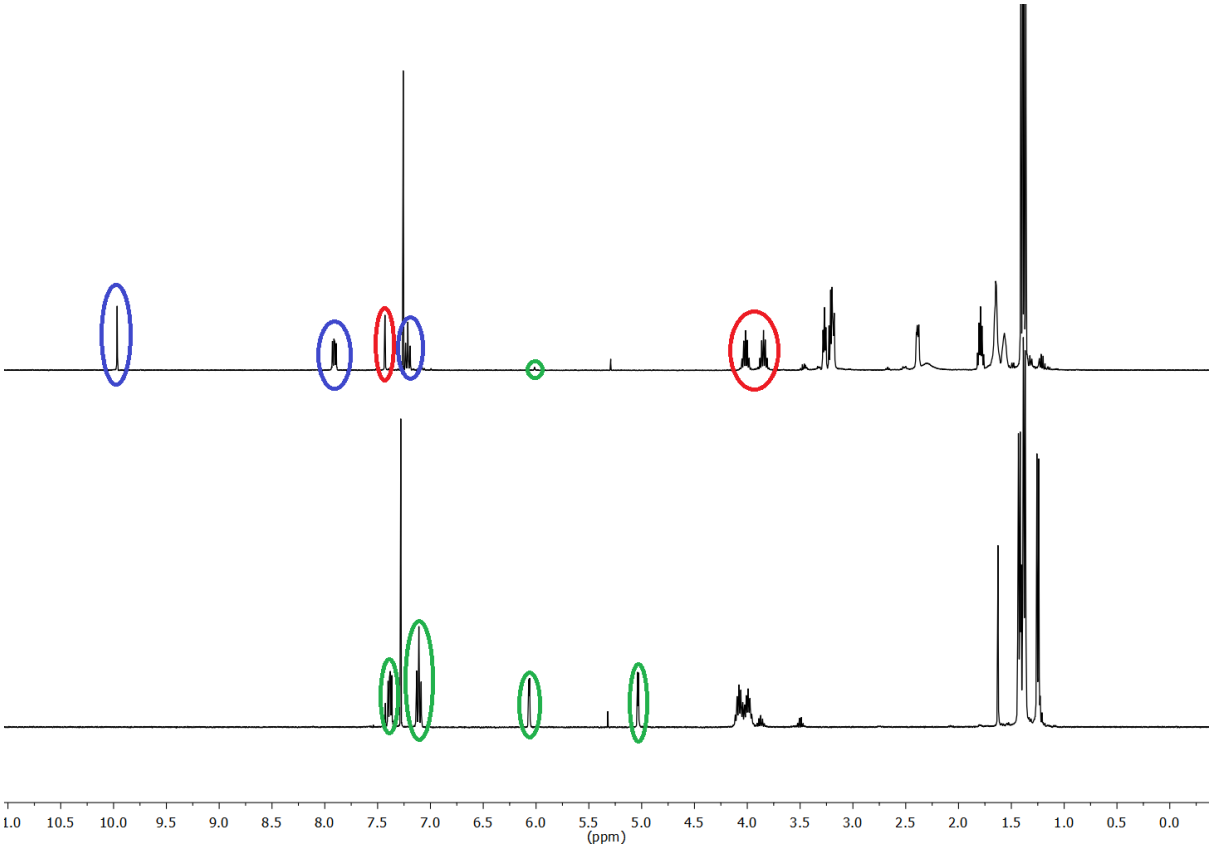

Changing solvent from d_4-MeOD to aprotic $CDCl_3$ resulted in a very rapid reaction of adducts **255** and **263** ($t_{1/2}$ < 4 min). The example of Figure 4.14 shows the rapid reaction of **263** (peaks of interest circled in green) to an equilibrium with BAC conjugate acid **163** (red) and aldehyde **262** (blue). D_2O (~20 µL) was added and the mixture vigorously shaken, however, H/D exchange was not observed at the adduct C(4)H position. Over time a decrease in the area of the peak associated with C3(H) of **163** was observed, either indicating decomposition or H/D exchange of this position.

4.2.3.2 *Estimation of the equilibrium constant between aldehyde, BAC and adduct in d_2-DCM.*

Scheme 4.28 Equilibrium of aldehyde and BAC with adduct

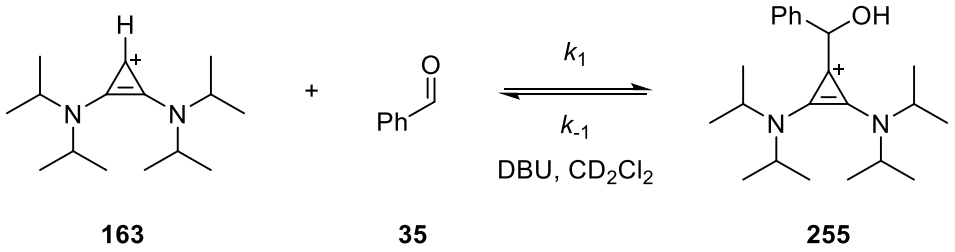

163 **35** **255**

At equilibrium, the rates of forward and reverse reaction are equal, and therefore the ratio of rate constants, k_1 and k_{-1}, describes the position of the equilibrium.

Equation 4.1

$$K = \frac{k_1}{k_{-1}} = \frac{[Adduct]}{[BAC][Aldehyde]}$$

Due to the inability of NEt_3 to effectively deprotonate the alcohol of **255**, this precluded attempts to precisely mimic our previous conditions utilised for analogous NHC studies of the equilibrium between NHC, adduct and aldehyde. In addition, as illustrated in Figure 4.14, the decomposition of adduct **255** in aprotic solvents was found to be too rapid to measure by ^{1}H NMR spectroscopy. The significant formation of solvent adducts **256**/**256'** in d_4-MeOD solutions in the presence of DBU, further complicated attempts to measure the forward and reverse rate constants under conditions akin to Collett et. al.[12]

Due to these factors, the equilibrium constants for adduct formation from BAC conjugate acid **163** and a range of aldehydes were estimated by measurement of relative peak areas of adduct to aldehyde in d_2-DCM. The relative peak areas were measured at relatively early reaction times before significant decomposition of both species in strongly basic solutions.

^{1}H NMR spectroscopic experiments were performed using equimolar solutions of **163** and the relevant aldehyde (each 5 mM), with 3.5 mM DBU (5 mM in the case of aldehyde **43**). Peak areas were measured relative to the singlet due to the internal standard of tetramethylsilane (TMS) at 0 ppm, the concentration of which does not change over the timeframe of these experiments. Unfortunately, each of the peaks

corresponding to BAC overlapped with adduct or aldehyde peaks. Therefore, *K* can only be approximated on the assumption that $[BAC]_t = [Aldehyde]_t$ as at t = 0. Over the short term this is reasonable, as the initial concentrations were precisely measured.

Equation 4.2

$$[Aldehyde]_{t0} = 0.05\ M = \frac{(A_{Ald})_{t0}/(A_{std})_{t0}}{C}$$

Equation 4.3

$$C = \frac{(A_{Ald})_{t0}/(A_{std})_{t0}}{0.05\ M}$$

Equations 4.2-4.3 relate the area of the aldehydic proton peak at ~10 ppm relative to standard TMS (0 ppm) to the pre-determined concentration by a constant C (M^{-1}). This constant C can then be used to convert the relative areas of the other peaks against TMS to concentration. A 17% correction was added to the aldehydic proton at ~10 ppm only, due to incomplete relaxation over the 7s turnover period.

Equation 4.4

$$[Aldehyde]_t = \frac{(A_{Ald})_t/(A_{std})_t}{C}$$

Equation 4.5

$$[Adduct]_t = \frac{(A_{Add})_t/(A_{std})_t}{C}$$

Equation 4.6

$$[BAC]_t = \frac{(A_{BAC})_t/(A_{std})_t}{C}$$

The concentrations at each time point were determined by equations 4.4-4.6. Representative spectra at three time points of the reactions, before and after initiation of the reaction with DBU are shown below with initial concentrations of 0.05 M of **163** and aldehyde in d_2-DCM solution.

Figure 4.16 Representative Spectra of the reaction of 0.05 M* 163 *and benzaldehyde* 35 *in d_2-DCM solution over time with 0.035 M DBU at room temperature.

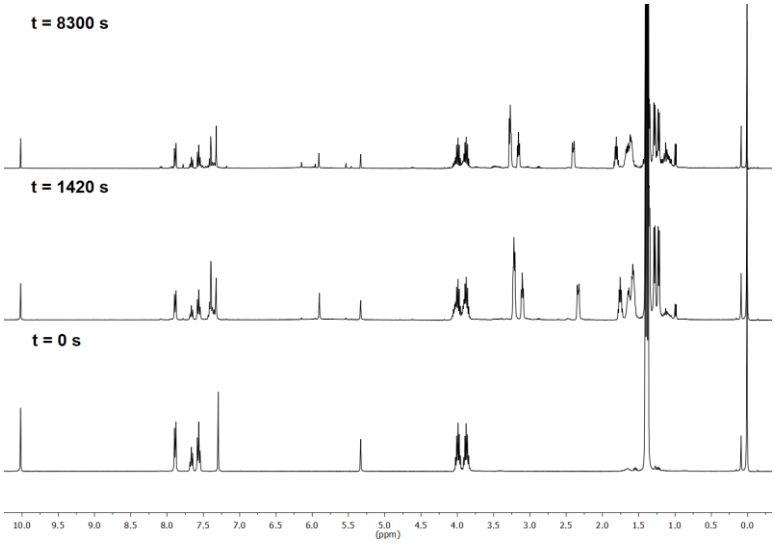

Figure 4.17 Representative Spectra of the reaction of 0.05 M* 163 *and 2-methoxybenzaldehyde* 241 *in d_2-DCM solution over time with 0.035 M DBU at room temperature.

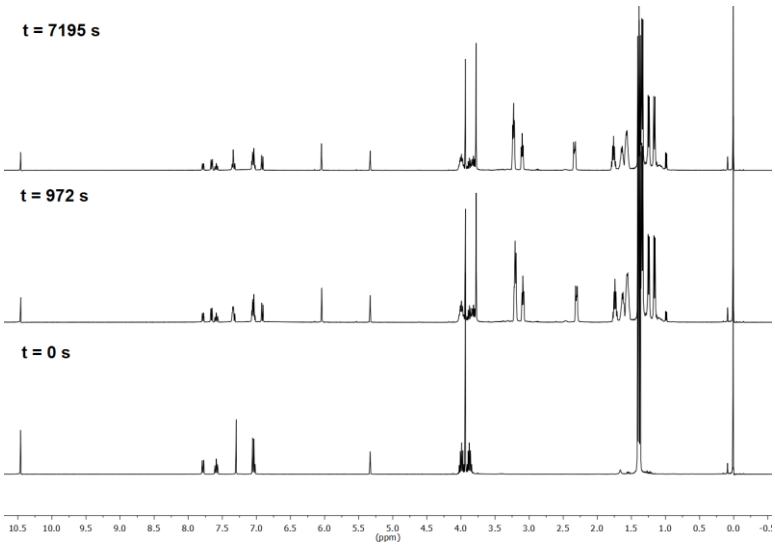

Figure 4.18 Representative Spectra of the reaction of 0.05 M* 163 *and 4-methoxybenzaldehyde* 43 *in d_2-DCM solution over time with 0.035 M DBU at room temperature.

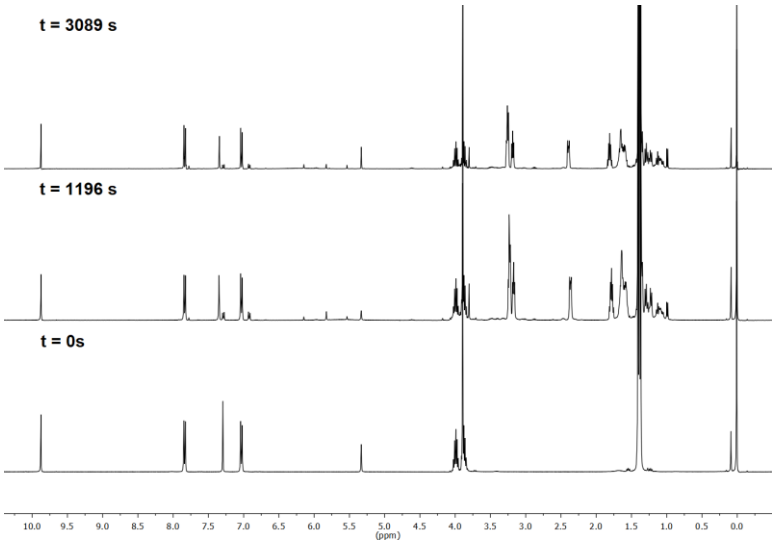

Figure 4.19 Concentration of 255* (■) *and benzaldehyde 3* (●) *over time in d_2-DCM with DBU

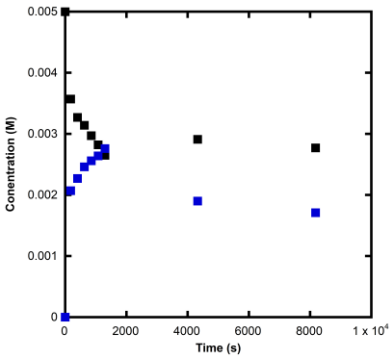

Figure 4.20 Concentration of 273 (■) and 2-methoxybenzaldehyde 241 (●) over time in d_2-DCM with DBU

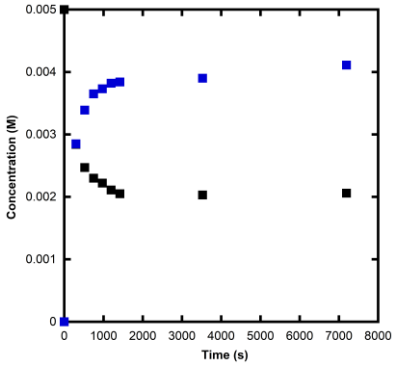

Figure 4.21 Concentration of 274 (■) and 4-methoxybenzaldehyde 43 (●) over time in d_2-DCM with DBU

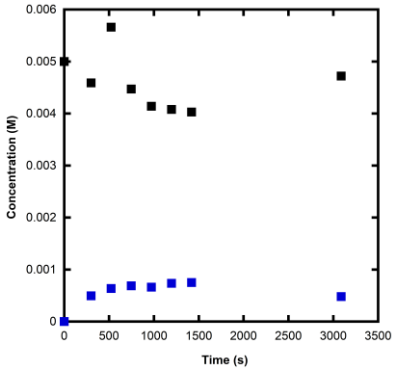

In each case, a rise in adduct concentration was observed, followed by a decrease over a much longer period (slow increases in decomposition product peaks can be seen in Figures 4.16-4.18) Reaction with 2-methoxybenzaldehyde **241** showed relatively little decomposition over time, compared to the other two examples. The later reaction of adduct or precatalyst **163** resulted in a parallel slow increase in the concentration of aldehyde in each case. The equilibrium position is estimated at the maximum concentration of adduct, before the decomposition becomes significant.

Table 4.6 Estimated equilibrium constants for hydroxyaryl adduct formation

Aldehyde	R =	K^{est} (M^{-1})

35	Ph	391
43	4-OMeC_6H_5	34.3
241	2-OMeC_6H_5	923

4.2.3.3 H/D Exchange experiments

As previously discussed, placing hydroxy-aryl adducts **255** and **263-265** in highly basic conditions results in a rapid reversion to the aryl aldehyde and BAC **23**, which makes studying the deprotonation of the C4(H) position more difficult. In order to probe the mechanism of organocatalytic reactions involving BACs, the H/D exchange of alkylated adducts **269** and **272-274** were studied by ^{1}H NMR spectroscopy under basic conditions.

Scheme 4.29 H/D exchange of 269.

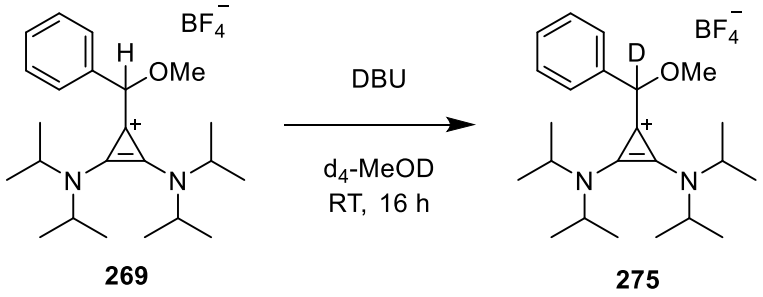

269 **275**

Firstly, **269** was dissolved in d_4-MeOD with equimolar DBU, in order to probe whether H/D exchange occurs under typical organocatalytic conditions. H/D exchange was monitored by ^{1}H NMR spectroscopy over 16 hours at 25 °C

Figure 4.22 Representative ^{1}H NMR spectra (400 MHz) of the H/D exchange of 269 in d_4-MeOD with DBU.

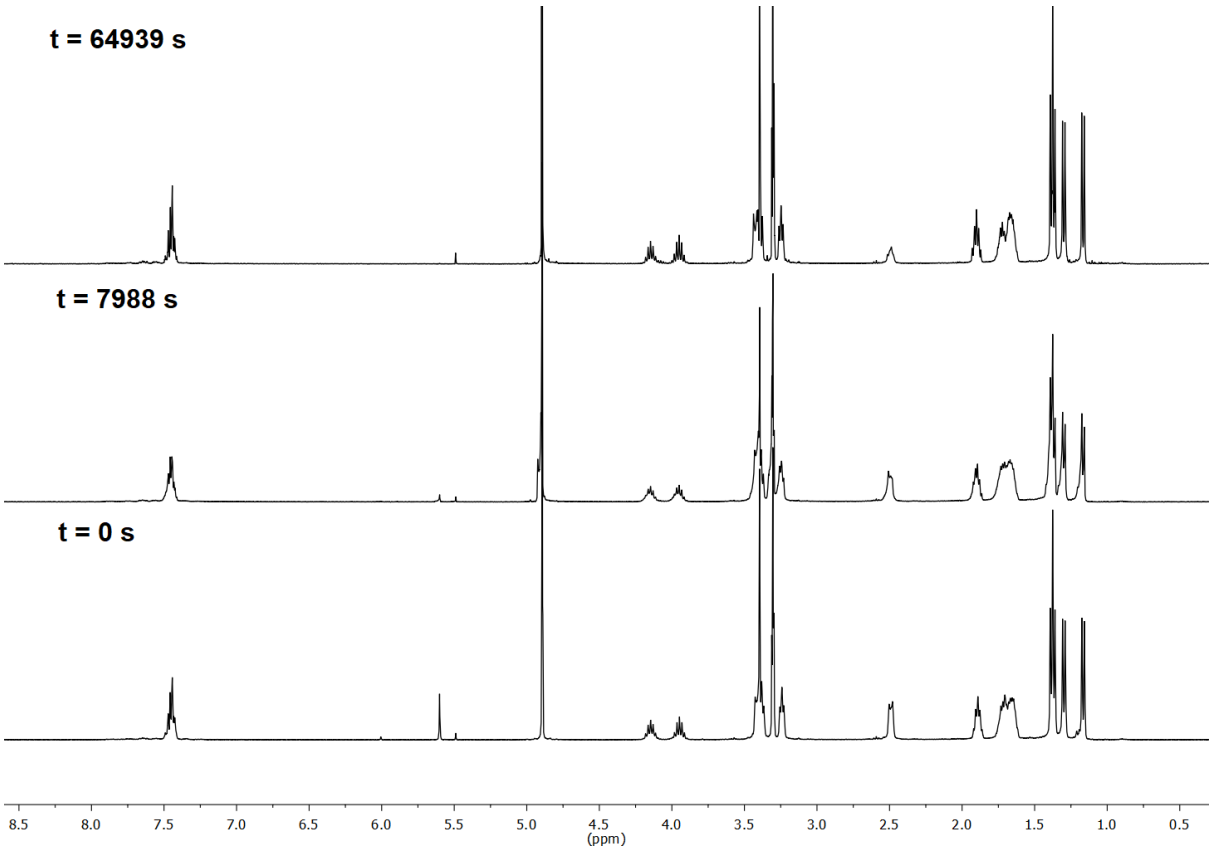

Exchange of the C(4)H proton signal at 5.6 ppm was observed in a pseudo first-order process with a $t_{1/2}$ of ~80 minutes. Over the duration of the experiment, additional reactions of **269** were not observed to a significant degree.

More detailed studies of the H/D exchange of the C(4)H position of adducts were performed in D_2O solutions of dilute NaOD at 25 °C and I = 0.5 (KCl) with an internal standard of tetramethylammonium deuteriosulfate (~1 mM). Due to the poor solubility of the adducts in D_2O, 25 % (v/v) d_3-MeCN cosolvent was added. Due to the very high p*Ds* involved, readings using a p*H* meter would be inaccurate, therefore the p*D* is estimated by concentration of added deuteroxide. In each reaction, parallel decomposition of the substrate was observed.

The progress of deuterium exchange was followed by the decrease of the area of the singlet signal at ~5.5 ppm, corresponding to the C(4) proton of the adducts. The rate of decomposition of adducts was monitored by the decrease of the singlet signal of the methoxy protons at ~3.5-4 ppm. All peaks were integrated relative to the internal

standard peak at ~3 ppm, corresponding to the twelve methyl protons of NMe_4DSO_4, which are known to be non-exchanging under these conditions.

Equation 4.7

$$f(H) = \frac{f(s)}{f(eth)}$$

Equation 4.8

$$f(s) = \frac{(A_{C(4)H}/A_{(std)})_t}{(A_{C(4)H}/A_{(std)})_{t0}}$$

Equation 4.9

$$f(eth) = \frac{(A_{C(OMe)H}/A_{(std)})_t}{(A_{C(OMe)H}/A_{(std)})_{t0}}$$

The fraction of remaining protonated substrate was determined using equations 4.7-4.9. The fraction of remaining C(4)H signal is *f*(s) and the fraction of remaining (C-OMe) signal is *f*(eth). The fraction of remaining protonated substrate is therefore determined by *f*(H), assuming that the decomposition product does not have an overlapping signal with the C(4)H signal. Pseudo first-order rate constants for exchange, $\underline{k}_{ex}$ (s^{-1}), were determined from plots of *f*(H) against time, using non-linear least square fitting to a first-order exponential decay.

Equation 4.10

$$f(H) = e^{-kt}$$

From the data obtained in these experiments, second-order rate constants for deuteroxide catalysed exchange, k_{DO} (M^{-1} s^{-1}) could be determined.

Representative spectra of three time points during the reaction of phenyl adduct **269** in 0.05 M NaOD solution are shown in Figure 4.23. Disappearance of the singlet at 5.75 ppm over time is assigned to hydrogen-deuterium exchange of the C(4)H atom. Other signals corresponding to aryl hydrogens are present at ~7.5 ppm, methoxy hydrogens at 3.5 ppm and further alkyl signals are noted at 4.3, 4.0 and 1.5-1.2 ppm, respectively. Decomposition of parent compound **269** is noted over the timeframe of this reaction, and is monitored through disappearance of the singlet at 3.5 ppm.

Figure 4.23 Representative ^{1}H NMR spectra at 400 MHz of adduct 269 (~5 mM) during exchange of the C(4)-H (s, 5.7 ppm) for deuterium in D_2O:MeCN (3:1 v/v) at I = 0.5, 25°C, 0.05 M NaOD. [Internal standard tetramethylammonium deuteriosulfate (s, 3.2 ppm)]

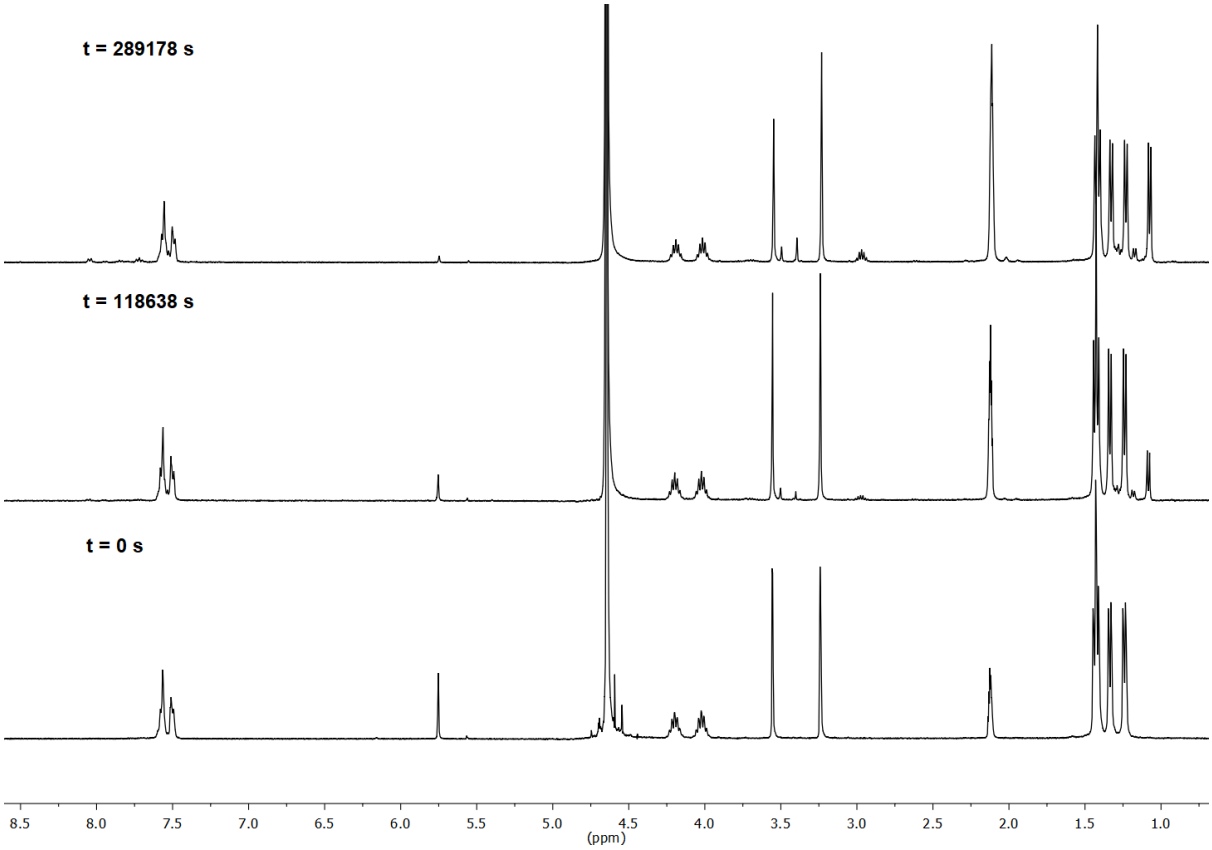

Similarly, hydrogen-deuterium exchange was followed for **272-274**. Representative spectra at three time points are shown for each adduct in Figure 4.23. Exchange was monitored by the decrease of the C(4)-H signal at ~ 5.75 ppm. Decomposition of each salt is noted and is monitored by the decay of the methoxy signal at ~3.5 ppm, against the internal standard at 3.2 ppm.

Figure 4.24 a-c) Representative ^{1}H NMR spectra at 500(a)/400(b-c) MHz of H/D exchange at I = 0.5, 25 °C of a) 272 in 0.45 M NaOD, b) 273 at 0.10 M NaOD, c) 274 at 0.25 M NaOD; in solutions of (3:1 v/v) D_2O:MeCN.

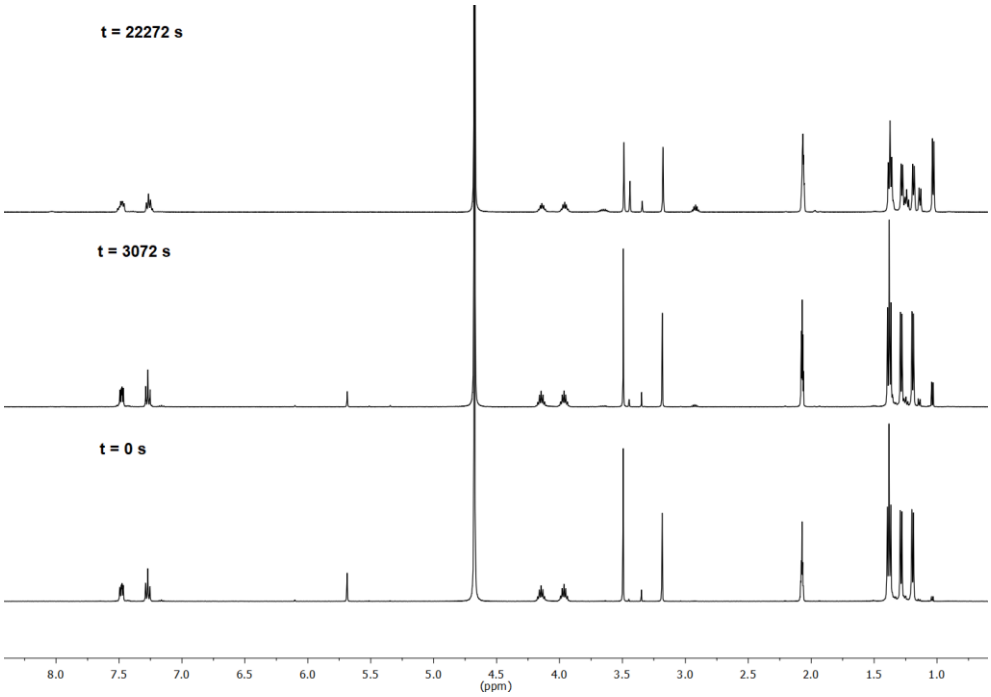

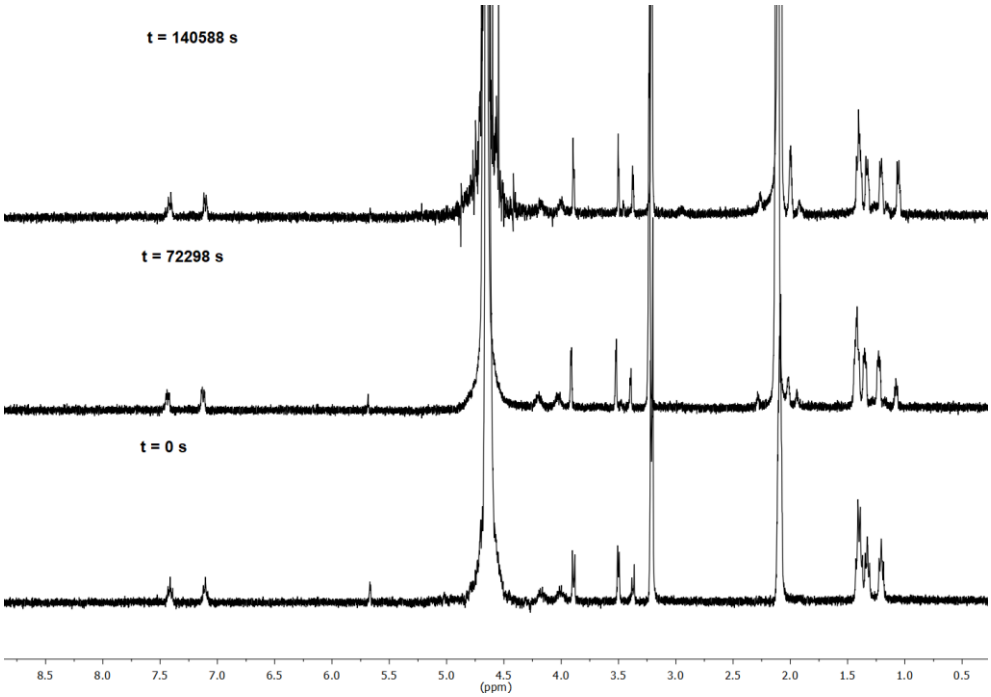

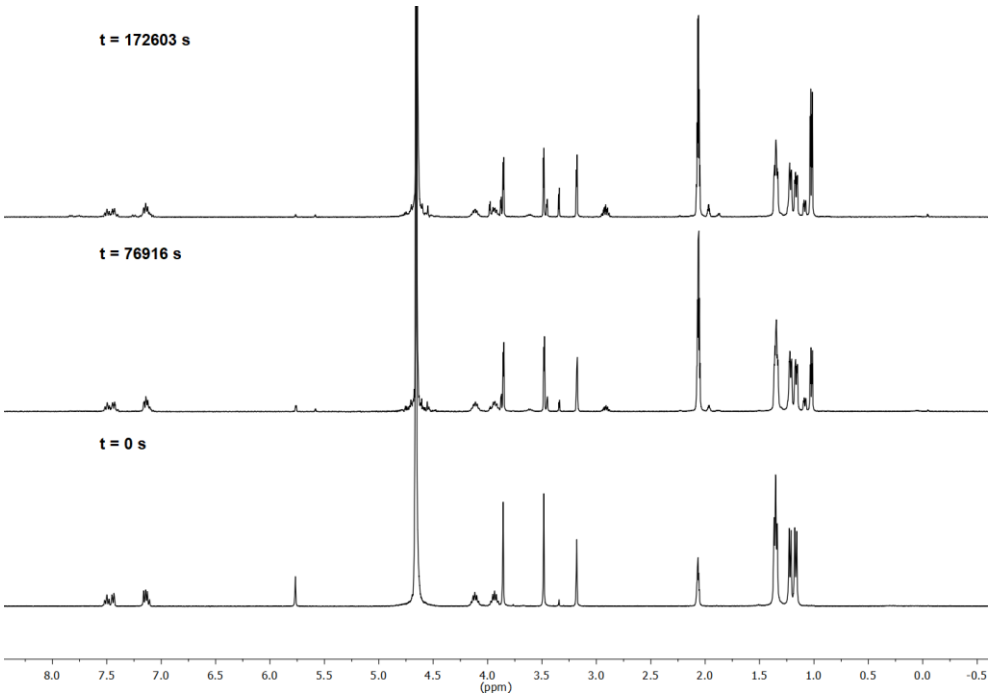

Example plots of *f*(H) against time with non-linear least square fitting are below (Figure 4.25)

Figure 4.25 (a-d) Representative plots of fraction of protonated substrate remaining against time at I = 0.5, 25 °C for adduct a) 269 at 0.025 M NaOD, b) 272 at 0.45 M NaOD, c) 273 at 0.10 M NaOD and d) 274 at 0.45 M NaOD.

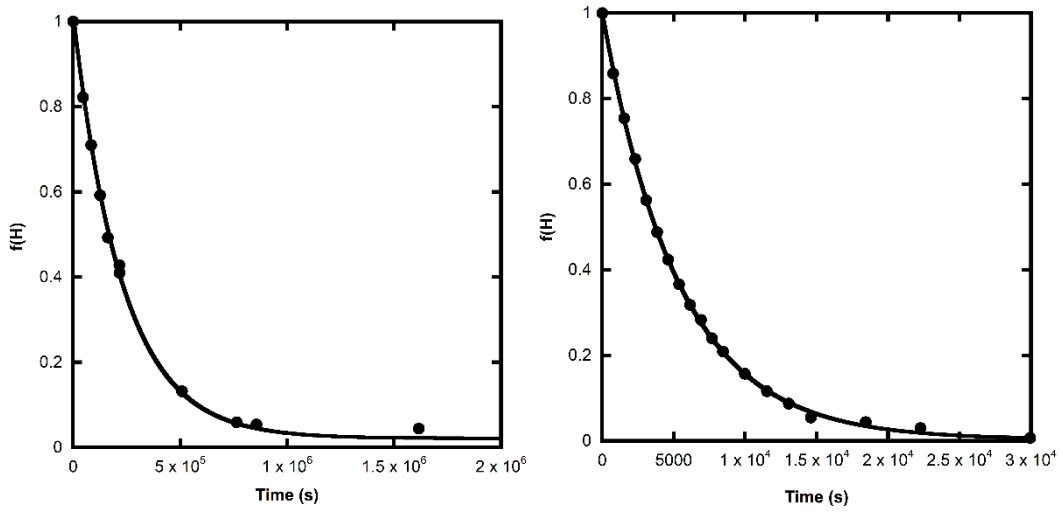

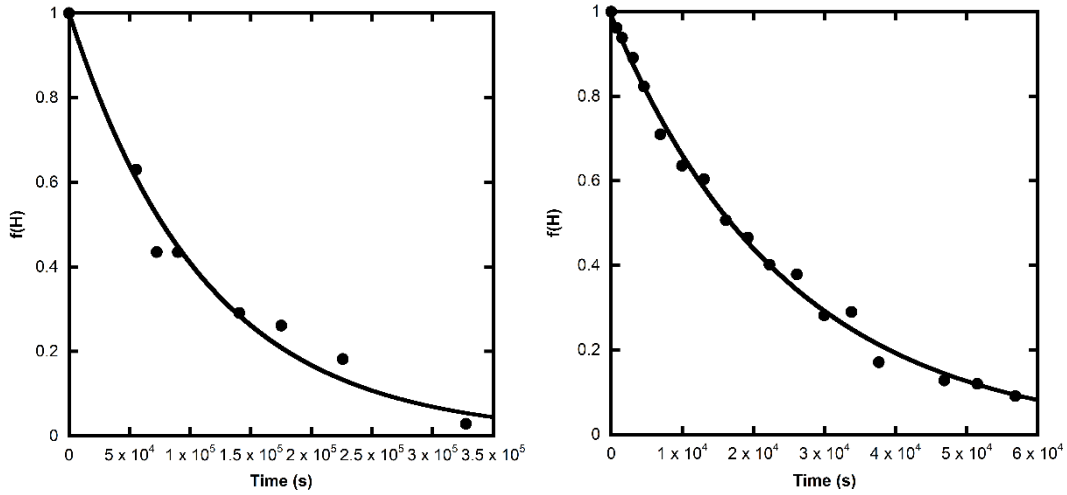

Table 4.7 details the reaction data and resulting k_{ex} values from these experiments. The concentration of deuteroxide is considered to be within error of the added NaOD solutions. The processes of H/D exchange and equilibration do not affect the p*D*, so it is assumed to be constant throughout the experiments.

Table 4.7 H/D exchange data for hydroxy-aryl adducts at I = 0.5 M, 25 °C

Adduct	Concentration NaOD (M)	k_{ex} (s^{-1})
269	0.45	1.19×10^{-4}
	0.25	5.89×10^{-5}
	0.15	3.55×10^{-5}
	0.1	2.27×10^{-5}
	0.05	6.74×10^{-5}
	0.025	4.38×10^{-6}
272	0.45	1.88×10^{-4}
	0.25	6.68×10^{-5}
	0.1	3.39×10^{-5}
	0.025	7.36×10^{-6}
273	0.45	6.76×10^{-5}
	0.1	8.98×10^{-6}
	0.045	4.50×10^{-6}
274	0.45	4.00×10^{-5}
	0.25	1.65×10^{-5}
	0.1	5.28×10^{-6}

	0.045	1.92×10^{-6}

The pseudo first-order rate constant for exchange k_{ex} (s^{-1}) includes kinetic terms for dependence on deuteroxide $k_{DO}[DO^-]$ M^{-1} s^{-1} and additional buffer catalysis ($k_B[B]$ M^{-1} s^{-1}) or solvent dependent deprotonation (k_{D2O}, s^{-1}) terms. As buffer was not employed in these experiments, the buffer term can be ignored. Initially, k_{D2O} is considered insignificant in this case.

Equation 4.11

$$k_{ex} = k_{DO}[DO^-]$$

The H/D exchange of adducts **269, 272-274** shows first-order dependence on $[DO^-]$, and therefore k_{DO} can be determined from the slope of the plots of k_{ex} against $[DO^-]$.

Figure 4.26 a-d) Second-order rate plots of the H/D exchange at I = 1.0, 25 °C of adducts a) 269, b) 272, c) 273, d) 274.

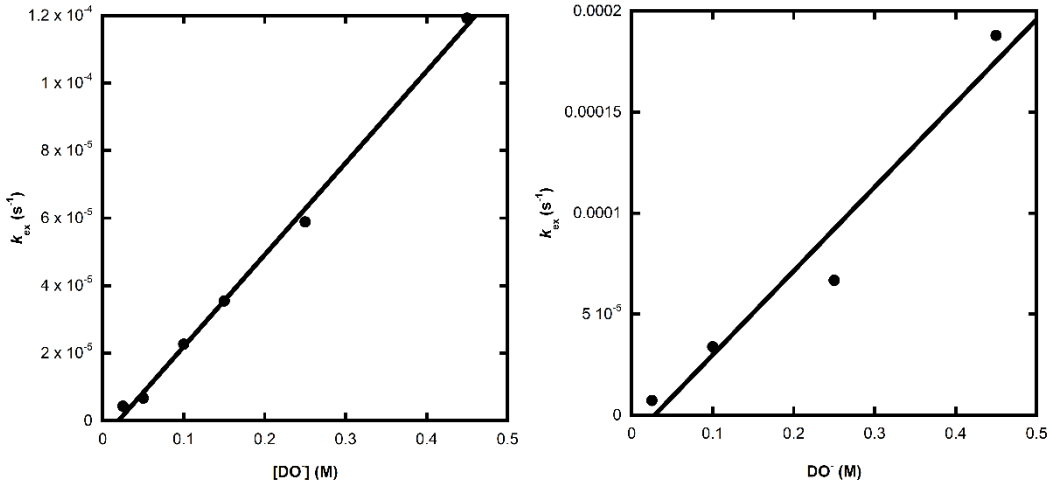

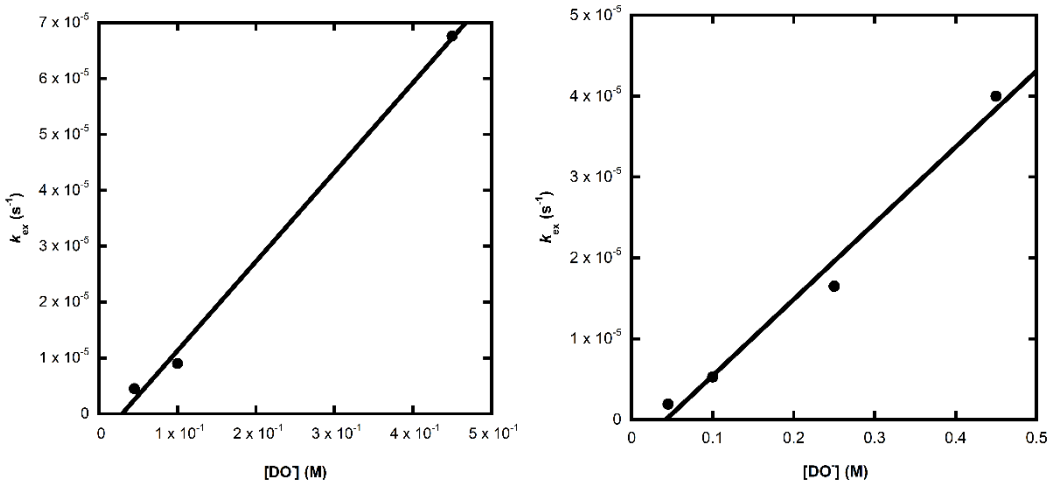

Table 4.8 Second-order rate constants of H/D exchange in adducts 269, 272-274 at I = 1, 25 °C

Adduct	k_{DO} (M^{-1} s^{-1})	k_{rel}[a]
269	2.71×10^{-4}	1
272	4.15×10^{-4}	1.5
273	1.60×10^{-4}	0.6
274	9.42×10^{-5}	0.3

(a) $k_{rel} = k_{DO}$(**x**)/k_{DO}(**269**)

Aside from the method of determination of k_{DO} using Equation 4.11, an alternate method to determine the values of k_{DO} was applied

Equation 4.12

$$f(s) = \mathrm{e}^{-k_{obs}\mathrm{t}}$$

Equation 4.13

$$f(eth) = \mathrm{e}^{-k_{dec}\mathrm{t}}$$

Equation 4.14

$$k_{\mathrm{obs}} - k_{\mathrm{dec}} = k'_{\mathrm{DO}}[\mathrm{DO}^-]$$

Equations 4.12-4.14 were used to calculate pseudo first-order rate constants of decomposition k_{dec} (s^{-1}) and of decrease of the C(4)H signal k_{obs} (s^{-1}), which when subtracted using Equation 4.14 allows for an independent calculation of second-order

rate constant, termed k'_{DO} (M^{-1} s^{-1}). The obtained values of k_{dec} were approximately one order of magnitude lower than k_{ex} in the case of every compound (Appendix B).

Table 4.9 Comparison of k_{DO} and k'_{DO} values

Adduct	k_{DO} (M^{-1} s^{-1})	k'_{DO} (M^{-1} s^{-1})
269	2.71×10^{-4}	2.72×10^{-4}
272	4.15×10^{-4}	4.07×10^{-4}
273	1.60×10^{-4}	1.43×10^{-4}
274	9.42×10^{-5}	9.37×10^{-5}

The differences between k'_{DO} and k_{DO} are relatively small, **269**, **272** and **274** have less than 1% deviation whereas **273** has an anomalously high 11% deviation. This is likely a result of relatively few data points being collected for **273**, and high error associated with k_{dec} estimation, due to reactions not being monitored to completion.

4.3 Discussion

4.3.1 Early Investigations.

Organocatalytic experiments involving BACs were followed by ^{1}H NMR spectroscopy, in order to compare and contrast them to earlier studies on NHC catalysis.

Wilde and co-workers had reported orthogonal BAC behaviour showing a lack of benzoin formation but effective catalysis of the Stetter reaction. To further explore this, initially the reaction of **163** with benzaldehyde only was followed by ^{1}H NMR spectroscopy. Rapid formation of an equilibrium with a hydroxyaryl adduct, similar to the initial step of the benzoin condensation was observed. The reaction appeared to not progress past this point, however, and D_2O shakes in addition to experiments in d_4-MeOD were inconclusive in confirming the presence or absence of H/D exchange through deprotonation of the C-(4)H of the aryl adducts, due to the relatively slow exchange in comparison to decomposition reactions of both the adduct and catalyst system.

In subsequent exploration of the potential intramolecular Stetter reaction of **239** in the presence of **163** or **140**, it was found that the steric bulk of the catalyst used was critical to the success of the reaction. In the presence of diethyl BAC precursor **140**, significant amounts of the product **240** were observed, whereas **163** gave mainly benzofuran **260** as product.

Previous experiments using triazolium based NHC catalysts in the presence of triethylamine did not result in significant amounts of side products during the course of the experiment[11]. The formation of the large number of side-products from this reaction is assigned to the higher basicity of DBU, which is known to be responsible for the base-catalysed formation of benzofuran **260** from **239**[13].

Figure 4.27 Proposed catalytic cycle of the BAC-catalysed Stetter reaction

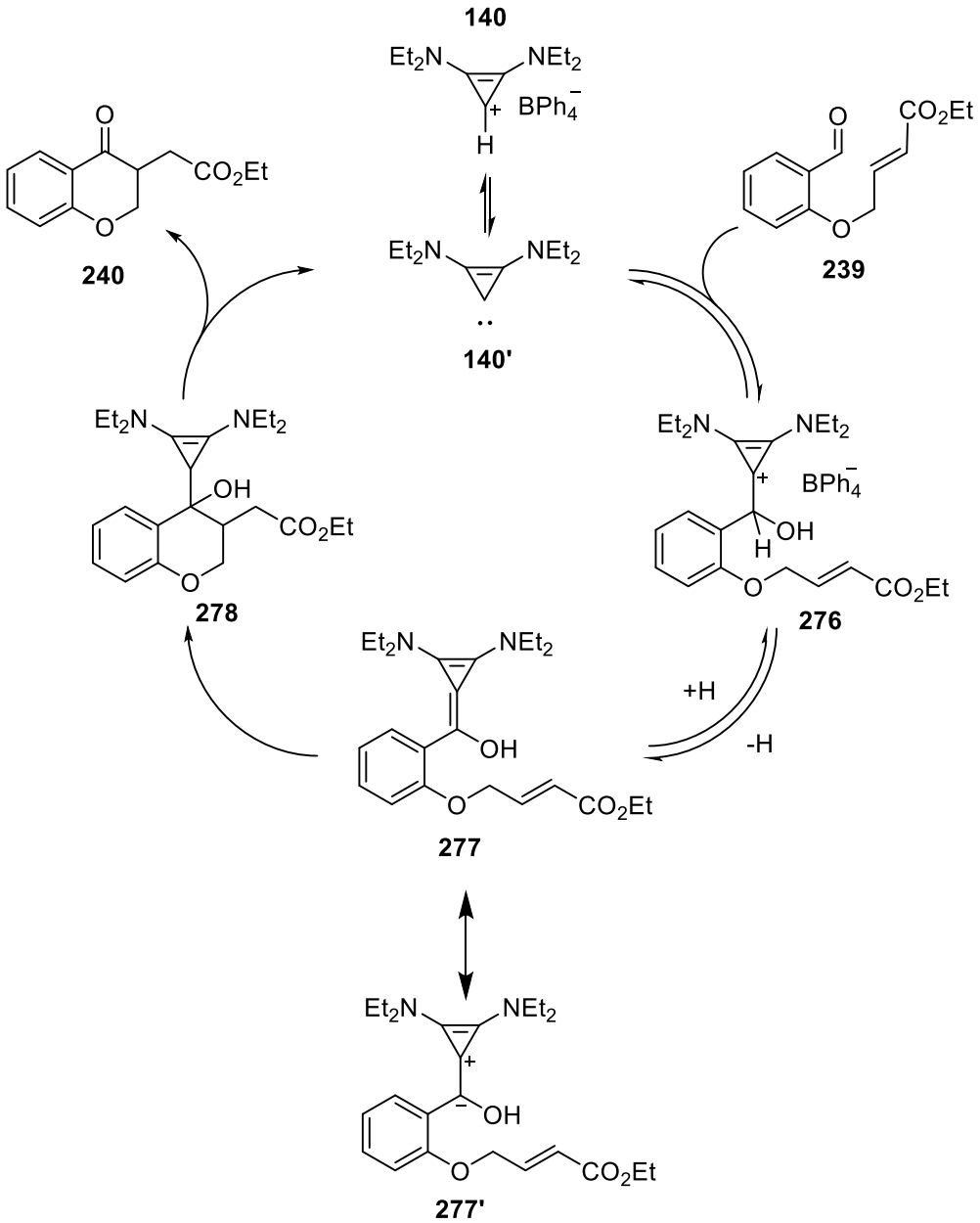

The peaks assigned to intermediates **259** and **276** in both the successful intramolecular Stetter reaction with **140** and unsuccessful reaction with **163** have similar chemical shifts and correct multiplicity to their equivalent peaks in the isolated intermediates

found by Collett. et. al. This suggests that in both cases, the reaction proceeded as far as the hydroxyaryl adduct stage but in the case of **163** no further onward reaction was observed. This is likely a similar factor in Wilde's observations of poor catalytic ability of **129**, the tetraphenyl borate salt of **163**[1].

4.3.2 Properties of hydroxyaryl adducts.

Several hydroxyaryl adducts were prepared from **163** by reaction with aryl aldehydes. Due to the lack of onward benzoin formation, the experimental yields for this process could be improved by the addition of more equivalents of aldehyde, pushing the equilibrium towards adducts. The mixtures were purified by removal of the non-ionic components of the mixture using diethyl ether, and subsequent recrystallization to ensure purity.

While the adducts were reasonably stable under mildly basic conditions with triethylamine, they also failed to undergo either reverse reaction to give benzaldehyde or H/D exchange of the C(4) proton which would indicate the formation of a d_1-acyl anion equivalent. Stronger bases caused deprotonation of the alcohol and reversion to aldehyde and BAC, but distinguishing H/D exchange of the C(4)H position from decomposition of BAC proved difficult.

Equilibrium constants were estimated from the maximum concentration of adduct compared to aldehyde to approximate the equilibrium position in d_2-DCM solution in the presence of DBU. The estimated values of *K* indicate a significant 2-substituent effect, as 2-methoxy adduct **264** has an ~18-fold higher *K* value than its 4-substituted counterpart **265**.

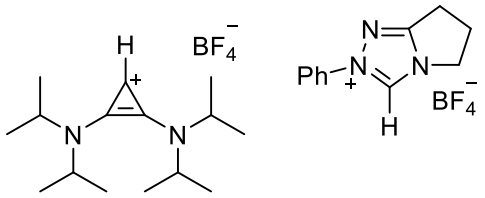

163 **105**

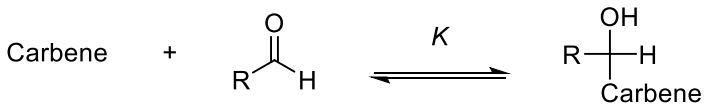

Table 4.10 Comparison of ortho-substituent effect in the addition of carbenes to aryl aldehydes

Carbene conjugate acid	Aldehyde	R =	K (M^{-1})
163[a]	**35**	Ph	391
163[a]	**242**	2-OMe-C_6H_4	923
163[a]	**43**	4-OMe-C_6H_4	34.3
105[b]	**35**	Ph	11.4
105[b]	**242**	2-OMe-C_6H_4	118
105[b]	**43**	4-OMe-C_6H_4	1.92

[a] determined by approximate equilibrium concentrations, CD_2Cl_2, DBU [b] determined by ratio of forward and reverse rate constants, d_4-MeOD, NEt_3/NEt_3HCl

Comparing our estimates of the equilibrium of addition of BACs into aldehydes with those determined by Collett et. al. for NHCs, a similar *ortho*-substituent effect can be observed, where 2-substituted **242** has significantly higher values of *K* than aldehydes **35** or **43**. Direct comparison of the absolute values of *K* cannot be made due to the use of different bases and solvents, but internal comparison clearly demonstrates the presence of this 2-substituent effect in BACs.

This effect has previously been suggested to originate from either destabilisation of the aldehyde starting material due to the steric bulk of the methoxy group, or stabilisation of the adduct due to internal hydrogen bonding between the adduct alcohol and methoxy group. The findings from this work confirm the presence of the 2-substituent effect. Destabilisation of the aldehyde by its 2-methoxy group would have the same effect in reaction with both NHCs and BACs. It is unknown whether the methoxy group has any stabilising interaction in the adduct of **242** and **163**. Significantly, a hydrogen bond is noted between the alcohol group of adduct **255** and its tetrafluoroborate counterion in the crystal structure (Figure 4.8)

Alkylation of the alcohol group of the adducts was difficult due to the poor nucleophilicity of the alcohol group of the positively charged adducts. **255** failed to react with common alkylating agents such as trimethyloxonium tetrafluoroborate and iodomethane under neutral or mildly basic conditions. Stronger bases such as DBU caused decomposition to aldehyde and cyclopropenium precursor, and no detectable alkylation. The use of **271** with tetrafluoroboric acid was more successful, causing

partial alkylation after the addition of several equivalents of **271**. However, this reaction did not go to completion, and product **269** could not be purified from **255**.

Figure 4.28 Mechanism of alkylation

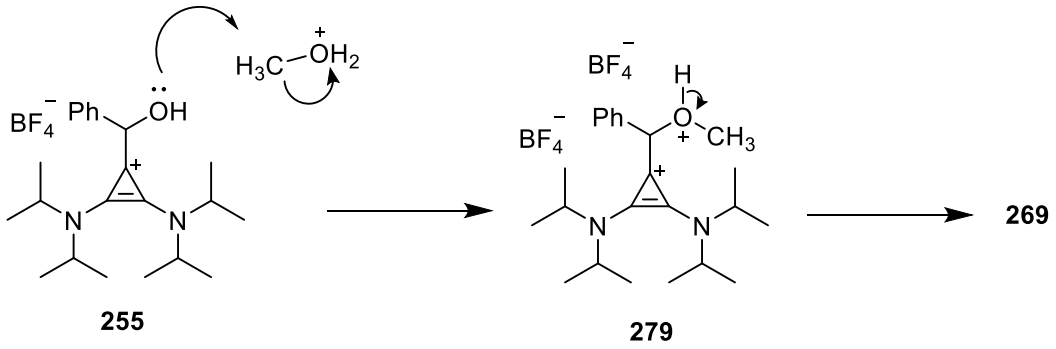

Successful alkylation was achieved using sulfuric acid and methanol under reflux over several days. The mechanism proposed for this reaction is the attack of the alcohol group on **255** with protonated methanol ($MeOH_2^+$ pK_a ~ −4[14]) *via* an S_N2 process. The more electron-rich adducts were found to react more rapidly under these conditions, due to the higher nucleophilicity of their alcohols. Competing elimination reactions that are common with alcohols under these conditions did not occur due to the use of primary alcohol methanol, and the lack of β-protons in the adducts. The disadvantage of this process is its incompatibility with functional groups, which are reactive under the harsh conditions used, possibly limiting the variety of substrates that can be used.

The C(4) proton of the alkylated adducts of more sterically hindered **163** was found to undergo H/D exchange with $t_{1/2}$ ~ 1 hour in d_4-MeOD by DBU. This suggests that this proton can be removed by DBU under organocatalytic conditions, and a lack of deprotonation of this position is not responsible for the chemoselectivity observed by Wilde[1,5].

Compared to known NHC examples, the rate of exchange is significantly slower in BAC adducts. Adduct **251** underwent H/D exchange with a k_2 (s^{-1}) value of 9.45 s^{-1}, ($t_{1/2}$ = 22 hours), whereas **255** did not show detectable H/D exchange under these conditions.**269** underwent H/D exchange in d_4-MeOD using DBU with a $t_{1/2}$ of ~80 minutes. It can be assumed that NHC adduct **247** would have a considerably lower $t_{1/2}$ under these conditions, considering the greatly higher basicity of DBU.

Quantitative studies of the deprotonation of alkylated adducts **269**, **272-274** found second-order rate constants of deprotonation by deuteroxide under basic conditions, which were found to be about 6-7 orders of magnitude slower than the deprotonation of the BAC in aqueous conditions.

Figure 4.29 Comparison of various carbene hydroxy-aryl adducts

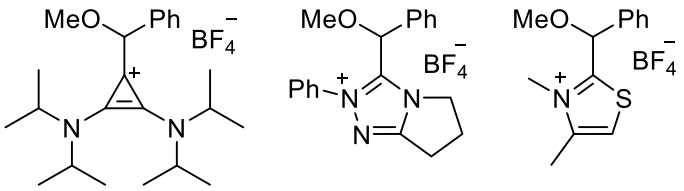

255 **280** **281**

Table 4.11 Comparison between NHC and BAC adducts of second-order rate constants of exchange by deuteroxide in D_2O solutions at 25 °C

Adduct	k_{DO} (M^{-1} s^{-1})
255[a]	2.17×10^{-4}
280[b]	2.08
281[c]	4.46×10^{-2}

a 3:1 D_2O:MeCN, I = 1.0 b 6.5:1 D_2O:MeOD, I = 1.0, [c] calculated from $k_{HO} = 1.86 \times 10^{-2}$, assuming $k_{DO}/k_{HO} = 2.4$, ionic strength was not constant

The second-order rate constants of H/D exchange of adducts **269**, **272-274** were approximately 2 and 4 orders of magnitude lower than those determined for methylated adducts of triazolyl[11] and thiazolyl[15] carbenes respectively. This change is broadly similar to the difference in the carbon acidity of the parent triazolium, thiazolium and bis(amino)cyclopropenium salts.

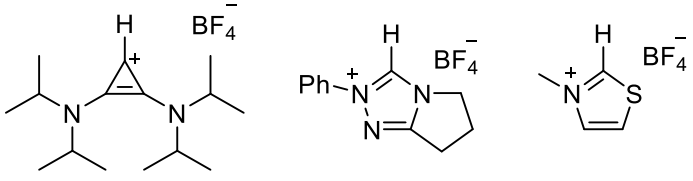

163 **105** **98**

Table 4.12 Carbon acidity and pK_a of BAC and NHC conjugate acids.

Conjugate acid	k_{DO} (M^{-1} s^{-1})	pK_a
163	1.95×10^{3}	22.1

105	6.82×10^7	19.5
98	3.40×10^5	17.5

Figure 4.30 Hammett plot of BAC-adducts 269, 272, 274* (●)*, with 273* (○) *not fitted.

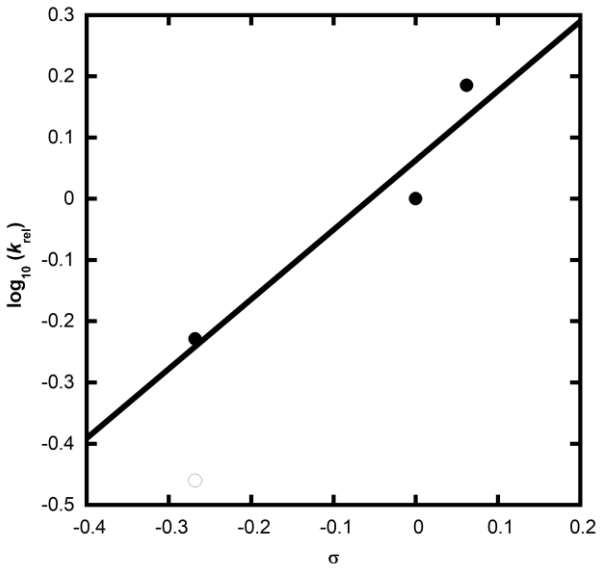

A Hammett plot can be prepared from the obtained values of k_{DO}. The obtained value of $\rho = 1.13$ is positive, indicating a build-up of partial negative charge during the reaction, and the magnitude suggests a relatively similar value obtained in Hammett's studies on the hydrolysis of aryl esters[16]. Although limited to three data points, the positive ρ value clearly supports negative charge build-up consistent with a deprotonation reaction.

Figure 4.31 Hammett plot of k_2 of 4-substituted (■) and 2-substituted (□) NHC adducts from Collett. et. al[12].

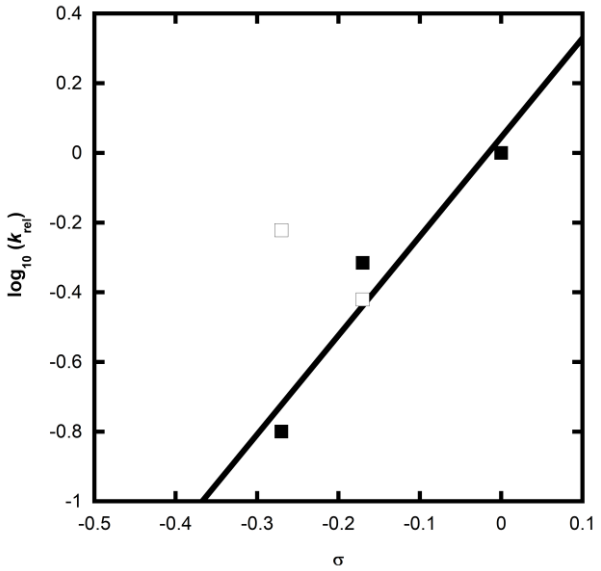

If we compare this data to the trend observed in k_2 values obtained by Collett et. al.[12], the onward reaction of 4-substituted aryl adducts of triazol-3-ylidenes gives a larger value of $\rho = 2.84$, which indicates a much greater dependence on the N-aryl substituent for the deprotonation step than observed for the BACs. This could be a result of a greater electronic or electrostatic stabilisation of the enol/ylide provided by the BAC relative to NHC thus a lesser reliance on the N-aryl group for stabilisation. It is important to note, however, that these experiments were performed in d_4-MeOD, rather than in D_2O:MeCN solutions, thus solvent effects could also account for differences in the absolute Hammett ρ values. More detailed Hammett analyses in both systems with a broad range of substituents under the same reaction conditions would provide a more reliable comparison.

The weaker substituent effect in BACs could have an additional origin. Examination of the obtained crystal structure of adduct **255** (Figure 4.8) indicates that the aryl ring is almost exactly perpendicular to the cyclopropenium ring. This is likely due to steric hindrance from the large isopropyl groups. If the aryl ring is out of plane with the developing partial negative charge during proton-transfer, there would be a limited ability for the substituents to stabilise or destabilise the reaction by resonance.

4.4 Conclusions and Further Work.

In this chapter, the mechanism of organocatalysis of BACs was probed and compared to the reactivity of similar NHC-catalysed processes.

Using BACs as catalysts in the intramolecular Stetter reaction confirmed the findings of Wilde et. al[1], that steric hindrance is of high importance in determining the utility of BACs in organocatalysis. Bulkier BAC **163** did not produce detectable quantities of product **240**, but the less bulky catalyst **140** successfully produced product **240**. The presence of a hydroxy-aryl adduct **259** in the BAC-catalysed intramolecular Stetter reaction was supported by comparison to previous ^{1}H NMR spectra of intermediates in the NHC-catalysed intramolecular Stetter reaction[11]. Additionally, the high basicity necessary to deprotonate BAC conjugate acids compared to triazolium-based NHCs has the undesired effect of introducing competing base-catalysed processes, such as the formation of benzofuran **260** from substrate **239** that do not occur under milder conditions.

Several hydroxy-aryl adducts were prepared, isolated and fully characterised. In mildly basic conditions the adducts are stable but do not undergo H/D exchange, indicating a lack of formation of an d_1-acyl anion equivalent. Stronger bases both successfully form this d_1-acyl anion equivalent but also cause the adduct to equilibrate with aldehyde and BAC. Reaction with 2-methoxybenzaldehyde **242** was significantly more favoured than with 4-methoxybenzaldehyde **43**, which suggests a similar *ortho*-substituent effect on adduct formation to that noted by Collett. et. al[12].

Methylation of the adducts was required in order to probe proton-transfer of the C4(H) position and was achieved by a harsh method involving refluxing sulfuric acid/methanol. This method could possibly be applied to the methylation of NHC adducts, which would eliminate the need to use TMS.Diazomethane **271**. Alkylated adduct **269** was shown to undergo H/D exchange of the C(4)H position under conditions used in organocatalytic reactions, with a $t_{1/2}$ of ~80 minutes using DBU in d_4-methanol. Further testing in aqueous systems showed that the adducts underwent H/D exchange significantly slower than existing NHC adducts. A moderate substituent effect on the values of the second-order rate constants of exchange (k_{DO}, $M^{-1}\,s^{-1}$) was found, which was lower in magnitude than observed for NHC adducts in methanol solutions.

4.5 Bibliography

1 M. M. D. Wilde and M. Gravel, *Angew. Chem. Int. Ed.*, 2013, **52**, 12651–12654.
2 Berkessel A., Elfert S., Yatham V. Reddy, Neudörfl Jörg-M., Schlörer Nils E. and Teles J. Henrique, *Angew. Chem. Int. Ed.*, 2012, **51**, 12370–12374.
3 Berkesselv A, Yatham V. Reddy, Elfert S. and Neudörfl Jörg-M., *Angew. Chem. Int. Ed.*, 2013, **52**, 11158–11162.
4 N. E. Wurz, C. G. Daniliuc and F. Glorius, *Chem. – Eur. J.*, 2012, **18**, 16297–16301.
5 M. M. D. Wilde and M. Gravel, *Org. Lett.*, 2014, **16**, 5308–5311.
6 B. T. Ramanjaneyulu, S. Mahesh and R. V. Anand, *Org. Lett.*, 2015, **17**, 3952–3955.
7 X. Lu and U. Schneider, *Chem Commun*, 2016, **52**, 12980–12983.
8 G. Kuchenbeiser, M. Soleilhavoup, B. Donnadieu and G. Bertrand, *Chem. - Asian J.*, 2009, **4**, 1745–1750.
9 V. Lavallo, Y. Ishida, B. Donnadieu and G. Bertrand, *Angew. Chem. Int. Ed Engl.*, 2006, **45**, 6652–6655.
10 V. Lavallo, Y. Canac, B. Donnadieu, W. W. Schoeller and G. Bertrand, *Science*, 2006, **312**, 722–724.
11 C. J. Collett, R. S. Massey, O. R. Maguire, A. S. Batsanov, A. C. O'Donoghue and A. D. Smith, *Chem. Sci.*, 2013, **4**, 1514–1522.
12 C. J. Collett, R. S. Massey, J. E. Taylor, O. R. Maguire, A. C. O'Donoghue and A. D. Smith, *Angew. Chem Int. Ed.*, 2015, **127**, 6991–6996.
13 S. Reddy, S. Thadkapally, M. Mamidyala, J. B. Nanubolu and R. S. Menon, *RSC Adv.*, 2015, **5**, 8199–8204.
14 J. Clayden, N. Greeves and S. Warren, *Organic Chemistry*, Oxford University Press, Oxford, New York, Second Edition., 2012.
15 G. L. Barletta, Y. Zou, W. P. Huskey and F. Jordan, *J. Am. Chem. Soc.*, 1997, **119**, 2356–2362.
16 L. P. Hammett, *J. Am. Chem. Soc.*, 1937, **59**, 96–103.

CHAPTER 5 – From Nitron to Novel Stable Benzotriazinyl Radicals.

5.0 Foreword

As discussed in chapter one, 1,2,4-benzotriazinyl radicals are an important family of organic radicals known for their high stability. This chapter focusses on work relating to the preparation of a family of novel benzotriazinyl radicals from the stable N-heterocyclic carbenoid compound Nitron **35**. Section 5.1 provides a literature review of modern benzotriazinyl chemistry and the chemistry of Nitron. Sections 5.2 and 5.3 presents the results of our investigation into this new synthetic route and the properties of the radicals. The research in this chapter has been partially published in Nature Communications[1], in collaboration with other researchers at the University of Durham and University of York.

5.1 Introduction

The study of organic magnetic materials is a field very much in its infancy. The majority of molecular magnetic materials are organometallic[2] complexes with low Curie temperatures (T_c), but some promising developments have been made in graphene research, including a report of room temperature ferromagnetism[3]. The ferromagnetism of graphene, however, is believed to be a result of defects in the graphene structure. Earlier work claimed to have discovered ferromagnetic behaviour in rhombohedral C_{60} fullerenes[4], however, was later retracted due to the discovered presence of iron impurities in the samples[5].

Figure 5.1 Dithiazolyl 282 and nitroxide 283 radicals

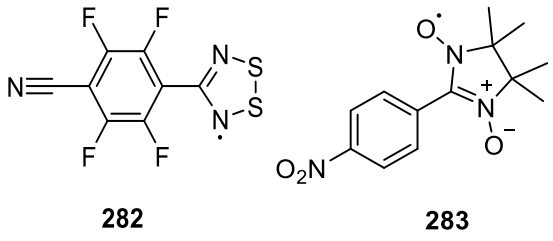

282 **283**

Purely organic magnetic materials are extremely rare and have low T_c values. A dithiadiazolyl radical **282** has been found with an unprecedentedly large T_c value of 36 K[6], above liquid helium temperature. Most dithiadiazolyl radicals, however, are diamagnetic in the solid state due to a spin-paired interaction between sulfur atoms[7].

Other organic magnetic materials mostly have extremely low T_c values. As an example, *p*-nitrophenyl nitronyl nitroxide **283** has a T_c of 0.6 K.[8]

The first stable benzotriazinyl radical discovered was the 1,3-diphenyl-1,2,4-benzotriazinyl radical **87** reported by Blatter[9] in 1968 (**Error! Reference source not found.**). The radical was f ound to have a stability comparable to the existing EPR standards of the time. Blatter's radical **87** was prepared by acid-catalysed ring closing of an iminobenzamidine **284**, followed by treatment with aqueous ethanolic KOH solution to give the black crystals of radical.

Scheme 5.1 Preparation of the first benzotriazinyl radical from triazabutadiene 284 by Blatter.

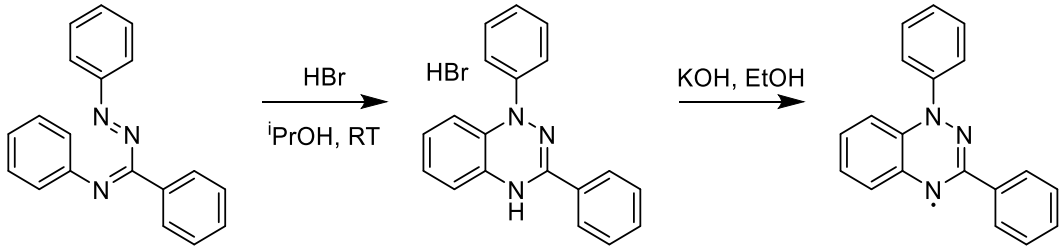

284 **285** **87**

Despite Blatter's first publication being as long ago as 1968, these radicals have seen relatively little focus until recently, where benzotriazinyl radicals have become of particular interest owing to their stability making them suitable building blocks for organic magnetic materials.[10]

5.1.1 Synthetic Methods

Scheme 5.2 Preparation of triazabutadiene 284

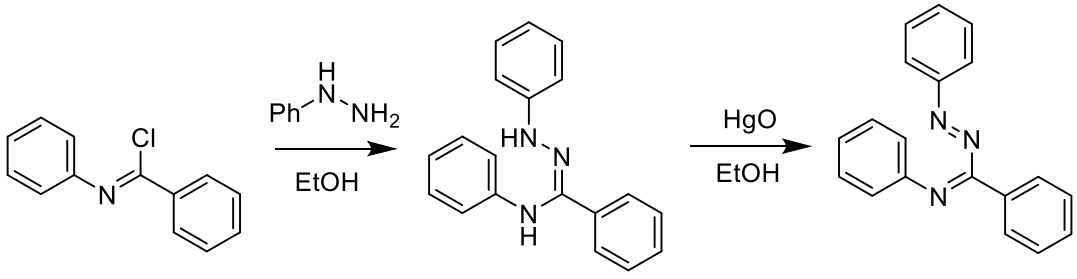

286 **287** **284**

In the original Blatter radical synthesis, iminobenzamidines **284** were accessed by oxidation of the amidrazone **287**, which was prepared from reaction of phenylhydrazine with N-phenylbenzimidoyl chloride **286**[11].

Scheme 5.3 Preparation of 4 by Neugebauer

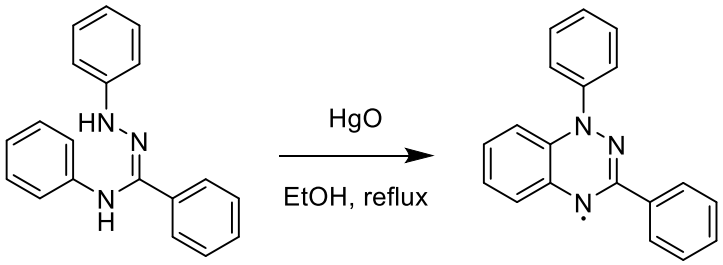

287 **87**

Other synthetic routes to the benzotriazinyl moiety have been reported. Neugebauer[12] improved the route to Blatter's radical by oxidation using HgO of N-phenylamidrazone **287** (Scheme 5.3).

Scheme 5.4 Improved preparation of benzotriazinyl radicals by Koutentis using palladium catalysis under basic conditions.

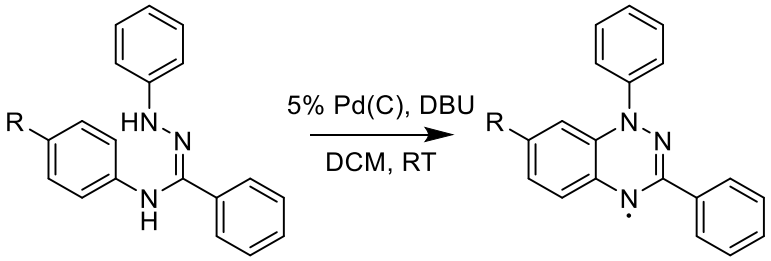

288a-g **289a-g**

a R = H **d R = Cl**
b R = Me **e R = Br**
c R= OMe **f R = I**
g R = CF_3

Further improvement to this synthetic pathway and the preparation of several derivatives (Scheme 5.4) were reported by Koutentis[13], using Pd(C) and DBU in air to oxidise the corresponding amidrazones **288a-g**. This method gave radicals **289a-g** on the gram scale and reasonably high yields (< 87%).

Scheme 5.5 Benzotriazinyl radical preparation by Takahashi starting from Ullman coupling of a hydrazide with aryl iodide.

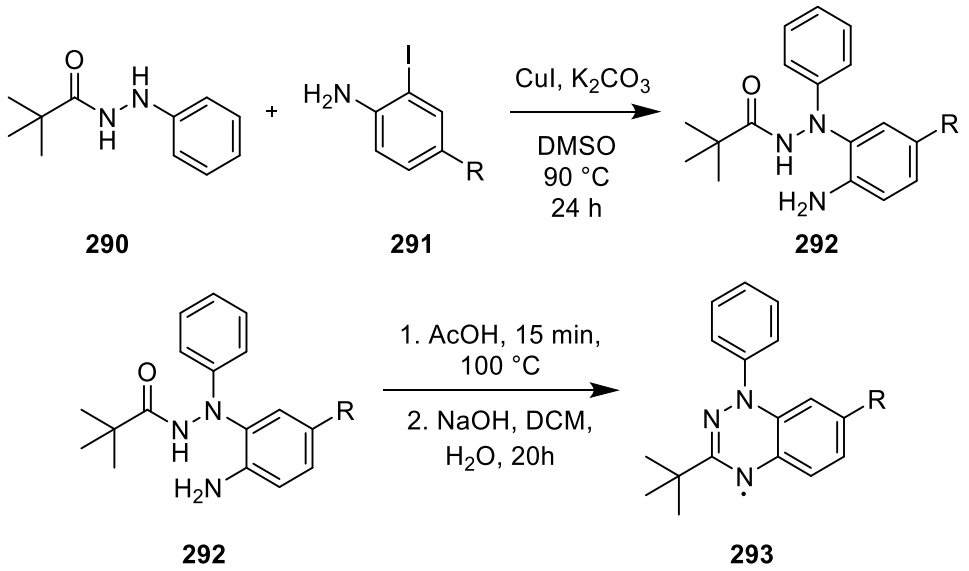

290 **291** **292** **292** **293**

Another preparation by Takahashi et al.[14] involved a modified route starting from N′-phenyl-N-pivaloylhydrazide **290** towards C3 ^{t}Bu-substituted Blatter radicals **293** (Scheme 5.5). The hydrazide **290** is coupled with 2-iodoaniline **291** by Ullmann coupling, followed by a ring closing reaction with acetic acid and subsequent oxidation in air to the benzotriazinyl radical.

Scheme 5.6 Synthesis of an aminopyrene-based benzotriazinyl radical from palladium and basic cyclization of an amidrazone.

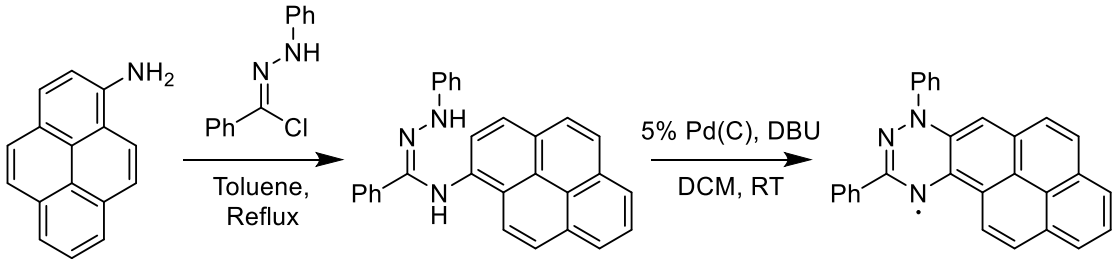

294 **295** **296**

Cicculo et al. reported the addition of a larger conjugated ring to the benzotriazinyl system by similar experimental methods using an aminopyrene **294** to create radical **296**.[15]

Scheme 5.7 Preparation of benzotriazinyl radicals from benzotriazines

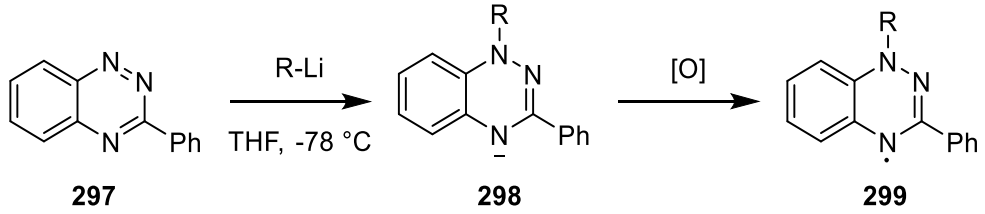

Benzotriazinyl radicals have also recently been accessed *via* an alternative method by Kaszyński[16] involving reaction of the corresponding benzotriazine **297** with aryl lithium species to give the benzotriazinamide anions **298**, which could be oxidised in air over 2-3 hours to give the benzotriazinyl radicals **299**.

Scheme 5.8 Preparation of thiazolobenzotriazinyl radicals from Blatter's radical 87.

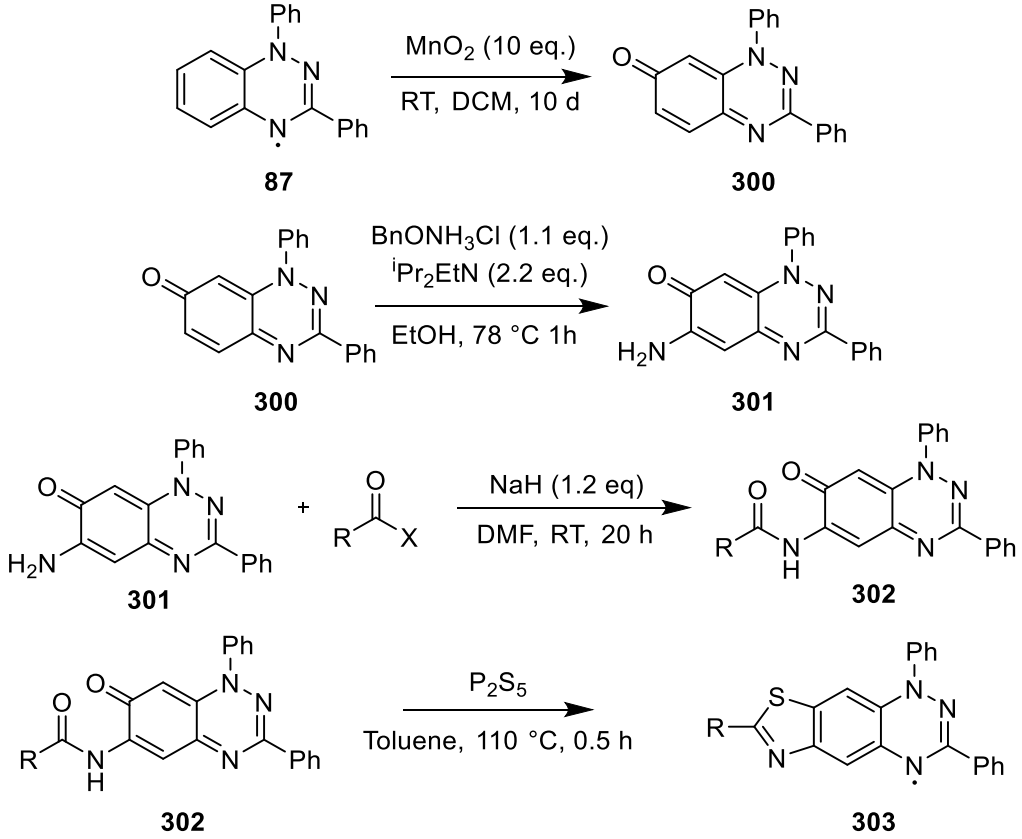

Derivatives of the benzotriazinyl structure have also been prepared by modification of the existing benzotriazinyl framework. Berezin[17] et al. prepared several 7-substituted 1,3-diphenyl-1,4-dihydrothiazolo[5′,4′:4,5]benzo[1,2-e][1,2,4]triazin-4-yl radicals **303** (Scheme 5.8). Initial oxidation on the 7-position of benzotriazinyl **87** yielded a benzotrianone **300**, which was subsequently reacted with 2-benzylhydroxylamine hydrochloride and Hünig's base in

refluxing ethanol. The resulting amine **301** was then acylated by either acyl halides or trifluoroacetic anhydride in the presence of sodium hydride, to an amide **302**, and subsequent reaction with P_2S_5 generated the desired thiazolobenzotriazinyls **303**.

Scheme 5.9 Suzuki coupling and reductive deprotection using H_2 of a benzotriazinyl radical

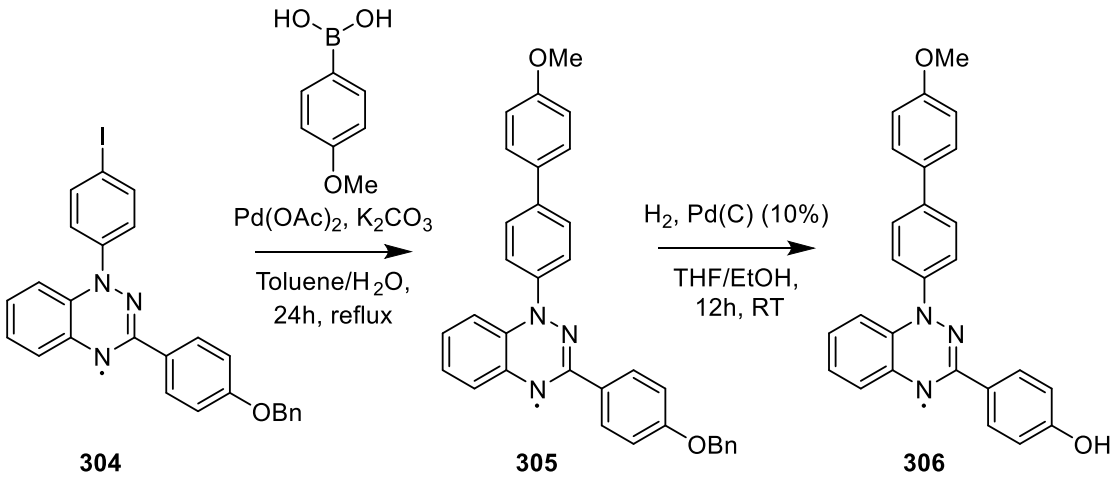

Bodzioch et al[18]. prepared several benzotriazinyl derivatives with halide, ester and ether functional groups and then utilised these new functionalities to investigate the incorporation of the benzotriazinyl moiety into larger molecular frameworks. The ester functional groups were exchanged by basic hydrolysis followed by either acylation or alkylation with several reagents. The benzyl ethers were deprotected using catalytic hydrogenation and reacted onwards in the same way as the other alcohols. The aryl iodides **304** were used in palladium-catalysed Heck, Sonogashira, Negishi, Suzuki (Scheme 5.9) and Molander cross-coupling reactions.

Scheme 5.10 Preparation of a planar benzotriazinyl from a benzotriazine.

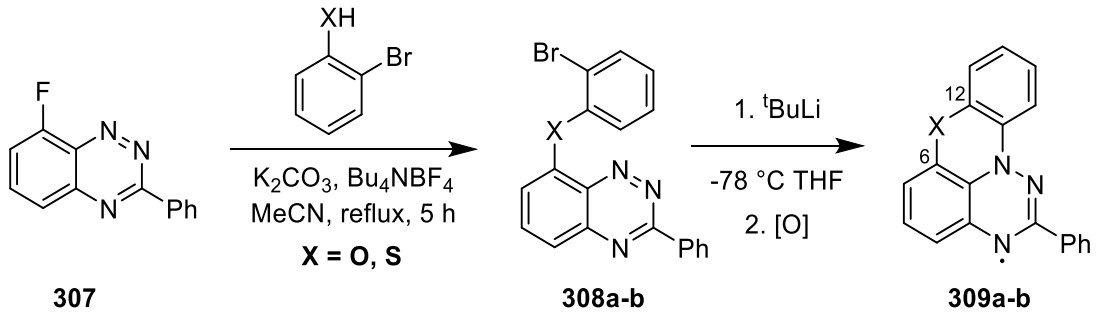

Planarization of the benzotriazinyl system was achieved by Kaszyński[19] et al. by connection of the C(6) and C(12) positions of the benzotriazine ring with S or O to bind the N1-aryl and benzotriazinyl ring together. The synthetic method started from a benzhydrazide, which was N-arylated with 2,3-difluoronitrobenzene to form a hydrazide, then reductively cyclized to **307**.

The fluorotriazine was reacted with 2-bromophenol or 2-bromothiophenol to introduce the chalcogen. Subsequent reaction of products **308a-b** with ^{t}BuLi generated the internal aryl lithium species by lithium halogen exchange, which could undergo intramolecular nucleophilic addition to the benzotriazine ring. Leaving the flask open to air allowed atmospheric oxidation to yield **309**[16].

The synthetic scope of the previous examples shows that the benzotriazinyl moiety is very robust and can survive under a wide range of reaction conditions, however the substituents directly attached to the benzotriazinyl moiety itself are more limited. Modification of the electron density around the benzotriazinyl centre has been done by attaching CF_3 groups[20] to the ring system. Overall, however, the chemistry is still somewhat limited in that each benzotriazinyl has only H or C substitution on the C3 position.

5.1.2.2 Magnetic Properties

Magnetic properties of several benzotriazinyl radicals have been studied. As discussed previously, the very high stabilities and ability to derivatise these radicals makes them highly suitable candidates for magnetic material research.

Figure 5.2 Benzotriazinyl radicals studied by SQUID

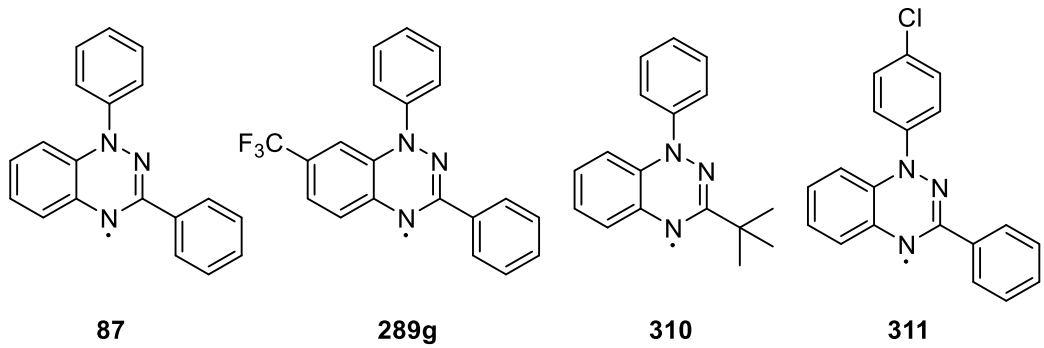

The first research into the magnetic properties of benzotriazinyl radicals was by Neugebauer et al[21] who used a SQUID (Superconducting QUantum Interference Device) to measure the magnetic behaviour of three benzotriazinyl radicals (Figure 5.2) at temperatures in the range of 4.2-300 K. Two of the radicals, **87** and **310** obeyed the Curie-Weiss law (do not show ordered magnetic behaviour; are paramagnetic) at all temperatures studied, with a negative Weiss constant. The third radical **311** however showed a broad maximum in magnetic susceptibility at 138 K as a result of Alternating Antiferromagnetic Heisenberg Linear Chains[22], which is further suggested by the crystal structure having the linear chains of spins in close proximity.

Constantinides[20] performed SQUID experiments on radical **289g**, which has a CF_3 substituent withdrawing electron density. Unlike the previous examples, **289g** showed a ferromagnetic exchange interaction at temperatures above 10 K, due to the slipped-stack packing of the crystal structure. At lower temperatures, however, antiferromagnetic behaviour was observed, which was assigned to interactions between different stacks.

5.1.2.3 Electrochemistry

Electrochemical activity is common to the family of benzotriazinyl radicals. Direct comparison between the literature results is difficult, however, due to variations in solvents, electrodes and standards in these systems. A wide range of benzotriazinyl radicals have been studied by cyclic voltammetry. The majority of benzotriazinyl radicals have two peaks corresponding to −1/0 and 0/+1 processes, which are fully reversible single electron processes.

Berezin et. al.[23] studied 13 radicals by cyclic voltammetry, comparing imidazolyl fused structures to their thiazolyl and parent benzotriazinyl analogues. It was found that for each radical the 0/+1 half-wave electrode potential ($E_{1/2}$) was slightly less positive (0.14-0.30 V) than ferrocene and the −1/0 peak was in a range of 1.22-1.49 V below the ferrocene reference. Each peak was fully reversible in dry solvent and an inert atmosphere.

Figure 5.3 Cyclic Voltammetry of imidazolo-fused benzotriazinyl 312

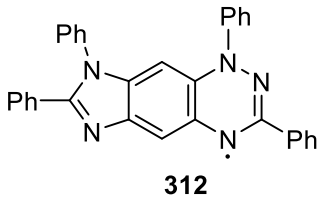

312

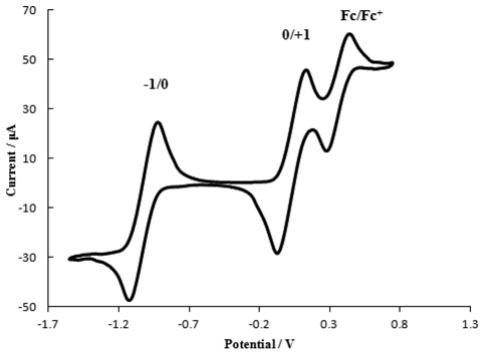

The potential of the 0/+1 wave was similar for the parent benzotriazinyl **87** (within 0.05 V) and each of the studied imidazolyl fused ring systems, e.g. **312**, however the thiazolyl substituted rings showed potential 0.10-0.15 V higher than the other simple benzotriazinyls. The −1/0 wave was found to be more significantly lower in potential for imidazolyl fused radicals than the parent benzotriazinyl ring by 0.1-0.18 V, whereas the thiazolyl fused radicals were found to have a higher reductive potential by 0.09 V.

The higher oxidative and lower reductive potentials indicate that the SOMO in these cases is stabilised by the larger conjugated ring system compared to **87**, which results in redox processes becoming more difficult.

5.1.2 Nitron and Recent Advances

Scheme 5.11 Nitron tautomerisation.

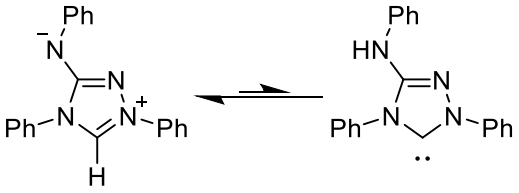

127 **127'**

Nitron **127** is an anilino-triazolium compound first discovered by Busch[24] in 1905. Nitron has found application as a gravimetric reagent[25] for the analysis of trace amounts of inorganic salts, such as nitrates, bromides, perchlorates and picrates, with which it forms salts of varying degrees of insolubility[26]. The structure is typically assigned as a zwitterion, however recently it was discovered that Nitron has some behaviour more consistent with N-heterocyclic carbene (NHC) tautomer **127'**[27]. The levels of the NHC proved too small to detect by NMR spectroscopy, but Nitron was found to react with trapping agents for nucleophilic carbenes such as CS_2.

Scheme 5.12 Grant's serendipitous preparation of benzotriazinyl radical 313.

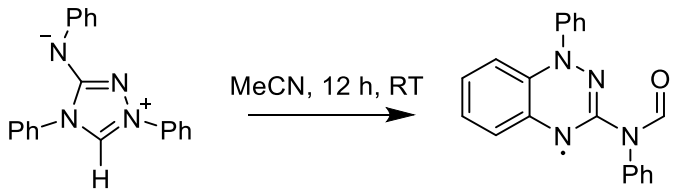

127 **313**

A MChem student in our research group, Jacob A. Grant, studied the proton-transfer behaviour of Nitron **127** as a continuation of the field of NHC proton-transfer chemistry discussed in sections 1 and 2. From our previous research on the proton-transfer chemistry of triazolium salts, the typical pK_a of the C(3) proton is around 16-18, which results in H/D exchange in D_2O solutions on a timescale accessible by NMR spectroscopy in the acidic region of the p*D* scale (0-4)[28,29]. As previously discussed, the stability of NHCs is increased by increased degrees of heteroatomic substitution in the central azolium ring. Nitron was therefore of interest due to its

exocyclic nitrogen atom, as well as its zwitterionic nature, in contrast to the previously studied NHC conjugate acid salts. Grant found that the H/D exchange occurred on a timescale too fast to measure by ^{1}H NMR spectroscopy, even in concentrated acidic solutions. When Nitron **1** was left overnight in a CD_3CN solution, however, the yellow solution became a dark red colour, of which the ^{1}H NMR spectrum showed weak, broad, poorly defined peaks. The procedure was repeated in MeCN and column chromatography of the resulting solution led to the purification of black crystals, which upon characterisation by mass spectrometry, EPR and X-ray crystallography identified a novel benzotriazinyl structure **313**.

The aims of this project were to follow up from these early findings, to confirm and optimize the synthetic route to the product, investigate the physical and chemical properties of the newly discovered radical and to explore the mechanism of this reaction.

5.2 Results

5.2.1 Early investigations and reaction optimization

The original procedure determined by Grant to produce benzotriazinyl radical **313** involved overnight stirring of an acetonitrile solution of Nitron **127** exposed to atmospheric oxygen and moisture, followed by evaporation of the solvent, washing with cold ethanol and subsequent purification by column chromatography (DCM:MeOH 98:2).

Scheme 5.13 Acetonitrile-based benzotriazinyl preparation

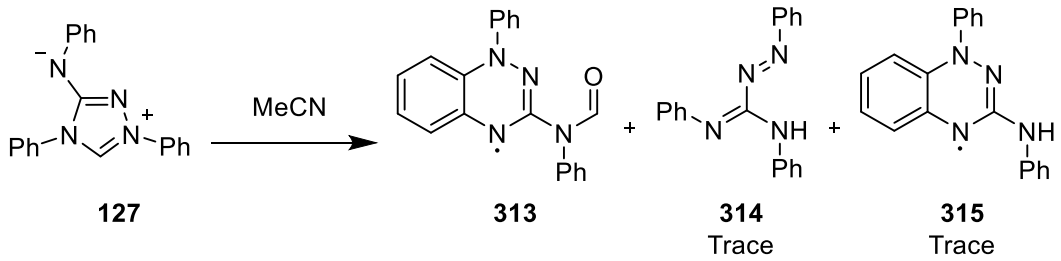

127 **313** **314** Trace **315** Trace

After repeating Grant's original procedure, obtaining a similar 58% yield, two side-products were collected in trace quantities during column chromatography of the reaction mixture. Mass spectral data supported the formation of triazabutadiene **314** and new C(3)-anilino radical **315**. Triazabutadiene **314** is a previously identified compound, which was reported but not fully characterised, and can be prepared in high yield by the reaction of Nitron **35** in water in strongly basic solutions.[24] The second minor product, **315**, was a new benzotriazinyl radical with a distinct green colour and was characterised initially by EPR, MS-MS and IR analysis.

Scheme 5.14 Benzotriazinyl formation in MeCN:H_2O (1:1)

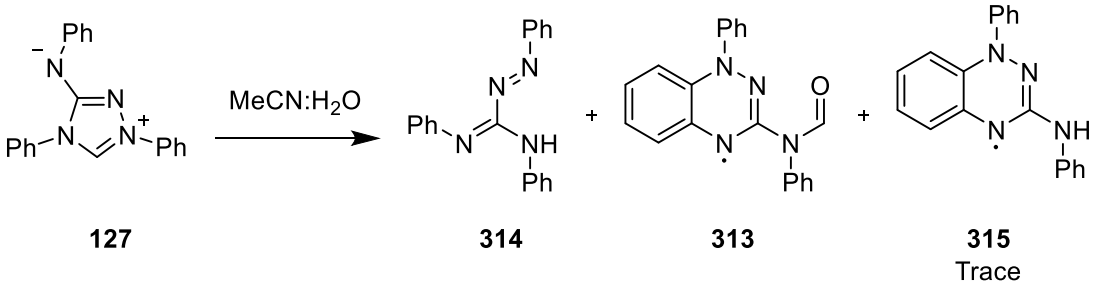

A range of solvents were trialled as alternatives to MeCN. Reaction in 50:50 acetonitrile:water provided only traces of **313**, however, instead an increased yield of the related triazabutadiene **314** (51 %) was obtained.

Scheme 5.15 Benzotriazinyl formation in MeOH

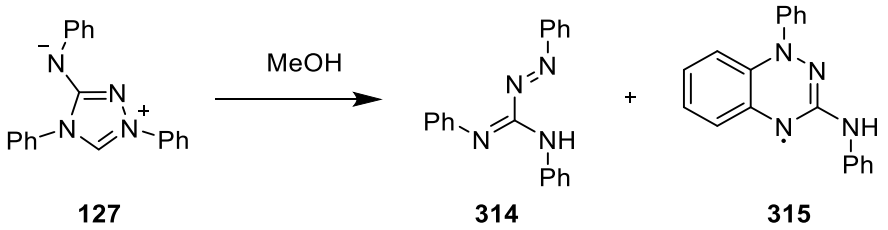

The use of pure methanol as solvent again provided mostly triazabutadiene **314**, albeit in a lower yield (15 %). Minor traces of the amido radical **313** were observed visually on column, but in very low yield and isolation was not attempted. Amino radical **315** was also collected in very small amounts (0.4 %).

Scheme 5.16 Further Attempts at production of benzotriazinyl radicals

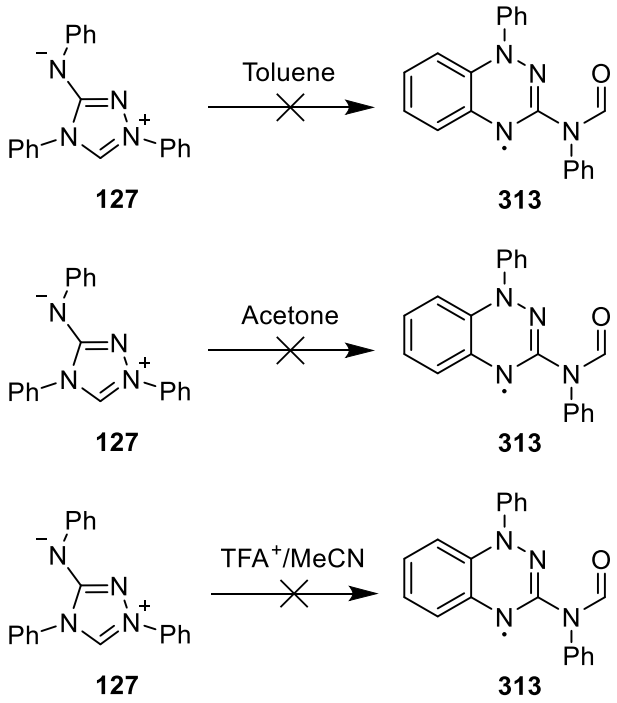

Changing the reaction solvent to acetone, however, slowed the progress of the reaction significantly, with only trace products of **313-315**. The use of toluene showed no reaction at all over 24 hours. Addition of trifluoroacetic acid (0.1%) in acetonitrile also showed a lack of reaction over 72 hours. The results of these experiments demonstrate that high levels of water or methanol cause the reaction to progress to the undesired side-product **314**.

Figure 5.4 Purification of radical 313 with visible unreacted Nitron 127.

In each of these reactions in alternative solvents, significant amounts of unreacted Nitron were observed by TLC and LCMS analysis, as well as being visibly retained during column chromatography as a yellow band with high retention factor. Heating the reaction neither provided an improved yield nor a significant increase in reaction speed.

Initial investigations by Grant determined that in dry degassed acetonitrile, Nitron is stable over several days, with no change in colour notable. It was therefore suspected that low levels of water are necessary for successful reaction although higher levels yielded mainly triazabutadiene **314**. Three alterations to the initial reaction procedure increased the overall isolated yield to 82%. This included the use of 99:1 MeCN:H_2O as solvent and a longer reaction time of 72 hours. Finally, recrystallization from hot ethanol provided a simpler and higher yielding purification than column chromatography, while retaining excellent purity of the C(3)-amido radical product **33**.

Scheme 5.17 Hydrolysis of 313 to 315

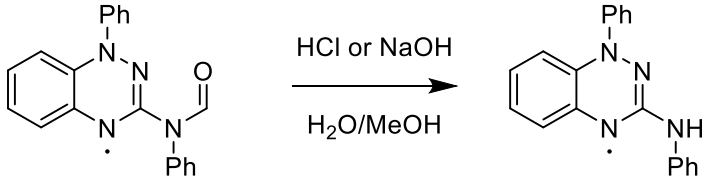

313 **315**

Additionally, it was found that green radical **315** could be produced through either acidic or basic amide hydrolysis in 1:1 (MeOH:H_2O) with purification by either column chromatography or recrystallization from hot ethanol and water. Recrystallization of the larger amounts of **315** produced by this process allowed a confirmation of the previously assigned structure by single-crystal X-ray diffraction, which by TLC, high-accuracy LCMS, and IR spectroscopy was determined to be identical to the data of **315** prepared under basic conditions.

Figure 5.5 Neutral (left) and acidic (right) solutions of 315 in acetonitrile.

An interesting side-note from this reaction is that under acidic conditions, the colour of solutions containing **315** are purple in colour instead of the characteristic green colour in non-protic solutions. Upon neutralization, the colour reverts to green again, indicating that the colour change is due to protonation of radical **315**. This process does not permanently change the radical structure; identical crystal structures were obtained for products isolated from both the acid and base catalysed processes, therefore the process is reversible.

5.2.2 Physical and Chemical Properties of Novel Benzotriazinyl Radicals

5.2.2.1 Structure of 313 and 315.

Single Crystal X-Ray Diffraction provided access to structures for both amido radical **313** and amino radical **315** after recrystallization of both species. Amido radical **313** was recrystallized from evaporation of DCM at room temperature. Amino radical **315** was recrystallized by slow evaporation of acetone from a solution of **315** at room temperature.

5.2.2.1.1 Crystal Structure of 313.

Figure 5.6 Crystal structure of two independent molecules of 313

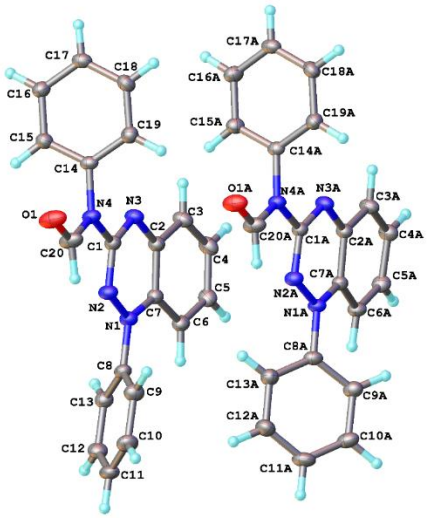

Figure 5.7 Crystal structure of 313 showing molecules stacked along the α-direction in a slipped stack packing motif.

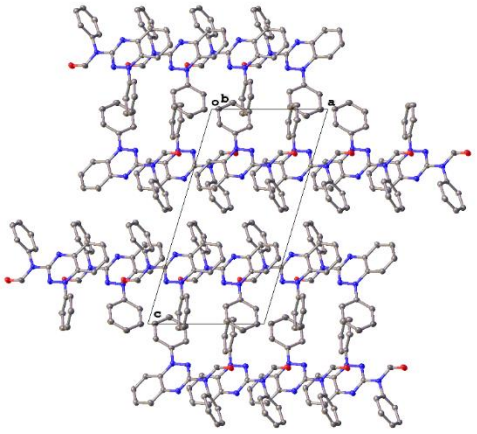

The crystal structure of **313** contains two crystallographically independent molecules which differ in their orientation of the phenyl substituent on N1 (Figure 5.6). The molecules of **313** form a slipped-stack packing motif along the α-direction (Figure 5.7), similar to the slipped-stack structure observed in other known crystal structures of benzotriazinyl radicals. The two independent molecules alternate in this stack with corresponding interplanar distances between the r.m.s planes of the benzotriazine structures of 3.68 and 3.61 Å. The shortest interatomic contacts between the benzotriazinyl ring planes are 3.62 and 3.53 Å, again, similar to the values for other benzotriazinyl radicals (3.3-3.8 Å). The slipped stacks are linked together into a 3-dimensional framework by weak hydrogen-bonding interactions. These hydrogen bonds are

very significant because the manipulation of these structures can affect the magnetic properties of these paramagnetic species and manipulation of these interactions allow control of the magnetic properties for possible applications in organic magnetic materials.

5.2.2.1.2 Crystal Structure of 315.

Figure 5.8 Partially disordered molecule 315.

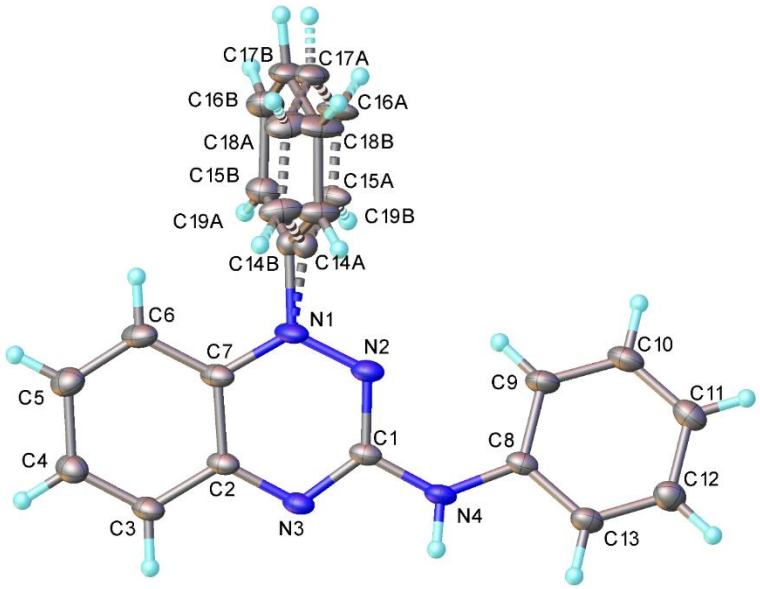

Figure 5.9 Hydrogen bonding between N4-H and N3 of two molecules of 315.

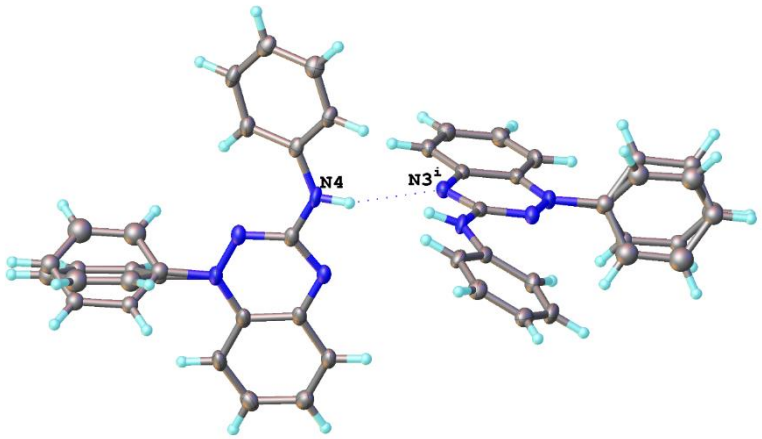

Figure 5.10 Packing of molecules 315 in the crystal showing slipped stacking along b-axis.

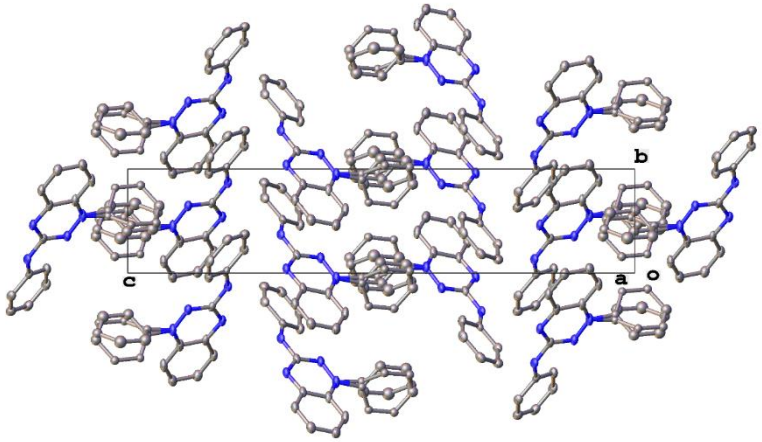

The crystal structure of **315** (Figure 5.8) is significantly different to that of **313**. The N1 Ph substituent in this case is completely disordered as to its conformation around the ring, as opposed to having two distinct conformations in amido radical **313**. There is significant hydrogen bonding between H4 and N3 of **315** with an intermolecular distance of 2.4 Å (Figure 5.9), which gives rise to the overall packing of the molecule into two slipped stacks in the b axis (Figure 5.10) in contrast to the α-stacking of **313**. This means that the planes of the benzotriazinyl rings are spaced significantly further apart (~6-7Å) and the closest contacts are the disordered atoms on the N1-Ph substituent and the benzotriazinyl ring. The presence of significant hydrogen bonding believed to be unique among benzotriazinyl radicals and could give rise to interesting magnetic properties.

5.2.2.2 Computed SOMO of 313 and 315

Figure 5.11 Computed SOMO (top) and spin density (bottom) of 313 and 315

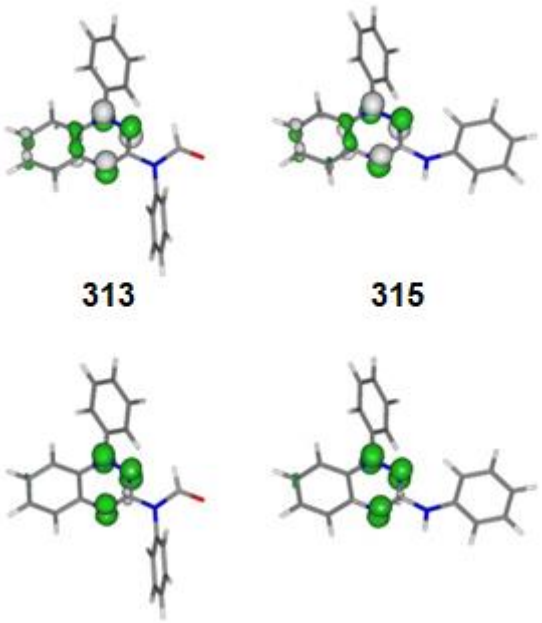

SOMO (Singly Occupied Molecular Orbital) and spin distribution were calculated for radicals **313** and **315** by Dr. Mark A. Fox at the hybrid-DFT UB3LYP/6-311+G(d,p) level with molecular orbitals and spin densities plotted using GABEDIT and orbital contributions determined with GAUSSSUM. Representations of the SOMO are in Figure 5.11 and calculated orbital contributions and spin density are in ***Table*** .

Figure 5.12 Nitrogen atom numbering.

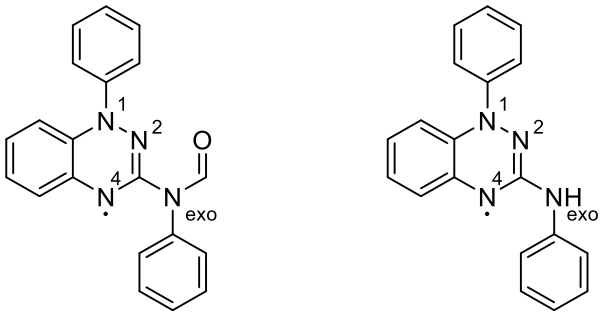

Table 5.1 Calculated SOMO contributions and Spin Density of radical 313 and 315 by DFT

	SOMO (%)		Spin Density (e)	
Atom	**313**	**315**	**313**	**315**

N1	18	18	0.23	0.26
N2	21	19	0.46	0.33
N4	17	18	0.35	0.30
N_{exo}	1	0	0.01	-0.02

This analysis shows that the SOMO is similar to those of literature Blatter radicals, with the majority of spin-density localised on the nitrogen atoms of the triazine ring, (N1, N2, N4) with the total orbital contributions of these at 56 %. The exocyclic nitrogen has very low contribution to this orbital, with the calculated orbital contribution within error of zero. These results suggest that the addition of the exocyclic nitrogen has comparatively little influence on the SOMO and spin density of the benzotriazinyl moiety.

5.2.2.3 Electron Paramagnetic Resonance (EPR) Experiments.

The radical nature of **313** and **315** was first suggested by the broad and weak ^{1}H NMR signals and by the geometries obtained in single crystal X-ray diffraction experiments. Single crystal X-ray diffraction, however, does not detect either the presence or the absence of hydrogen atoms, so the radical structure could only be inferred by valency, bond angles and lengths. Electron paramagnetic resonance experiments were performed where EPR spectra were recorded on a Bruker EMX Micro spectrometer operating at X-band (9.5 GHz frequency) on the radical samples in solutions of degassed toluene (0.1 mM). Simulations of these spectra are shown alongside the experimental readings.

Figure 5.13 EPR spectrum of 313

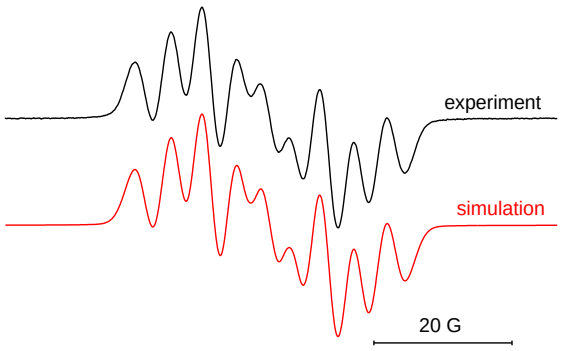

a_{N1} = 8.14 G, a_{N2} = 5.01 G, a_{N3} = 4.69 G

Figure 5.14 EPR spectrum of 315

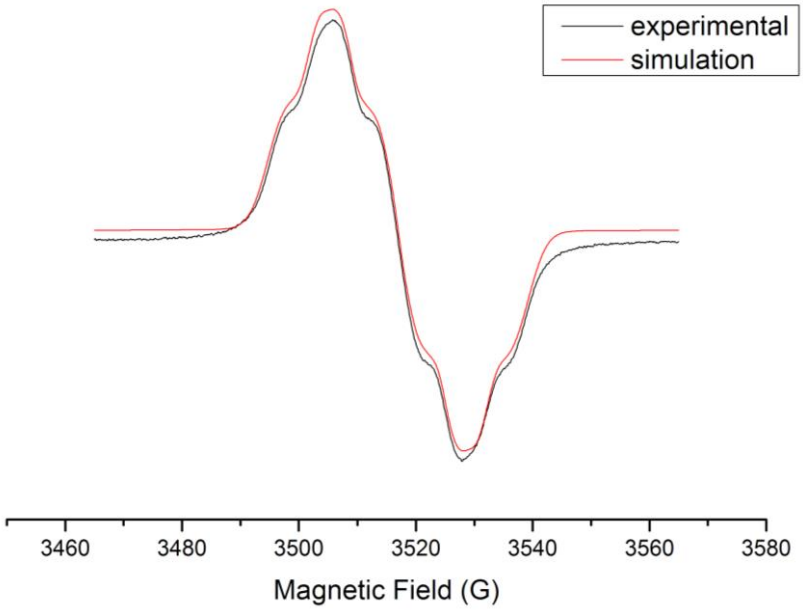

a_{N1} = 7.84 G, a_{N2} = 4.92 G, a_{N3} = 4.88 G

The EPR spectra above are both consistent with significant hyperfine coupling to three nitrogen atoms i.e. the benzotriazinyl moiety. The values of the hyperfine constants are about 8 G for the largest and 5 G for the two smaller splittings. This is consistent with the spectra of other benzotriazinyl radicals. In both the amido **313** and amino **315** cases, there is very little coupling to the exocyclic nitrogen atom, which again suggests that spin density on the exocyclic nitrogen is low. This implies that the addition of the exocyclic nitrogen atom does not dramatically affect the orbital structure of the benzotriazinyl moiety.

5.2.2.3.1 Behaviour of Blatter radical 315 under acidic conditions.

It was observed previously that **315** can be protonated at low p*H*. This is in contrast to **313**, which does not show an instantaneous colour change in acidic media (slow colour change due to hydrolysis to **315** is observed). EPR experiments were performed in two aqueous solutions (0.1 mM) with acid (0.1% HCl, 0.1% TsOH) and one in pure trifluoroacetic acid (1 mg/mL, 3.4 mM).

Figure 5.15 EPR spectrum of 315 (0.1 M) in hydrochloric acid solution (0.1%)

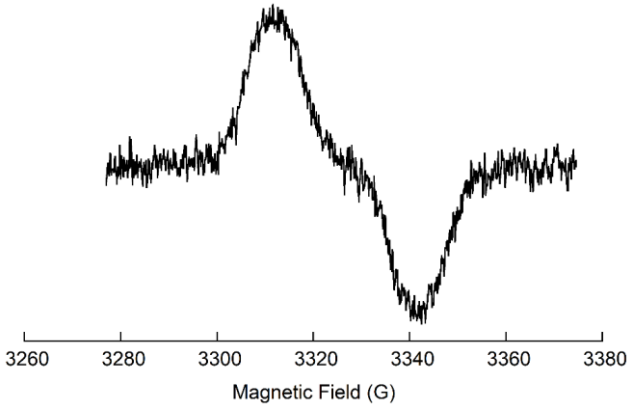

Figure 5.16 EPR spectrum of 315 (3.2 mM) in tosylic acid solution (0.1%)

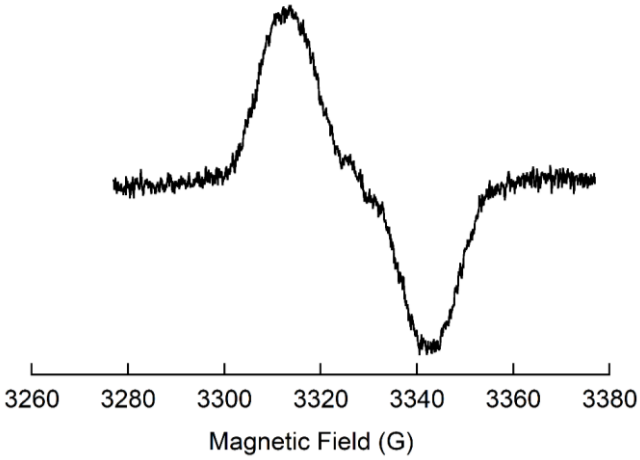

Figure 5.17 EPR spectrum of 315 (3.3 mM) in trifluoroacetic acid

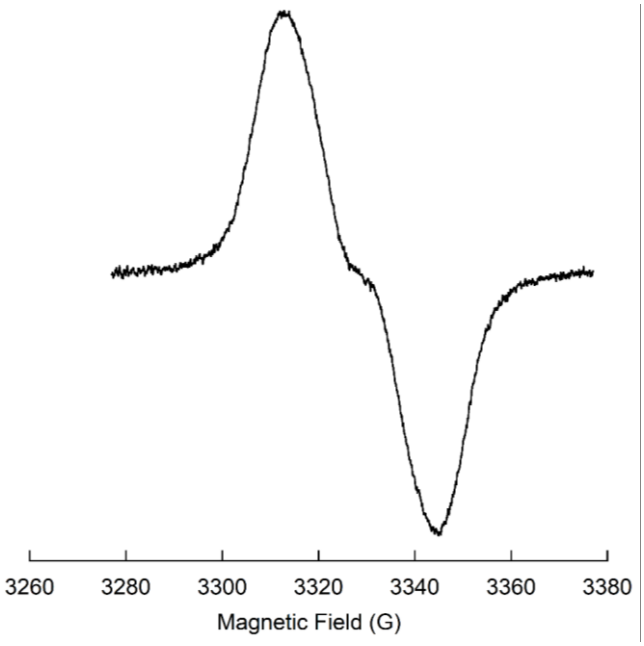

All of these spectra show a lower intensity than the spectra in toluene, which indicates that the protonated compound is not 100% radical under these conditions. The spectra are poorly resolved, possibly due to the low concentration of radical material, but show a large 15.7 G hyperfine coupling constant. This could possibly be assigned to significant coupling to a proton, suggesting that spin density is distributed among the added hydrogen atom in addition to the triazinyl moiety once the molecule is protonated. The hyperfine coupling to nitrogen is hidden in the high linewidth in this case, and is lower than 5 G in all cases. The g-factor, g_{iso} is approximately 2.04, compared to 1.93 in the case of the non-protonated species. This could indicate a radical cationic species is present in these reactions, however due to the poor resolution this cannot be conclusively stated.

5.2.2.4 Electrochemistry.

As previously discussed, benzotriazinyl radicals are known to have electrochemically active properties, and the majority of known benzotriazinyl radicals have two peaks, a 0/+1 oxidation and a 0/−1 reduction, both of which show fully reversible behaviour. In order to further study the electrochemistry of our two radicals, cyclic voltammetry and spectroelectrochemistry were employed.

Cyclic voltammetry measurements were performed on radicals **313** and **315** (1 mM) in degassed, dried acetonitrile with a supporting electrolyte of dried Bu_4NBF_4. An inert atmosphere was maintained during the experiments.

All potentials are quoted relative to the potential of the ferrocenium/ferrocene couple (Cp_2Fe^+/Cp_2Fe). Internal standards of ferrocene (Cp_2Fe) and decamethylferrocene (Cp^*_2Fe) (~1 mM) were used in the experiments of **313** and **315** respectively. Decamethylferrocene was used in place of ferrocene due to overlap of the peaks corresponding to (Cp_2Fe^+/Cp_2Fe) and 0/+1 of radical **313**. ($Cp^*_2Fe^+/Cp^*_2Fe$) and (Cp_2Fe^+/Cp_2Fe) were determined to have a difference in $E_{1/2}$ values of −0.50 V in this system.

Figure 5.18 (a-b) Cyclic voltammogram of (a) 313 and (b) 315 in MeCN (1 mM) with a supporting electrolyte of $Bu_4N\ BF_4$ at RT scanned at 50 mV/s

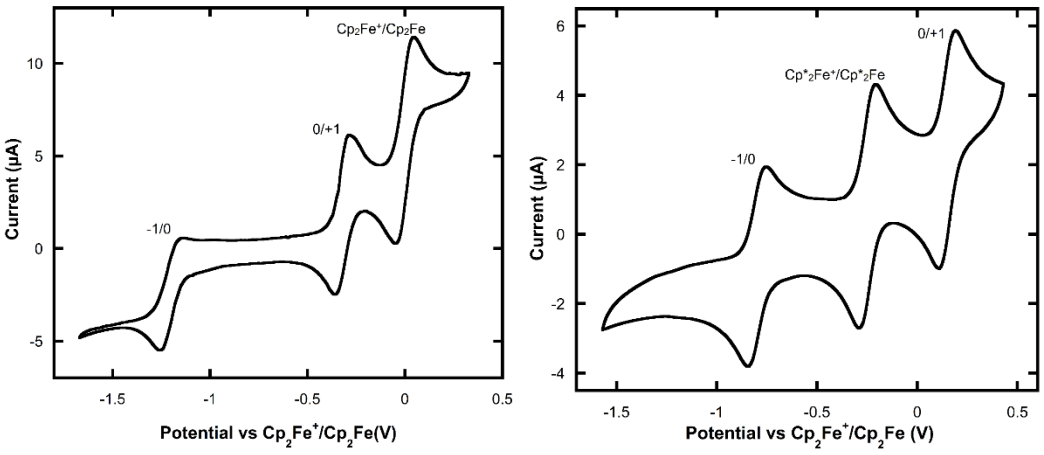

Table 5.2 Half-wave potentials for radicals 33 and 35

Radical	$E_{1/2}$ (0/+1)	$E_{1/2}$ (−1/0)	E_{cell} (V)
313	−0.11	−1.06	0.97
315	−0.35	−1.21	0.89

Every peak in this system is fully reversible, as demonstrated by both the repeating pattern of the cyclic voltammogram and the Nernstian 0.58 mV gap between the values of E_{peak} and $E_{1/2}$[30]. This indicates that both the oxidation and reduction of both radicals occurs under these conditions and timescales giving reasonably stable products that do not immediately derivatise.

5.2.2.4.1 Spectroelectrochemistry.

Spectroelectrochemistry experiments were performed by Dr. Mark A. Fox on a solution of **315** in dichloromethane (1 mM) with a supporting electrolyte of Bu_4NBF_4 under an inert atmosphere. UV-Visible spectra were taken of the solution at neutral and the extremes of positive and negative potential, scanned a single time over 8 hours.

The results show that the cationic species generated at high potential is essentially stable for several hours, but the anionic species was not stable, and underwent significant decomposition. These results were determined by observing the intensity of the returned spectrum of the neutral species once the experiment had returned to neutral potential. In the case of negative potentials, there was ~ 70 % return to the neutral radical **315** after 3-4 hours in the anionic state, indicating partial decomposition.

Figure 5.19 UV-Visible spectra (200-800 nm) of 315 in the 0 (—), +1 (—), and −1 (—) oxidation states.

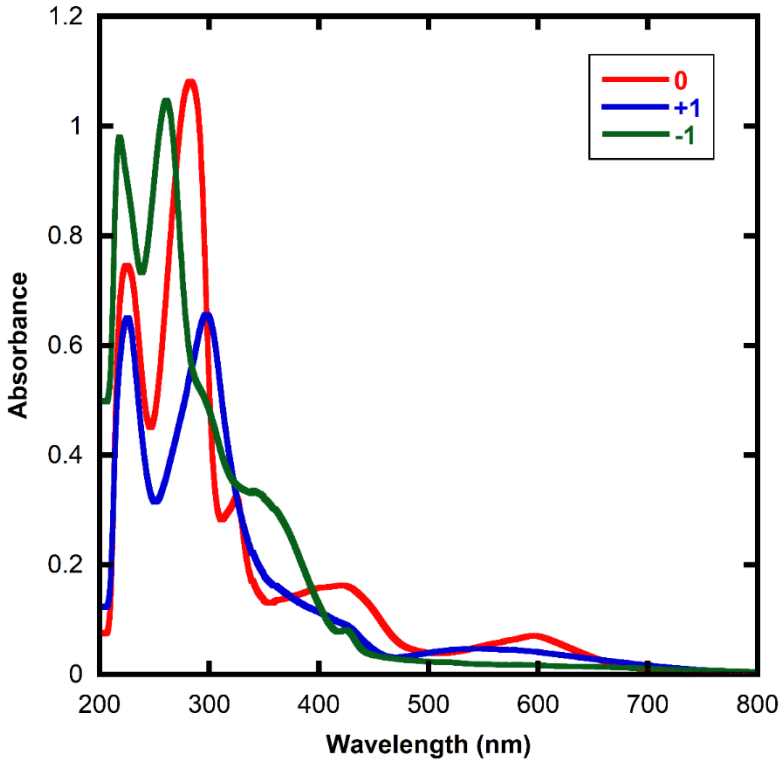

Calculated structures were also obtained by Dr. Mark A. Fox of the cationic, neutral and anionic species, as well as calculated UV-Visible spectra. The calculated spectra show good agreement to the experimental data, which could possibly indicate that the calculated geometries of the cationic and anionic species are accurate, although this cannot be conclusively determined without isolation and further characterisation of these species.

***Figure 5.20a-c Calculated geometry of 315 in oxidation state (a)* +1, *(b)* 0 *and (c)* −1**

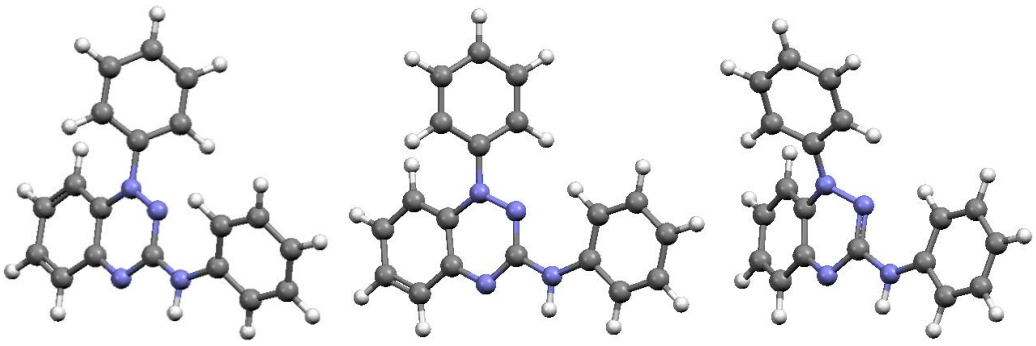

The calculated geometry of the neutral species (Figure 19b) is similar in appearance to the independently experimentally determined crystal structure of **315**, not accounting for the

disordered aryl ring attached to N1. The cationic species has slight differences to the neutral state, around the rotation of the exocyclic nitrogen. The anionic species, however, has a dramatic difference in that the triazinyl ring is no longer planar and N1 has a double bond to its exocyclic ring. This highly unstable suggested structure implies that the anion is likely to decompose immediately, rather than retain the calculated geometry. Regardless of the accuracy of this computational analysis, the anionic state is known to be unstable from lack of full regeneration of the neutral spectrum.

5.2.3 Mechanistic Studies into the formation of Benzotriazinyl Radicals

5.2.3.1 Studies on 1,2,4-triphenyltriazolium tetrafluoroborate

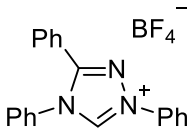

128

The unprecedented formation of a benzotriazinyl radical **313** from N-heterocyclic carbene Nitron **127** prompted further investigation of other structurally related 1,2,4-triazolium ring systems and their reactions under similar conditions. To this end NMR spectroscopy studies of 1,2,4-triazolium tetrafluoroborate were undertaken to compare the reactivity of **127** to a triazolium ring without the exocyclic anilino substituent.

1,2,4-triazolium tetrafluoroborate **128** was placed in a series of NMR tubes and dissolved under three different sets of conditions: in pure acetonitrile, in acetonitrile with trace D_2O, and in basic D_2O with an added oxidant.

Figure 5.21 Representative spectra of 128 in d_3-MeCN under ambient conditions over 1 week.

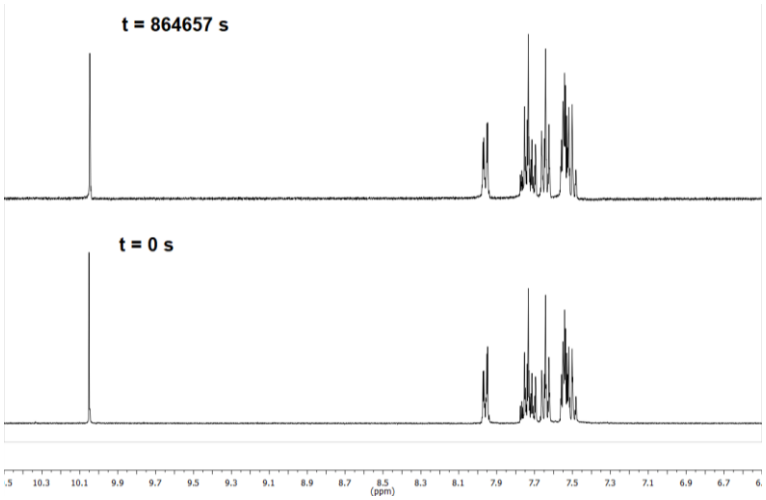

Figure 5.22 Representative spectra of 128 in 1% D_2O/99% d_3-MeCN (v/v %) under ambient conditions over 4 days.

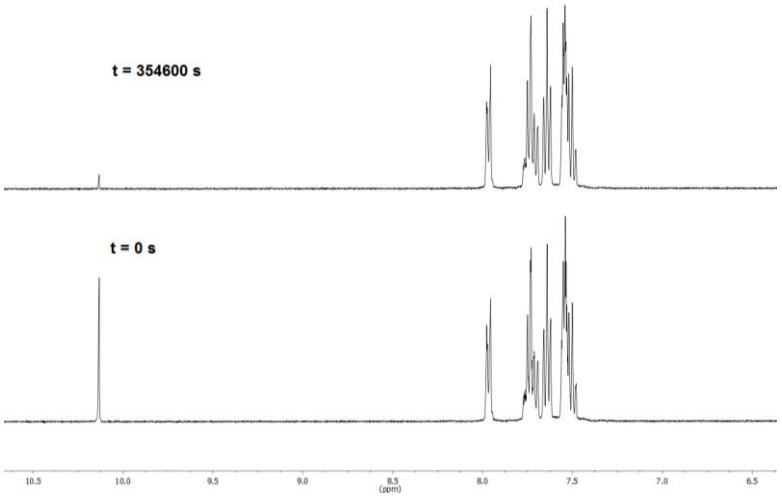

In each of these conditions, the only quantitative change of the ^{1}H NMR spectrum of **128** is H/D exchange of the C3 proton in the experiments containing D_2O. The exchange is *via* an NHC intermediate as discussed in chapter 2. This indicates that **128** does not undergo any analogous reaction to Nitron **127** under these conditions and therefore the presence of the exocyclic nitrogen is necessary for the radical forming reaction.

Figure 5.23 Representative spectra of 128 in 1 M NaOD 1% D_2O/99% d_3-MeCN (v/v %) in a suspension of excess Ag_2O under ambient conditions over 4 days.

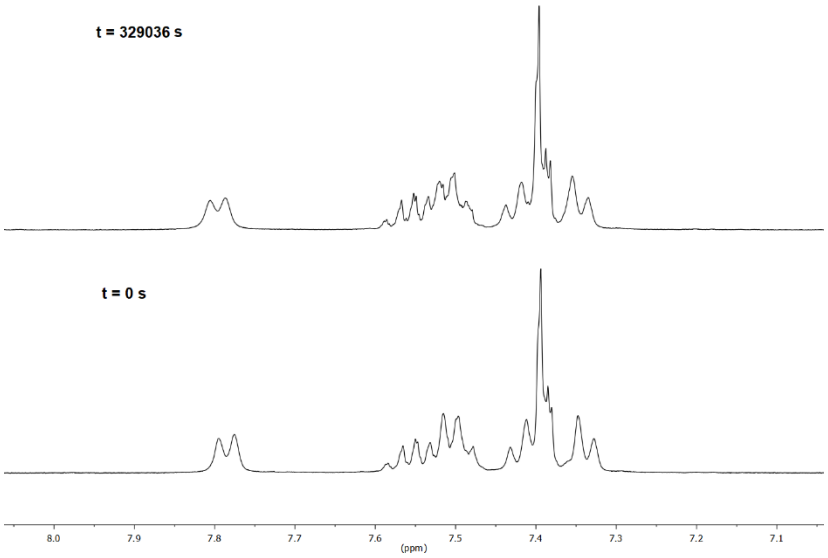

Significant broadening of the peaks is present in the spectra of the suspension of Ag_2O due to the inhomogeneity introduced by the solid particles of oxidant. Whilst ring-opening of **128** under these conditions could have occurred, EPR experiments by Victor Chechik under the same conditions did not detect radical formation.

5.2.3.2 Formation and role of triazabutadiene 314

Scheme 5.18 Production of triazabutadiene 314

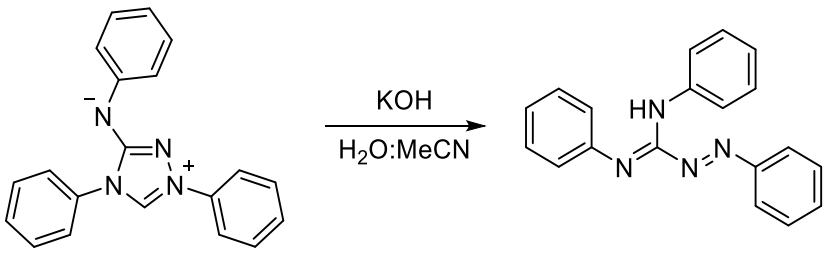

127 **314**

Triazabutadiene **314** is a previously reported species[24] that was discovered nearly 100 years ago from the hydrolysis of Nitron in alkaline solution. In this work, the hydrolysis was reproduced and gave the same product, which was fully characterised by ^{1}H and ^{13}C NMR spectroscopy, mass spectrometry, IR and UV spectroscopy, and single crystal X-ray diffraction. The addition of 0.33 M KOH increases the yield in 2:1 H_2O:MeCN to 71% from 51% achieved without base in 1:1 H_2O:MeCN over a longer timescale.

Scheme 5.19 Non-reaction of triazabutadiene 314

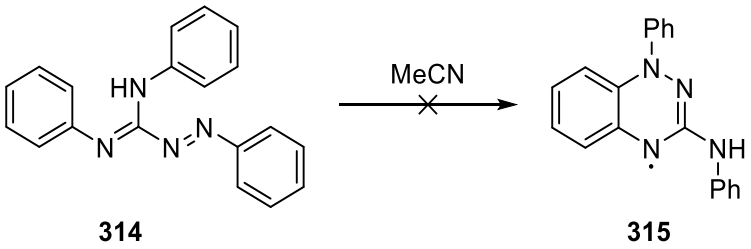

314 **315**

The triazabutadiene, left over several days in acetonitrile as used in the reaction to form the amido radical **313**, did not go on to form the respective amino radical **315**, indicating that it is not likely an intermediate in a process to form **315**.

Figure 5.24 Representative spectra of 314 1% D_2O/99% d3-MeCN (v/v %) under ambient conditions over 5 days.

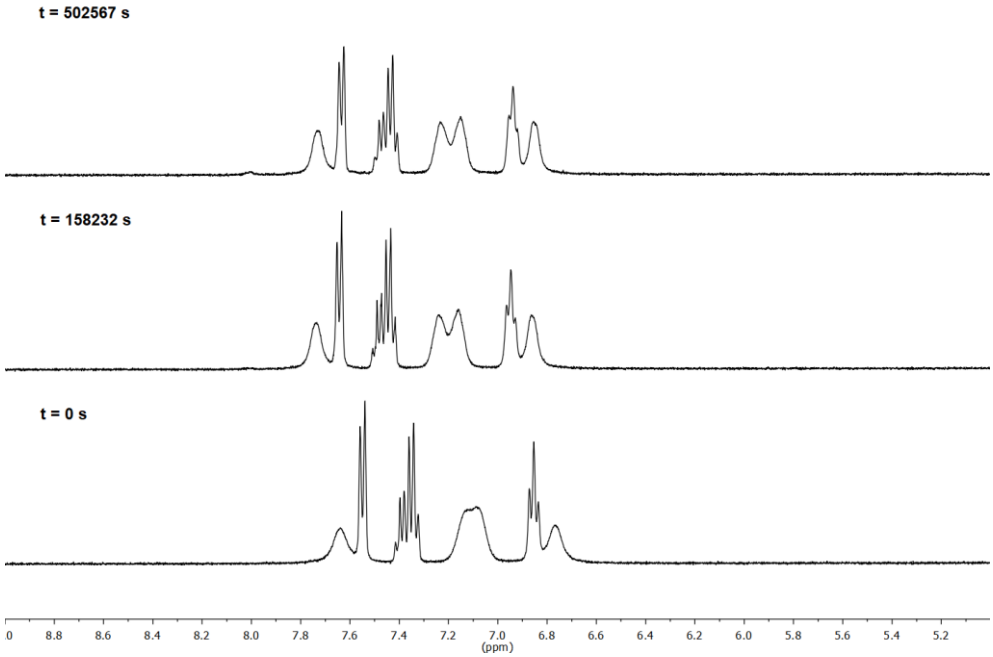

Furthermore, under conditions of 99:1 MeCN:D_2O over five days, there was no appreciable change in the spectrum of **314**. The spectrum has notably broad peaks for some of the aryl protons however this is assigned to rapid *cis-trans* isomerism, which is explored in Section 5.2.2.3.2.

Figure 5.25 Reference spectra of 314 in 1 M NaOD 1% D_2O/99% d3-MeCN (v/v %) a) and b-c) in a suspension of excess Ag_2O under ambient conditions over 6 days.

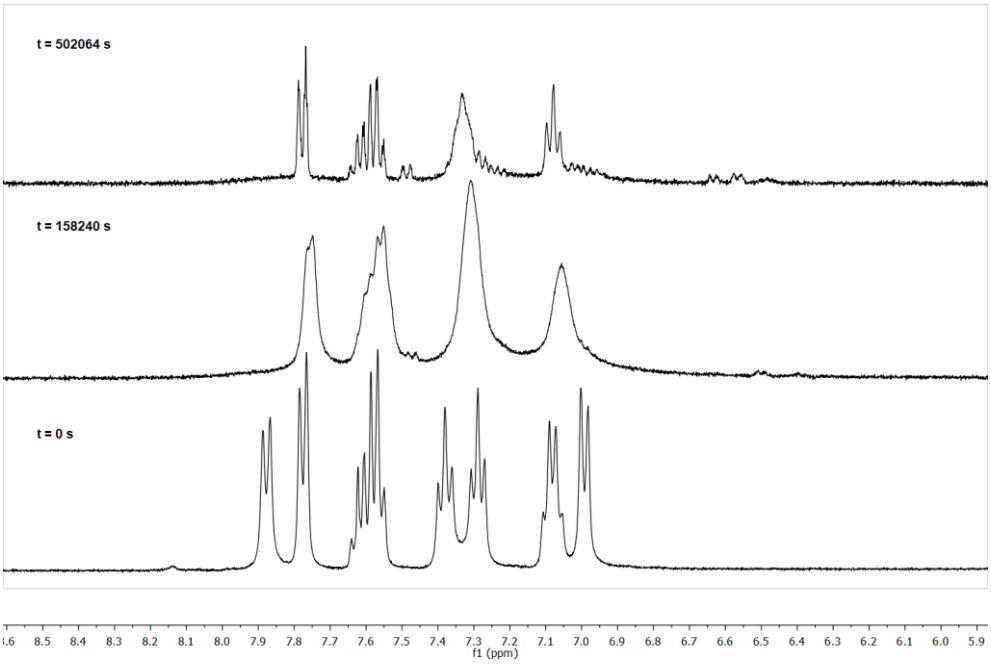

The use of 1% 1 M NaOD in D_2O solution with the presence of Ag_2O as oxidant also failed to convert **314** to **315**. The presence of solid Ag_2O causes inhomogeneity, resulting in broadened spectra. The coalescence of peaks was also observed, which was assigned to variation in the speed of bond rotation by change in p*H*. The spectral changes could also be due to the reaction of **314** under these conditions, however, the formation of **315** could be excluded after LCMS analysis. Additionally, there was no colour change observed over time. The broad peaks are assigned to coalescence of the two sets of aryl protons by rapid *cis-trans* isomerism (Section 5.2.2.3.2), the rate of which is at least somewhat solvent dependent.

Figure 5.26 Crystal structure of triazabutadiene 314.

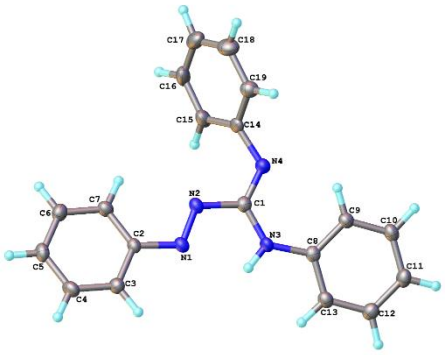

The mechanism to form benzotriazinyl radical **315** (by electrocyclization only) would require the triazabutadiene **314** to take a *cis* conformation across the N1-N2 bond. The crystal structure of **314** however shows the triazabutadiene N1-N2 bond in a *trans* conformation (Figure 5.26) To investigate the *cis-trans* isomerism energy barrier, a dual approach was used, theoretical computational analysis and practical EXSY NMR spectroscopic experiments. Computational analysis was additionally performed by our collaborator Dr. Mark A Fox as an alternative approach to investigate the *cis-trans* isomerism of **314**.

Triazabutadiene **314** was studied at B3LYP/6-331+G(d,p) using GAUSSIAN09 package to determine the optimized ground state. The ground states were confirmed as true minima by frequency calculations. The optimized geometry of **314** was found to have good agreement with the pre-collected crystallographic data (Figure 5.26).

The results of these experiments determined triazabutadiene **314** to have a small preference for the *trans* conformation, which corroborates the data found by X-ray crystallography. The rotational energy barrier is 5.4 kcal mol^{-1}, which is partially due to a favourable internal hydrogen bond with a computed N…H-N distance of 2.06 Å.

5.2.3.2.1 Conformational analysis by EXSY NMR Spectroscopy

EXSY (EXchange SpectroscopY) was used to investigate the *cis-trans* isomerism of **314**. A solution of **314** in stock $CDCl_3$ was placed in an NMR tube and EXSY spectra were taken by 2D 600 MHz NMR spectroscopy.

Figure 5.27 Representative EXSY pulse sequence

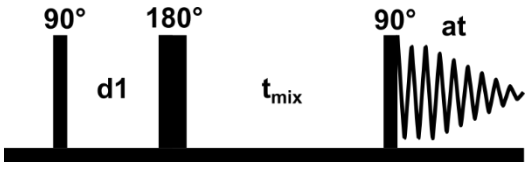

EXSY is functionally identical in pulse sequence to the more commonly known NOESY NMR method, which can be used to detect atoms that are in close proximity in space by the Nuclear Overhauser Effect (NOE). EXSY detects peaks that chemically exchange during the mixing time t_{mix}. The spectrum shows cross-peaks with an intensity proportional to the proportion of the signal that has exchanged within the mixing time.

Figure 5.28 EXSY spectrum of 314 with mixing time 0.3 s, with exchanging peaks circled in red.

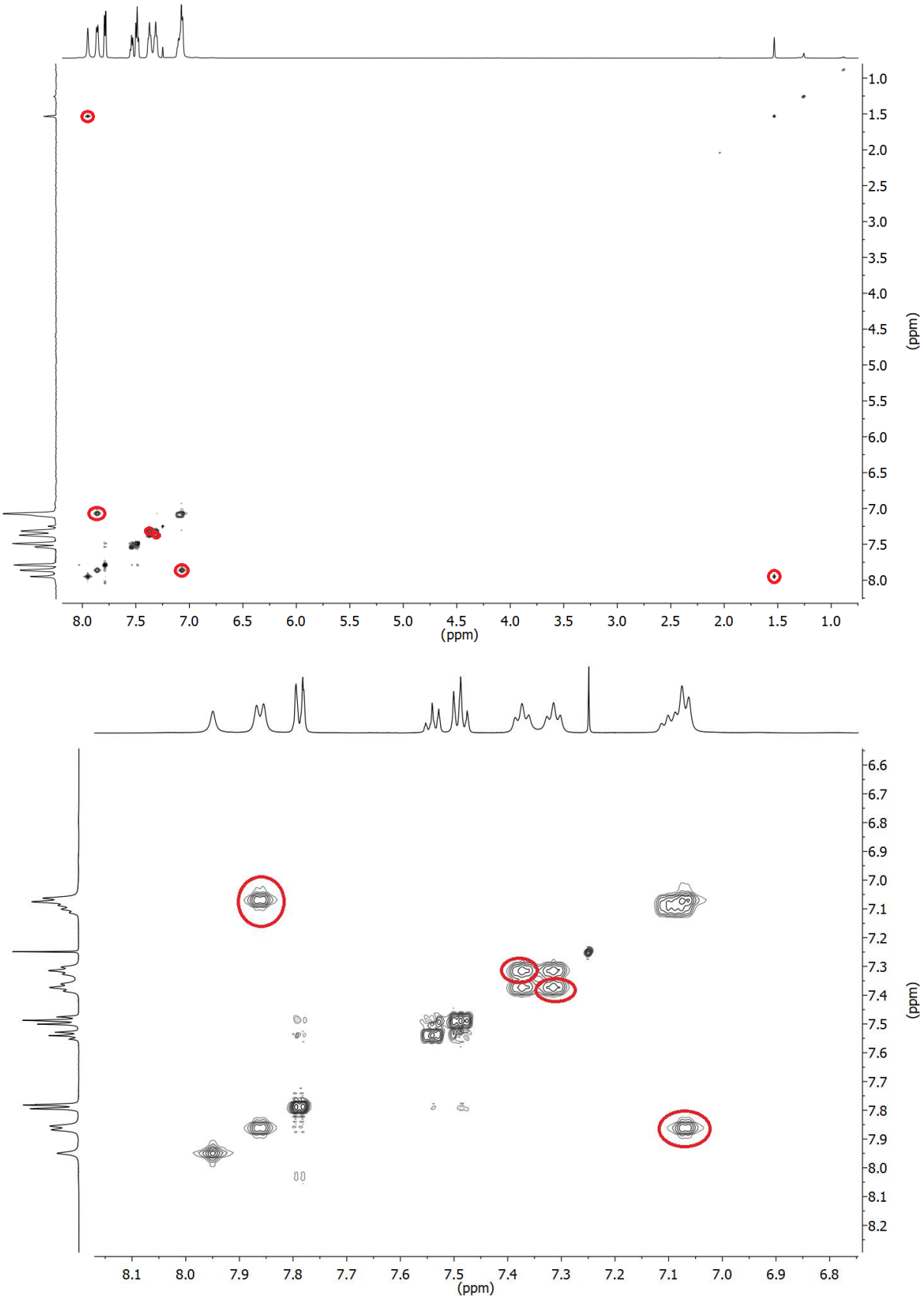

Two spectra were taken, an EXSY spectrum with mixing time of 0.3 s (Figure 5.28), and a reference EXSY spectrum without a mixing time. The reference spectrum is used to distinguish COSY and NOESY-type signals that could mimic exchanges.

From integration of the cross-peaks on the 2D EXSY spectrum, a minimum rate constant for exchange was determined, using free EXSYcalc software provided by Mestrelab Research SL to calculate the rate constant. Using EXSYCalc and integrals of the peaks in question from MestReNova, the rate constant is determined to be k_{ex} = 7 s^{-1}. Although this method can be used to determine a close estimate for the rate constant in most cases, due to the integrals of the cross peaks being close to 100% of the non-exchange peaks, this constitutes a lower limit for the rate constant. As the peaks are distinct and not coalesced, it can also be determined that the rate constant must be less than the rate constant required for peak coalescence, which is described by Equation 5.1, where Δν is the difference in chemical shift in Hz.

Equation 5.1

$$k = \pi\Delta\nu/\sqrt{2}$$

From both of these methods, a rate constant range can be determined, where k_{ex} the rate of exchange of the peaks, which is potentially equal to the rate of *cis-trans* isomerism.

$$7 \leq k_{ex}(s^{-1}) \leq 80$$

The results of this experiment are in disagreement with our computational energy barrier of 5.4 kcal mol^{-1}. The latter would equate to a rate constant of ~ 10^6 s^{-1} which would result in coalescence of the ^{1}H NMR peaks. The computational methods, however, assume reaction of **314** in the gas phase unlike the EXSY experiments. Previous data from experiments on **314** in solution phase NMR spectroscopy indicate that the rotation around the bond varies significantly with the solvent, however, the range given above applies only for this experiment in stock $CDCl_3$.

A second possible explanation accounting for the discrepancy is an alternative mechanism for the exchange in the EXSY experiment. Tautomerisation between the N-H group and C=N groups, mediated by water in the solvent, would result in *cis-trans* isomerism without rotation around the N=N bond. There is an exchange between the N-H groups and the peak corresponding to trace water in the $CDCl_3$, with a rate constant determined by EXSY of k_{OH} =

1.58 s^{-1}. This value is lower than the minimum rate constant of 7 s^{-1}, however, which indicates that tautomerisation is not the predominant mechanism for *cis-trans* isomerism in this reaction, although the associated rate would be within similar order of magnitude.

5.3.3.3 Alkylation of Triazabutadiene 314

To further investigate whether a benzotriazinyl radical could be formed from triazabutadiene **314**, alkylation of the triazabutadiene was attempted. It was hypothesised that the seemingly large energy barrier to cyclization of this system could be bypassed by alkylating the N-H group of the triazabutadiene, resulting in formation of a benzotriazinyl moiety.

Scheme 5.20 Attempted alkylation by trimethyloxonium tetrafluoroborate

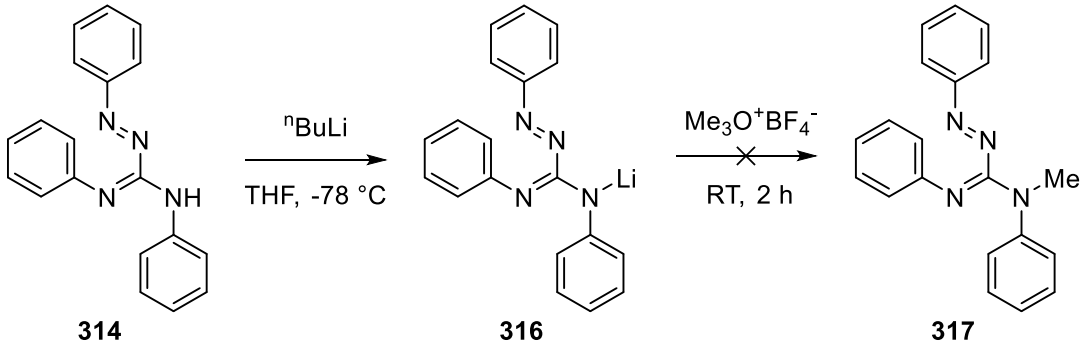

Alkylation was attempted first by the usage of trimethyloxonium tetrafluoroborate. The products of the reaction were analysed and found to be predominantly the starting triazabutadiene **314** and a small peak in LCMS with mass corresponding to alkylated form **317** was detected. However, the product could not be isolated in any quantity significant enough for further analysis.

Scheme 5.21 Attempted alkylation by iodomethane

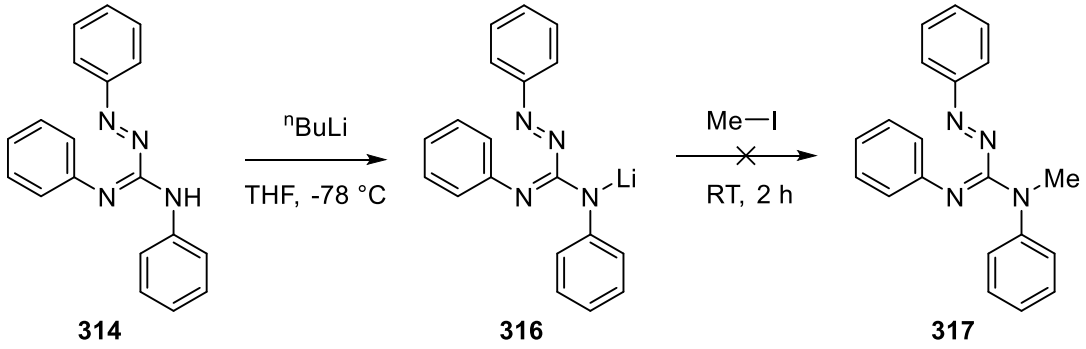

Further attempts at alkylation were made by first preparing the lithium amide salt **316** of triazabutadiene **314** at 0 °C, followed by addition of iodomethane in an attempt to achieve

alkylation. This again resulted in only trace amounts of potentially alkylated triazabutadiene which could not be isolated in any significant quantities. In this reaction, although there was an initial observed colour change from red to dark green in the presence of ^{n}BuLi (similar in colour to solutions of amino radical **315**), upon addition of iodomethane and stirring, the solution slowly returned to the red colour of the triazabutadiene. This suggests that the green colour is the presence of the lithium amide which is unreactive towards iodomethane and is slowly quenched back to the starting material **314**.

5.3 Discussion

Following the serendipitous discovery by Grant of the novel benzotriazinyl radical formed by the decomposition of the NHC precursor Nitron in solutions of acetonitrile, this chapter aimed to further investigate the mechanism of this reaction, as well as to determine the physical and chemical properties of the newly formed radical. Initial investigations by Grant determined that in dry degassed acetonitrile, Nitron is stable over several days, with no change in colour notable. Triazabutadiene **314** is also a known decomposition product of Nitron **127**, by base hydrolysis[24].

Optimisation of the preparation of **313** determined that addition of excess water caused the reaction to form **314** to become predominant. However, the use of less hygroscopic solvents like toluene slow the reaction substantially. Empirically, the addition of 1% v/v water to acetonitrile was sufficient to increase the speed of reaction without substantially increasing the formation of **314**. Purification of **313** by recrystallization from ethanol proved simple and effective.

Amino radical **315** was discovered during a preparation of **313** during column chromatography as a distinctive green coloured solution eluting after **33**. Further investigation determined that **315** could be prepared through acidic or basic hydrolysis of **313**. Triazabutadiene **314** was not found to react to form **315** under ambient conditions in acetonitrile, or under basic conditions in the presence of an oxidising agent.

Scheme 5.22 Proposed mechanism of formation of 313, 314 and 315.

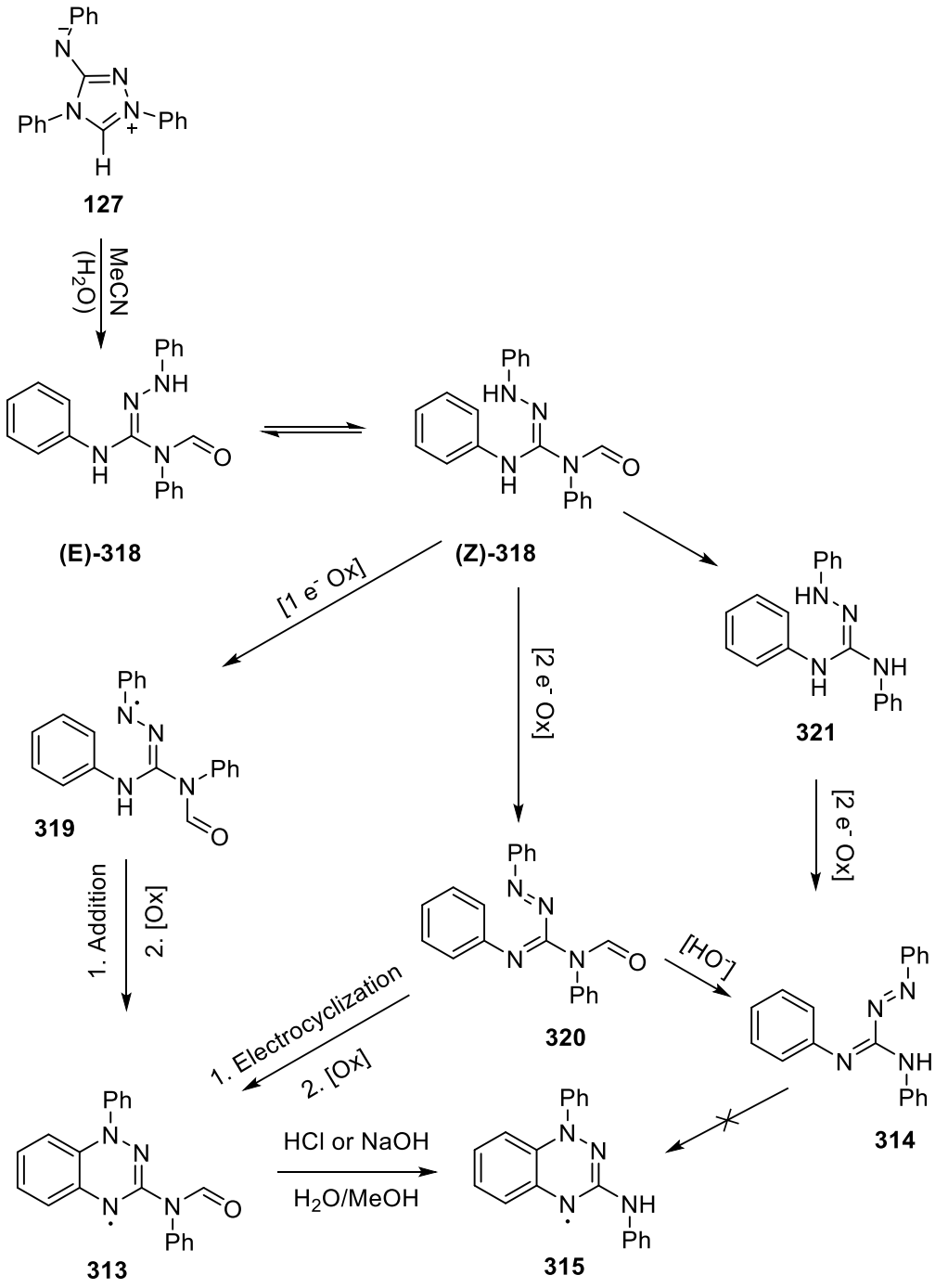

The results of these experiments, in conjunction with the proposed literature route to C(3)-aryl/alkyl Blatter radicals, allow a mechanism to be proposed for the formation and reactions of **313**, **314** and **315**. Due to the lack of reaction of Nitron **127** under acidic or anhydrous conditions, the initial step is believed to be a ring opening by water or hydroxide, to form amidrazone **318**. *Cis-trans* isomerism is required to form the correct conformation for either a single electron oxidation to amidrazonyl radical **319** or a two electron oxidation to

triazabutadiene **320**. Radical ring-closure of **319** and subsequent oxidation could then give **313**. Alternatively, triazabutadiene **320** could undergo electrocyclization followed by a 2-electron oxidation to give **313**. The unique preference for acetonitrile as a solvent over other polar protic or aprotic solvents could be a result of the role of solvent in promoting the 1e or 2e electron transfer steps. Solvents with low dielectric relaxation times are known to increase the rate of simple electron-transfer reactions, and acetonitrile's low relaxation time could enhance the reactivity via these mechanisms[31–33].

Triazabutadiene **314** is believed to originate from either hydrolysis and oxidation of amidrazone **321** hydrolysis of **320**. It was also not found to react onwards to form radical **315** under the tested conditions. This explains why higher levels of water or methanol decrease yields of amido radical **313** and do not increase formation of green radical **315**.

It was considered that the reason for a lack of formation of amino radical **315** from triazabutadiene **314** is a high barrier to *cis-trans* isomerism, preventing onward reaction. It was found by computational research by Dr. Mark A Fox that the *trans* isomer of **318** is the ground state but the C1-N1 rotational barrier for triazabutadiene **314** is predicted to be under 5.4 kcal mol^{-1}. EXSY NMR experiments disagree with this finding, and determined that the first-order rate constant of *cis-trans* isomerism of **314** in $CDCl_3$ solution is between 7 s^{-1} and 80 s^{-1}, much slower than computational analysis suggests. Both the computational and EXSY experiments confirm, however, that the barrier to *cis-trans* isomerism is relatively low. Furthermore, the barrier to electrocyclization in related triazabutadiene **284** has previously been determined computationally to be 38.6 kcal mol^{-1}, making it a more likely rate determining step[18]. Therefore, the amide group of **320** is possibly activating towards onward electrocyclization than the aniline group of **314**, allowing the reaction to proceed to **315** in the former case.

Several hypotheses were suggested for the origin of amino radical **315**. One possible route to **315** is by electrocyclization and subsequent oxidation of triazabutadiene **314** by analogy with the proposed literature route to other Blatter-type radicals. Another possible route to **315** is parallel generation of **315** alongside the reaction conditions that generated amido radical **313**. A third possible route is amide hydrolysis of **331** by opportunistic water during either the original reaction or during column chromatography. Given the lack of reactivity of **314** under a variety of reaction conditions, it is most likely that **315** forms in a post-cyclization hydrolysis of **313**

Scheme 5.23 Lack of reaction of 128

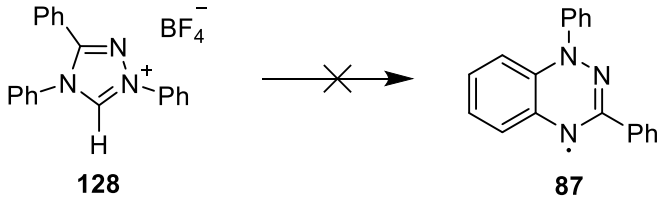

The related 1,2,4-triphenyl-triazolium salt **128** was found not to undergo any analogous reactions under neutral, basic and oxidising conditions. This demonstrates that the exocyclic nitrogen atom is necessary in this reaction motif. Scheme 5.24 shows a potential mechanism by which **128** could form benzotriazinyl radical **87**, through two sequential hydrolyses to amidrazone **323**, followed by a cyclization reaction.

Scheme 5.24 Potential pathway to form 87 from 128

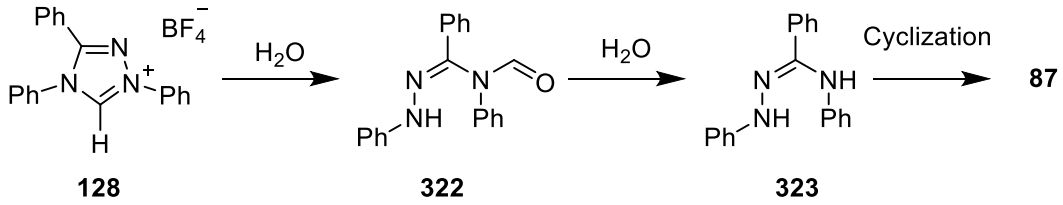

As no change was observed in the ^{1}H NMR spectra or LCMS data for **128**, it can be shown that there was no initial ring opening, precluding any further reactions.

In conclusion, the reaction of Nitron **127** in acetonitrile provides a novel and facile route to the benzotriazinyl moiety. The mechanism of this reaction is an unprecedented ring-opening and cyclization mechanism, which has been optimized to a yield of 82%. Radicals **313** and **315** are unique among benzotriazinyl radicals in having heteroatom substitution at the 3-position. This synthetic handle could provide a valuable route to a wide range of derivatives, which could be useful in the fields of spin labelling or organic magnetic materials.

5.3.1 Properties of benzotriazinyl radicals 313 and 315

As previously stated, radicals **313** and **315** have a unique 3-heteratom substituted benzotriazinyl moiety. A series of experiments were performed to probe the physical and chemical properties of these two radicals and any effects of their 3-amido/amino substituents.

EPR experiments with the assistance of Dr. Victor Chechik and computational chemistry experiments by Dr. Mark A Fox were undertaken in order to determine the orbital structure of radicals 1 and 2. The EPR spectra indicate there is a large 8 G hyperfine coupling to one

nitrogen atom and two 5 G couplings to two further nitrogen atoms. The computed orbitals of **313** and **315** indicate roughly equal distribution of spin density between N1, N2 and N4, with negligible spin density on the exocyclic nitrogen atom. It can therefore be suggested that the 3-amino substituent does not largely influence the nature of the benzotriazinyl radical, and the chemistry would be expected to be related to known examples.

The electrochemistry of **313** and **315** was studied by cyclic voltammetry. **313** and **315** are both insoluble in water, therefore the experiments were performed in acetonitrile with a supporting electrolyte of $Bu_4N\ BF_4$. **313** and **315** both show two fully reversible waves corresponding to (−1/0) and (0/+1) redox processes. In the presence of oxygen, the (−1/0) peak of **315** becomes irreversible. Reversible (−1/0) and (0/+1) peaks are common to most other benzotriazinyl radicals. The half-wave potentials of **315** are notably lower than for **313**, and this is assigned to the electron-withdrawing effect of the amido group of **313**, compared to the less withdrawing anilino substituent of **315**, reducing the energy of the SOMO. Compared to results found by Berezin[23], amino radical **315** was similar in 0/+1 potential to the more electron-withdrawing fused imidazolyl benzotriazinyl radicals, whereas **313** was significantly higher in potential, similar to the thiazolyl fused system. However, comparison to these results is difficult, due to the different solvent systems, electrolytes and electrodes used.

Figure 5.29 Verdazyl radical

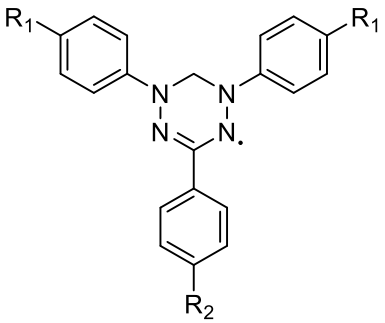

86, 324a-d

Table 5.3 Verdazyl radical redox potentials obtained through cyclic voltammetry

Radical	R_1 =	R_2 =	$E_{1/2}$ (0/+1)	$E_{1/2}$ (−1/0)
313	–	–	−0.11	−1.06
315	–	–	−0.35	−1.21
86	H	H	−0.22	−1.23
324a	OMe	Me	−0.39	−1.33

324b	Me	Me	−0.31	−1.29
324c	H	Me	−0.24	−1.26
324d	Cl	Me	−0.15	−1.14

Electrochemical studies on verdazyl radicals performed by Hicks et. al[34]. in acetonitrile with Bu_4NBF_4 (0.1 M) electrolyte, with platinum counter electrode and glassy carbon instead of our platinum electrode show broadly similar potentials in comparison to the internal standard of the Fc/Fc+ couple as the benzotriazinyl species **313** and **315.**

Figure 5.30 Oxoverdazyl radicals

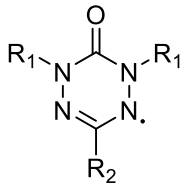

325a-d

Table 5.4 Oxoverdazyl radical redox potentials obtained through cyclic voltammetry.

Radical	R_1 =	R_2 =	$E_{1/2}$ (0/+1)	$E_{1/2}$ (−1/0)
325a	Ph	Ph	+0.44	−0.94
325b	Me	Ph	*+0.27*	−1.28
325c	^{i}Pr	Ph	*+0.18*	−1.38
325d	^{i}Pr	2-pyridyl	*+0.20*	−1.36

Oxoverdazyl radicals in the same system however showed significantly higher 0/+1 potentials from but roughly similar −1/0 potentials. Again, both peaks were fully reversible in the examples shown.

Both radicals were found to be stable indefinitely under ambient conditions, although benzotriazinyl radicals are known to decompose slowly by oxidation[13,23]. This oxidation process was not observed for **313** or **315**, but cannot be ruled out as an eventual decomposition pathway. Strongly acidic or basic conditions cause **313** to undergo base hydrolysis to **315**. Under acidic conditions, **315** could be protonated causing a distinctive colour change, however, the site of protonation is unknown. A weak EPR signal could be detected under highly acidic conditions, including neat trifluoroacetic acid. The resulting spectrum was broad and poorly resolved and appears to show a large 15 G hyperfine coupling. Unfortunately, due to the poor resolution and lack of other data, the protonated species cannot be characterised and requires further investigation.

5.4 Summary

In this work, the mechanism of Grant's serendipitous formation of a novel benzotriazinyl radical **313** was probed by a range of synthetic, spectroscopic and computational techniques.

Synthetic experiments determined that acetonitrile was a facile and useful solvent for the formation of radical **313**, with the addition of small amounts of water enhancing the yield. Surplus water largely resulted in the formation of triazabutadiene **314**, and other solvents either resulted in triazabutadiene **314** formation, or slow reaction rate. Acetonitrile may have a role in promoting the necessary electron-transfer processes in cyclization reactions to form **313**[32].

A second novel benzotriazinyl radical **315** was discovered during preparations of **313** and is believed to originate from further hydrolysis of **313** under the reaction conditions or during purification. Both radicals were fully characterised by EPR spectroscopy, MS and X-ray crystallography, which confirmed the assigned structures and 100% radical character. EPR spectral data, combined with computational predictions showed that the exocyclic nitrogen atom adjacent to the benzotriazinyl moiety has a minimal effect on the SOMO orbital structure. Electrochemistry of both radicals showed two fully reversible single electron redox waves in acetonitrile, which is consistent with other benzotriazinyl radicals[23].

Further investigation into the mechanism of benzotriazinyl formation showed that the exocyclic nitrogen atom of **313** is necessary for its formation, as related triazolium salt **128** failed to form a benzotriazinyl radical under similar conditions. Additionally, triazabutadiene **314** was found to not undergo cyclization under typical reaction conditions, possibly indicating the necessity of the carbonyl group of potential intermediate **318** to permit further reaction via 1e or 2e oxidative routes. Alkylation of **314** under standard conditions was unsuccessful, which was assigned to low nucleophilicity of **314**.

5.4 Bibliography

1 J. A. Grant, Z. Lu, D. E. Tucker, B. M. Hockin, D. S. Yufit, M. A. Fox, R. Kataky, V. Chechik and A. C. O'Donoghue, *Nat. Commun.*, 2017, **8**, 15088.

2 J. S. Miller, *Inorg. Chem.*, 2000, **39**, 4392–4408.

3 Y. Wang, Y. Huang, Y. Song, X. Zhang, Y. Ma, J. Liang and Y. Chen, *Nano Lett.*, 2009, **9**, 220–224.

4 T. L. Makarova, B. Sundqvist, R. Höhne, P. Esquinazi, Y. Kopelevich, P. Scharff, V. A. Davydov, L. S. Kashevarova and A. V. Rakhmanina, *Nature*, 2001, **413**, 716–718.

5 T. L. Makarova, B. Sundqvist, R. Höhne, P. Esquinazi, Y. Kopelevich, P. Scharff, V. Davydov, L. S. Kashevarova and A. V. Rakhmanina, *Nature*, 2006, **440**, 707–707.

6 A. J. Banister, N. Bricklebank, I. Lavender, J. M. Rawson, C. I. Gregory, B. K. Tanner, W. Clegg, M. R. J. Elsegood and F. Palacio, *Angew. Chem. Int. Ed. Engl.*, 1996, **35**, 2533–2535.

7 J. M. Rawson, A. J. Banister and I. Lavender, in *Advances in Heterocyclic Chemistry*, ed. A. R. Katritzky, Academic Press, 1995, vol. 62, pp. 137–247.

8 M. Kinoshita, *Jpn. J. Appl. Phys.*, 1994, **33**, 5718.

9 H. M. Blatter and H. Lukaszewski, *Tetrahedron Lett.*, 1968, **9**, 2701–2705.

10 I. Ratera and J. Veciana, *Chem. Soc. Rev.*, 2011, **41**, 303–349.

11 M. Busch and R. Ruppenthal, *Berichte Dtsch. Chem. Ges.*, 1910, **43**, 3001–3011.

12 F. A. Neugebauer and I. Umminger, *Chem. Ber.*, 1980, **113**, 1205–1225.

13 P. A. Koutentis and D. L. Re, *Synthesis*, 2010, **2010**, 2075–2079.

14 Y. Takahashi, Y. Miura and N. Yoshioka, *New J. Chem.*, 2015, **39**, 4783–4789.

15 F. Ciccullo, N. M. Gallagher, O. Geladari, T. Chassé, A. Rajca and M. B. Casu, *ACS Appl. Mater. Interfaces*, 2016, **8**, 1805–1812.

16 C. P. Constantinides, E. Obijalska and P. Kaszyński, *Org. Lett.*, 2016, **18**, 916–919.

17 A. A. Berezin, C. P. Constantinides, C. Drouza, M. Manoli and P. A. Koutentis, *Org. Lett.*, 2012, **14**, 5586–5589.

18 A. Bodzioch, M. Zheng, P. Kaszyński and G. Utecht, *J. Org. Chem.*, 2014, **79**, 7294–7310.

19 P. Kaszyński, C. P. Constantinides and V. G. Young, *Angew. Chem. Int. Ed.*, 2016, **55**, 11149–11152.

20 C. P. Constantinides, P. A. Koutentis, H. Krassos, J. M. Rawson and A. J. Tasiopoulos, *J. Org. Chem.*, 2011, **76**, 2798–2806.

21 K. Mukai, K. Inoue, N. Achiwa, J. B. Jamali, C. Krieger and F. A. Neugebauer, *Chem. Phys. Lett.*, 1994, **224**, 569–575.

22 W. Duffy and K. P. Barr, *Phys. Rev.*, 1968, **165**, 647–654.

23 A. A. Berezin, C. P. Constantinides, S. I. Mirallai, M. Manoli, L. L. Cao, J. M. Rawson and P. A. Koutentis, *Org. Biomol. Chem.*, 2013, **11**, 6780–6795.

24 M. Busch, *Berichte Dtsch. Chem. Ges.*, 1905, **38**, 856–860.

25 S. Shahine and S. Khamis, *Microchem. J.*, 1975, **20**, 409–414.

26 W. C. Cope and J. Barab, *J. Am. Chem. Soc.*, 1917, **39**, 504–514.

27 C. Färber, M. Leibold, C. Bruhn, M. Maurer and U. Siemeling, *Chem. Commun.*, 2011, **48**, 227–229.

28 R. S. Massey, C. J. Collett, A. G. Lindsay, A. D. Smith and A. C. O'Donoghue, *J. Am. Chem. Soc.*, 2012, **134**, 20421–20432.
29 D. E. Tucker, P. Quinn, R. S. Massey, C. J. Collett, D. J. Jasiewicz, C. R. Bramley, A. D. Smith and A. C. O'Donoghue, *J. Phys. Org. Chem.*, 2015, **28**, 108–115.
30 G. A. Mabbott, *J. Chem. Educ.*, 1983, **60**, 697.
31 W. R. Fawcett and C. A. Foss, *J. Electroanal. Chem. Interfacial Electrochem.*, 1991, **306**, 71–85.
32 H. Heitele, *Angew. Chem. Int. Ed. Engl.*, 1993, **32**, 359–377.
33 J. J. Warren and J. M. Mayer, *J. Am. Chem. Soc.*, 2008, **130**, 7546–7547.
34 J. B. Gilroy, S. D. J. McKinnon, B. D. Koivisto and R. G. Hicks, *Org. Lett.*, 2007, **9**, 4837–4840.

Chapter 6 Experimental

6.1 General Instrumentation

6.1.1 General Instrumentation.

Chromatography

Thin layer chromatography was performed using silica-backed Machery-Nagel Polygram SILG/UV_{254} plates obtained from Fisher Scientific. Column chromatography was performed using 60Å silica gel obtained from Fluorochem.

6.1.2 Supply of Materials

Chemicals used in this thesis were purchased from Sigma Aldrich, Tokyo Chemical Industries, Acros Organics, Fisher Scientific, Fluorochem, Manchester Organics, Alfa Aesar and Apollo Scientific.

Flash column chromatography was conducted using silica gel supplied from Sigma Aldrich and Fluorochem and monitored by thin layer chromatography (TLC) analysis. All synthetic solvents were obtained from Fisher Chemicals: methanol and acetonitrile were obtained as HPLC grade (99.9% min assay by GC); acetone and toluene were obtained as analytical reagent grade.

$CDCl_3$ (99.8% D) was obtained from Apollo Scientific, and all other deuterated solvents (CD_2Cl_2, CD_3CN, CD_3OD, d_6-DMSO, D_2O, DCl Soln., NaOD soln.) were obtained from Cambridge Isotope Laboratories.

Triazolium salts **120** and **121** were previously prepared by a MChem student in our research group – Chris Bramley – and were independently characterised.

Imidazolium salts **122** and **123** were prepared by Dr. Paul Davies of the University of Birmingham and were independently characterised.

6.1.3 Computational Methods

The geometry optimizations in Chapter 5 were carried out by Dr. Mark A. Fox of Durham University at the B3LYP[1,2]/6-311+G(d,p)[3,4] level using the GAUSSIAN09[5] package and confirmed as true minima by frequency calculations.

Electronic structure (molecular orbital, spin density, EPR) data in the radical species **313** and **315** were obtained at the hybrid-DFT UB3LYP/6-311+G(d,p) with molecular orbitals and spin densities plotted using GABEDIT[6] and orbital contributions determined with GAUSSSUM[7]. The SOMO in the radical species is assumed here to be

the highest alpha(α) singly occupied molecular orbital, α-HOSO, where α- and β- single orbitals are treated as separate orbitals in open-shell calculations at UB3LYP/6-311+G(d,p). The model chemistry B3LYP/EPR-II[8] was used on UB3LYP/6-311+G(d,p) optimised geometries as it is considered to be more suitable for predicting EPR parameters.

6.1.4 Instrumental Methods

Nuclear Magnetic Resonance Spectroscopy (NMR)

NMR samples were prepared in a wide variety of solvents: chloroform-d_1, deuterium oxide-d_2, dichlormethane-d_2, dimethylsulfoxide-d_6, acetonitrile-d_3 and methanol-d_4. Additionally, several samples for ^{31}P NMR spectroscopy were collected in non-deuterated H_2O when stated. Chemical shifts are reported relative to residual solvent peaks[9,10] as stated in Table 1, unless stated relative to a particular internal standard.

Table 1 Solvent residual signals

Solvent	δ_H (ppm)	δ_C (ppm)
Acetonitrile-d_3	1.94	1.3, 118.3
Chloroform-d_1	7.26	77.2
Deuterium oxide-d_2	4.79	-
Dichloromethane-d_2	5.32	53.8
Dimethylsulfoxide-d_6	2.50	39.5
Methanol-d_4	3.31	49.0

Data is presented in the following format: chemical shift (ppm), integration, multiplicity (br = broad, m = multiplet. s = singlet, d = doublet, t = triplet, q = quartet, quintet and septet) coupling constants (J = x Hz) and assignment where appropriate. NMR spectra at 400, 500, 600 and 700 MHz were recorded using Varian Mercury-400, Bruker Ultrashield 400, Varian Inova-500, Varian VNMR 600, and Varian VNMR 700 instruments operated at 25 ˚C unless otherwise stated.

Elemental Analysis

Elemental analysis was performed by the Microanalytical Unit (Department of Chemistry, Durham University), and performed on an Exeter CE-440 Elemental Analyser.

Electron Paramagnetic Resonance Spectroscopy.

EPR spectra were recorded by Dr, Victor Chechik of the University of York on a Bruker EMX Micro spectrometer operating at X-band (9.5 GHz frequency), power 5 mW, modulation frequency 100 kHz, modulation amplitude 1 G. The spectra were recorded at room temperature using 0.1 mM solutions of radicals in degassed toluene unless otherwise stated.

Cyclic Voltammetry

A potentiostat (Ivium Compactstat.e) interfaced with a personal computer was used for the electrochemical measurements. A three-electrode cell containing a Pt wire pseudo-reference electrode, a Pt foil (area = 1 cm^2) counter electrode and a Pt working electrode were used in a Faraday cage.

Cyclic voltammetry measurements were performed on **313** and **315** at 1 mM concentrations in Bu_4NBF_4 solutions (0.1 M) in degassed, dried acetonitrile. The electrolyte, Bu_4NBF_4, was dried before use and inert conditions were maintained during measurements. Decamethylferrocene (Cp^*_2Fe) and ferrocene (Cp_2Fe) were used as internal references for radicals **313** and **315** respectively. A scan rate of 50 mV/s was used for all measurements unless stated otherwise. All potentials are quoted relative to the ferrocenium/ferrocene (Cp_2Fe^+/Cp_2Fe) couple. The decamethylferrocenium/decamethylferrocene[11] ($Cp^*_2Fe^+/Cp^*_2Fe$) couple has a half-cell potential of −0.50 V relative to the Cp_2Fe^+/Cp_2Fe couple in this setup.

Infrared spectra

IR spectra were taken of solid or neat liquid samples using a Perkin-Elmer Spectrum 2 FTIR infrared spectrophotometer at room temperature.

UV-visible spectra

UV-Visible spectra were determined in acetonitrile solution using a Varian Cary 100 Bio UV-visible spectrophotometer at 25 °C.

Single Crystal X-ray Crystallography

The X-ray single crystal data in this project has been collected by the Crystallography Department of Durham University using λMoKα-radiation (λ=0.71073Å) at 120.0K using a Bruker SMART CCD 6000 (fine-focus sealed tube, graphite monochromator), or using a Bruker D8Venture (Photon100 CMOS detector, IμS-microsource, focusing mirrors) or on an Agilent Gemini S-Ultra (Sapphire-3 CCD detector, fine-focus sealed

tube, graphite monochromator) diffractometers equipped with Cryostream (Oxford Cryosystems) open-flow nitrogen cryostat. The structures were solved by a direct method and refined by full-matrix least squares on F^2 for all data using Olex2S[12] and SHELXTL[13] software. All non-hydrogen atoms were refined with anisotropic displacement parameters, and H-atoms were located on the difference map and refined isotropically.

Mass Spectrometry

Liquid chromatography-mass spectrometry (LC-MS) spectra were obtained using either a Waters (UK) TQD mass spectrometer with low resolution ESI+, electrospray in positive ion mode, (ES+) or a Waters (UK) QToF Premier mass spectrometer (QToF+) (low resolution ESI+ ionisation) running either water-acetonitrile gradient or water-methanol gradient methods.

6.2 Synthetic Procedures for Chapter 3

Bis(diisopropylamino)cyclopropenium tetraphenylborate 129

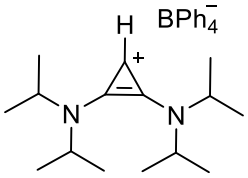

129

Diisopropylamine (7.01 mL, 50.0 mmol) was added dropwise at 0 ºC to a stirred solution of tetrachlorocyclopropene **3** (1.78 g, 10.0 mmol) in DCM (100 mL), under an inert atmosphere in a flask fitted with septum cap and stirrer bar. After 6 hours at 0 ºC, the solution was warmed to room temperature and sodium tetraphenylborate (3.42 g, 10.0 mol) was added. The suspension was stirred overnight, and then refluxed for 4 hours. After cooling the solution to room temperature, triphenylphosphine (2.62 g, 10.0 mmol) was added. Immediately after addition of the triphenylphosphine, water (70 mL) was added and the mixture was stirred overnight with a vent to open air. The organic layer was separated and washed with water (3 × 150 mL). Then the organic phase was dried with anhydrous Na_2SO_4 and concentrated under vacuum. After washing with hexane (70 mL), and drying under vacuum, the cyclopropenium salt was obtained as an orange-yellow solid in a crude yield of 4.93 g. Recrystallization from DCM/Et_2O at −20 ºC yielded white crystals of bis(diisopropylamino)cyclopropenium tetraphenylborate

129 (0.42 g, 9%); ν_{max} (cm^{-1}) 3101, 3054, 2982, 1878, 1567, 1541, 1480, 1437, 1426, 1373, 1345, 1312, 1265, 1183, 1138, 1121, 1074, 1032, 997, 964, 899, 838, 786, 745, 729, 702, 624, 612, 597, 539, 515, 500, 466, 401, 389; δ_H (700MHz, $CDCl_3$): 7.44 (8H, m, B-Ar-*H*), 7.03 (8H, t, *J* = 7.4 Hz, *m*-Ar-*H*), 6.88 (4H, t, *J* = 7.2 Hz, *p*-Ar-*H*), 4.95 (1H, s, Cp-*H*), 3.78 (2H, septet, *J* = 6.8 Hz, N-C*H*), 3.58 (2H, septet, *J* = 6.8 Hz, N-C*H*), 1.25 (12H, d, *J* = 6.8 Hz, CH_3), 1.12 (12H, d, *J* = 6.8 Hz, CH_3); δ_C (176 MHz, $CDCl_3$): 164.22 (q, *J* = 49.3 Hz), 136.24 – 136.14 (m), 133.07, 125.55 (q, *J* = 2.7 Hz), 121.66, 100.34, 55.12, 50.12, 21.06, 20.76; m/z (ES+): 237 $[M-BPh_4]^+$; HRMS (ES+): $C_{15}H_{29}N_2$ requires: 237.2331; found: 237.2346.

Bis(diisopropylamino)cyclopropenium tetrafluoroborate 163

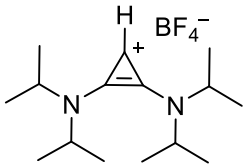

163

Diisopropylamine (2.69 mL, 1.94 g, 19.2 mmol) was added dropwise at 0 ºC to a stirred solution of tetrachlorocyclopropene (0.49 mL, 0.71 g, 4.00 mmol) in DCM (100 mL) under an inert atmosphere in a flask fitted with a septum cap and stirrer bar. After 1 hour at 0 ºC, the solution was warmed to room temperature and sodium tetrafluoroborate (0.44 g, 4 mmol) was added. The suspension was stirred overnight. Triphenylphosphine (1.05 g, 4 mmol) was added, immediately followed by water (100 mL) and the mixture was stirred overnight with a vent to open air. The organic layer was separated and washed with water (3 x 100 mL). Then the organic phase was dried with anhydrous Na_2SO_4 and concentrated under vacuum. The crude product was purified by recrystallization from DCM/Et_2O at −20 °C to give the product as fluffy white crystals of **163** (1.14 g, 87 %); m.p 177-178 °C (dec.), CHN: (Found C 55.5, H 8.9, N 8.6 %, Required for $C_{15}H_{29}N_2BF_4$ C 55.6, H 9.0, N 8.6 %); ν_{max} (cm^{-1}): 3438, 2982, 1909, 1558, 1495, 1447, 1396, 1375, 1355, 1248, 1213, 1186, 1156, 1140, 1117, 1070, 1043, 1023, 988, 929, 916, 855, 827, 762, 749, 734, 701, 682, 645, 615, 587, 554, 517, 386; δ_H (700MHz, $CDCl_3$): 7.44 (1H, s, Cp-*H*), 4.02 (2H, septet, *J* = 6.8 Hz, N-C*H*), 3.85 (2H, septet, *J* = 6.8 Hz, N-C*H*), 1.40 (12H, d, *J* = 6.8 Hz, CH_3), 1.37 (12H, d, *J* = 6.8 Hz, CH_3); δ_C (700MHz, $CDCl_3$): 133.81, 99.28, 56.86, 49.21, 20.83, 20.72; m/z (ES+) : 237 $[M-BF_4]^+$ HRMS (ES+): $C_{15}H_{29}N_2$ requires: 237.2331; found: 237.2352.

Bis(dicyclohexylamino)cyclopropenium tetrafluoroborate 142

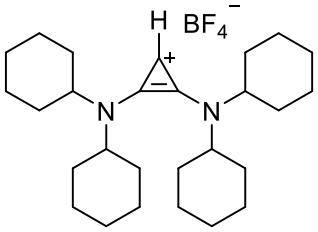

142

Dicyclohexylamine (7.88 mL, 40.0 mmol) was added dropwise at 0 ºC to a stirred solution of tetrachlorocyclopropene (1.78 g, 1.22 mL, 10.0 mmol) in DCM (100 mL) under an inert atmosphere in a flask fitted with a septum cap and stirrer bar. After 6 hours at 0 ºC, the solution was warmed to room temperature and sodium tetrafluoroborate (1.09 g, 10.0 mmol) was added. The suspension was stirred overnight, and then refluxed for 4 hours. After cooling the solution to room temperature, triphenylphosphine (2.62 g, 10.0 mmol) was added. Immediately after addition of the triphenylphosphine, water (70 ml) was added and the mixture was stirred overnight with a vent to open air. The organic layer was separated and washed with water (3 x 150 mL). The organic phase was dried over Na_2SO_4 and dried under reduced pressure to give the crude product as yellow crystals. Recrystallization from hot THF gave the product bis(dicyclohexylamino)cyclopropenium tetrafluoroborate **142** as off-white crystals (1.25 g, 26%); m.p 176-178 °C (dec.); CHN: (Found C 66.5, H 9.2, N 5.6, Required for $C_{27}H_{45}N_2BF_4$ C 66.9, H 9.4, N 5.8); ν_{max} (cm^{-1}): 3115, 2931, 2858, 1881, 1557, 1451, 1373, 1323, 1277, 1176, 1156, 1048, 869, 867, 848, 832, 729, 645, 520, 398; δ_H (700 MHz, $CDCl_3$): 7.58 (1H, s, Cp-*H*), 3.53 (2H, tt, *J* = 12.2, 3.8 Hz, N-C*H*), 3.35 (2H, tt, *J* = 11.8, 4.3 Hz, N-C*H*), 2.00-1.10 (40H, m, Cy-*H*); δ_C (176 MHz, $CDCl_3$): 134.32, 100.59, 64.68, 58.32, 31.22, 30.83, 25.67, 25.61, 24.76, 24.56; m/z (ES+): 397 $[M-BF_4]^+$; HRMS (ES+): required for $C_{27}H_{45}N_2BF_4$ 397.3583, found 397.3577.

Tris(N-Methylanilino)cyclopropenium tetrafluoroborate 181

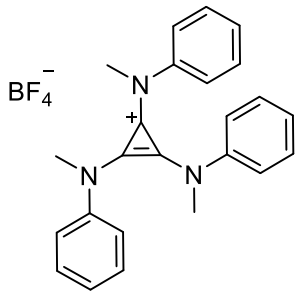

181

N-Methylaniline (8.65 mL, 8.57 g, 80.0 mmol) was added slowly to a stirring solution of tetrachlorocyclopropene (3.55 g, 2.45 mL, 20.0 mmol) in DCM (100 mL) at 0 °C under an inert atmosphere. The reaction mixture was slowly warmed to room temperature and stirred for 2 hours. Sodium tetrafluoroborate (2.19 g, 20 mmol) was then added and stirred for 1 hour. The reaction mixture was decanted into a separating funnel and washed with water (3 × 40 mL), and the organic layer was dried under reduced pressure to yield the product tris(N-methylanilino)-cyclopropenium tetrafluoroborate **181** as brown crystals (6.24 g, 71%); δ_H (700 MHz, $CDCl_3$): 7.24 (6H, d, *J* = 8.2 Hz, *o*-Ar-*H*), 7.15 (6H, t, *J* = 7.8 Hz, *m*-Ar-*H*), 7.06 (3H, t, *J* = 7.5 Hz, *p*-Ar-*H*), 3.28 (9H, s, N-CH_3); δ_C (176 MHz, $CDCl_3$): 143.8, 129.5, 127.0, 122.9, 117.8, 42.2; m/z (ES+): 354 $[M-BF_4]^+$, HRMS (ES+): required for $C_{24}H_{24}N_3$ 354.1970, found 354.1956.

Bis(N-Methylanilino)cyclopropenone 149

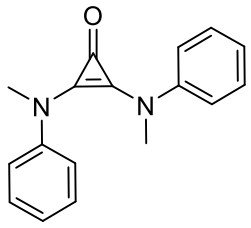

149

Tris(N-methylanilino)-cyclopropenium tetrafluoroborate **181** (6.62 g, 15.0 mmol) was dissolved in methanol (120 mL) and 0.3% aq. NaOH (250 mL) was added and stirred at room temperature for 4 days. Filtration of the precipitate and subsequent recrystallization from acetone gave white needles of the product bis(N-methylanilino)-cyclopropenone **149** (0.93 g, 23%); ν_{max} (cm^{-1}) : 3060, 2981, 1923, 1901, 1596, 1582, 1541, 1505, 1479; 1376, 1326, 1300, 1285, 1195, 1140, 1111, 1069, 1032, 1006, 992,

950, 886, 793, 773, 748, 716, 688, 673, 551, 532, 512, 462, 405, 384; δ_H (400 MHz, $CDCl_3$): 7.46 – 7.34 (8H, m, Ar-*H*), 7.11 (2H, t, *J* = 6.8 Hz, Ar-*H*), 3.47 (6H, s, N-C*H*$_3$); m/z (ES+): 265 $[M+H]^+$; HRMS (ES+): required for $C_{17}H_{16}N_2O$ 265.1341, found 265.1340.

1,2-Bis(N-Methylanilino)-3-chloro-cyclopropenium tetrafluoroborate 183

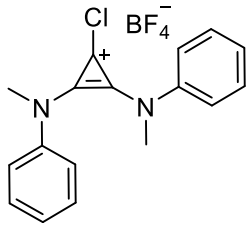

183

Bis(N-Methylanilino)-cyclopropenone 149 (0.80 g, 5.71 mmol) was placed in a dry flask under an inert atmosphere fitted with a stirrer bar and oxalyl chloride (10 mL) was added dropwise with stirring. The reaction mixture was concentrated under reduced pressure to yield the crude 1-chloro,2-3-bis(N-methylanilino)cyclopropenium chloride **182** (0.88 g, 4.50 mmol, 78%) as a sticky brown solid. The sticky brown solid was dissolved in acetonitrile and sodium tetrafluoroborate (0.49 g, 4.50 mmol) was added. The solution was filtered and the filtrate concentrated under reduced pressure to yield the product 1-chloro-2,3-bis(N-Methylanilino)-cyclopropenium tetrafluoroborate **183** (0.84 g, 76%) as a sticky pale brown solid, which was used directly in an impure state; m/z (ES+): 283 $[M-BF_4]^+$

Tris(dimethylamino)cyclopropenium tetrafluoroborate 174

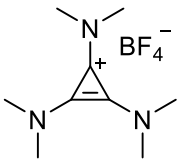

174

Tetrachlorocyclopropene (0.70 mL, 1.02 g, 5.75 mmol) was dissolved in acetonitrile (30 mL) under an inert atmosphere and stirred at 0 °C. Dimethylamine solution in water (5.6 M, 5 mL, 28 mmol) was slowly added and the mixture was stirred for 1 hour, before being allowed to warm to room temperature. Sodium tetrafluoroborate (0.63 g, 5.75 mmol) was then added and the reaction mixture stirred for 15 minutes. The solvent was then removed under reduced pressure, and the product collected from the residue using

dichloromethane, filtered, and concentrated under reduced pressure to give the product **174** as a light orange solid (0.45 g, 31 %); δ_H (400 MHz, $CDCl_3$): 3.10 (18H, s, C*H*$_3$), δ_C (100 MHz, $CDCl_3$): 118.3, 42.6; δ_F (377 MHz, $CDCl_3$) −154.2 (4F, s, B*F*$_4$); m/z (ESI+): 168 $[M-BF_4]^+$; HRMS (ESI+): $C_9H_{18}N_3$ requires: 168.1502; found: 168.1501.

Bis(dimethylamino)cyclopropenone 175

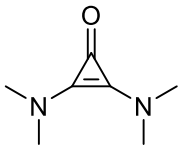

175

174 (0.45 g, 1.79 mmol) was dissolved in 15 % NaOH solution (50 mL) and heated to 70 °C for 1 hour. The resulting solution was cooled to room temperature, carefully neutralized using sodium bicarbonate, and decanted into a separating funnel. The aqueous phase was washed with DCM (3 × 50 mL) and the organic phases were combined, dried over Na_2SO_4 and evaporated under reduced pressure to yield **175** as a clear oil (0.11 g, 43 %); δ_H (400 MHz, $CDCl_3$): 2.98 (12H, s, N-C*H*$_3$), δ_C (50 MHz, $CDCl_3$): 134.0, 121.44, 41.6; m/z (ES+): 141 $[M+H]^+$; HRMS (ES+): $C_7H_{13}N_2O$ requires: 141.1028; found: 141.1021.

1,2-Bis(dimethylamino)-3-chloro-cyclopropenium tetrafluoroborate 177

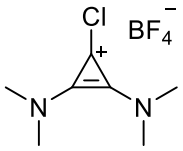

177

Cyclopropenone **175** (0.50 g, 0.87 mmol) was placed in a flask equipped with stirrer bar under an inert atmosphere and was cooled to 0 °C. Oxalyl chloride (7 mL, 10.5 g, 95 mmol) was then added dropwise. The solution was concentrated under reduced pressure to yield a crude solid. The solid was dissolved in acetonitrile, and sodium tetrafluoroborate (0.20 g, 1.82 mmol) was added and stirred for 30 minutes. The solution was concentrated under reduced pressure and DCM (10 mL) was added. The solution was filtered, and the solvent was evaporated under reduced pressure to yield the product **177** as a hygroscopic solid (0.85 g, 97 %); δ_H (400 MHz, $CDCl_3$): 3.36 (6H, s, N-C*H*$_3$), 3.28 (6H, s, N-C*H*$_3$); δ_C (100 MHz, $CDCl_3$): 134.9, 91.8, 43.0, 42.0; δ_F (377 MHz, $CDCl_3$) −154.6 (4F, s, B*F*$_4$); m/z (ESI+) 159 $[M^+-BF_4]$.

Bis(diethylamino)cyclopropenium tetraphenylborate 140

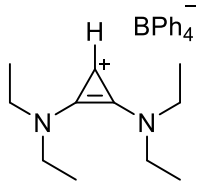

140

Sodium tetraphenylborate (2.73 g, 8.0 mmol) was suspended in dry DCM (100 mL) under an inert atmosphere in a flask fitted with a septum cap and stirrer bar and cooled to −78 °C. Tetrachlorocyclopropene (0.98 mL, 1.42 g, 8.0 mmol) was then added. Diethylamine (1.58 mL, 1.17 g, 16.0 mmol) was dissolved separately in DCM to a total volume of 50 mL and added slowly to the stirring tetrachlorocyclopropene solution over 45 minutes by means of a syringe pump. The reaction mixture was stirred for 1 hour at −78 °C before being slowly warmed to room temperature and stirred overnight. Triphenylphosphine (2.09 g, 8 mmol) was then added and the solution rapidly turned red, followed by water (100 mL) after which the diphasic mixture was stirred vigorously for 2 hours with exposure to air. The mixture was then decanted into a separating funnel and washed with water (2 x 100 mL) and brine (100 mL) before being dried over sodium sulfate and concentrated under reduced pressure to yield the crude product **140** as a red residue.

The red residue was then stirred in refluxing methanol (50 mL) and filtered to remove the insoluble component. Water was then slowly added to the stirring methanol solution until the solution became cloudy, and the solution was refrigerated at 5 °C to promote precipitation. The solution was then filtered to yield the product **140** as a yellow powder (0.18 g, 4.6 %); m.p. 128-130 °C (dec); CHN: (Found C 83.6, H 8.2, N 5.5, Required for $C_{35}H_{41}BN_2$: C 84.0, H 8.3, N 5.6); ν_{max} (cm^{-1}) : 3112, 3055, 2981, 1899, 1584, 1480, 1454, 1427, 1383, 1350, 1312, 1282, 1213, 1175, 1151, 1085, 1068, 1033, 1005, 962, 849, 789, 769, 732, 702, 626, 614, 605, 527, 479, 462, 397, 385; δ_H (700 MHz, $CDCl_3$): 7.50-7.42 (5H, m, Ar-*H*), 6.98 (10H, t, Ar-*H*), 6.85 (5H, tt, J = 7.2, 1.4 Hz, Ar-*H*), 4.30 (1H, s, Cp-*H*), 3.01 (4H, q, J = 7.3 Hz, N-CH_2), 3.00 (4H, q, J = 7.3 Hz, N-CH_2), 1.10 (6H, t, J = 7.3 Hz, N-CH_2-CH_3), 1.04 (6H, t, J = 7.3 Hz, N-CH_2-CH_3); δ_C (176 MHz, $CDCl_3$): 164.3 (q, J = 49.2 Hz), 136.1, 135.2, 125.7 (q, J = 2.7 Hz), 121.7, 98.3, 47.9, 46.7, 14.1, 12.8; m/z (ES+): 181 $[M-BPh_4]^+$; HRMS (ES+): $C_{11}H_{21}N_2$ requires: 181.1705; found: 181.1713.

Bis(diethylamino)cyclopropenium tetrafluoroborate 167

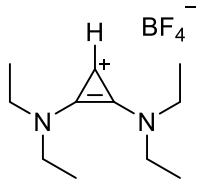

167

Diethylamine (1.58 mL, 1.17 g, 16.0 mmol) was dissolved in DCM (24 mL) and added dropwise over the course of 45 minutes by means of a syringe pump to a stirring solution of tetrachlorocyclopropene (0.98 mL, 1.42 g, 8 mmol) in DCM (100 mL) at −78°C. The resulting solution was stirred for 30 minutes then slowly warmed to room temperature over 2 hours. Sodium tetrafluoroborate (0.88 g, 8 mmol) was then added and stirred for 30 minutes. Triethyl phosphite (1.37 mL, 1.33 g, 8 mmol) was then added and the reaction mixture stirred overnight. The reaction was found to have not gone to completion (using LCMS) by morning so a second aliquot of triethyl phosphite (1 mL) was added and stirred for a further 2 hours. The reaction mixture was then decanted into a separating funnel and washed with water (2×100 mL) and brine (50 mL). The organic layer was collected, concentrated under reduced pressure, washed with Et_2O (2×50 mL) and dried under reduced pressure to yield a yellow oil containing intermediate **172**.

The yellow oil was dissolved in a solution of K_2CO_3 in water (0.2 M, 40 mL) and stirred at room temperature for 72 hours. The solution was decanted into a separating funnel and extracted with DCM (3 × 50 mL), dried over sodium sulfate and concentrated under reduced pressure to yield the crude product **167** (0.89 g)

The crude mixture was then purified by HPLC using a reverse phase Sunfire C18 19x100mm 5 µm column with an isocratic water:methanol (80:20) system at 10 mL/min with UV-Visible detector too give **167** as a brown ionic liquid (0.016 g, 0.4%); δ_H (400 MHz, $CDCl_3$) : 7.21 (1H, s, Cp-*H*), 3.62 (4H, q, J = 7.3 Hz, N-CH_2), 3.58 (4H, q, J = 7.3 Hz, N-CH_2), 1.38 (12H, q, J = 7.3 Hz, N-CH_2-CH_3); δ_C (100 MHz, $CDCl_3$): 136.6, 97.6, 48.4, 47.3, 14.1, 12.8; δ_F (167 MHz, $CDCl_3$): 153.35 (4F, s, BF_4); m/z (ESI+): $[M-BF_4]^+$ 181, HRMS (ESI+): $C_{11}H_{21}N_2$ requires: 181.1705 found 181.1707

1,2-Bis(diethylamino)-3-ethylphosphonato-cyclopropenium tetrafluoroborate 173

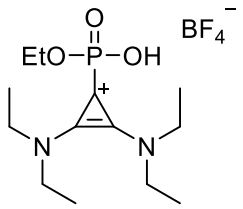

173

Tetrachlorocyclopropene (1.47 mL, 2.13 g, 12.0 mmol) was dissolved in DCM (100 mL) under an inert atmosphere and cooled to −78°C. Diethylamine (2.37 mL, 1.76 g, 24 mmol) was then added slowly while stirring vigorously. The reaction was then warmed slowly to room temperature and stirred overnight. Sodium tetrafluoroborate (1.31 g, 12 mmol) was then added and the reaction stirred for 15 minutes. Triethyl phosphite (2.05 mL, 1.99 g, 12 mmol) was then added and the reaction rapidly changed colour from clear to yellow. After stirring for 3 hours, water (100 mL) was added and the biphasic system stirred vigorously for another 3 hours. The two-phase mixture was decanted into a separating funnel and the organic layer was washed with water (3×50 mL) before being dried under reduced pressure to yield a yellow oil.

The yellow oil was then triturated using Et_2O (50 mL), and the ether was discarded. The yellow oil was then dissolved in aqueous sodium carbonate solution (0.1 M, 40 mL) and stirred overnight. DCM (3 × 50 mL) was then added and the chlorinated layer collected to yield an impure yellow oil of the product bis(diethylamino)cyclopropenium tetrafluoroborate mixed with a minor product of tris(diethylamino)cyclopropenium tetrafluoroborate.

The aqueous layer was decanted and dried under reduced pressure. DCM (50 mL) was then added, filtered and evaporated under reduced pressure to yield of 1,2-bis(diethylamino)-cyclopropenium-3-diethylphosphonate tetrafluoroborate as a brown ionic liquid **173** (0.14 g, 3%); δ_H (700 MHz, $CDCl_3$): 3.91 (2H, quintet, J =, 7.2 Hz P-O-CH_2), 3.66 (4H, q, J = 7.3 Hz, N-CH_2), 3.36 (4H, q, J = 7.3 Hz, N-CH_2), 1.27 (6H, t, J = 7.3 Hz, N-CH_2-CH_3), 1.20 (6H, t, J = 7.3 Hz, N-CH_2-CH_3), 1.17 (3H, J = 7.3 Hz, O-CH_2-CH_3); δ_C (167 MHz, $CDCl_3$): 137.0 (d, J = 4.9 Hz), 110.5 (d, J = 175.8 Hz), 60.8 (d, J = 6.0 Hz), 47.4, 47.3,16.8 (d, J = 6.9 Hz), 14.2, 13.3; δ_P (167 MHz, $CDCl_3$): −10.76 (1P, t J = 7.7 Hz); m/z (ES+) 289 $[M-BF_4]^+$; HRMS (ES+): $C_{13}H_{26}N_2O_3P$ requires: 289.1681; found: 289.1684.

Bis-1,2-(diisopropylamino)-3-chlorocylopropenium tetrafluoroborate 190

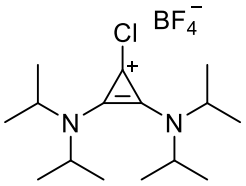

190

Diisopropylamine (1.34 mL, 0.97 g, 4.00 mmol) was added dropwise at 0 ºC to a stirred solution of tetrachlorocyclopropene (0.49 mL, 0.71 g, 4.00 mmol) in DCM (100 mL) under an inert atmosphere in a flask fitted with septum cap and stirrer bar. After 1 hour at 0 ºC, the solution was warmed to room temperature and sodium tetrafluoroborate (0.44 g, 4.00 mmol) was added. The solution was then decanted into a separating funnel and washed with water (3 × 100 mL). The chlorinated layer was collected, dried over Na_2SO_4 and concentrated under reduced pressure. The resulting residue was purified by recrystallization from DCM/Et_2O at −20 °C to yield the product **190** as white crystals (0.74 g, 51%) m.p 175-176 °C (dec.); CHN: (Found: C 50.3, H 7.8, N 7.7, Required for $C_{15}H_{28}N_2BF_4Cl$: C 50.2, H 7.9, N 7.8); ν_{max} (cm^{-1}) : 2983, 2941, 1928, 1582, 1453, 1425, 1375, 1350, 1208, 1182, 1140, 1094, 1043, 1025, 893, 789, 659, 749, 659, 573, 542, 518, 405, 388; δ_H (400 MHz, $CDCl_3$) : 4.15 (2H, sept, J = 6.7 Hz, N-C*H*), 3.87 (2H, sept, J = 6.7 Hz, N-C*H*), 1.43 (12H, J = 6.7 Hz, N-CH-CH_3), 1.42 (12H, J = 6.7 Hz, N-CH-CH_3); δ_C (100 MHz, $CDCl_3$) : 132.2, 93.2, 58.0, 48.3, 22.4, 20.6; δ_F (376 MHz, $CDCl_3$) −153.45 (4F, m, BF_4); m/z (ES+): 271 $[M-BF_4]^+$; HRMS (ES+): required for $C_{15}H_{29}N_2Cl$ 271.1941, found 271.1936.

Bis-1,2-(diisopropylamino)-3-iodocylopropenium iodide 196

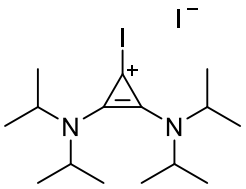

196

190 (0.19 g, 1.90 mmol) was dissolved in acetone (30 mL) and an excess of potassium iodide (0.75 g, 4.50 mmol) was added. The resulting suspension was stirred at room temperature overnight and the solution changed from clear to yellow. The solvent was removed under reduced pressure and the resulting solid was collected by washing first

in DCM (50 mL) and water (50 mL). The DCM layer was collected and washed with water (2 × 50 mL). The DCM layer was then collected, dried over Na_2SO_4 and the solvent removed under reduced pressure to yield the pure product bis-1,2-(diisopropylamino)-3-iodocylopropenium iodide **196** as a yellow solid (0.19 g, 74%), δ_H (400 MHz, $CDCl_3$) : 4.05 (2H, d, J = 6.8 Hz), 3.98 (2H, d, J = 6.8 Hz), 1.51 (12H, d, J = 6.8 Hz), 1.40 (12H, d, J = 6.8 Hz); δ_C (100 MHz, $CDCl_3$) 139.5, 56.99, 49.23, 22.50, 21.15; m/z (ES+): 363 $[M-I]^+$; HRMS (QToF+): $[M-I]^+$ $C_{15}H_{29}N_2I$ requires 363.2971 found 363.1303

The structure was confirmed by single crystal X-ray diffraction analysis (Appendix B)

Bis-1,2-(diisopropylamino)-3-iodocylopropenium tetrafluoroborate 197

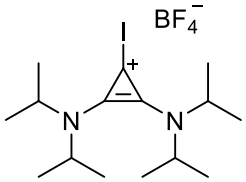

190 (0.70 g, 1.95 mmol) was dissolved in acetone (50 mL) and an excess of potassium iodide (2.5 g, 15 mmol) was added. The resulting suspension was stirred at room temperature overnight and the solution changed from clear to yellow. The solvent was removed under reduced pressure and the resulting solid was collected by washing first in DCM (50 mL) and water (50 mL). The DCM layer was collected and washed with water (2 × 50 mL), and then shaken vigorously with 1 M $NaBF_4$ solution (50 mL) and left to stand for 15 minutes. The DCM layer was collected, dried over Na_2SO_4 and the solvent removed under reduced pressure to yield the pure product bis-1,2-(diisopropylamino)-3-iodocylopropenium tetrafluoroborate **197** as an off-white solid (0.76 g, 87%) m.p. 165 (dec); CHN (Found C 38.7, H 6.0, N 6.0%, Required for $C_{15}H_{28}N_2BF_4I$ C 40.0, H 6.3, N 6.2%); ν_{max} (cm^{-1}) 2980, 1878, 1557, 1456, 1426, 1404, 1374, 1342, 1319, 1209, 1157, 1138, 1054, 1020, 889, 732, 636, 560, 533, 519, 417; δ_H (600 MHz, d_6-DMSO) : 4.19 (2H, septet, J = 6.7 Hz, N-C*H*), 3.95 (2H, septet, J = 6.7 Hz, N-C*H*), 1.35 (12H, d, J = 6.7 Hz, N-CH(CH_3)$_2$)), 1.27 (12H, d, J = 6.7 Hz, N-CH(CH_3)$_2$)); δ_C (151 MHz, d_6-DMSO) : 140.9, 57.9, 48.4, 22.7, 20.3; δ_F (376 MHz, $CDCl_3$) −153.87 (4F, m, BF_4); m/z (QToF+): 363 $[M-BF_4]^+$; HRMS (QToF+) $C_{15}H_{28}N_2I$ requires 363.1297, found 363.1311

6.2.1 Preparation of phosphonate cyclopropenium salts.

Bis-1,2-(diisopropylamino)-3-(diethylphosphonato)cyclopropenium tetrafluoroborate 191

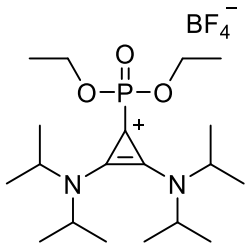

191

190 (0.57 g, 1.59 mmol) was placed in a round bottomed flask equipped with a stirrer bar and condenser and dissolved in THF (50 mL). Triethyl phosphite (1.76 mL, 1.70 g, 10.0 mmol) was added and the solution was refluxed overnight. A color change from clear to yellow was observed. The solvent was removed under reduced pressure and the resulting yellow residue was triturated with diethyl ether (30 mL), precipitating a white solid. The white solid was recrystallized from DCM/Et_2O at −20°C to yield the product bis(1,2-diisopropylamino)-3-(diethylphosphonato)-cyclopropenium tetrafluoroborate **191** as a white solid (0.35 g, 47%). m.p. 136-137 °C; CHN (found C 49.5, H 8.3, N 6.0, required for $C_{19}H_{38}N_2O_3PBF_4$ C 49.6, H 8.3, N 6.1) ν_{max} (cm^{-1}) : 2981, 1880, 1578, 1460, 1392, 1378, 1350, 1265, 1090, 1049, 998, 795, 670, 594, 508, 418; δ_H (700 MHz, $CDCl_3$) : 4.27 (4H, dq, J = 7.2, 3.5 Hz, P-O-C*H*$_2$), 4.17 (2H, septet, J = 6.8 Hz, N-C*H*), 3.96 (2H, septet, J = 6.8 Hz, N-C*H*), 1.46 (12H, d, J = 6.8 Hz, N-CH(C*H*$_3$)$_2$), 1.40 (12 H, d, J = 6.8 Hz, N-CH(C*H*$_3$)$_2$), 1.37 (6H, J = 7.2 Hz t, O-CH_2C*H*$_3$); δ_C (176 MHz, $CDCl_3$) : 136.5 (d, J =5.3 Hz), 94.7 (d, J = 231.6 Hz), 64.3 (d, J = 5.7 Hz), 57.6, 50.2, 20.6, 20.2, 16.1 (d, J = 7 Hz); δ_P (162 MHz, $CDCl_3$) : −3.70 (1P, quintet, J = 7.8 Hz); m/z (ES+) : 373 $[M-BF_4]^+$, HRMS (QToF+): $[M-BF_4]^+$ $C_{19}H_{38}N_2O_3P$ requires 373.2604 found 373.2600.

Bis-1,2-(diisopropylamino)-3-(diisopropylphosphonato)cyclopropenium tetrafluoroborate 193

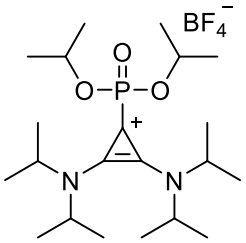

193

190 (0.25 g, 0.7 mmol) was placed in a 5 mL microwave vial with stirrer bar and seal and dissolved in acetonitrile (5 mL). Triisopropyl phosphite (0.13 mL, 0.29 g, 1.4 mmol) was then added and the mixture was heated by microwave at 80 °C for 1 hour. The reaction mixture was allowed to slowly cool to room temperature and transferred to a round bottomed flask. The solvent was removed under reduced pressure to yield a yellow residue. The mixture was recrystallized from DCM/Et_2O at −20 °C to yield the product bis-1,2-(diisopropylamino)-3-(diisopropylphosphonato)cyclopropenium tetrafluoroborate **193** as white crystals (0.24 g, 65%) m.p. 135-137 °C; CHN (found C 51.3, H 8.6, N 5.7 %, required for $C_{21}H_{42}N_2O_3PBF_4$ C 51.6, H 8.7, N 5.7 %) ν_{max} (cm^{-1}) 2981, 2942, 1886, 1572, 1464, 1350, 1378, 1259, 1151, 1051, 1035, 892, 771, 594, 473.1, 387.4; δ_H (600 MHz, $CDCl_3$) : 4.86 (2H, doubled septet, J = 7.0. 6.2 Hz, P-OC*H*), 4.21 (2H, septet, 6.9 Hz, N-C*H*), 3.99 (2H, septet, 6.8 Hz, N-C*H*), 1.48 (12H, d, J = 6.8 Hz, N-CH(CH_3)$_2$), 1.42 (12H, d, J = 6.8 Hz, N-CH(CH_3)$_2$), 1.40 (6H, d, J = 6.2 Hz, O-CH(CH_3)$_2$), 1.37 (6H, d, J = 6.2 Hz, O-CH(CH_3)$_2$); δ_C (151 MHz, $CDCl_3$) : 135.9 (d, J = 5.4 Hz), 95.9 (d, J = 233.1 Hz), 74.4 (d, J = 6.0 Hz), 57.6, 50.2, 24.0 (d, J = 4.1 Hz), 23.8 (d, J = 5.5 Hz), 20.7, 20.3; δ_P (243 MHz, $CDCl_3$) −6.15 (1P, t, J = 7.5 Hz); m/z (ES+) : 401; HRMS (QToF+) : $[M-BF_4]^+$ $C_{21}H_{42}N_2O_3P$ requires 401.2933, found 401.2931

Bis-1,2-(diisopropylamino)-3-(dimethylphosphonato)cyclopropenium tetrafluoroborate 192

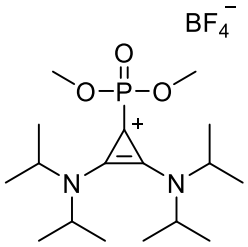

192

190 (0.20 g, 0.6 mmol) was placed in a 5 mL microwave vial with stirrer bar and seal and dissolved in acetonitrile (5 mL). Trimethyl phosphite (0.34 mL, 0.14 g, 1.2 mmol) was then added and the mixture was heated by microwave at 80 °C for 1 hour. The reaction mixture was allowed to slowly cool to room temperature and transferred to a round bottomed flask. The solvent was removed under reduced pressure to yield a yellow residue. The mixture was recrystallized from DCM/Et_2O at −20 °C to yield the product bis-1,2-(diisopropylamino)-3-(diisopropylphosphonato)cyclopropenium tetrafluoroborate **192** as a white solid (0.16 g, 63%) m.p. 173-175 °C; CHN (found C 46.6, H 7.8, N 6.4, required for $C_{17}H_{34}N_2O_3PBF_4$ C 47.2, H 7.9, N 6.5 %); ν_{max} (cm^{-1}): 2982, 1883, 1582, 1462, 1392, 1379, 1355, 1271, 1210, 1182, 1153, 1093, 1048, 1036, 1005, 893, 839, 800, 671, 593, 549, 506, 460, 421, 399; δ_H (600 MHz, $CDCl_3$) : 4.18 (2H, septet, J = 6.8 Hz N-C*H*), 3.96 (2H, septet, J = 6.9 Hz, N-C*H*), 3.91 (6H, d, J = 11.9 Hz, P-O-CH_3) 1.47 (12H, d, J = 6.9 Hz, N-CH(CH_3)$_2$), 1.42 (12H, d, J = 6.9 Hz, N-CH(CH_3)$_2$); δ_C (151 MHz, $CDCl_3$): 136.8, 93.7 (d, J = 233.5 Hz), 57.7, 54.1 (d, J = 5.5 Hz), 50.3, 20.6, 20.1; δ_P (243 MHz, $CDCl_3$) : −0.92 (1P, septet, J = 11.9 Hz); m/z (ES+): 345 $[M-BF_4]^+$; HRMS (QToF+): $[M-BF_4]^+$ $C_{17}H_{34}N_2O_3P$ requires 345.2307, found 345.2316.

6.3 Synthetic procedures for Chapter 4

4-(2-formyl-phenoxy)-but-2-eneoyl ethyl ester

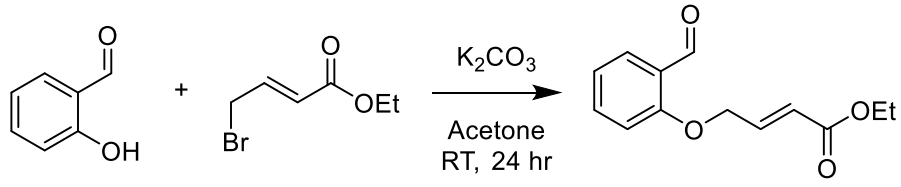

239

Ethyl 4-bromocrotonate (8.11 g, 5.80 mL, 42 mmol) was added to a stirring mixture of salicylaldehyde (4.89 g, 4.26 mL, 40 mmol) and potassium carbonate (8.29g, 60 mmol) in acetone (75 mL) and stirred overnight. The reaction was then quenched with water and the organic layer extracted with diethyl ether. The organic layer was then washed with 5% NaOH and water followed by brine, dried over Na_2SO_4 and concentrated under reduced pressure. The crude mixture underwent column chromatography (4:1 Hexane:EtOAc) to yield an impure mixture. This solid was subsequently recrystallized from cold ethyl acetate to yield the 4-(2-formyl-phenoxy)-but-2-eneoyl ethyl ester **239** as a white solid (0.45 g, 5 %); m.p 68 °C; CHN (found C 66.4, H 6.0, required for $C_{13}H_{14}O_4$ C 66.6, H 6.0); ν_{max} (cm^{-1}): 2981, 2869, 1712, 1684, 1666, 1598, 1483, 1461, 1438, 1402, 1383, 1366, 1301, 1288, 1273, 1247, 1183, 1157, 1109, 1075, 1039, 1023, 970, 946, 871, 850, 838, 820, 766, 683, 661, 615, 532, 468, 442, 385; δ_H (400 MHz, $CDCl_3$) 10.58 (1H, d, J = 0.8 Hz, O=C-*H*), 7.89 (1H, dd, J = 7.8, 1.8 Hz, Ar-*H*),7.57 (1H, ddd, J = 8.4, 7.3, 1.8 Hz, Ar-H), 7.18-7.06 (2H, m,), 6.97 (1H, dd, J =8.5, 0.9 Hz,) 6.24 (dt, J = 15.8, 2.1 Hz), 4.86 (2H, J = 4.0, 2.1 Hz) 4.25 (2H, q, J = 7.1 Hz, O=C-O-C*H*$_2$), 1.33 (3H, t, J = 7.1 Hz, O-CH_2-C*H*$_3$); δ_C (101 MHz, $CDCl_3$): 189.3, 165.8, 160.2, 141.2, 135.9, 128.9, 125.2, 122.6, 121.5, 112.5, 77.4, 77.0, 76.7, 66.9, 60.8, 14.2. m/z (ESI+) 235 $[M+H]^+$, (ESI−), 233 $[M-H]^-$

X-ray crystallography confirmed the structure identical to previous crystallizations of x. (FOHCUB)

6.3.1 Preparation of hydroxy-aryl adducts.

Preparation of 1-hydroxybenzyl-2,3-bis(diisopropylamino)cyclopropenium tetrafluoroborate 255

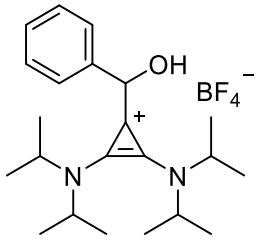

255

163 (1.16 g, 3.6 mmol) was placed in a dry round bottomed flask (50 mL) equipped with septum and stirrer bar and placed under an inert atmosphere. Dry dichloromethane (30 mL) was then added by cannula and the mixture cooled to 0 °C. Benzaldehyde (1.84

mL, 1.91 g, 18 mmol) was added and stirred, followed by DBU (0.65 mL, 0.66 g, 4.3 mmol). The reaction was stirred for 1 hour and a rapid colour change from clear to yellow followed by a slower change to green were observed. An aqueous HCl solution (1M, 1 mL) was added to quench the solution and the mixture was stirred for 10 minutes at room temperature. The mixture was decanted into a separating funnel, diluted to 50 mL DCM and washed with aqueous HCl solution (1M, 30 mL), followed by water (2 × 30 mL) and brine (30 mL). The organic phase was collected, dried over Na_2SO_4, filtered and concentrated under reduced pressure to yield a yellow oil. Hexane was slowly added to triturate a white solid of crude product. The product was purified by recrystallization from DCM:Et_2O and filtered to yield the pure product **255** (0.84 g, 54%) as a white solid. m.p. 195 °C; CHN (found C 61.4, H 8.2, N 6.5, required for $C_{23}H_{37}N_2OBF_4$ C 61.4, H 8.2, N 6.5 %); ν_{max} (cm^{-1}) : 3438, 2982, 1909, 1558, 1396, 1375, 1338, 1213, 1043, 1023, 929, 916, 749, 734, 517; δ_H (600 MHz, $CDCl_3$) 7.40-7.29 (5H, m, Ar-*H*), 6.03 (1H, s, *H*COH), 4.04 (2H, septet, J = 6.8 Hz, N-C*H*), 3.93 (2H, septet, J = 6.8 Hz, N-C*H*), 1.37 (6H, d, J = 6.8 Hz, N-CH(CH_3)$_2$) 1.33 (6H, d, J = 6.8 Hz, N-CH(CH_3)$_2$), 1.31 (6H, d, J = 6.8 Hz, N-CH(CH_3)$_2$), 1.20 (6H, d, J = 6.8 Hz, N-CH(CH_3)$_2$); δ_C (151 MHz, $CDCl_3$) : 137.70, 132.6, 128.9, 128.8, 126.7, 111.24, 99.2, 68.0, 53.4, 51.3, 21.3, 21.2, 21.1, 21.0; m/z (ES+) : 343 $[M-BF_4]^+$; HRMS (QToF+) : $[M-BF_4]^+$ $C_{22}H_{35}N_2O$ requires 343.2749, found 343.2744.

Preparation of 1-(4-fluorohydroxybenzyl)-2,3-bis(diisopropylamino)cyclopropenium tetrafluoroborate 263

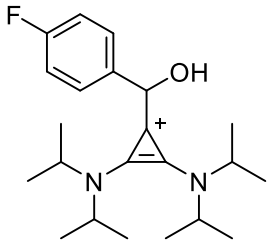

263

Bis(diisopropylamino)cyclopropenium tetrafluoroborate **163** (0.65 g, 2.00 mmol) was dissolved in DCM (40 mL) under an inert atmosphere at room temperature and 4-fluorobenzaldehyde (0.25 g, 0.21 mL, 2.00 mmol) was added. DBU (0.36 mL, 0.37 g, 2.40 mmol) was then added and the solution stirred for 2 hours. Aqueous HCl (20 mL, 0.1M) was then added to quench the DBU. The mixture was washed with water (2×30 mL) and brine (30 mL) and the chlorinated layers collected. The chlorinated layer was

dried under reduced pressure and triturated with diethyl ether. The crude mixture was then recrystallized from DCM/Et_2O to give the product **263** as an off-white solid (0.40 g, 41%) m.p. 138 °C (dec); CHN (found C 58.4 , H 7.6, N 6.2, required for $C_{22}H_{34}N_2O_2BF_5$ C 58.9, H 7.6, N 6.2 %); ν_{max} (cm^{-1}): 3453, 2985, 1888, 1567, 1414, 1351, 1183, 1118, 1049, 1035, 687, 550, 417; δ_H (600 MHz, $CDCl_3$) 7.35, (2H, dd, J = 8.6, 5.3 Hz, Ar-*H*), 7.07 (2H, t, J = 8.6 Hz, Ar-*H*), 6.03 (1H, s, HO-C*H*), 5.00 (1H, br, HC-O*H*), 4.04 (2H, septet, J = 6.8 Hz, N-C*H*), 3.96 (2H, septet, J = 6.8 Hz, N-C*H*), 1.38 (6H, d, J = 6.8 Hz, N-CH(CH_3)$_2$), 1.35 (6H, d, J = 6.8 Hz, N-CH(CH_3)$_2$), 1.33 (6H, d, J = 6.8 Hz, N-CH(CH_3)$_2$), 1.21 (6H, d, J = 6.8 Hz, N-CH(CH_3)$_2$); δ_C (151 MHz, $CDCl_3$) 163.44, 162.03, 133.62 (d, J = 3.3 Hz), 128.62 (d, J = 8.3 Hz), 115.90 (d, J = 21.8 Hz) 110.84, 67.43, 55.45, 51.25, 21.26, 21.04; δ_F (376 MHz, $CDCl_3$) −112.62 (1F, tt, J = 8.4, 5.2 Hz, Ar-*F*), −152.25 (4F, s, BF_4); m/z (ES+): 361 $[M-BF_4]^+$; HRMS (QToF+) $C_{22}H_{34}N_2OF$ found 361.2652, required 361.2655.

Preparation of 1-(4-methoxyhydroxybenzyl)-2,3-bis(diisopropylamino)cyclopropenium tetrafluoroborate 264

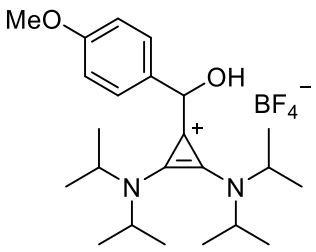

163 (0.10 g 0.30 mmol) was placed in a 25 mL round bottomed flask equipped with stirrer bar and septum and placed in an inert atmosphere. 4-Methoxybenzaldehyde (1.0 mL, 1.14g, 8.40 mmol) was added followed by DBU (0.13 mL, 0.13 g, 0.87 mmol). The reaction mixture was stirred for 30 minutes at room temperature and aqueous HCl (0.1 M, 2 mL) was added to quench the reaction. The mixture was stirred for 5 minutes, decanted into DCM (30 mL) and washed with aqueous HCl (1M, 30 mL), water (2 × 30 mL) and brine (30 mL). The organic layer was collected, dried over Na_2SO_4 and concentrated under reduced pressure to give an orange oil. The oil was triturated by slow addition of Et_2O to yield the pure product **264** as an orange solid (0.092 g, 72%). m.p. 148-152 °C; CHN (found C 59.6, H 8.1, N 6.1, required for $C_{23}H_{37}N_2O_2BF_4$ C 60.0, H 8.1, N 6.1 %); ν_{max} (cm^{-1}) : 3443, 2981, 2943, 1895 1603, 1557, 1462, 1349, 1235, 1209, 1074, 987, 867, 761, 501, 485; δ_H (700 MHz, $CDCl_3$) : 7.30-7.24 (2H, m,

Ar-*H*), 6.93-6.88 (2H, m, Ar-*H*), 5.99 (1H, d, J = 1.5 Hz, *H*COH), 4.84 (1H, d, J =3.2 Hz, 1H), 4.05 (2H, septet, J = 6.9 Hz, N-C*H*), 4.02-3.97 (2H, m, N-C*H*), 3.80 (3H, s, O-CH_3), 1.39 (6H, d, J = 6.8 Hz, N-CH(CH_3)$_2$), 1.36 (6H, d, J = 6.8 Hz, N-CH(CH_3)$_2$), 1.34 (6H, d, J = 6.9 Hz, N-CH(CH_3)$_2$), 1.21 (6H, d, J = 6.8 Hz, N-CH(CH_3)$_2$); δ_C (176 MHz, $CDCl_3$) : 159.9, 132.5, 129.7, 128.2, 114.3, 111.8, 68.0, 55.3, 21.3, 21.1; m/z (QToF+) 375 $[M-BF_4]^+$; HRMS (QToF+) $C_{23}H_{37}N_2O_2$ requires 373.2855, found 373.2851.

Preparation of 1-(2-methoxy-hydroxybenzyl)-2,3-bis(diisopropylamino)cyclopropenium tetrafluoroborate 265

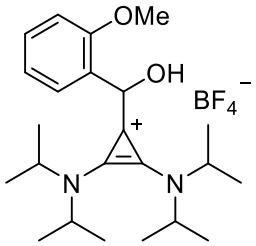

163 (0.11 g, 0.35 mmol) and 2-methoxybenzaldehyde (1.10 g, 10.5 mmol) were placed in a 25 mL round bottomed flask equipped with stirrer bar and septum and placed under an inert atmosphere. DCM (2 mL) was then added followed by DBU (0.15 mL, 0.15 g, 1.0 mmol). The reaction was stirred for 30 minutes at room temperature and 2 mL aqueous HCl (0.1 M) was added to quench the reaction. The mixture was stirred for 5 minutes, decanted into DCM (30 mL) and washed with aqueous HCl (1 M, 30 mL), water (2 × 30 mL) and brine (30 mL). The organic layer was collected, dried over Na_2SO_4 and concentrated under reduced pressure to give a yellow oil. Et_2O was added to the oil to precipitate the crude product, which was purified by recrystallization from DCM:Et_2O to yield the pure product **265** as an off-white solid (0.11 g, 71%). m.p. : 142-146 °C; CHN (found C 59.9, H 8.0, N 6.0, required for $C_{23}H_{37}N_2O_2BF_4$ C 60.0, H 8.1, N 6.1 %); ν_{max} (cm^{-1}) : 3443, 2981, 2844, 1895, 1557, 1462, 1350, 1235, 1074, 985, 908, 761, 639, 518 485; δ_H (700 MHz, $CDCl_3$) 7.58 (1H, dd, J = 7.6, 1.7 Hz, Ar-*H*), 7.31 (1H, td, J = 7.8, 1.7 Hz Ar-*H*), 7.02 (1H, td, J = 7.6, 1.0 Hz, Ar-*H*), 6.88 (1H, dd, J = 8.3 Hz, 1.0 Hz, Ar-*H*), 6.14 (1H, s, *H*COH), 4.68 (1H, br s, O*H*), 4.02 (2H, septet, J = 6.9 Hz, N-C*H*), 3.85 (2H, septet, J = 6.8 Hz, N-C*H*), 3.79 (3H, s, O-CH_3), 1.36 (6H, d, J = 6.9 Hz, N-CH(CH_3)$_2$), 1.33 (6H, d, J = 6.9 Hz, N-CH(CH_3)$_2$), 1.24 (6H, d, J = 6.9 Hz, N-CH(CH_3)$_2$), 1.22 (6H, d, J = 6.9 Hz, N-CH(CH_3)$_2$); δ_C (176 MHz, $CDCl_3$) : 156.1, 132.3, 129.9, 127.9, 121.0, 111.0, 62.6, 55.5, 53.5, 50.9, 21.2, 21.0, 20.8, 20.7; m/z

(QToF+): 375 $[M-BF_4]^+$; HRMS (QToF+): $C_{23}H_{37}N_2O_2$ requires 373.2855, found 373.2858

Preparation of 1-hydroxyethyl-2,3-bis(diisopropylamino)cyclopropenium tetrafluoroborate 267

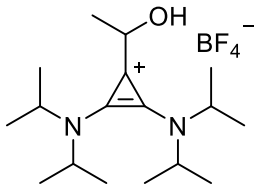

163 (0.32 g, 1.0 mmol) was placed in a 50 mL round bottomed flask equipped with stirrer bar and septum under an inert atmosphere. DCM (50 mL) was added, along with acetaldehyde (2.81 mL, 2.20 g, 50 mmol) and DBU (0.18 mL, 0.18 g, 1.20 mmol). The solution was stirred at room temperature for 2 hours. The mixture was washed with water (2×50 mL) and brine (50 mL) and the chlorinated layers collected. Aqueous HCl (20 mL, 0.1 M) was then added to quench the reaction and the mixture was stirred for 5 minutes. The chlorinated layer was dried under reduced pressure to yield the pure product **267** as a brown solid (0.20 g, 54%); CHN (found C 58.1 H 9.4, N 7.9, required for $C_{17}H_{33}N_2OBF_4$ C 55.5, H 8.4, N 7.6 %); ν_{max} (cm^{-1}) : 3129 (br.), 2980, 1904, 1550, 1455, 1375, 1353, 1209, 1188, 1141, 1115, 1049, 1032, 915, 890, 767, 674, 619, 564, 520, 454, 405, 389; δ_H (600MHz, $CDCl_3$): 5.50 (s, 1H, O-*H*), 5.11, (1H, q, J = 6.8 Hz. *H*C-OH), 3.98 (4H, sept, 7.1 Hz, N-C*H*), 1.47 (3H, d, J = 6.8 Hz, (HO)CH-CH_3), 1.42 (6H, d, J = 6.8 Hz, N-CH-CH_3), 1.35 (6H, d, J = 6.8 Hz, N-CH-CH_3), 1.33 (6H, d, J = 6.8 Hz, N-CH-CH_3); δ_C (151 MHz, $CDCl_3$): 131.9, 114.2, 61.9, 53.4 50.9, 21.3, 21.1, 20.1, 20.9; m/z (ESI+) : 281 $[M-BF_4]^+$; HRMS (ES+): $C_{17}H_{33}N_2O$ requires: 281.2593; found: 281.2584.

6.3.2 Alkylation of Hydroxy-aryl Adducts

Preparation of 1-methoxybenzyl-2,3-bis(diisopropylamino)cyclopropenium tetrafluoroborate.

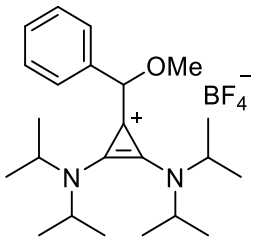

255 (0.23 g, 0.54 mmol), was placed in a round bottomed flask and dissolved in a methanol:H_2SO_4 mixture (80:20 v/v, 60 mL). The solution was heated to reflux and stirred for 4 days. Reaction progress was monitored by LCMS. The reaction was then allowed to cool to room temperature and decanted into water (100 mL). The mixture was neutralised by slow addition of $NaHCO_3$ (~20 g) and solvent removed under reduced pressure at 60 °C. The residue was redissolved in water (250 mL) and DCM (250 mL) to make a biphasic mixture. The mixture was separated and the water phase washed with DCM (3 × 100 mL). The organic phases were combined and washed with brine (100 mL) and the organic phase concentrated under reduced pressure to give an orange liquid. The liquid was dissolved in water (50 mL) and sodium tetrafluoroborate (1 g) was added and left to stand for 15 minutes. The solution was then washed with DCM (3 × 50 mL) and the organic phases were combined, dried over Na_2SO_4, concentrated under reduced pressure and dried under high vacuum overnight to yield the pure product **269** as a white solid (0.16 g, 64%). m.p. 150 °C (dec); CHN (found C 61.6, H 8.2, N 6.1, required for $C_{23}H_{37}N_2OBF_4$ C 62.2, H 8.4, N 6.3) ν_{max} (cm^{-1}) : 2982, 2934, 2822, 1903, 1562, 1449, 1316, 1139, 1048, 1035, 1000, 912, 881, 700, 653, 585, 519, 399; δ_H (700 MHz, $CDCl_3$): 7.44-7.40 (2H, m, Ar-H), 7.40-7.34 (2H, m, Ar-H), 5.44 (1H, s, *H*C-OCH_3), 4.06 (2H, septet, J= 6.8 Hz, N-C*H*), 3.80-3.65 (2H, m, N-C*H*), 3.38 (3H, s, O-CH_3), 1.36 (6H, d, J = 6.8 Hz, N-CH(CH_3)$_2$), 1.35 (6H, d, J = 6.8 Hz, N-CH(CH_3)$_2$), 1.23 (6H, d, J = 6.8 Hz, N-CH(CH_3)$_2$), 1.15 (6H, d, J = 6.8 Hz, N-CH(CH_3)$_2$); δ_C (176 MHz, $CDCl_3$) : 136.8, 132.9, 129.5, 129.2, 127.9, 108.8, 77.8, 57.1, 54.4, 50.7, 21.1, 21.1, 21.0, 20.7; m/z (QToF+) 357 $[M-BF_4]^+$; HRMS (QToF+) : $[M-BF_4]^+$ required for $C_{23}H_{37}N_2O$ requires 357.2906, found 357.2909.

Preparation of 1-(4-fluoromethoxybenzyl)-2,3-bis(diisopropylamino)cyclopropenium tetrafluoroborate 272

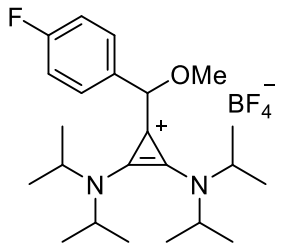

272

4-Fluorophenyl adduct **263** (0.10 g, 0.22 mmol) was placed in a round bottomed flask and dissolved in a methanol:H_2SO_4 mixture (80:20 v/v, 30 mL). The solution was heated to reflux and stirred for 8 days. Reaction progress was monitored by LCMS. The reaction was then allowed to cool to room temperature and decanted into water (100 mL). The mixture was neutralised by slow addition of $NaHCO_3$ (~10 g) and solvent removed under reduced pressure at 60 °C. The mixture was separated and the water phase washed with DCM (3 × 100 mL) and the organic phases were combined and washed with brine (100 mL). The organic phase was concentrated under reduced pressure to give a brown ionic liquid. The ionic liquid was dissolved in water (50 mL) and sodium tetrafluoroborate (1 g) was added and left to stand for 15 minutes. The solution was then washed with DCM (3 × 50 mL) and the organic phases were combined, dried over Na_2SO_4, concentrated under reduced pressure and dried under high vacuum overnight to yield the pure product **272** as an orange solid (0.065 g, 63%); m.p. 166 (dec); CHN (found C 59.8, H 7.8, N 5.9, required for $C_{23}H_{36}N_2OBF_5$ C 59.8, H 7.8, N 6.00); ν_{max} (cm^{-1}) : 2982, 1908, 1602, 1562, 1507, 1456, 1377, 1353, 1310, 1283, 1217, 1183, 1164, 1138, 1083, 1047, 1035, 1008, 976, 956, 915, 882, 853, 821, 797, 735, 624, 601, 554, 519, 423, 398; δ_H (600 MHz, $CDCl_3$) : 7.46-7.39 (2H, m, Ar-*H*), 7.12 (2H, t, J = 2.8 Hz, Ar-*H*), 5.48 (1H, s, *H*C-O-CH_3), 4.07 (2H, septet, J = 6.9 Hz, N-C*H*), 3.70 (2H, septet, J = 6.9 Hz, N-C*H*), 3.38 (3H, s, O-CH_3), 1.39-1.34 (12H, m, N-CH(CH_3)$_2$), 1.23 (6H, d, J = 6.9 Hz, N-CH(CH_3)$_2$), 1.18 (6H, d, J = 6.9 Hz, N-CH(CH_3)$_2$); δ_C (151 MHz, $CDCl_3$) : 163.1 (d, J = 249.2 Hz), 133.2, 131.8 (d, J = 3.3 Hz), 129.9 (d, J = 8.4 Hz), 116.2 (d, J = 21.7 Hz), 108.4, 57.1, 54.5, 50.6, 21.1, 21.0, 20.7; m/z (ES+) : 375 $[M-BF_4]^+$; HRMS (QToF+) : $C_{23}H_{36}N_2OF$ requires 375.2812, found 375.2813.

Preparation of 1-(4-methoxymethoxybenzyl-2,3-bis(diisopropylamino)cyclopropenium tetrafluoroborate 273

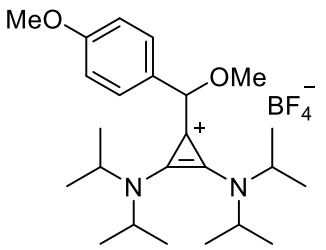

273

4-Methoxyphenyl adduct **264** (0.05 g, 0.11 mmol) was placed in a round bottomed flask and dissolved in a methanol:H_2SO_4 mixture (80:20 v/v) (40 mL). The solution was heated to reflux and stirred for 3 days. Reaction progress was monitored by LCMS. The reaction was then allowed to cool to room temperature and decanted into water (100 mL). The mixture was neutralised by slow addition of $NaHCO_3$ (~13 g) and solvent removed under reduced pressure at 60 °C. The mixture was separated and the water phase washed with DCM (3 × 100 mL) and the organic phases were combined and washed with brine (100 mL) and the organic phase concentrated under reduced pressure to give a brown ionic liquid. The ionic liquid was dissolved in water (50 mL) and sodium tetrafluoroborate (1 g) was added and left to stand for 15 minutes. The solution was then washed with DCM (3 × 50 mL) and the organic phases were combined, dried over Na_2SO_4, concentrated under reduced pressure and dried under high vacuum overnight to yield the pure product 273 as a hygroscopic brown solid (0.044 g, 85%); m.p. 148-152 °C (dec); CHN (found C 61.3, H 8.2, N 6.0 %, required for $C_{24}H_{39}N_2O_2BF_4$ C 60.8 H 8.3, N 5.9 %); ν_{max} (cm^{-1}) 2989, 2937, 1905, 1609, 1553, 1511, 1456, 1393, 1376, 1353, 1306, 1251, 1210, 1179, 1153, 1084, 1049, 1033, 975, 915, 881, 822, 797, 783, 734, 624, 600, 556, 520, 423, 399; δ_H (700 MHz, $CDCl_3$): 7.35-7.30 (2H, m, Ar-*H***)**, 6.96-6.92 (2H, m, Ar-*H*), 5.48 (1H, s, *H*COH), 4.11 (2H, septet, J = 6.6 Hz, N-C*H*), 3.81 (3H, s, Ar-O-CH_3), 3.79 (2H, m, N-C*H*), 3.36 (3H, s, C-O-CH_3), 1.42-1.32 (12H, m, N-CH(CH_3)$_2$), 1.27 (6H, d, J = 6.8 Hz, N-CH(CH_3)$_2$)), 1.17 (6H, d, J = 6.8 Hz, N-CH(CH_3)$_2$); δ_C (176 MHz, $CDCl_3$): 160.4, 132.8, 129.4, 127.6, 114.6, 109.3, 77.6, 56.8, 55.4, 54.5, 50.6, 21.2, 21.2, 21.1, 20.8; m/z (QToF+): 387 $[M-BF_4]^+$; HRMS (QToF+) : $[M-BF_4]^+$ $C_{24}H_{39}N_2O_2$ requires 387.3012, found 387.3033.

Preparation of 1-(2-methoxy-methoxybenzyl)-2,3-bis(diisopropylamino)cyclopropenium tetrafluoroborate 274

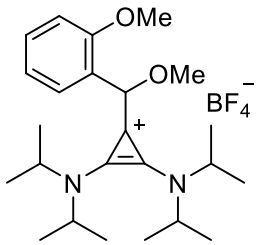

274

2-Methoxyphenyl adduct **265** (0.10 g, 0.22 mmol) was placed in a round bottomed flask and dissolved in a methanol:H_2SO_4 mixture (80:20 v/v, 40 mL). The solution was heated to reflux and stirred for 3 days. Reaction progress was monitored by LCMS. The reaction was then allowed to cool to room temperature and decanted into water (100 mL). The mixture was neutralised by slow addition of $NaHCO_3$ (~13 g) and solvent removed under reduced pressure at 60 °C. The mixture was separated and the water phase washed with DCM (3 × 100 mL). The organic phases were combined and washed with brine (100 mL) then concentrated under reduced pressure to give a white residue. The residue was dissolved in water (50 mL) and sodium tetrafluoroborate (1 g) was added and left to stand for 15 minutes. The solution was then washed with DCM (3 × 50 mL) and the organic phases were combined, dried over Na_2SO_4, concentrated under reduced pressure and dried under high vacuum overnight to yield the pure product **274** as a white solid (0.098 g, 95%); m.p. 148-152 °C; CHN (found C 61.0, H 8.3, N 5.8, required for $C_{24}H_{39}N_2O_2BF_4$ C 60.8 H 8.3, N 5.9) ν_{max} (cm^{-1}) 2980, 1912, 1602, 1549, 1495, 1456, 1377, 1357, 1319, 1299, 1252, 1188, 1154, 1120, 1093, 1047, 1036, 1021, 968, 951, 924, 894, 844, 762, 659, 626, 572, 560, 520, 398; δ_H (700 MHz, $CDCl_3$) : 7.35 (1H, ddd, J = 8.3, 7.4, 1.8 Hz, Ar-*H*), 7.32 (1H, dd, J = 7.6, 1.7 Hz, Ar-*H*), 7.02 (1H, td, J = 7.5, 1.0 Hz, Ar-*H*), 6.94 (1H, dd, J = 8.3, 1.0 Hz, Ar-*H*), 5.66 (1H, s, *H*C-OCH_3), 4.07 (2H, septet, J = 6.9 Hz, N-C*H*), 3.81 (3H, s, C-O-CH_3), 3.79 (2H, m, N-C*H*), 3.39 (2H, s, Ar-O-CH_3), 1.35 (12H, t, J = 6.5 Hz, N-CH(CH_3)$_2$), 1.19 (6H, d, J = 6.8 Hz, N-CH(CH_3)$_2$), 1.15 (6H, d, J = 6.9 Hz, N-CH(CH_3)$_2$); δ_C (176 MHz, $CDCl_3$) : 157.0, 132.2, 131.0, 128.5, 123.2, 121.1, 111.2, 109.1, 72.2, 57.5, 55.7, 54.8, 50.3, 21.1, 21.1, 20.8, 20.6; m/z (QToF+) : 387 $[M-BF_4]^+$; HRMS (QToF+): $[M-BF_4]^+$ $C_{24}H_{39}N_2O_2$ requires 387.3012, found 387.3006.

6.4 Synthetic procedures for Chapter 5

6.4.1 Optimized Synthetic Procedures

Optimized method for conversion of Nitron 2 to C(3)-amido Blatter-type radical 313

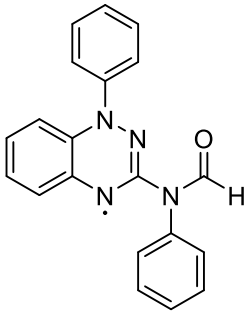

Nitron **127** (0.99 g, 16 mmol) was dissolved in acetonitrile (99 mL) along with 1% water (1 mL) and stirred with exposure to air for 72 hours. The solution was then dried *in vacuo* to give crude black crystals. Column chromatographic purification of the crude black crystals (98:2 DCM:MeOH), where the major product **313** eluted as a dark red fraction, followed by concentration under reduced pressure, yielded a black solid. The solid was then recrystallized from minimum hot ethanol to yield amido radical **313** as black crystals (0.85 g, 82%). m.p. 143-145 °C; CHN: (found: C 73.2, H 4.6, N 17.1, required for $C_{20}H_{15}N_4O$ C 73.4, H 4.6, N 17.1 %); λ_{max}(MeCN) nm (ε dm^3 mol^{-1} cm^{-1}): 560 (925), 533 (923), 471 (934), 370 (5006), 320 (6998), 254 (34189); ν_{max} (cm^{-1}): 3070, 2925, 1681, 1586, 1483, 1370, 1204, 1077, 841, 760, 692, 612, 552, 495 cm^{-1}; m/z (ES+): 327 $[M]^+$. HRMS (ES+): $C_{20}H_{15}N_4O$ requires: 327.1246; found: 327.1252.

Preparation of amino radical 315 by hydroxide-promoted hydrolysis

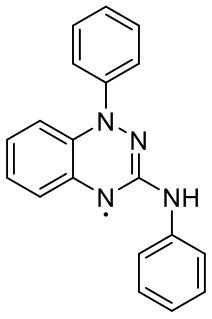

Radical **127** (0.39 g, 1.19 mmol) was dissolved in a 1 M NaOH solution in 50:50 H_2O:MeOH (40 mL) and stirred for 72 hours. The solvent was removed under reduced pressure and the green residue dissolved in DCM (100 mL), washed with 1 M HCl (1 x

50 mL), sat. $NaHCO_3$(aq) (1 x 50 mL), water (3 x 50 mL) and brine (1 x 50 mL). The organic layer was dried over Na_2SO_4, filtered and dried *in vacuo*. The residue was dissolved in the minimum volume of DCM and purified by column chromatography (98:2 DCM:MeOH). The product containing fractions were collected and dried *in vacuo* to give radical **315** (0.25 g, 70 %); m.p. 151-154 °C; λ_{max}(MeCN) nm (ε dm^3 mol^{-1} cm^{-1}): 594 (1176), 413 (2675), 281 (30588); ν_{max} (cm^{-1}): 3305, 1598, 1530, 1481, 1419, 1339, 1214, 746, 690, 614, 486; R_f = 0.45 (98:2 DCM:MeOH); m/z (ESI+): 299 $[M]^+$; HRMS (QToF+): $C_{19}H_{15}N_4$ requires 299.1297, found: 299.1294.

The structure was confirmed by independent X-Ray analysis.

Preparation of amino radical 315 by acid-catalysed hydrolysis 315

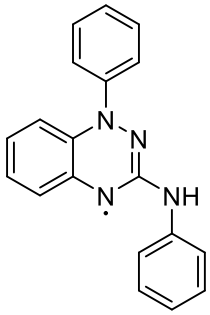

Radical **127** (0.250 g, 1.19 mmol) was dissolved in a 5 M HCl solution in 50:50 H_2O:MeOH (40 mL) and stirred for 2 hours. The solvent was removed under reduced pressure and the green residue dissolved in DCM (100 mL) and washed with 1 M Na_2CO_3 (1 x 50 mL) then water (3 x 50 mL) and finally brine (1 x 50 mL). The organic layer was dried over Na_2SO_4, filtered and dried *in vacuo*. The residue was dissolved in the minimum volume of DCM and purified by column chromatography (98:2 DCM:MeOH) The product containing fractions were collected and dried *in vacuo* to give radical **315** (0.098 g, 43%). The structure was confirmed by independent X-ray analysis.

Reaction of Nitron 127 in aqueous KOH solution in degassed acetonitrile 314

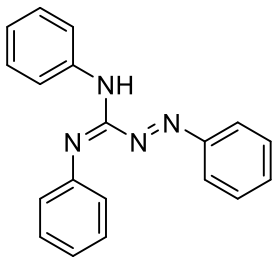

Nitron **127** (0.10 g, 0.32 mmol) was dissolved in degassed acetonitrile (10 mL) and added to a KOH solution (0.5 M, 20 mL). Immediately, a red oil formed above the aqueous layer. The solution was stirred for 48 hours and red crystals were precipitated. The product was collected by filtration and was purified by recrystallization, first from DCM and then from acetonitrile, to yield triazabutadiene **314** as red crystals (0.072 g, 75%); m.p. 107-108 °C; R_f = 0.35 (95:5 Hexane:EtOAc); δ_H ($CDCl_3$, 600 MHz,): 7.95 (s, 1H, N-*H*), 7.86 (d, *J* = 8.0 Hz, 2H, Ar-*H*), 7.73-7.80 (m, 2H, Ar-*H*), 7.52-7.57 (m, 1H, Ar-*H*), 7.49 (t, *J* = 7.3 Hz, 2H, Ar-*H*), 7.37 (t, *J* = 7.7 Hz, 2H, Ar-*H*), 7.31 (t, *J* = 7.6 Hz, 2H, Ar-H), 7.02-7.15 (m, 4H, Ar-*H*); δ_C ($CDCl_3$, 151 MHz,): 150.7, 148.8, 147.3, 138.7, 133.3, 129.4, 129.0, 128.0 124.4, 123.9, 123.1, 122.8, 119.1; m/z **(**ES+): 301 $[M+H]^+$; HRMS (ES+): $C_{19}H_{17}N_4$ requires 301.1453 found 301.1457.

6.5 Preparation of Solutions for NMR kinetic analysis.

Solutions of DCl and NaOD in D_2O were prepared by dilution of their commercially available stock solutions, the concentrations of which were titrated against commercially available standard solutions of KOH or HCl.

Acetate buffers were prepared by addition of DCl and KCl solutions to stock solutions of potassium acetate, giving various buffer solutions at differing free-base ratios at set ionic strengths.

Phosphate buffers were prepared from stock solutions of K_2DPO_4 and KD_2PO_4 in D_2O. K_2DPO_4 and KD_2PO_4 were prepared by repeated (4 times) dissolution of their analogous protonated salts, followed by removal of solvent by freeze-drying to give the solid compounds. Phosphate buffers in D_2O were prepared by mixing the stock solutions with KCl solution (where necessary) to give buffer solutions at various free-base ratios and ionic strengths.

Carbonate buffers in H_2O were from stock solutions of K_2CO_3 and $KHCO_3$ in H_2O, with addition of KCl solution where necessary to give buffer solutions at various free-base ratios and ionic strengths.

Carbonate buffers in D_2O were prepared by addition of DCl solutions to stock solutions of potassium carbonate in D_2O with vigorous agitation (to minimise loss of carbonate as CO_2 from locally acidic regions of solution) to the desired free-base ratio. If

necessary, addition of solutions of KCl in D_2O adjusted the ionic strength of these solutions.

Measurement of p*H*, p*D* and determination of activity coefficient of hydroxide ion (γ_{HO})

The p*H* of each of the solutions used in determination of carbon acidity were determined at 25 °C using a MeterLab™ PHM 290 p*H*-Stat controller equipped with a Radiometer combination electrode filled with saturated KCl solution. This apparatus was standardised between p*H* 1.6 – 4, 4 – 7, 7 – 12.45 to encompass the p*H* of the solution in question. Commercially available standard p*H* solutions (Fisher scientific) were used for standardising the p*H* of 1.6, 4 and 7. Saturated calcium hydroxide solution was used to standardise the electrode at 12.45. p*D* can be determined by simple addition of 0.4 to the value found from the p*H* meter.

The activity coefficient of hydroxide ion (γ_{HO}) was determined from the fit of observed pH of series of titrimetrically-known standard solutions of KOH at 25 °C at constant ionic strength. At I = 1.0 M, the previously determined value of γ_{HO} = 0.73 was used. At I = 0.4 M (Figure 1) and at I = 0.5 M (Figure 2), γ_{HO} was determined by the slope of a plot of a_{HO} against concentration of KOH (Equation 1).

Equation 2

$$10^{\mathrm{p}H-\mathrm{p}K_\mathrm{w}} = a_{HO} = \gamma_{\mathrm{HO}}[\mathrm{HO}^-]$$

Figure 2 Plot of a_{HO} against concentration of KOH at I = 0.4 M

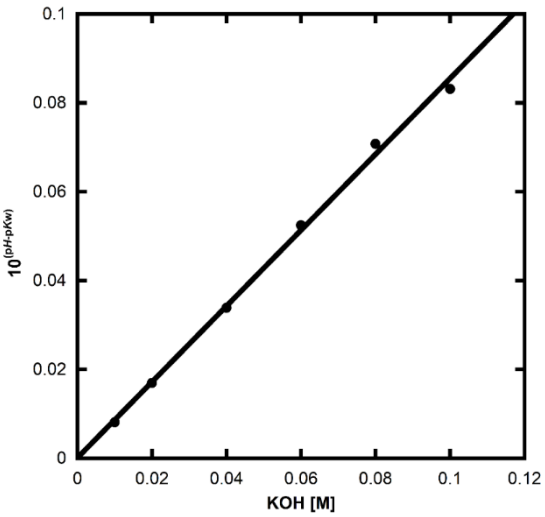

$$y = 0.85x$$

$$R^2 = 0.997$$

Figure 3 Plot of a_{OH} against concentration of KOH at I = 0.5 M

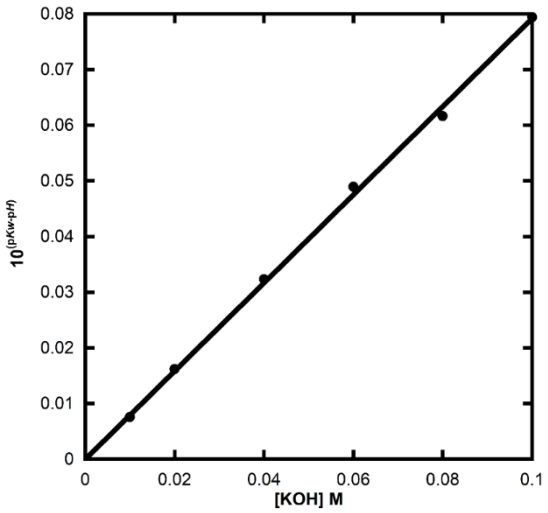

$$y = 0.79x$$

$$R^2 = 0.998$$

6.6 General procedures for kinetic NMR experiments

For H/D exchange experiments of triazolium, imidazolium, bis(amino)cyclopropenium and its hydroxy-aryl adduct salts, experiments were recorded on either a Bruker Ultrashield 400 MHz or Varian Inova 500 MHz spectrometer. ^{1}H NMR spectra were run with an acquisition time of 4 s and 90° pulse angle and a relaxation delay of 20 s, over 32 transients (~13 min). Peak areas were measured after a first-order drift correction and manual phasing. Integration was performed relative to the 12 methyl protons of the internal standard NMe_4 D_2SO_4.

For the hydrolysis of cyclopropenium phosphonates, experiments were recorded on the same instruments as above. ^{31}P NMR spectra were obtained using an acquisition time of 1s, 90° pulse angle and relaxation delay of 9s over 32 transients (~9 min). The T_1 relaxation times of all species except diethyl phosphate were found to be on the order of 2-3 s. Experiments at 32.5, 40 and 50 °C, were thermostated at their respective temperatures by the Varian Inova 500 MHz spectrometer. The experiment at 4 °C was cooled using (freezer) and temperature monitored by periodic thermometer readings, to within ±0.5 °C. Readings were taken at room temperature using Bruker Ultrashield 400

MHz spectrometer, before rapidly cooling back to the controlled temperature. Peak areas were corrected as above and integrated relative to the external standard K_3PO_4 (sat.) in D_2O locktube.

For studies of BAC organocatalysis in organic solvents, including determination of equilibrium constants in d_2-DCM, experiments were recorded on the same instruments as previously. ^1H NMR spectra were recorded with an acquisition time of 2 s, 45° pulse angle and relaxation delay of 5 s over 32 transients (~5 minutes). Peak areas were corrected as above, and integrated relative to an internal standard of TMS, which was considered not to change in concentration over the time period of the reaction.

6.5 Bibliography

1 A. D. Becke, *J. Chem. Phys.*, 1993, **98**, 5648–5652.
2 C. Lee, W. Yang and R. G. Parr, *Phys. Rev. B*, 1988, **37**, 785–789.
3 G. A. Petersson and M. A. Al-Laham, *J. Chem. Phys.*, 1991, **94**, 6081–6090.
4 G. A. Petersson, A. Bennett, T. G. Tensfeldt, M. A. Al-Laham, W. A. Shirley and J. Mantzaris, *J. Chem. Phys.*, 1988, **89**, 2193–2218.
5 F. M. J, *Gaussian 09*, Gaussian Inc., Wallingford CT, 2016.
6 A.-R. Allouche, *J. Comput. Chem.*, 2011, **32**, 174–182.
7 O'boyle Noel M., Tenderholt Adam L. and Langner Karol M., *J. Comput. Chem.*, 2008, **29**, 839–845.
8 Recent Advances in Density Functional Methods, https://www.worldscientific.com/worldscibooks/10.1142/2914,
9 H. E. Gottlieb, V. Kotlyar and A. Nudelman, *J. Org. Chem.*, 1997, **62**, 7512–7515.
10 G. R. Fulmer, A. J. M. Miller, N. H. Sherden, H. E. Gottlieb, A. Nudelman, B. M. Stoltz, J. E. Bercaw and K. I. Goldberg, *Organometallics*, 2010, **29**, 2176–2179.
11 I. Noviandri, K. N. Brown, D. S. Fleming, P. T. Gulyas, P. A. Lay, A. F. Masters and L. Phillips, *J. Phys. Chem. B*, 1999, **103**, 6713–6722.
12 Dolomanov Oleg V., Bourhis Luc J., Gildea Richard J., Howard Judith A. K. and Puschmann Horst, *J. Appl. Crystallogr.*, 2009, **42**, 339–341.
13 G. M. Sheldrick, *Acta Crystallogr. A*, 2008, **64**, 112–122.

CHAPTER 7 Conclusions and Future Work

Conclusions

The overall theme of this project was investigation of the chemistry of stable carbenes. Stable carbenes, primarily NHCs are of high importance in chemistry due to their versatile organocatalytic properties, as being useful as ligands in organometallic chemistry. As NHCs are typically generated *in situ* by deprotonation of their conjugate acids, investigations of this process are of significant interest.

Following work by Massey et. al. we have probed the kinetics of proton-transfer at the C(3)H position of two triazolium salts with o*rtho*-heteroatom substituents. The kinetic acidities of these positions were determined by H/D exchange experiments monitored by ^{1}H NMR spectroscopy in D_2O solutions at 25 °C and ionic strength = 1.0. The pseudo first-order rate constants of exchange, k_{ex} (s^{-1}) of these triazolium salts were determined at various p*D*s and were used to determine second-order rate constants of exchange k_{DO} (M^{-1} s^{-1}), and subsequently the pK_a of these systems. Similar to the pentafluoro triazolium **49** studied by Massey, plots of $\log_{10} k_{DO}$ against p*D* showed significant deviation from first-order dependence on deuteroxide at low p*D*, which is assigned to a mechanism involving protonation of the N1 position of the triazolium system to create a dicationic triazolium species, which is much more labile to deprotonation. *Ortho*-heteroatom substitution increases the significance of this mechanism, possibly due to unfavourable interactions between the nitrogen and heteroatom lone-pairs raising the pK_a of the N1 position, allowing protonation to be observed at a kinetically relevant p*D*. The presence of this *ortho*-substituent effect on the proton-transfer of N-aryl triazolium salts is now well established, and its potential effects on the organocatalytic behaviour of **120** and **121** could be investigated.

Two imidazolium species **122** and **123** provided by Dr. Paul Davies of Birmingham University were also investigated by similar methods. The proton-transfer chemistry of both salts showed no deviation from first-order dependence on deuteroxide. The kinetic acidity of these species was unusually high compared to other imidazolium salts, a factor which was assigned to the fused furyl ring in the ring system. The exocyclic sulfonamide substituents were thought not to be influential during proton-transfer. Exchange experiments on these imidazolium salts required a large amount of acetonitrile cosolvent due to their large hydrophobic substituents. Preparation of more

soluble furo-imidazolium systems could be used to further probe their unusually acidic nature compared to other imidazolium ions without the requirement for cosolvent.

Bis(amino)cyclopropenylidenes are a relatively new class of stable carbenes, and the only examples with no α-heteroatoms to the carbene centre. These species were of particular interest as there is a lack of current literature available on their proton-transfer chemistry. Preparation of the cyclopropenium conjugate acids of BACs proved to be somewhat difficult due to preferential formation of their tris(amino)cyclopropenium counterparts. Using H/D exchange experimental conditions identical to those used for triazolium salts, second-order rate constants of exchange k_{DO} of BACs were determined. Mechanistic investigation suggested that proton-transfer occurred *via* a BAC, in an analogous mechanism to that of NHCs. Assuming rate-determining reprotonation, the k_{DO} values were used to estimate the pK_as of BACs (~22), between that of N-aryl and N-alkyl imidazolium salts. The unexpectedly high carbon acidity of cyclopropenium salts was assigned to the very acute C-C-C bond angle at the carbene centre, and stabilising effects from the β-nitrogen atoms.

Only a few examples of BACs were studied during these experiments, and future work to produce a wider array of derivatives has a lot of potential. Using the new synthetic method developed herein involving triethyl phosphite could potentially be applied to produce further BAC conjugate acids which are considered difficult to access such as N-aryl BACs. Furthermore, this method could allow for easier purification of a variety of other BAC conjugate acids, due to the ease of purification compared to the difficult to remove triphenylphosphine oxide related impurities. Additionally, counterion control, using Lewis acidic species such as $SbCl_5$ or $AlCl_3$, could potentially allow successful preparation of BACs with unhindered amine substituents, which has the potential to allow specific tuning of BACs for organocatalysis or in organometallic chemistry.

During our research on the preparation of BAC conjugate acids, a serendipitous discovery of stable phosphonato cyclopropenium salts was made. Several phosphonates were prepared and were found to be stable under ambient conditions. Hydrolysis under basic conditions resulted in ejection of either an alkoxide or BAC. Unusually, the leaving group with higher pK_a – a BAC – was found to preferentially leave compared to alkoxides. ^{31}P NMR spectroscopic experiments probed these experiments and found

first-order dependence on deuteroxide. Less substituted alcohols were found to be better leaving groups (Me>Et>^{i}Pr), but BAC was the predominant leaving group in each case. It was also determined that there was no significant solvent kinetic isotope effect in these experiments. Furthermore, variable temperature experiments determined that the mechanism is likely associative in nature. The ratio of products for **191** was consistent throughout any change of conditions. The data suggested two possible mechanisms of hydrolysis, a concerted $S_N2@P$ process, or a stepwise A_N+D_N mechanism involving rate-limiting pseudorotation of the pentahedral intermediate.

Future work on this topic could include further kinetic data on a range of phosphonates to confirm current findings, and to find more precise knowledge of rate constants, as well as further probe the mechanism. Phosphonates with electron-withdrawing ester groups were not successfully prepared in this project. They could potentially be prepared by alternative synthetic pathways, such as the use of PCl_3 or phosphonate transesterification. Further, use of different cyclopropenium substituents could provide information about the mechanism of hydrolysis. Nucleophilic substitution using nucleophiles other than lyoxides could also be an area of interest. Additionally, preparation of azolium phosphonates using NHCs could be of significant interest, if they can be prepared by a similar method.

Studies on the kinetics of organocatalytic properties of BACs were undertaken using ^{1}H NMR spectroscopy. It was found that despite the lack of a benzoin product detected in reactions involving BACs and aryl aldehydes, the formation of an aldehyde-BAC adduct, or hydroxy-aryl adduct is common to BACs and NHCs. The intramolecular Stetter reaction was found to be highly sensitive to the steric bulk of the BAC used, bulky catalyst **163** failed to produce any product, however the formation of a hydroxy-aryl adduct was common to both catalysts. The lack of difference in carbon acidities between **163** and **167** suggests these catalysts are similar electronically. The strong base DBU used to generate the BAC *in situ* was unfortunately found to catalyse other reactions concurrently to the desired processes, which did not occur under the milder conditions associated with triazolium catalysts, which hindered more detailed analysis.

The aforementioned hydroxy-aryl adducts could be prepared synthetically in four examples. and were successfully isolated. The adducts were found to rapidly revert to equilibrium with BAC and aldehyde under strongly basic conditions. Alkylation of the

alcohol groups of these adducts was achieved under harsh acidic conditions and prevented the return to equilibrium. In D_2O solutions, H/D exchange experiments at 25 °C and I = 1.0 monitored by ^1H NMR spectroscopy determined that exchange occurs under strongly basic conditions, confirming the formation of a d_1-acyl anion equivalent is present in BAC organocatalysis. A moderate aryl substituent effect was observed.

The equilibrium constants between aldehyde, BAC and adduct were estimated by ^1H NMR spectroscopic measurement of their equilibrium concentrations in d_2-DCM. A similar substituent effect to that found by Collett. et. al.[2] causing adducts to be favoured in the case of *ortho*-substituted aryl aldehydes was found using BACs. The effect was potentially as a result of destabilisation of the ground state of the aldehyde, or as a result of favourable interactions between the alcohol proton and ether oxygen of 2-substituted adducts.

Relatively few equilibrium constants were identified, and the study of other aldehydes and BACs could probe the 2-substituent effect further. The kinetic profiles of BAC organocatalytic reactions may be studied better with the use of a milder base than DBU, but stronger than NEt_3, if it simultaneously is capable of forming the BAC and does not initiate undesired side-reactions. The proposed d_1-acyl anion intermediate was formed transiently during our H/D exchange experiments, but further experimentation could potentially isolate and directly characterise this intermediate. The lack of homobenzoin product currently does not have a mechanistic explanation, and further studies could uncover the origin of this behaviour. Additionally, the lack of a homobenzoin product in reactions involving BACs could be synthetically useful in further catalytic procedures.

Following from the serendipitous discovery by Grant of a novel Blatter-type (benzotriazinyl) radical x formed by the hydrolysis and oxidation of carbenoid species Nitron **127**, the mechanism of this process was investigated. It was found that high concentrations of water formed predominantly triazabutadiene **314**, instead of a benzotriazinyl radical. Data from synthetic experiments and suggested the mechanism involves hydrolytic ring-opening of Nitron to form an amidrazone, which is then either hydrolysed to form triazabutadiene **314** or undergoes an oxidation and cyclization to form benzotriazinyl radical **313**. **313** was also found to undergo amide hydrolysis under basic or acidic conditions to form amino radical **315**.

Triazabutadiene **314** was found not to form amino radical x under any of the conditions tested. The lack of radical formation was could have been due to a lack of *cis-trans* isomerism, however EXSY NMR spectroscopy experiments showed that *cis-trans* isomerism occurs rapidly. It is instead suggested that the loss of the electron-withdrawing amido group disfavours the cyclization necessary to form a benzotriazinyl radical.

Both radicals **313** and **315** were found to be fully radical in nature by EPR spectroscopy, and crystal structures were obtained in both cases. The crystal structure of **313** showed a slipped-stack structure. Unusually, **315** showed interaction between the radical and amine N-H positions of different molecules of **315** in its crystal structure, which could potentially show interesting magnetic properties. Protonation of **315** under acidic conditions shows a noted colour change, and formation of an uncharacterized species with lower radical character, but the remaining radical species showed very high hyperfine coupling to a hydrogen atom. Cyclic voltammetry of both radicals showed fully reversible (−1/0) and (0/+1) redox processes, results similar to those determined for other benzotriazinyl radicals. The addition of the exocyclic heteroatom to the system was found by computational and EPR spectroscopic data not to significantly affect the SOMO orbital structure of the benzotriazinyl moiety.

The novel benzotriazinyl structure found in these experiments has the potential for significant derivatization, especially at the synthetic “handle” of the exocyclic nitrogen atom. Substitution at this site could potentially bring a wide variety of new Blatter type radicals. Furthermore, the magnetic properties of radicals **313** and **315** have not been investigated. Further applications for stable radicals, such as mediators in radical polymerisation, or attachment to biologically relevant molecules may be aided by the addition of the exocyclic nitrogen atom.

Acknowledgements

I would like to thank Dr. AnnMarie O’Donoghue for her excellent support, knowledge and guidance. AnnMarie is an exceptionally helpful and kind supervisor and I am very grateful for her assistance throughout the course of these studies.

I would also like to thank the staff of Durham University who were of assistance with technical aspects of this project: Dr. Dmitry Yufit and Dr. Andrei Batsanov for their X-

ray crystallographic work, Prof. Alan Kenwright, Dr. Juan Aguilar Malavia and Mrs. Catherine Heffernan for assistance and guidance in NMR spectroscopy, Dr. Jackie Mosely and Dr. David Parker for help with Mass Spectrometry, Dr. Ritu Kataky for help with electrochemistry, Dr. Aileen Congreve for guidance on HPLC and Dr. Mark A. Fox for spectroelectrochemical data and computational chemistry. Thanks also to Prof. Ian Baxendale and Prof. Patrick Steel for the use of their microwave reactors. Additionally, I would like to thank Dr. Victor Chechik of the University of York for his help with EPR Spectroscopy and Dr. Paul Davies of the University of Birmingham for providing two imidazolium salts.

Thank you to Chris Bramley and Peter Quinn for their assistance with Chapter 2, and Jacob Grant, for his original finding of the benzotriazinyl radical in Chapter 5. I have thoroughly enjoyed my work in laboratory CG115, especially thanks to the two named above, as well as Oliver Maguire, David Wong-Pascua, Jiayun Zhu, Kevin Maduka, Hector Macrae, Lami Mnamonu and Niamh Ainsworth. Thanks are also extended to the 4th year project students Isabell Pickles, Bryony Hockin, Natalie Farmer, Ryan Williams, James Pemberton, Elin Pyke and Bethany Taylor. I would also like to thank the members of the Sandford Group for their assistance and support throughout this project and the many tea breaks that went into it.

Finally, I would like to thank my parents and Catherine for their constant support.

APPENDIX A – NMR MONITORED EXPERIMENT DATA

Triazolium Salt H/D Exchange Kinetics

121

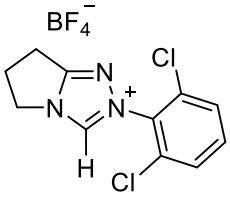

Table 2 H/D exchange kinetics for 120 in D_2O solutions at I = 1.0, 25 °C

Condition	p*D*	Time, (s)	*f*(s)	k_{ex} (s^{-1})
2 M DCl	−0.10	0	1.000	2.29×10^{-6}
		76525	0.794	
		104813	0.759	
		164946	0.660	
		287132	0.500	
		357425	0.437	
1 M DCl	0.37	0	1	6.71×10^{-6}
		9520	0.959	
		74837	0.570	
		83358	0.620	
		94954	0.536	
		354154	0.101	
		948521	0.009	
0.75 M DCl	0.61	0	1.000	8.13×10^{-6}
		5307	0.961	
		63970	0.597	
		73456	0.553	
		594140	0.012	
0.5 M DCl	0.53	0	1	8.61×10^{-6}
		10398	0.928	
		18115	0.884	
		85537	0.493	

		100731	0.419	
		352348	0.049	
		362761	0.050	
		688163	0.013	
0.25 M DCl	0.71	0	1	9.52×10^{-6}
		10622	0.9667	
		18064	0.881	
		89697	0.532	
		100775	0.482	
		360696	0.080	
		688207	0.145	
0.175 M DCl	1.17	0	1	1.28×10^{-5}
		2244	0.871	
		65169	0.419	
		73956	0.379	
		594765	0.011	
0.1 M DCl	1.09	0	1	1.40×10^{-5}
		9515	0.899	
		81270	0.307	
		93802	0.261	
		102648	0.253	
		696977	−0.004	
0.05 M DCl	1.41	0	1	2.08×10^{-5}
		9534	0.815	
		81578	0.162	
		94092	0.128	
		102691	0.106	
0.025 M DCl	1.80	0	1	4.30×10^{-5}
		5768	0.787	
		11536	0.607	
		17304	0.489	
		23072	0.380	
		28840	0.302	

		34608	0.233	
		40376	0.195	
		46144	0.149	
		51912	0.120	
0.01 M DCl	2.99	0	1	5.73×10^{-4}
		768	0.648	
		1536	0.420	
		2304	0.281	
		3072	0.185	
		3840	0.112	
		4608	0.078	
		5376	0.061	
		6144	0.043	
		6912	0.036	
1 M Acetate	2.20	0	1.000	8.21×10^{-5}
		2700	0.771	
		5400	0.683	
		8100	0.495	
		12000	0.381	
		14700	0.286	
		17400	0.272	
		20100	0.198	
		23100	0.189	
		86700	0.032	
1 M Acetate	3.40	0	1.000	1.01×10^{-3}
		1068	0.369	
		2118	0.154	
		3168	0.072	
		4218	0.066	
		5268	0.048	
		7368	0.043	
		9468	0.033	
1 M Acetate	3.65	0	1.000	2.42×10^{-3}

318	0.473	
590	0.244	
875	0.147	
1185	0.083	
1575	0.051	
2490	0.008	

121

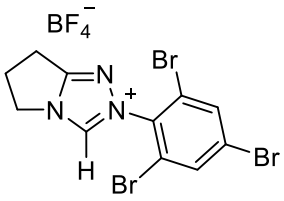

Table 3 H/D exchange kinetics for 121 in D_2O solutions at I = 1.0, 25 °C

Condition	p*D*	Time, (s)	*f*(s)	k_{ex}, (s^{-1})
2 M DCl	−0.13	0	1.000	4.59×10^{-6}
		76414	0.678	
		102733	0.607	
		164901	0.476	
		287113	0.270	
		357312	0.189	
		509678	0.103	
1 M DCl	0.22	0	1.000	1.37×10^{-5}
		12998	0.832	
		22959	0.738	
		83384	0.321	
		102486	0.259	
		172668	0.094	
		342394	0.012	
0.5 M DCl	0.43	0	1.000	1.70×10^{-5}
		11607	0.842	
		66715	0.325	
		84747	0.242	

		98152	0.196	
		156588	0.072	
		183328	0.053	
0.25 M DCl	0.70	0	1.000	1.91×10^{-5}
		12258	0.809	
		21649	0.658	
		82595	0.194	
		93211	0.162	
		111344	0.116	
		183313	0.023	
0.1 M DCl	0.97	0	1.000	2.58×10^{-5}
		8768	0.801	
		17536	0.633	
		26304	0.513	
		35072	0.409	
		43840	0.317	
		52608	0.256	
		61376	0.195	
		70144	0.166	
		78912	0.129	
		87680	0.102	
		96448	0.084	
		105216	0.063	
		113984	0.048	
0.05 M DCl	1.25	0	1.000	3.37×10^{-5}
		5768	0.812	
		11536	0.682	
		17304	0.551	
		23072	0.454	
		28840	0.373	
		34608	0.330	
		40376	0.243	
		46144	0.199	

		51912	0.167	
0.025 M DCl	1.60	0	1.000	4.98×10^{-5}
		5088	0.792	
		10176	0.617	
		15264	0.473	
		20352	0.368	
		25440	0.281	
		30528	0.226	
		35616	0.145	
		40704	0.128	
		45792	0.102	
0.005 M DCl	2.25	0	1.000	1.50×10^{-5}
		3568	0.601	
		7136	0.354	
		10704	0.209	
		14272	0.127	
		17840	0.084	
		21408	0.052	
		24976	0.042	
		28544	0.023	
		32112	0.029	
0.0015 M DCl	2.45	0	1.000	2.48×10^{-5}
		960	0.771	
		1920	0.622	
		2880	0.485	
		3840	0.375	
		4800	0.306	
		5760	0.236	
		6720	0.187	
		7680	0.154	
		8640	0.118	
0.001 M DCl	2.55	0	1.000	3.14×10^{-4}
		768	0.779	

1536	0.612
2304	0.480
3072	0.378
3840	0.292
4608	0.247
5376	0.188

Imidazolium salt H/D exchange

122

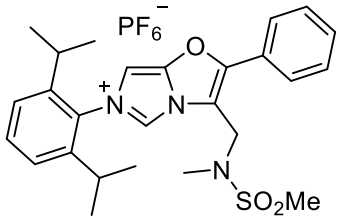

Table 4 H/D exchange kinetics for imidazolium 122 in D_2O:MeCN (3:2) at I = 0.40, 25 °C

Buffer	pD_{corr}	Time (s)	f(s)	k_{ex} (s^{-1})
10% fb Formate	3.20	0	1	1.20×10^{-5}
		72338	0.423	
		161568	0.156	
		174920	0.146	
		226408	0.090	
		314380	0.046	
17.5% fb Formate	3.52	00	1.000	2.09×10^{-5}
		7273	0.863	
		13136	0.789	
		17523	0.718	
		23540	0.613	
		31219	0.531	
		74816	0.197	
		102271	0.106	
		111553	0.091	

		188168	0.022	
25% fb Formate	3.68	0	1	3.37×10^{-5}
		4903	0.864	
		55113	0.159	
		65508	0.124	
		82843	0.064	
		131039	0.030	
50% fb Formate	4.20	0	1.000	1.04×10^{-4}
		4060	0.670	
		8699	0.417	
		16116	0.197	
		19759	0.146	
		25010	0.084	
		84710	0.014	
		89938	0.026	
75% fb Formate	4.70	0	1.000	3.55×10^{-4}
		768	0.775	
		1536	0.580	
		2304	0.467	
		3072	0.356	
		3840	0.268	
		4608	0.220	
		5376	0.169	
		6144	0.134	
		6912	0.128	
		8448	0.067	
		10752	0.051	
		14592	0.029	
		22272	0.020	
		37632	0.020	
		52992	0.022	

123

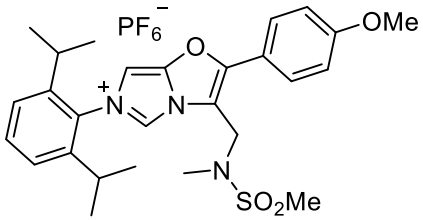

Table 5 H/D exchange kinetics for imidazolium 123 in D_2O:MeCN (3:2) at I = 0.40, 25 °C

Buffer	pD_{corr}	Time (s)	f(s)	k_{ex} (s^{-1})
10% fb Formate	3.36	0	1.000	7.52×10^{-6}
		6128	0.878	
		58551	0.607	
		82013	0.497	
		164985	0.250	
		253598	0.144	
		320325	0.073	
17.5% fb Formate	3.56	0	1.000	1.55×10^{-5}
		6232	0.892	
		13497	0.820	
		22540	0.699	
		27007	0.666	
		32768	0.608	
		40340	0.545	
		84347	0.247	
		101299	0.203	
		114493	0.164	
		122981	0.138	
		197648	0.042	
25% fb Formate	3.68	0	1.000	2.72×10^{-5}
		8840	0.773	
		17680	0.610	
		26520	0.483	
		35360	0.381	

		44200	0.300	
		53040	0.235	
		61880	0.190	
		70720	0.150	
		79560	0.123	
		86632	0.113	
		95472	0.083	
		104312	0.066	
		121992	0.042	
		139672	0.034	
		157352	0.020	
		175032	0.016	
50% fb Formate	4.23	0	1.000	7.44×10^{-5}
		4263	0.740	
		9002	0.525	
		14479	0.336	
		18292	0.268	
		21967	0.186	
		27274	0.129	
		31410	0.100	
		83612	0.008	
25% fb Acetate	4.82	0	1.000	4.63×10^{-4}
		768	0.687	
		1536	0.488	
		2304	0.342	
		3072	0.247	
		3840	0.176	
		4608	0.124	
		5376	0.089	
		6144	0.061	

Cyclopropenium H/D exchange

163

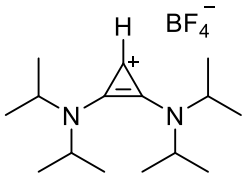

Table 6 H/D exchange kinetics for 163 in D_2O solutions at I = 1.0, 25 °C

Buffer	p*D*	Time (s)	f(s)	k_{ex} (s^{-1})
10% fb Phosphate 0.1 M	5.51	0	1.000	1.04×10^{-6}
		90446	0.902	
		162525	0.844	
		236403	0.771	
		499921	0.582	
		607935	0.507	
		696292	0.470	
		1358911	0.279	
25 % fb Phosphate 0.1 M	6.13	0	1.000	3.30×10^{-6}
		14603	0.954	
		92698	0.734	
		169151	0.562	
		510285	0.183	
		605303	0.146	
		706611	0.101	
50% fb Phosphate 0.1 M	6.73	0	1.000	1.95×10^{-5}
		8153	0.860	
		21448	0.670	
		86534	0.187	
		172034	0.040	
75% fb Phosphate 0.1 M	7.13	0	1.000	2.98×10^{-5}
		7865	0.819	
		22089	0.523	
		79517	0.080	

		100243	0.046	
		177237	0.013	
90% fb Phosphate 0.1 M	7.70	0	1.000	1.33×10^{-4}
		1968	0.771	
		3936	0.591	
		5904	0.457	
		7872	0.354	
		9840	0.275	
		11808	0.203	
		13776	0.167	
		15744	0.129	
		17712	0.099	
90% fb Phosphate 0.05 M	6.20	0	1.000	4.00×10^{-6}
		9378	0.988	
		79062	0.749	
		98685	0.695	
		330543	0.270	
		514478	0.140	
90% fb Phosphate 0.025 M	6.17	0	1.000	3.66×10^{-6}
		7708	0.964	
		76995	0.746	
		96478	0.677	
		328376	0.300	
		510305	0.160	

167

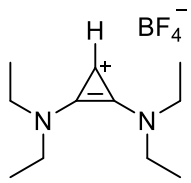

Table 7 H/D exchange kinetics for 167 in D_2O solutions at I = 1.0, 25 °C

Buffer	p*D*	Time (s)	f(s)	k_{ex} (s^{-1})

75% fb Acetate 0.1 M	5.52	0	1.000	2.58×10^{-6}
		17853	0.923	
		75147	0.855	
		94352	0.800	
		170479	0.659	
		192901	0.621	
		272874	0.500	
		353145	0.410	
		514455	0.222	
		709794	0.080	
		1049959	−0.006	
10% fb Phosphate 0.1 M	5.88	0	1.000	6.58×10^{-6}
		52700	0.800	
		76529	0.542	
		145721	0.383	
		226348	0.260	
		341917	0.029	
50% fb Phosphate 0.1 M	6.90	0	1.000	8.11×10^{-5}
		1788	0.819	
		3576	0.655	
		5364	0.622	
		7152	0.548	
		8940	0.481	
		10728	0.392	
		12516	0.368	
		14304	0.342	
		16092	0.280	
		17880	0.191	
		19668	0.194	
		23244	0.129	
		26820	0.133	
		30396	0.066	
		41124	0.037	

		48276	0.008	
		55428	0.032	
75 % fb Phosphate 0.1 M	7.48	0	1.000	2.52×10^{-4}
		1788	0.650	
		3576	0.417	
		5364	0.253	
		7152	0.144	
		8940	0.104	
		10728	0.067	
90% fb Phosphate 0.1 M	7.56	0	1.000	3.29×10^{-4}
		768	0.756	
		1536	0.586	
		2304	0.476	
		3072	0.365	
		3840	0.291	
		4608	0.231	
		5376	0.182	
		6144	0.149	
		6912	0.121	
		7680	0.100	
		8448	0.087	

Kinetics of phosphonato cyclopropenium hydrolysis.

Hydrolysis of 191 in H_2O

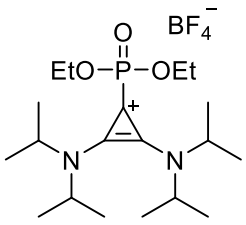

Table 8 Kinetics of the hydrolysis of 181 in H_2O solutions at I = 1.0, 25 °C

Buffer	p*H* start	p*H* end	Time (s)	f(s)	k_{obs} (s^{-1})
	9.32	9.28	0	1.000	3.51×10^{-5}

20% fb Carbonate 0.5 M			4642	0.860	
			8927	0.754	
			55810	0.123	
			75678	0.029	
			152092	0.024	
30% fb Carbonate 0.5 M	9.51	9.48	0	1.000	7.95×10^{-5}
			3838	0.751	
			7363	0.531	
			16607	0.288	
			21467	0.216	
			64221	0.025	
40 % fb Carbonate 0.5 M	9.73	9.72	0	1.000	1.29×10^{-4}
			4168	0.608	
			8894	0.371	
			12437	0.224	
			16248	0.174	
			75702	0.059	
			106508	0.053	
50% fb Carbonate 0.5 M	9.91	9.86	0	1.000	1.94×10^{-4}
			3556	0.508	
			7096	0.276	
			11381	0.130	
			15004	0.074	
			29819	0.034	
40% fb Carbonate 0.25 M	9.76	9.59	0	1.000	9.69×10^{-5}
			7672	0.473	
			12435	0.324	
			18334	0.220	
			30513	0.061	
			516024	0.044	
40% fb Carbonate 1.0 M	9.76	9.77	0	1.000	1.54×10^{-4}
			3218	0.698	
			6189	0.446	

		10023	0.191	
		14730	0.106	
		71693	0.054	
		81546	0.037	

Hydrolysis of 191 in D_2O

Table 9 Kinetics of the hydrolysis of 181 in D_2O solutions at I = 1.0, 25 °C

Buffer	p*D*	Time (s)	f(s)	k_{obs} (s^{-1})
20% fb Carbonate 0.5 M	9.24	0	1.000	6.76×10^{-6}
		6078	0.967	
		14511	0.967	
		78337	0.550	
		93337	0.540	
		108744	0.459	
		162814	0.393	
		190073	0.287	
		253970	0.202	
		278209	0.175	
		338071	0.091	
		593574	0.005	
		604238	0.016	
		774236	0.025	
30% fb Carbonate 0.5 M	10.29	0	1.000	6.83×10^{-5}
		4962	0.666	
		10311	0.493	
		16453	0.342	
		23037	0.227	
		29181	0.145	
		39655	0.104	
		81868	0.024	
	10.70	0	1.000	1.83×10^{-4}
		4648	0.424	

40% fb Carbonate 0.5 M		7173	0.320	
		12131	0.127	
		26324	0.008	
		77693	0.063	
50% fb Carbonate 0.5 M	10.29	0	1.000	8.20×10^{-5}
		3128	0.839	
		7340	0.574	
		13277	0.408	
		17658	0.280	
		21953	0.207	
		28015	0.151	
		77993	0.060	
		91903	0.088	

Variable Temperature Hydrolysis of 191 in D_2O

Table 10 Kinetics of the hydrolysis of 181 in D_2O solutions (50% f.b. K_2CO_3) at I = 1.0

Temperature (°C)	p*D*’	[DO^-] (M)	Time (s)	f(s)	k_{obs} (s^{-1})
4	10.55	9.97×10^{-6}	0	1.000	1.43×10^{-5}
			73575	0.365	
			111562	0.215	
			159297	0.118	
			194918	0.046	
			1369941	0.031	
32.5	10.22	5.50×10^{-5}	320	1.000	2.62×10^{-4}
			960	0.653	
			1600	0.683	
			2240	0.579	
			2880	0.521	
			3520	0.341	
			4160	0.369	

			4800	0.330	
			5440	0.246	
			6080	0.188	
			6720	0.226	
			7360	0.182	
			8000	0.159	
			8640	0.113	
			9280	0.022	
			9920	0.046	
			10560	0.090	
			11200	0.094	
			11840	0.049	
			12480	0.015	
			13120	0.087	
40	10.18	8.54×10^{-5}	320	1.000	5.44×10^{-4}
			960	0.691	
			1600	0.462	
			2240	0.369	
			2880	0.205	
			3520	0.208	
			4160	0.141	
			4800	0.154	
			5440	0.052	
			6080	0.028	
50	10.12	1.42×10^{-4}	160	1.000	1.54×10^{-3}
			480	0.577	
			800	0.464	
			1120	0.105	
			1440	0.071	
			1760	0.147	
			2080	0.153	
			2400	0.051	
			3040	0.166	

3680	0.005		

Kinetics of hydroxy-aryl adduct H/D exchange and decomposition

269

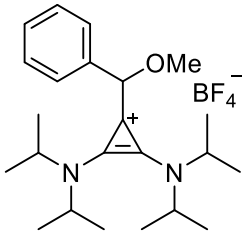

Table 11 H/D exchange and decomposition kinetics for adduct 269 in D_2O:MeCN (3:1) at I = 0.5, 25 °C

NaOD (M)	Time (s)	*f*(S)	*f*(eth)	*f*(H)	k_{ex} (s^{-1})	k_{obs} (s^{-1})	k_{dec} (s^{-1})
0.45 M	0	1.000	1.000	1.000	1.19×10^{-4}	1.31×10^{-4}	1.09×10^{-5}
	768	0.884	0.972	0.909			
	1536	0.791	0.959	0.825			
	2304	0.725	0.956	0.758			
	3072	0.671	0.932	0.720			
	3840	0.596	0.933	0.639			
	4608	0.545	0.932	0.585			
	5376	0.514	0.923	0.557			
	6144	0.455	0.920	0.495			
	6912	0.413	0.910	0.453			
	7680	0.376	0.896	0.420			
	8448	0.337	0.910	0.371			
	9984	0.175	0.862	0.202			
	13056	0.159	0.855	0.186			
	14592	0.145	0.833	0.175			
	19200	0.065	0.834	0.078			
	23808	0.031	0.765	0.040			
	26112	0.016	0.731	0.022			

	29952	0.010	0.700	0.015		
	37632	0.001	0.634	0.001		
	45312	0.009	0.590	0.016		
	52992	0.003	0.537	0.005		
0.25 M	0	1.000	1.000	1.000	5.89×10^{-5}	6.04×10^{-5}	4.40×10^{-6}
	4122	0.803	0.983	0.817			
	12599	0.495	0.941	0.526			
	27302	0.185	0.829	0.224			
	36594	0.101	0.809	0.125			
	86965	0.004	0.620	0.006			
	276768	0.029	0.323	0.091			
0.15 M	0	1.000	1.000	1.000	3.55×10^{-5}	3.85×10^{-5}	2.57×10^{-6}
	5637	0.799	0.980	0.815			
	12431	0.626	0.946	0.662			
	25049	0.400	0.925	0.433			
	33921	0.259	0.884	0.293			
	84668	0.041	0.763	0.054			
	276977	0.011	0.489	0.023			
0.10 M	0	1.000	1.000	1.000	2.27×10^{-5}	2.41×10^{-5}	1.80×10^{-6}
	4478	0.842	0.998	0.844			
	21879	0.594	0.971	0.612			
	30741	0.483	0.949	0.508			
	78769	0.133	0.855	0.156			
	92556	0.071	0.835	0.085			
	275822	0.017	0.618	0.027			
0.05 M	0	1.000	1.000	1.000	6.74×10^{-6}	7.26×10^{-6}	5.79×10^{-7}
	78153	0.612	0.967	0.633			
	97448	0.533	0.947	0.563			
	118638	0.441	0.913	0.484			
	158484	0.291	0.894	0.326			
	195405	0.222	0.865	0.256			
	249003	0.134	0.837	0.160			
	289178	0.085	0.804	0.106			

	541067	0.019	0.707	0.027			
	800024	0.016	0.648	0.025			
0.025 M	0	1.000	1.000	1.000	4.38×10^{-6}	4.81×10^{-6}	2.07×10^{-7}
	46059	0.795	0.968	0.822			
	84232	0.690	0.973	0.710			
	126248	0.560	0.946	0.592			
	163100	0.459	0.931	0.493			
	216553	0.391	0.913	0.428			
	217173	0.372	0.909	0.410			
	598791	0.107	0.811	0.132			
	764460	0.046	0.779	0.059			
	857344	0.041	0.765	0.054			
	1615682	0.033	0.747	0.044			

272

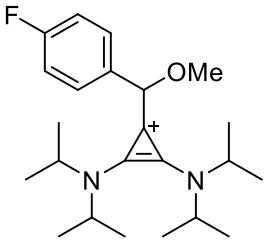

Table 12 H/D exchange and decomposition kinetics for adduct 272 in D_2O:MeCN (3:1) at I = 0.5, 25 °C

NaOD (M)	Time (s)	*f*(S)	*f*(eth)	*f*(H)	k_{ex} (s^{-1})	k_{obs} (s^{-1})	k_{dec} (s^{-1})
0.45 M	0	1.000	1.000	1.000	1.88×10^{-4}	2.02×10^{-4}	1.69×10^{-5}
	768	0.862	1.004	0.859			
	1536	0.739	0.979	0.754			
	2304	0.633	0.960	0.659			
	3072	0.539	0.956	0.563			
	3840	0.463	0.948	0.488			
	4608	0.396	0.933	0.424			
	5376	0.340	0.927	0.366			

	6144	0.292	0.915	0.318		
	6912	0.256	0.903	0.283		
	7680	0.214	0.891	0.240		
	8448	0.183	0.879	0.209		
	9984	0.134	0.854	0.157		
	11520	0.098	0.838	0.116		
	13056	0.070	0.807	0.087		
	14592	0.043	0.788	0.055		
	18432	0.033	0.739	0.044		
	22272	0.021	0.693	0.030		
	29952	0.004	0.610	0.007		
0.25 M	0	1.000	1.000	1.000	6.88×10^{-5}	6.54×10^{-5}	7.28×10^{-6}
	3273	0.874	1.117	0.783			
	5883	0.703	1.062	0.662			
	9601	0.587	1.056	0.556			
	14614	0.388	1.012	0.383			
	20739	0.239	0.965	0.248			
	72491	0.022	0.663	0.033			
0.10 M	0	1.000	1.000	1.000	3.39×10^{-5}	3.42×10^{-5}	2.72×10^{-6}
	6761	0.826	0.977	0.846			
	11924	0.599	0.990	0.604			
	18005	0.546	1.005	0.544			
	23090	0.456	0.940	0.485			
	27474	0.408	0.936	0.436			
	31650	0.379	0.899	0.422			
	94806	0.066	0.792	0.084			
	104737	0.040	0.754	0.052			
0.025 M	0	1.000	1.000	1.000	7.36×10^{-6}	8.28×10^{-6}	4.90×10^{-7}
	11837	0.815	0.973	0.838			
	23937	0.757	0.964	0.786			
	31656	0.719	0.943	0.763			
	78122	0.477	0.919	0.520			
	101009	0.419	0.943	0.445			

113621	0.394	0.900	0.439
175739	0.257	0.890	0.288
198748	0.213	0.857	0.248
264951	0.143	0.804	0.178
341552	0.101	0.787	0.129
441891	0.083	0.770	0.107
780409	0.025	0.687	0.037

273

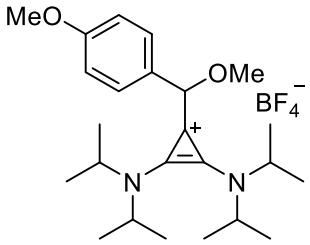

Table 13 H/D exchange and decomposition kinetics for adduct 272 in D_2O:MeCN (3:1) at I = 0.5, 25 °C

NaOD (M)	Time (s)	*f*(S)	*f*(eth)	*f*(H)	k_{ex} (s^{-1})	k_{obs} (s^{-1})	k_{dec} (s^{-1})
0.45 M	0	1.000	1.000	1.000	6.76×10^{-5}	7.02×10^{-5}	8.56×10^{-6}
	3316	0.696	0.910	0.765			
	7805	0.590	0.942	0.626			
	11577	0.433	0.929	0.466			
	16577	0.374	0.848	0.441			
	22694	0.238	0.807	0.295			
	74672	0.084	0.512	0.164			
0.10 M	0	1.000	1.000	1.000	8.98×10^{-6}	1.05×10^{-5}	9.89×10^{-7}
	55392	0.588	0.934	0.630			
	72298	0.398	0.915	0.435			
	89877	0.389	0.895	0.435			
	140588	0.257	0.881	0.291			
	175223	0.217	0.832	0.261			
	225929	0.148	0.811	0.182			

	327485	0.020	0.703	0.029			
	0	1.000	1.000	1.000			
	59394	0.729	0.957	0.762			
	154050	0.454	0.879	0.516			
	224993	0.332	0.831	0.399			
0.045 M	266518	0.274	0.821	0.333	4.50×10^{-6}	5.48×10^{-6}	5.41×10^{-7}
	311002	0.232	0.799	0.290			
	409749	0.175	0.767	0.229			
	517450	0.133	0.724	0.184			
	749286	0.094	0.673	0.140			

274

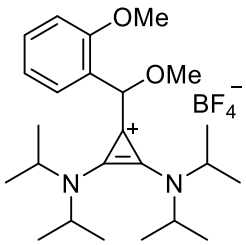

Table 14 H/D exchange and decomposition kinetics for adduct 274 in D_2O:MeCN (3:1) at I = 0.5, 25 °C

NaOD (M)	Time (s)	*f*(S)	*f*(eth)	*f*(H)	k_{ex} (s^{-1})	k_{obs} (s^{-1})	k_{dec} (s^{-1})
	0	1.000	1.000	1.000			
	768	0.969	1.007	0.962			
	1536	0.932	0.994	0.938			
	3072	0.874	0.981	0.891			
	4608	0.808	0.982	0.823			
0.45 M	6912	0.709	0.998	0.710	4.00×10^{-5}	4.19×10^{-5}	1.95×10^{-6}
	9984	0.630	0.990	0.636			
	13056	0.584	0.966	0.604			
	16128	0.499	0.984	0.507			
	19200	0.452	0.970	0.466			
	22272	0.388	0.964	0.402			

	26112	0.344	0.907	0.379			
	29952	0.267	0.947	0.282			
	33792	0.272	0.939	0.290			
	37632	0.160	0.933	0.171			
	46848	0.117	0.908	0.128			
	51456	0.110	0.917	0.120			
	56832	0.081	0.890	0.091			
0.25 M	0	1.000	1.000	1.000	1.65×10^{-5}	2.05×10^{-5}	2.48×10^{-6}
	5159	0.943	0.977	0.966			
	13736	0.769	0.918	0.837			
	30483	0.559	0.882	0.634			
	76916	0.242	0.756	0.320			
	97785	0.177	0.717	0.247			
	110493	0.161	0.708	0.227			
	172603	0.085	0.623	0.137			
	197847	0.064	0.583	0.110			
	261698	0.049	0.524	0.094			
0.10 M	0	1.000	1.000	1.000	5.28×10^{-6}	6.49×10^{-6}	6.54×10^{-6}
	10264	0.907	0.995	0.912			
	22797	0.896	0.974	0.920			
	80345	0.602	0.936	0.643			
	105699	0.517	0.872	0.593			
	171988	0.332	0.828	0.401			
	253349	0.238	0.770	0.309			
	289257	0.202	0.744	0.272			
	333692	0.176	0.718	0.245			
	852762	0.090	0.617	0.146			
0.045 M	0	1.000	1.000	1.000	1.92×10^{-6}	2.54×10^{-6}	3.84×10^{-7}
	8447	1.018	0.999	1.018			
	71733	0.816	0.933	0.874			
	160293	0.610	0.904	0.675			
	238008	0.520	0.869	0.598			
	272925	0.481	0.855	0.563			

348445	0.443	0.853	0.519
416206	0.359	0.817	0.439
493249	0.329	0.784	0.419
755726	0.239	0.762	0.313

Kinetics of the equilibrium between 163, adduct and aldehyde.

Aldehyde	Time (s)	Aldehyde concentration (M)	Adduct concentration (M)
35	0	5.00×10^{-3}	0
	300	3.57×10^{-3}	1.77×10^{-3}
	524	3.27×10^{-3}	1.94×10^{-3}
	748	3.14×10^{-3}	2.11×10^{-3}
	972	2.97×10^{-3}	2.19×10^{-3}
	1196	2.82×10^{-3}	2.25×10^{-3}
	1420	2.65×10^{-3}	2.36×10^{-3}
	4448	2.91×10^{-3}	1.63×10^{-3}
	8300	2.77×10^{-3}	1.47×10^{-3}
241	0	5.00×10^{-3}	0
	300	2.84×10^{-3}	2.44×10^{-3}
	524	2.47×10^{-3}	2.90×10^{-3}
	748	2.30×10^{-3}	3.12×10^{-3}
	972	2.22×10^{-3}	3.19×10^{-3}
	1196	2.11×10^{-3}	3.27×10^{-3}
	1420	2.05×10^{-3}	3.28×10^{-3}
	3527	2.03×10^{-3}	3.33×10^{-3}
	7195	2.06×10^{-3}	3.51×10^{-3}
43	0	5.00×10^{-3}	0
	300	4.60×10^{-3}	4.89×10^{-4}
	524	5.66×10^{-3}	6.28×10^{-4}
	748	4.47×10^{-3}	6.79×10^{-4}
	972	4.14×10^{-3}	6.55×10^{-4}

1196	4.08×10^{-3}	7.27×10^{-4}
1420	4.03×10^{-3}	7.43×10^{-4}
3089	4.72×10^{-3}	4.76×10^{-4}